

**CARBON CYCLE VARIABILITY  
OF THE NORTH ATLANTIC OCEAN AND LAKE SUPERIOR**

by

**Val Bennington**

**A thesis submitted in partial fulfillment of  
the requirements for the degree of**

**Doctor of Philosophy**

**(Atmospheric and Oceanic Sciences)**

at the

**University of Wisconsin – Madison**

**2010**

UMI Number: 3448883

All rights reserved

**INFORMATION TO ALL USERS**

The quality of this reproduction is dependent upon the quality of the copy submitted.

In the unlikely event that the author did not send a complete manuscript and there are missing pages, these will be noted. Also, if material had to be removed, a note will indicate the deletion.



UMI 3448883

Copyright 2011 by ProQuest LLC.

All rights reserved. This edition of the work is protected against unauthorized copying under Title 17, United States Code.



ProQuest LLC  
789 East Eisenhower Parkway  
P.O. Box 1346  
Ann Arbor, MI 48106-1346

CARBON CYCLE VARIABILITY  
OF THE NORTH ATLANTIC OCEAN AND LAKE  
SUPERIOR

submitted to the Graduate School of the  
University of Wisconsin-Madison  
in partial fulfillment of the requirements for the  
degree of Doctor of Philosophy

By

VALERIE SUSANNE BENNINGTON

Date of final oral examination: October 11, 2010

Month and year degree to be awarded: November 2010

The dissertation is approved by the following members of the Final Oral Committee:

Galen A. McKinley, Assistant Professor, Atmospheric and Oceanic Sciences

Dan Vimont, Assistant Professor, Atmospheric and Oceanic Sciences

Ankur Desai, Assistant Professor, Atmospheric and Oceanic Sciences

Chin Wu, Professor, Civil and Environmental Engineering

Noel Urban, Professor, Civil and Environmental Engineering

(Michigan Technological Institute)

# CARBON CYCLE VARIABILITY OF THE NORTH ATLANTIC OCEAN AND LAKE SUPERIOR

Val Bennington

Under the supervision of Galen A. McKinley

## Abstract

The importance of biology to the ocean carbon sink is often quantified in terms of export, the removal of carbon from the ocean surface layer. Satellite images of sea surface chlorophyll indicate variability in biological production, but how these variations affect export and air-sea carbon fluxes are poorly understood. We investigate this in the North Atlantic using an ocean general circulation model coupled to a medium-complexity ecosystem model. We find that biological CO<sub>2</sub> drawdown is significant on the mean and dominates the seasonal cycle of pCO<sub>2</sub>, but variations in the annual air-sea CO<sub>2</sub> flux and export are not significantly correlated. Large year-to-year variability in summertime pCO<sub>2</sub> occurs, due to changing bloom timing, but integrated bloom strength and associated carbon uptake and export do not vary substantially. The model indicates that small biological variability, quantitatively consistent with SeaWiFS (1998-2006), is not sufficient to be a first-order control on annual subpolar air-sea CO<sub>2</sub> flux variability.

Previous observations and modeling studies of Lake Superior have only partly elucidated its large-scale circulation, in terms of both the climatological state and interannual variability. We use an eddy resolving, three-dimensional hydrodynamic model to bridge this gap. We simulate Lake Superior circulation and thermal structure from 1979 to 2006 and consider the mechanisms responsible for the flow. Model results are compared to available direct observations of



temperature and currents. Circulation in the lake is primarily cyclonic during all seasons, and a two-gyre structure is present. Surface circulation patterns in winter mimic wind directions, but become organized in summer by the presence of thermal gradients. On the annual mean, near-shore currents are controlled by thermal gradients, while offshore flow is primarily determined by the wind. From a uniform bathymetry simulation, we determine that topographic variations cause small-scale structures in the open lake flow and are critical to the development of near shore-offshore temperature gradients. The lake exhibits significant variability in current speed and direction on synoptic timescales, but coherent patterns of inter-annual variability are not found. Long-term trends due to changing meteorological forcing are found. Model results suggest the increase in lake surface temperature ( $0.37^{\circ}\text{C}/\text{decade}$ ) is significantly correlated to increases in wind speed above the lake ( $0.18\text{ m/s}/\text{decade}$ ), increased current speeds ( $0.37\text{ cm/s}/\text{decade}$ ), and declining ice coverage ( $-886\text{ km}^2/\text{yr}$ ).

The carbon budget of Lake Superior has remained imbalanced from extrapolation of sparse observations to annual-average lake-wide budgets. Respiration estimates are an order of magnitude larger than primary production estimates; and a large efflux of carbon dioxide ( $\sim 3\text{ TgC}/\text{yr}$ ) is deduced. Using two separate ecosystem models coupled to the general circulation model at 10 km horizontal resolution, the internal carbon cycle of Lake Superior is simulated between 1979 and 2006. Modeled chlorophyll and  $\text{pCO}_2$  in the open lake are captured reasonably well, and the model suggests that although it is super-saturated and a source of atmospheric carbon dioxide during two of four periods of the year, it may not be a significant source of  $\text{CO}_2$  on annual time scales. The modeled seasonal cycles of  $\text{pCO}_2$  and  $\text{CO}_2$  fluxes are driven by the thermal structure of Lake Superior, its overturning, and biological productivity. Year-to-year

variability in the flux is driven by temperature, not biological variability, and one model suggests annual  $p\text{CO}_2$  is significantly correlated with the Southern Oscillation Index. Spatially coherent patterns of annual variability suggest that the near shore and open waters of the lake act out of sync and calls attention to the need for more open lake observations that would constrain the carbon cycle.

The modeled internal carbon cycle of Lake Superior is unable to capture high  $p\text{CO}_2$  estimated near shore along the Keweenaw Peninsula. By adding river inputs of DOC, DIC, and alkalinity from the nine rivers of largest flow, the model is able to capture a near to offshore gradient in  $p\text{CO}_2$  of observed order of magnitude. Open lake  $p\text{CO}_2$  cycles remain largely unchanged by the addition of rivers, although a background pool of DOC believed to be slowly remineralizing increases background  $p\text{CO}_2$ . The model suggests that river DOC is a more important component of the whole lake carbon budget, although river DIC causes a significant impact immediately at the river mouth. Near shore respiration rates along the Keweenaw Peninsula in 1999 are captured reasonably well with the model, and the model indicates that there exists an order of magnitude difference in respiration rates between waters impacted by rivers and those further from shore. Such a gradient, suggested but needing to be confirmed by observations, would bring the carbon budget of Lake Superior in balance. It appears that the least studied aspect of the carbon cycle, respiration, could not be extrapolated to whole-lake estimates from previous observations. Thus, the lake is likely a small annual source of carbon dioxide to the atmosphere (tenths of a  $\text{TgC/yr}$ ) with primary production between 6 and 10  $\text{TgC/yr}$ , and respiration of the same order of magnitude. Although only a small source of  $\text{CO}_2$  on the annual mean, Lake Superior's rate of

efflux can exceed 10 TgC/yr on a windy winter day, and its seasonal cycle of fluxes may be relevant to understanding the regional and downwind terrestrial carbon budgets.

## Acknowledgements

I dedicate this work to my father, Greg Benesh, who dreamed of putting his children through college and taught me the value of education. I thank both of my parents for their never ending belief in me and for their love and patience over the past thirty years.

I would like to thank my advisor, Galen A. McKinley for her guidance and dedication during the last five years. Galen is not only a brilliant scientist, but a supportive advisor, and her compassion and respect have made this work possible.

I would like to thank my entire committee: Galen McKinley, Noel Urban, Ankur Desai, Chin Wu, and Dan Vimont. Over the past years, you have put in countless hours to improve this research. Your expertise, direction, and ideas have not gone unnoticed. I would also like to thank Stephanie Dutkiewicz for teaching me how to use the MITgcm and for letting me steal her ecosystem model. I thank Dierk Polzin for his technical support and for teaching me how to get around on a supercomputer.

I would like to thank my fellow graduate students and postdoctoral scientists, particularly Amanda Fay and Nazan Atilla, for making the office a fun place to be.

I thank my partner, Ninfa, for making me laugh for the past eleven years. My successes are exponentially greater with your support. I thank our daughter, Lia, for her smile and wonder in the world

# Table of Contents

<b>ABSTRACT</b> .....	<b>I</b>
<b>ACKNOWLEDGEMENTS</b> .....	<b>V</b>
<b>TABLE OF CONTENTS</b> .....	<b>VI</b>
<b>CHAPTER 1</b> .....	<b>1</b>
<b>INTRODUCTION</b> .....	<b>1</b>
1.1 REFERENCES .....	10
<b>CHAPTER 2</b> .....	<b>13</b>
<b>IMPACTS OF BIOLOGICAL VARIABILITY ON NORTH ATLANTIC CO<sub>2</sub> FLUXES</b> .....	<b>13</b>
2.1 INTRODUCTION .....	14
2.2 MODEL DESCRIPTION .....	17
2.2.1 <i>The Physical Model</i> .....	17
2.2.2 <i>Ecosystem Model</i> .....	18
2.2.3 <i>Model-Data Comparisons</i> .....	20
2.3 RESULTS.....	23
2.3.1 <i>Bloom timing and pCO<sub>2</sub></i> .....	23
2.3.2 <i>Export and CO<sub>2</sub> Fluxes</i> .....	24
2.3.3 <i>Biological Variability</i> .....	27
2.4 DISCUSSION AND CONCLUSIONS .....	30
ACKNOWLEDGMENTS.....	32
REFERENCES .....	33
FIGURE CAPTIONS.....	36
2.5 SUPPLEMENTARY TEXT.....	46
<i>Supplementary Figure Captions</i> .....	48
<i>Supplementary Figures</i> .....	49
<b>CHAPTER 3.</b> .....	<b>52</b>
<b>THE GENERAL CIRCULATION OF LAKE SUPERIOR:</b> .....	<b>52</b>
<b>MEAN, VARIABILITY, AND TRENDS FROM 1979-2006</b> .....	<b>52</b>
ABSTRACT .....	53
3.1 INTRODUCTION.....	54
3.2 MODEL.....	58
3.2.1 <i>Physical Model</i> .....	58
3.2.2 <i>Model - Observation Comparisons</i> .....	60
3.2.2.1 <i>Model-Observation Temperature Comparisons</i> .....	60
3.2.2.2 <i>Warm Bias in NARR Forcing</i> .....	62
3.2.2.3 <i>Model-Observation Current Comparisons</i> .....	64
3.3 RESULTS.....	67
3.3.1 <i>General Circulation</i> .....	67
3.3.2 <i>Current Mechanisms</i> .....	70
3.3.3 <i>Trends</i> .....	74
3.4 DISCUSSION AND CONCLUSIONS .....	75
ACKNOWLEDGMENTS.....	79

	vii
REFERENCES .....	80
FIGURE CAPTIONS.....	83
TABLES .....	86
FIGURES.....	88
SUPPLEMENTARY .....	98
<i>Section 1: Model Forcing</i> .....	98
<i>Supplementary Section 2: Circulation Sensitivity Studies</i> .....	99
<i>Supplementary References</i> .....	101
<i>Supplementary Table Captions</i> .....	101
<i>Supplementary Figure Captions</i> .....	102
<i>Supplementary Tables</i> .....	104
<i>Supplementary Figures</i> .....	105
<b>CHAPTER 4 .....</b>	<b>111</b>
<b>INTERNAL CARBON CYCLING IN LAKE SUPERIOR.....</b>	<b>111</b>
4.1 INTRODUCTION.....	111
4.2 METHODS.....	116
4.3 PHYSICAL MODEL .....	117
4.4 ECOSYSTEM MODEL 1 – PHOSPHORUS BASED MODEL.....	117
4.4.1 <i>Nutrient Cycling</i> .....	118
4.4.2 <i>Explicit Ecosystem Model</i> .....	119
4.5 NO PHOSPHORUS MODEL DESCRIPTION .....	124
4.5.1 <i>Nutrient Cycling</i> .....	124
4.5.2 <i>No Phosphorus Ecosystem Model</i> .....	125
4.6 MAIN DIFFERENCES BETWEEN MODELS .....	128
4.6 MODEL – OBSERVATION COMPARISONS .....	129
4.6.1 OBSERVATIONS OF PCO <sub>2</sub> .....	132
4.6.2 MODEL-OBSERVATION PCO <sub>2</sub> COMPARISONS.....	133
4.7 RESULTS.....	137
4.7.1 <i>Mechanisms of CO<sub>2</sub> Flux Variability</i> .....	140
<i>Phosphorus Model</i> .....	141
<i>No Phosphorus Model Mechanisms</i> .....	144
<i>El Niño, Southern Oscillation</i> .....	146
4.7.2 <i>Empirical Orthogonal Function (EOF) Analysis</i> .....	147
<i>Physical Model Principal Components</i> .....	148
<i>Phosphorus Model Principal Components</i> .....	149
<i>No Phosphorus Model Principal Components</i> .....	151
4.8 DISCUSSION AND CONCLUSIONS .....	153
TABLE CAPTIONS .....	159
FIGURE CAPTIONS.....	161
FIGURES.....	172
<b>CHAPTER 5. ....</b>	<b>191</b>
<b>IMPACT OF RIVER RUNOFF .....</b>	<b>191</b>
<b>ON THE CARBON CYCLE OF LAKE SUPERIOR .....</b>	<b>191</b>
5.1 INTRODUCTION.....	191
5.2 METHODS.....	193
5.3 MODEL-OBSERVATION COMPARISON .....	198

	viii
5.4 RESULTS.....	200
5.4 DISCUSSION AND CONCLUSIONS .....	202
FIGURE CAPTIONS.....	206
FIGURES.....	208
<b>CHAPTER 6 .....</b>	<b>221</b>
<b>RESPIRATION RATES IN LAKE SUPERIOR.....</b>	<b>221</b>
6.1 INTRODUCTION.....	221
6.2 OBSERVATIONS OF RESPIRATION.....	222
6.3 MODEL-OBSERVATION COMPARISONS .....	223
6.4 LAKE-WIDE RESPIRATION RATES .....	224
6.5 A NEW CARBON BUDGET FOR LAKE SUPERIOR .....	226
6.6 DISCUSSION AND CONCLUSIONS .....	227
FIGURE CAPTIONS.....	230
TABLES .....	231
FIGURES.....	232
<b>CHAPTER 7 .....</b>	<b>235</b>
<b>CONCLUSIONS AND FUTURE WORK .....</b>	<b>235</b>
7.1 NORTH ATLANTIC FLUX VARIABILITY .....	235
7.1.2 <i>Key Issues in North Atlantic Flux Variability</i> .....	235
7.2 LAKE SUPERIOR'S CARBON CYCLE.....	236
7.2.1 <i>Key Issues</i> .....	240
7.3 FUTURE WORK.....	243
<b>APPENDIX A: RIVER FLOW AND CONSTITUENTS .....</b>	<b>246</b>
APPENDIX A.1. AGUASABON RIVER .....	247
APPENDIX A.2 NIPIGON RIVER .....	248
APPENDIX A.3 KAMINISTQUIA RIVER.....	249
APPENDIX A.4 MICHIPICOTEN RIVER.....	250
APPENDIX A.5 PIC RIVER.....	251
APPENDIX A.6 WHITE RIVER .....	252
APPENDIX A.7 BLACK STURGEON RIVER.....	253
APPENDIX A.8 ST. LOUIS RIVER.....	254
APPENDIX A.9 ONTONAGON RIVER .....	255
<b>APPENDIX A.2 LOADBEST MODEL AND COEFFICIENTS.....</b>	<b>256</b>
<b>REFERENCES.....</b>	<b>259</b>

# Chapter 1

## Introduction

Since the Industrial Revolution, human activities such as fossil fuel burning, cement production, and land use change have increased the global atmospheric concentration of carbon dioxide (CO<sub>2</sub>) from 280 ppm in 1850 to over 390 ppm in 2010 [Keeling *et al.*, 2005]. The terrestrial biosphere and oceans serve as natural sinks of this greenhouse gas, cutting the net accumulation of carbon dioxide in the Earth's atmosphere to about half of the total emissions [Solomon *et al.*, 2007], thereby reducing anthropogenic impacts on the climate. The percentage of anthropogenic emissions that accumulates in the atmosphere each year varies considerably [Conway *et al.*, 1994; Peylin *et al.*, 2005], and this fraction appears to be increasing [Raupach *et al.*, 2007; Canadell *et al.*, 2007]. This suggests that climate variability significantly alters the magnitude of the Earth's natural carbon dioxide sinks; thus, a mechanistic understanding of these sinks is necessary to project how the Earth's sinks and atmospheric concentration of CO<sub>2</sub> may change in the future.

The global ocean serves as the largest reservoir of the Earth's carbon and a significant sink of carbon dioxide, having absorbed about one quarter of anthropogenic emissions, thus reducing current atmospheric carbon dioxide concentrations by an estimated 55 ppm [Solomon *et al.*, 2007]. This oceanic sink is highly variable in both space and time [Sarmiento and Gruber, 2006; Corbiere *et al.*, 2007; Takahashi *et al.*, 2002; Sabine *et al.*, 2004], driven by heterogeneity and



variability in ocean physics and biology. Variations in climate cause significant changes in ocean temperature, circulation, and chemistry, all of which affect the ocean carbon cycle [McKinley *et al.*, 2004].

Warmer (colder) ocean temperatures increase (decrease) the partial pressure of CO<sub>2</sub> (pCO<sub>2</sub>) in the ocean and reduce (increase) its capacity to take carbon dioxide up from the atmosphere. This solubility pump interacts with the ocean circulation. Warmer (colder) waters flowing to colder (warmer) regions cool (warm) and increase (decrease) their ability to take up carbon dioxide (or increase efflux). Deep-water formation moves cold surface waters high in carbon dioxide to depths, where the carbon can be isolated from the atmosphere for thousands of years. Regions of upwelling return inorganic carbon from depths to the surface ocean. The older the upwelled water, the higher the concentration of inorganic carbon. Biological productivity can reduce (increase) the resulting efflux to the atmosphere (influx) by utilizing part of the upwelled dissolved inorganic carbon (DIC), depending on limitations of other macro and micronutrients. Biological productivity maintains a large gradient in DIC from the ocean depths to surface waters, and the biological pump can move carbon dioxide absorbed from the atmosphere to great depths by exporting organic carbon to deep water where it is remineralized or accumulates in sediments. Ocean productivity also alters ocean alkalinity via the utilization of CO<sub>2</sub> and the formation of calcium carbonate shells. Location, strength, and timing of the biological and calcium carbonate pumps are driven by temperature, light, and nutrient availability, which are results of latitude, season, and ocean circulation.

The interannual variability in the global ocean's annual sink of CO<sub>2</sub> is driven by El Niño, but the mechanisms controlling variability in the subtropical and subpolar oceans are largely unknown [McKinley *et al.*, 2004; Gurney *et al.*, 2002; Keeling *et al.*, 1996; Peylin *et al.*, 2005; Baker *et al.*, 2006]. Although the North Atlantic Ocean is only 15% of the global ocean surface, it accounts for an estimated 23% of the oceanic sink of all anthropogenic carbon dioxide emitted since 1800, and Takahashi *et al.* [2002] estimated that the entire Atlantic basin absorbs 41% of the annual global oceanic sink for a 1995 reference year [Sabine *et al.*, 2004].

The subpolar North Atlantic Ocean is a region of deep-water formation, large biological productivity, and deep winter mixing. The seasonal cycle of pCO<sub>2</sub> in the subpolar North Atlantic is controlled the seasonal cycles of biological productivity and convective mixing [Ullman *et al.*, 2009; Takahashi *et al.*, 1993]. Although the surface ocean is cold during winter, supply of dissolved inorganic carbon to the surface ocean causes elevated oceanic pCO<sub>2</sub> and an out-gassing. Biological productivity begins after spring stratification [Follows and Dutkiewicz, 2001] and reduces surface pCO<sub>2</sub> during the spring bloom, causing an influx of atmospheric CO<sub>2</sub>. It is thus reasonable to hypothesize that inter-annual variability in the strength of the biological pump in this region may be a first order control of year-to-year variability in the regional carbon sink.

Satellites, such as the Sea-Viewing Wide Field-of-View Sensor (SeaWiFS), provide estimates of chlorophyll at fine spatial and temporal resolution, but it is uncertain what these year-to-year variations in satellite observations mean in terms of oceanic carbon sink variability. Chlorophyll is not a direct measurement of biomass and is dependent upon temperature, light, and nutrients [Geider *et al.*, 1998], and biomass is not a direct measurement of the export of organic matter out

of the surface ocean. Do larger peaks in satellite estimates of chlorophyll suggest a larger carbon sink in the region? Are years of larger annual average chlorophyll also years of a larger influx of carbon dioxide into the North Atlantic Ocean? In **Chapter 2**, I use a medium complexity biogeochemical model coupled to the MIT general ocean circulation model to determine whether biological productivity is a first order control of inter-annual variability in the North Atlantic CO<sub>2</sub> sink and the importance of satellite estimates of oceanic chlorophyll.

Aside from the global ocean, the terrestrial biosphere removes approximately the remaining quarter of each year's anthropogenic emissions (1/4 into ocean, 1/2 into atmosphere). Lakes and rivers serve as conduits between the terrestrial biosphere and the global ocean. Carbon stored on land runs off into lakes and rivers, where it is partially decomposed and re-emitted to the atmosphere before the remainder reaches the ocean. These inland waters receive 2.9 Pg C (10<sup>15</sup> g) from land each year, of which only 0.9 Pg C reaches the ocean. Lakes, rivers, and other inland waters return 1.4 Pg C to the atmosphere and store 0.6 Pg C in their sediments each year. This source is of the same order of magnitude as uptake by the global oceans (1.6 Pg C) [*Sarmiento and Gruber, 2006*], making them a significant component of the global carbon cycle [*Cole et al., 1994; Tranvik et al., 2009; revised from Cole et al., 2007*].

Inverse model results suggest the North American continent is a large natural sink of carbon dioxide (although fossil fuel emissions from the region exceed the magnitude of this sink).

Inverse model results suggest this sink is due to forest re-growth and a reduction in forest fires [*Field et al., 2007*]. However, inverse models do not currently separate fluxes from inland waters from land, nor do they consider the Great Lakes. Thus, any net flux from the Great Lakes is

being aliased to the surrounding land in these studies. Primary productivity in the Great Lakes is of the same order of magnitude as the surrounding forest [Vollenweider *et al.*, 1974], suggesting they are an important component of the regional carbon budget. Carbon cycling in the Great Lakes may not respond to climatic variability with comparable magnitude or even flux direction as the surrounding land. To determine mechanisms controlling the inter-annual CO<sub>2</sub> flux variability in the Great Lakes region, the carbon cycle of these water bodies must be considered.

Lake Superior is the largest of the Laurentian Great Lakes, and the largest freshwater lake in the world by surface area (82,000 km<sup>2</sup>), approximately the size of South Carolina. Small lakes with large drainage basin to surface area ratios, brief residence times (months to several years), and significant biological productivity bury 23 TgC/yr in sediments [Dean and Gorham, 1998] but also process large amounts of carbon from their watersheds and respire ~100 TgC/yr to the atmosphere [Cole *et al.*, 2007]. These small lakes are highly productive, and their sedimentation rate is primarily due to autotrophic production [Dean and Gorham, 1998]. Lake Superior is oligotrophic (low-nutrient) with a watershed to lake surface area of only 1.5 and a residence time of 178 years [Quinn, 1992]. Thus, internal processes likely dominate the lake's carbon cycle. Lake Superior is also the deepest of the Great Lakes, with an average depth of 150 m, and its deepest point exceeds 400 m. Lake Superior is also positioned at a latitude where large lakes generally transition from being sinks of atmospheric CO<sub>2</sub> (lower latitudes) to sources (higher latitudes) [Alin and Johnson, 2007].

Previous estimates of Lake Superior's carbon cycle have been limited by seasonal and spatial bias in observations and large uncertainty due to indirect methods of estimating lake pCO<sub>2</sub> [eg. *Urban et al.*, 2005; *Cotner et al.*, 2004]. These studies suggest Lake Superior may be a regionally significant source of CO<sub>2</sub> to the atmosphere, but are unable to balance carbon inputs with carbon outputs. Only two time series of direct observations of pCO<sub>2</sub> exist [*Kelly et al.*, 2001; *Atilla et al.*, 2010], and both of these observations suggest Lake Superior is in near equilibrium or under-saturated with CO<sub>2</sub> relative to the atmosphere at the observation locations during summer.

*Urban et al.* [2005] put together the most comprehensive carbon cycle for Lake Superior and suggested an annual flux of 3 Teragrams of carbon (Tg C) to the atmosphere per year based on respiration and productivity measurements off the Keweenaw Peninsula. Respiration in their study far exceeds photosynthesis, but no known carbon input to the lake is large enough to subsidize the respiration estimates. It appears that respiration and/or photosynthesis cannot easily be extrapolated from the observation locations and seasons to a lake wide annual flux. Due to the fact that Lake Superior is a heterogeneous system, with large spatial and temporal variations in temperature and currents (**Chapter 3**), a three dimensional model is an appropriate technique to attempt to determine whether spatial heterogeneity in the physical and biological systems of the lake are causing an imbalance in carbon budgets estimated from regional studies.

The large-scale circulation of Lake Superior will have a significant impact on its carbon cycle but has been understudied. Due to its northerly position, Lake Superior mixes twice each year when the water warms (spring) to 3.98°C and cools (fall) to 3.98°C. This thermal structure allows

nutrients to mix from the lake bottom to the surface, given adequate winds. This turnover replenishes surface waters with nutrients and highlights the fact that, unlike the ocean, long-term carbon storage in Lake Superior would only be possible in its sediments. Weak stratification [Assel, 2003] and biological productivity during winter is possible when surface waters cool below 3.98°C, although no winter-time observations of Lake Superior productivity have been made due to its harsh winters and annual coastal ice coverage.

In Lake Superior, the spring stratification begins along the southern coast, isolating some phytoplankton and bacteria within the euphotic zone and allowing for increased biological productivity. A strong near to offshore temperature gradient persists, often referred to as the thermal bar, until the deep waters of Lake Superior stratify during summer, generally in late June or July. The thermal bar reduces transport from the near to offshore regions [Auer and Gatzke, 2004], but the strong temperature gradient also creates a coastal jet called the Keweenaw Current which transports material rapidly along the coastline from west to east and may cause mixing during eddy events [Chen *et al.*, 2001]. The open waters experience cooler temperatures due to their great depth, thereby reducing primary productivity, which is dependent on light and temperature [Sterner, 2010]. Storm and wind mixing events during summer stratification may supply phosphorus to the euphotic zone in this highly oligotrophic system. In **Chapter 3**, I adapt the MIT general circulation model to Lake Superior bathymetry and utilize the model to determine the general circulation of Lake Superior, its mechanisms, and trends between 1979 and 2006.

Lake Superior is a vast, heterogeneous system. *In situ* measurements of its carbon cycle have been restricted by location, season, and indirect techniques ( $p\text{CO}_2$ ), forcing great extrapolation to whole-lake and annual carbon cycle estimates. Biological productivity that draws down DIC and reduces lake surface  $p\text{CO}_2$  is possible during the stratified season(s) and may have a stronger effect on  $p\text{CO}_2$  than temperature [Atilla *et al.*, 2010]. Winter and spring mixing likely cause an increase in surface  $p\text{CO}_2$ , and a resulting efflux dependent on ice coverage. In **Chapter 4**, I couple two ecosystem models of the lake's internal carbon cycle to a lake circulation model to understand the seasonal cycle of surface  $p\text{CO}_2$  and  $\text{CO}_2$  fluxes, variability, and the mechanisms controlling them.

Since Lake Superior has no capacity for long term storage of carbon in its deepest waters, the internal carbon cycle allows for only a small net influx/efflux during any one year when neglecting the impact of sediment re-suspension and formation. However, climate variability causes year-to-year changes in the length and strength of the growing season; nutrient supply to the euphotic zone; lake temperatures and resulting chemistry; and the magnitude of horizontal transports (via current strength and direction), all of which may affect the amplitude of its annual fluxes.

The lake is likely a source of atmospheric carbon dioxide, although carbon budgets derived from *in situ* observations limited by space, time, and indirect techniques remain largely unbalanced [Urban *et al.*, 2005; Cotner *et al.*, 2004; Sterner, 2010]. Low sedimentation rates [Baker *et al.*, 1991; McManus *et al.*, 2003] and a long residence time allows time for the lake to process carbon from its surrounding drainage basin. Indirect estimates of near shore  $p\text{CO}_2$  suggest the

regions near shore are more supersaturated with CO<sub>2</sub> [*Urban*, unpublished data], and respiration of terrestrial carbon is one possible cause of this gradient. Seasonality in river carbon concentrations [*Raymond et al.*, 2007], DOC lability [*Holmes et al.*, 2008], alkalinity [*Keller*, 1983], and pH [*Keller*, 1983] have been shown to exist in the arctic or Lake Superior tributaries. Thus, it is possible that large river inflows high in inorganic and organic carbon and low in alkalinity after the spring- melt are transported along the coastline, causing elevated pCO<sub>2</sub> near shore. In **Chapter 5**, I add river flows from nine of the largest sub-drainage basins to the model, allowing river alkalinity, dissolved inorganic carbon, and dissolved organic carbon to impact the lake carbon cycle. Can river inputs cause a larger near shore efflux? How do they modify annual fluxes and seasonality of pCO<sub>2</sub>?

In **Chapter 6**, I re-examine the carbon budget of Lake Superior by investigating the spatial heterogeneity in modeled respiration. Respiration is the largest flow of carbon in any direction in estimated carbon budgets [*Cotner et al.*, 2004; *Urban et al.*, 2005], yet least studied in space and time. I provide my own estimates of the carbon budget for Lake Superior and discuss what observations are necessary to confirm or disprove my estimates.

I conclude my thesis in **Chapter 7**, as well as discuss key issues concerning my findings and work that needs to be done in the future.



## 1.1 References

- Alin, S. R., and T. C. Johnson (2007), Carbon cycling in large lakes of the world: A synthesis of production, burial, and lake-atmosphere exchange estimates, *Global Biogeochem. Cycles*, 21, GB3002, doi:10.1029/2006GB002881.
- Atila et al., (2010), Observed variability of Lake Superior pCO<sub>2</sub>, *Limnol. Oceanogr.*, in press.
- Auer, M.T. and T.L. Gatzke (2004) The spring runoff event, thermal bar formation, and cross margin transport in Lake Superior, *J. Great Lakes Res.*, 30 (Supplement 1): 64-81.
- Baker, J.E., Eisenreich, S.J., Eadie B.J. (1991), Sediment trap fluxes, and benthic recycling of organic carbon, polycyclic aromatic hydrocarbons, and polychlorobiphenyl congeners in Lake Superior. *Environ. Sci. Technol.* 25, 500-509.
- Baker, D., et al. (2006), TransCom 3 inversion intercomparison: Impact of transport model errors on the interannual variability of regional CO<sub>2</sub> fluxes, 1988 – 2003, *Global Biogeochem. Cycles*, 20, GB1002, doi:10.1029/2003GL018597.
- Canadell, J.G., C. Le Quééré, M.R. Raupach, C.B. Field, E.T. Buitenhuis, P. Ciais, T.J. Conway, N.P. Gillett, R.A. Houghton, and G. Marland, (2007), Contributions to accelerating atmospheric CO<sub>2</sub> growth from economic activity, carbon intensity, and efficiency of natural sinks, PNAS:0702737104.
- Chen, C.S., J.R. Zhu, E. Ralph, S.A. Green, J.W. Budd, and F.Y. Zhang (2001), Prognostic modeling studies of the Keweenaw current in Lake Superior. Part I: Formation and evolution, *J. Phys. Oceanog.*, 31(2), 379-395.
- Cole, J. J., N. F. Caraco, G. W. Kling, AND T. K. Kratz (1994), Carbon dioxide supersaturation in the surface waters of lakes, *Scienc,e* 265:1568–1570.
- Cole et al., (2007). Plumbing the global carbon cycle: Integrating inland waters into the terrestrial carbon budget. *Ecosystems* 10:171–184.
- Conway, T. J., P.P. Tans, L.S. Watermann, K.W. Thoning, D.R. Kitzis, K.A. Masarie, and N. Zhang (1994), Evidence for interannual variability of the carbon cycle from the National Oceanic and Atmospheric Administration/Climate Monitoring and Diagnostics Laboratory Global Air Sampling Network, *J. Geophys. Res.*, 99(D11), 22,831–22,855.
- Cotner, J.B., B.A. Biddanda, W. Makino, and E. Stets (2004). Organic carbon biogeochemistry of Lake Superior. *Aquatic Ecosystem Health and Management*, 7(4), 451-464.
- Dean, W. E., and E. Gorham (1998). Magnitude and significance of carbon burial in lakes, reservoirs, and peatlands. *Geology* 26: 535–538.
- Field, C.B., J. Sarmiento, and B. Hales (2007), The carbon cycle of North America in a global context. In: *The First State of the Carbon Cycle Report (SOCCR); The North American Carbon Budget and Implications for the Global Carbon Cycle*. A Report by the U.S. Climate Change Science Program and the Subcommittee on Global Change Research. National Oceanic and Atmospheric Administration, National Climatic Data Center, Asheville, NC, USA, pp. 21-28.
- Follows, M. and S. Dutkiewicz, (2001), Meteorological modulation of the North Atlantic spring bloom, *Deep Sea Res. II*, 49, 1-3, 321-344.

- French, C.R., J.J. Carr, E.M. Daugherty, L.A.K. Eidson, J.C. Reynolds, M.D. DeGrandpre (2002) Spectrophotometric pH measurements of freshwater. *Analytica Chimica Acta*, 453,13-20.
- Geider, R.J., H.L. MacIntyre, and T.M. Kana, (1998), A dynamic regulatory model of phytoplanktonic acclimation to light, nutrients, and temperature, *Limnol. Oceanogr.*, 43(4), 679-694.
- Gurney, K., et al. (2002), Towards robust regional estimates of CO<sub>2</sub> sources and sinks using atmospheric transport models, *Nature*, 415, 626–630.
- Holmes, R. M., J. W. McClelland, P. A. Raymond, B. B. Frazer, B. J. Peterson, and M. Stieglitz (2008), Lability of DOC transported by Alaskan rivers to the Arctic Ocean, *Geophys. Res. Lett.*, 35, L03402, doi:10.1029/2007GL032837.
- Keeling, R. F., S. C. Piper, and M. Heimann (1996), Global and hemispheric CO<sub>2</sub> sinks deduced from changes in atmospheric O<sub>2</sub> concentration, *Nature*, 381, 150–155.
- Keeling, C.D. and T.P. Whorf (2005), Atmospheric CO<sub>2</sub> records from sites in the SIO air sampling network. In Trends: A Compendium of Data on Global Change. Carbon Dioxide Information Analysis Center, Oak Ridge National Laboratory, U.S. Department of Energy, Oak Ridge, Tenn., U.S.A.
- Keller, W. (1983) Spring pH and alkalinity depressions in Lake Superior tributaries. *J. Great Lakes Res.* 9(3):425-429.
- Kelly, C.A., E. Fee, P.S. Ramlal, J.W. Rudd, R.H. Hesslein, C. Cnema, and E.U. Schindler (2001) Natural variability of carbon dioxide and net epilimnetic production in surface waters of boreal lakes of different sizes, *Limnol. Oceanogr.*, 46(5), 1054-1064.
- McKinley, G. A., M. J. Follows, and J. Marshall (2004), Mechanisms of air-sea CO<sub>2</sub> flux variability in the equatorial Pacific and the North Atlantic, *Global Biogeochem. Cycles*, 18, GB2011, doi:10.1029/2003GB002179.
- McManus, J., Heinen, E.A., Baehr, M.M. (2003), Hypolimnetic oxidation rates in Lake Superior: role of dissolved organic material on the lake's carbon budget. *Limnol. Oceanogr.* 48, 1624-1632.
- Peylin, P., P. Bousquet, C. Le Quéré, S. Sitch, P. Friedlingstein, G. McKinley, N. Gruber, P. Rayner, and P. Ciais (2005), Multiple constraints on regional CO<sub>2</sub> flux variations over land and oceans, *Global Biogeochem. Cycles*, 19, GB1011, doi:10.1029/2003GB002214.
- Quinn, F.H. (1992) Hydraulic residence times for Laurentian Great Lakes, *J. Great Lakes Res.*, 18, 22-28.
- Raupach, M., G. Marland, P. Ciais, C. Le Quéré, J. Canadell, G. Klepper, and C. B. Field, (2007), Global and regional drivers of accelerating CO<sub>2</sub> emissions, *PNAS*, 104(24), 10288-10293.
- Raymond, P. A., J. W. McClelland, R. M. Holmes, A. V. Zhulidov, K. Mull, B. J. Peterson, R. G. Striegl, G. R. Aiken, and T. Y. Gurtovaya (2007), Flux and age of dissolved organic carbon exported to the Arctic Ocean: A carbon isotopic study of the five largest arctic rivers, *Global Biogeochem. Cycles*, 21, GB4011, doi:10.1029/2007GB002934.
- Rödenbeck, C., S. Houweling, M. Gloor, and M. Heimann (2003), CO<sub>2</sub> flux history 1982-2001 inferred from atmospheric data using a global inversion of atmospheric transport, *Atmos. Chem. Phys.*, 3, 1919-1964,
- Rödenbeck, C. (2005), Estimating CO<sub>2</sub> sources and sinks from atmospheric concentration measurements using a global inversion of atmospheric transport, *Tech. Rep., Max-Planck-Institute for Biogeochemistry*, 6, 53.

- Sabine, C. L., R. Feely, Y. Wantanabe, and M. Lamb (2004), Temporal evolution of the North Pacific CO<sub>2</sub> uptake rate, *J. Oceanogr.*, 60, 5-15.
- Sarmiento, J. L. and N. Gruber, *Ocean Biogeochemical Dynamics*, Princeton University Press, Princeton, NJ, 526pp, 2006.
- Solomon, S., D. Qin, M. Manning, eds. (2007), *Climate Change 2007: The Physical Science Basis, Fourth IPCC Report*, Cambridge University Press, Cambridge.
- Sterner, R.W. (2010), In situ-measured primary production in Lake Superior, *Journal of Great Lakes Research*, 36:139–149.
- Takahashi, T., J. Olafsson, J. G. Goddard, D.W. Chipman, and S. Sutherland (1993), Seasonal variation of CO<sub>2</sub> and nutrients in the high-latitude surface oceans: A comparative study, *Global Biogeochem. Cycles*, 7(4), 843–878, doi:10.1029/93GB02263.
- Takahashi, T., et al. (2002), Global sea-air CO<sub>2</sub> flux based on climatological surface ocean pCO<sub>2</sub>, and seasonal biological and temperature effects, *Deep Sea Res., Part II*, 49, 1601–1622.
- Tranvik et al. (2009), Lakes and reservoirs as regulators of carbon cycling and climate, *Limnol. Oceanogr.*, 54(6 part 2), 2298-2314.
- Ullman, D. J., G. A. McKinley, V. Bennington, and S. Dutkiewicz (2009), Trends in the North Atlantic carbon sink:1992–2006, *Global Biogeochem. Cycles*, 23, GB4011, doi:10.1029/2008GB003383.
- Urban, N.R., M.T. Auer, S.A. Green, X. Lu, D.S. Apul, K.D. Powell and L. Bub (2005) Carbon Cycling in Lake Superior. *J. Geophys. Res.* 110, C06S90, doi:10.1029/2003JC002230.
- Vollenwider, R. A., M. Munawar, and P. Stadelmann (1974) A comparative review of phytoplankton and primary production in the Laurentian Great Lakes. *J. Fish. Res. Bd. Can.*, 31, 739-762.

## Chapter 2

# Impacts of biological variability on North Atlantic CO<sub>2</sub> fluxes

This chapter appeared in full as Bennington, V, G.A. McKinley, S. Dutkiewicz, D. Ullman (2009) What does chlorophyll variability tell us about export and air-sea CO<sub>2</sub> flux variability in the North Atlantic? *Global Biogeochemical Cycles*, 23, GB3002, doi:10.1029/2008GB00341. Reproduced by permission of American Geophysical Union.

The importance of biology to the ocean carbon sink is often quantified in terms of export, the removal of carbon from the ocean surface layer. Satellite images of sea surface chlorophyll indicate variability in biological production, but how these variations affect export and air-sea carbon fluxes are poorly understood. We investigate this in the North Atlantic using an ocean general circulation model coupled to a medium-complexity ecosystem model. We find that biological CO<sub>2</sub> drawdown is significant on the mean and dominates the seasonal cycle of pCO<sub>2</sub>, but variations in the annual air-sea CO<sub>2</sub> flux and export are not significantly correlated. Large year-to-year variability in summertime pCO<sub>2</sub> occurs, due to changing bloom timing, but integrated bloom strength and associated carbon uptake and export do not vary substantially. The model indicates that small biological variability, quantitatively consistent with SeaWiFS (1998-2006), is not sufficient to be a first-order control on annual subpolar air-sea CO<sub>2</sub> flux variability.

## 2.1 Introduction

Although we can quantify the amount of carbon dioxide pumped into and remaining in the atmosphere each year, we are currently unable to fully explain why the relative magnitude of terrestrial and oceanic sinks appears to be decreasing [Raupach *et al.*, 2007; Canadell *et al.*, 2007]. The difficulty of distinguishing trends from inter-annual variability is one confounding factor. In order to understand the current and future trajectory of the oceanic carbon sink, the mechanisms that control its strength and year-to-year variations must be understood. Currently, direct observations at the global scale can only provide the climatological mean and seasonal cycle of the oceanic sink [Takahashi *et al.*, 2002].

Ocean biology is critical to maintaining the gradient of  $p\text{CO}_2$  between the surface ocean and atmosphere, significantly modifying air-sea gas exchange and its spatial distribution.

Photosynthesis reduces oceanic  $p\text{CO}_2$  by converting dissolved inorganic carbon (DIC) into organic carbon, and sinking organic matter creates a mass of carbon that remineralizes back to DIC at depth. This biological cycle causes a net movement of carbon from the surface to depth and is often referred to as the “biological pump.” Behrenfeld *et al.* [2006] estimated that more than one million tons of carbon is fixed into organic matter as  $\text{CO}_2$  each day by ocean biology. Falkowski *et al.* [2000] estimate that atmospheric  $p\text{CO}_2$  would be 150-200  $\mu\text{atm}$  greater than its current value if it were not for the biological control on the gradient of DIC in the ocean. It is reasonable to hypothesize that in regions of large chlorophyll blooms, interannual fluctuations in biological productivity may alter the annual sink of carbon dioxide. The subpolar North Atlantic is one such region, with a pronounced spring bloom and a large annual mean net uptake of

carbon dioxide. *Sabine et al.* [2004] estimate the North Atlantic has taken up 23% of the total anthropogenic CO<sub>2</sub>, even though it is only 15% of the global ocean surface area. Recent studies suggest this important sink may be changing. *Schuster and Watson* [2007], based on their analysis of pCO<sub>2</sub> data, conclude that the North Atlantic sink between 20°N and 65°N has declined by 50% between 1994 and 2005.

Coupled ocean-atmosphere model results suggest that a future increase in ocean temperatures and stratification will alter chlorophyll and export production [*Sarmiento, 1999; Bopp et al., 2001*]. Increases in export production in the subpolar region [*Bopp et al., 2001*] and decreases in the subtropical region are anticipated. *Behrenfeld et al.* [2006] investigated recent (1999-2006) satellite data and suggested that global biological productivity within the subtropics has already declined, but they were unable to make any conclusions about trends in the high latitudes. To better address these ideas, we need to understand to what extent year-to-year variability of biological activity impacts the oceanic carbon sink in the present day subpolar North Atlantic.

Satellites, such as the Sea-viewing Wide Field-of-view Sensor (SeaWiFS), provide estimates of chlorophyll at fine spatial and temporal resolution, but it is uncertain what these year-to-year variations in satellite observations mean in terms of oceanic carbon sink variability. Chlorophyll is not a direct measurement of biomass and is dependent upon temperature, light, and nutrients [*Geider et al., 1998*]. Biomass itself is also not a direct measurement of export, as the sinking velocities of particulate matter are dependent upon size and density. Yet, *Lutz et al., [2007]* show that patterns of biological export do match patterns of productivity, with export occurring nearly simultaneously at low latitudes and lagging production by about two months at high

latitudes. Do larger peak chlorophyll observations indicate more biomass and export for the entire year? Satellite chlorophyll estimates do not correlate well with simultaneous measurements of oceanic  $p\text{CO}_2$  because of differing air-sea gas exchange and remineralization timescales [Lueger *et al.*, 2008], but still years of greater biological productivity might be expected to be years of greater uptake of atmospheric  $\text{CO}_2$ . Are years of greater daily average chlorophyll years of a greater oceanic carbon sink? What can these satellite estimates of chlorophyll tell us about interannual export variability?

We use an ocean general circulation model coupled to an ecosystem-biogeochemical component to determine whether biology is a first order control of interannual  $\text{CO}_2$  flux variability in the North Atlantic subpolar gyre. We seek to understand how year-to-year variations in biomass affect the annual sink of carbon dioxide in the region and to learn what satellite observations can tell us about a year's anomalous sink. We also consider controls of North Atlantic bloom variability [Follows and Dutkiewicz, 2002; Ueyama and Monger, 2005] and the lack of a significant trend in production in observations in the subpolar North Atlantic [Behrenfeld *et al.*, 2006].

This paper is organized as follows. The next section will describe the model used, experimental setup, and model evaluation. The third section will discuss model results, and the final section includes discussion and conclusions.

## 2.2 Model Description

We use a medium-complexity ecosystem model coupled to a three-dimensional North Atlantic regional ocean circulation model.

### 2.2.1 The Physical Model

We use the MIT general ocean circulation model [Marshall *et al.*, 1997a, 1997b] configured to the bathymetry of the North Atlantic with a horizontal resolution of  $0.5^\circ \times 0.5^\circ$ . The model uses a z-coordinate system of 23 vertical layers. The uppermost layers have finest resolution, with layer depths of 10 meters, becoming coarser with depth to 500 meters below 2500 meters. The Gent-McWilliams [Gent and McWilliams, 1990] eddy parameterization and KPP vertical mixing scheme [Large *et al.*, 1994] simulate effects of sub-grid scale processes. The bathymetry extends from  $20^\circ$  South to  $81.5^\circ$  North. At the southern boundary, there is a sponge layer in which tracers are rapidly restored to climatology, and the Mediterranean, Labrador and Norwegian Seas have closed boundaries. Temperature and salinity are relaxed to climatology at the Strait of Gibraltar. Model tracers have a time step of 40 minutes, and momentum is integrated more rapidly with a time step of 200 seconds. The physical model is forced with daily winds, heat, freshwater, and radiation data taken from the National Centers for Environmental Protection (NCEP) Reanalysis I between 1980 and 2006 [Kalnay *et al.*, 1996]. The physical model is spun up for eighty years while relaxing sea surface temperature and salinity to monthly climatology [Boyer *et al.*, 2004] with timescales of 2 weeks and 1 month, respectively. The relaxation forcings during spin up are saved out of the model, and during model experiments discussed here, the relaxations are turned off, but the climatological relaxation forcings are added



to interannually varying forcing terms. This increases modeled physical variability.

### 2.2.2 Ecosystem Model

The ecosystem model is that of the *Dutkiewicz et al.* [2005] updated to include the cycling of carbon, alkalinity, and oxygen. The model considers the fate of phosphorus, iron, silicon, carbon, and oxygen (results from the latter element are not discussed in this paper) as they pass from dissolved inorganic form to phytoplankton, to zooplankton, and to detritus in both dissolved and sinking particulate forms. Detritus is remineralized back to dissolved inorganic forms. The model includes two phytoplankton functional groups (diatoms and other small phytoplankton) and one zooplankton class. Phytoplankton growth can be limited by multiple nutrients (phosphate, iron, and silicic acid) and light. As an additional update to *Dutkiewicz et al.* [2005] we include temperature dependence on the growth rate following *Eppley* [1974]. To incorporate this latter change, we have altered the phytoplankton growth rates from those used in *Dutkiewicz et al.* [2005] to  $1/1.3 \text{ d}^{-1}$  for small phytoplankton and  $1/1.1 \text{ d}^{-1}$  for diatoms. Particulate organic carbon remineralizes at the rate of  $1/70 \text{ d}^{-1}$  and sinks at a rate of 8 m/d. A schematic of the ecosystem model is shown in Supplemental Figure 2-1. We refer the reader to *Dutkiewicz et al.* [2005] for further details of the model and parameter selection, and discuss here only the pertinent updates to the model to include the carbon and alkalinity cycle.

Dissolved inorganic carbon (DIC) is taken up by phytoplankton with a fixed C:P ratio of 120 [*Anderson and Sarmiento, 1994*]. As is done with other nutrients in *Dutkiewicz et al.* [2005], carbon passes through phytoplankton into zooplankton and detrital matter, which in turn

reminerals with constant timescales back to DIC. Additionally, though, carbon is exchanged with the atmosphere. The flux of carbon dioxide between the ocean and atmosphere is parameterized according to *Wanninkhof* [1992] using daily winds. We define a positive air-sea flux as one directed into the ocean. The pH and DIC in the ocean model surface layers are used to determine the concentration of CO<sub>2</sub> gas and H<sub>2</sub>CO<sub>3</sub>, which determine oceanic pCO<sub>2</sub>. Seawater alkalinity, temperature, salinity, DIC, PO<sub>4</sub>, and silicate concentrations determine pH according to *Follows et al.* [2006]. Changes in particulate inorganic carbon (PIC) and nutrient concentrations alter alkalinity following OCMIP protocols [*Najjar and Orr*, 1999]. PIC, representing sinking calcium carbonate shells, is explicitly included, with 7% of phytoplankton assumed to be calcifiers. Dissolution of PIC occurs with a timescale of 360 d.

Photosynthetically available radiation (PAR) is assumed to be 40% of the daily NCEP Reanalysis I data 24 hour averaged shortwave radiation, a reasonable assumption according to *Frouin and Pinker*, [1995] and *Olofsson et al.* [2007]. Fractional ice coverage is prescribed with daily resolution from NCEP Reanalysis I data, and its presence blocks the same fraction of incoming radiation and gas exchange. The model allows for self-shading as in *Dutkiewicz et al.* [2005]. As also in that paper, phytoplankton biomass ( $\mu\text{M P}$ ) is converted to chlorophyll for diagnostic purposes using the *Doney et al.* [1996] parameterization. We assume that because POC constitutes the majority of carbon removed from the surface ocean, it is also the most important component to interannual variability of export. We neglect the removal of biomass and dissolved carbon by lateral and vertical mixing. For the purpose of this analysis, carbon export is defined to be the rate of removal of particulate organic carbon through 100 meters, as done by *Bopp et al.* [2001]. Export defined in this manner will capture new growth in the photic zone, but

the export that does not sink below the depth of the maximum mixed layer may return to the surface ocean during winter mixing.

The biogeochemical model spin up begins in winter and is initialized with GLODAP [Key *et al.*, 2004; Lee *et al.*, 2006] DIC and ALK climatology, World Ocean Atlas 2005 [Garcia *et al.*, 2005a, 2005b] nutrients and oxygen, and very low values of phytoplankton and zooplankton. The ecosystem component is turned on after the eighty-year physical model spin up, and the coupled model is spun up for twenty years with a constant atmospheric pCO<sub>2</sub> of 360 ppm. The coupled model is then run for twenty-seven years with daily forcing between 1980 and 2006, and seasonally varying atmospheric pCO<sub>2</sub> increasing according to Mauna Loa observations [Keeling *et al.*, 2001]. The years 1980 and 1981 are ignored in model analysis to allow for adjustment. In order to separate a bloom and the subsequent export from the bloom and export of the following year, a year is considered to be December 1 – November 31 for analysis.

### **2.2.3 Model-Data Comparisons**

The physical model produces realistic surface ocean temperatures which affect pCO<sub>2</sub> and bloom timing. With Figure 2-1, we show that the physical model adequately replicates the observed pattern of annual average SST with the exception of a small region off the northeastern coast of North America. The model also captures the amplitude of the seasonal SST cycle. The model produces a realistic pattern of observed interannual SST root mean square (RMS) in the subpolar region, but overestimates this RMS by about 0.25 degrees.

Timing of the bloom is dependent upon both the physical and chemical state of the ocean and may affect the annual biomass and export. For example, blooms that begin later in the subpolar gyre may be limited by the length of the growing season, and those years may have reduced net biomass and export. Timing of modeled bloom peak dates is evaluated using SeaWiFS satellite data from 1998-2006. To isolate bloom peak dates, SeaWiFS, 8-day chlorophyll data and daily model chlorophyll were smoothed using a four week median filter as in *Ueyama and Monger* [2005], and the peak was defined as the first day between December 1 and November 31 of the maximum chlorophyll value. Figure 2-2 shows the agreement between the climatological calendar day of peak chlorophyll in the model and satellite data. Bloom start dates (not shown) are determined using the cumulative variance technique as in *Ueyama and Monger* [2005]. We fit a sigmoidal curve to the cumulative variance of the chlorophyll time series in each model grid cell. The start of the bloom is determined as the first day the slope of the curve reaches twenty percent of its maximum value. We find that the bloom begins in the fall in the lower latitudes and progresses northward through the spring and summer, similar to that found by *Ueyama and Monger* [2005].

The climatology of modeled and observed chlorophyll and standard deviation of chlorophyll during the subpolar bloom peak in the model and eight years of observations are shown in Figure 2-3. The depth to which SeaWiFS is retrieving ocean color varies in both space and time. For the model, the surface chlorophyll concentration is considered to be the mean value in the top 55 meters. Results and patterns are robust with differing selections of the depth to which model chlorophyll is averaged. The model replicates the pattern and cycle of observed chlorophyll well, but overestimates the magnitude of peak chlorophyll in the subpolar region by a factor of

two to three. The model underestimates chlorophyll in the subtropical region, a problem common in models that do not explicitly model eddies [McGillicuddy *et al.*, 2007; Oschlies and Garçon, 1998]. One additional potential reason for our underestimation of chlorophyll is that we neglect nitrogen fixation. However, satellite retrieval of surface chlorophyll does have an error on the order of 30% globally [Gregg and Casey, 2004].

Surface ocean pCO<sub>2</sub> is affected by temperature (SST), alkalinity (ALK), salinity (SSS), and dissolved inorganic carbon (DIC). In order to understand how biology affects the pCO<sub>2</sub>, we separate the temperature-driven pCO<sub>2</sub> (pCO<sub>2</sub>-T) from the effects of alkalinity, salinity, and DIC (pCO<sub>2</sub>-nonT) according to the equations of Takahashi *et al.* [2002], based upon experimental results of Takahashi *et al.* [1993]. This separation is valuable in the study of the subpolar North Atlantic because DIC and temperature are the two dominating controls on pCO<sub>2</sub> in the region [Ullman *et al.*, 2009]. pCO<sub>2</sub>-nonT can be understood primarily as the effect of DIC.

$$pCO_2 - T = \overline{pCO_2} \times \exp(0.0423 \times (SST - \overline{SST})) \quad (2-1)$$

$$pCO_2 - nonT = pCO_2 \times \exp(0.0423 \times (\overline{SST} - SST)) \quad (2-2)$$

The bar represents a time averaged mean value. Although the equations are not linear, when separating daily model output pCO<sub>2</sub>, the temperature and non-temperature components sum to within a couple μatm of total pCO<sub>2</sub>.

We can compare these components of the model's carbon cycle to observations. In Figure 2-4, the seasonal cycle of total pCO<sub>2</sub> and each of the pCO<sub>2</sub> components are shown compared to the

climatology of *Takahashi et al.* [2002]. The seasonal cycle is defined as the mean over the late summer/early fall months (August, September, October) minus the three-month winter mean (January, February, March). The model does well capturing the observed pattern of the seasonal cycle of  $p\text{CO}_2$ , clearly illustrating the dominance of temperature to the cycle in the subtropics and the dominance of DIC cycling in the subpolar region. The cycle of  $p\text{CO}_2\text{-nonT}$  is slightly stronger than observed in the subpolar region due to the large model bloom there. The weak bloom in the subtropical region causes a weaker seasonal cycle of  $p\text{CO}_2\text{-nonT}$  than observed. The seasonal cycle of  $p\text{CO}_2\text{-T}$  is a bit strong at subtropical locations.

In summary, the coupled model does a good job capturing the timing and pattern of the spring bloom and the seasonal cycle of SSTs and  $p\text{CO}_2$  throughout much of the North Atlantic basin. The primary deficiency is that mean chlorophyll is too low in the subtropical region. Despite this, patterns of variability in chlorophyll (Figure 2-3) are consistent with data across the basin, and thus we conclude the model is an adequate tool for understanding the effect of biological variability on air-sea  $\text{CO}_2$  fluxes.

## 2.3 Results

### 2.3.1 Bloom timing and $p\text{CO}_2$

We would like to understand whether interannual variations in the magnitude of the North Atlantic spring bloom have an effect on yearly export and  $\text{CO}_2$  fluxes. In Figure 2-5a, we show the standard deviation of 25 years of monthly-averaged June  $p\text{CO}_2\text{-nonT}$  from the model. The

subpolar region shows large variability in the magnitude of June  $p\text{CO}_2$  during the height of the bloom due to interannual variability in DIC changes from biological activity. Zooming in on the boxed region near Iceland shown in Figure 2-5a, we show the seasonal cycle of weekly  $p\text{CO}_2$  and its standard deviation (black dashed) in Figure 2-5b. The largest variability in total  $p\text{CO}_2$  occurs during June and is due to changes in the  $p\text{CO}_2\text{-nonT}$  component, that is, in turn, due to bloom timing and magnitude variability. This maximum in variability occurs during the time of maximum change in the seasonal cycle of total  $p\text{CO}_2$ . This suggests that variability in the bloom timing might impact yearly  $\text{CO}_2$  fluxes.

The importance of the bloom to the seasonal cycle of  $p\text{CO}_2$  is shown in Figure 2-6a, where significant positive correlations between the bloom peak date and the date of minimum oceanic  $p\text{CO}_2$  are shown. Positive correlations north of  $45^\circ\text{N}$  indicate that bloom timing affects the date of the annual minimum  $p\text{CO}_2$ . Earlier blooms shift this minimum earlier, and later blooms shift the minimum  $p\text{CO}_2$  later. The correlation between  $30^\circ\text{N}$  and  $45^\circ\text{N}$  is surprising, because temperature controls  $p\text{CO}_2$  in this region. Here, minimum  $p\text{CO}_2$  occurs when the water is coldest and mixing most vigorously. Chlorophyll peaks at the same time, because the mixing supplies nutrients, and at the same time DIC (Figure 2-6b) to the surface, but it is the cold that causes the  $p\text{CO}_2$  minimum, not biology.

### **2.3.2 Export and $\text{CO}_2$ Fluxes**

Ocean biology controls summertime  $p\text{CO}_2$  in the subpolar region, but does this summertime control of  $p\text{CO}_2$  exert a first order control on the annual  $\text{CO}_2$  fluxes in the region? SeaWiFS provides satellite-derived estimates of year-to-year variations in ocean chlorophyll. It is

expected that years with larger chlorophyll peaks and annually integrated chlorophyll are years of greater export of particulate organic carbon, even though chlorophyll is not a direct measurement of biomass. We test this expectation.

The correlation between modeled integrated annual biomass in the top 55 meters (December – November) and integrated export over the same time period is significantly correlated almost everywhere in the North Atlantic (Figure 2-6c). Thus, greater biological productivity does result in more export, but do larger blooms create an anomalous influx of CO<sub>2</sub> for the year? We consider this by correlating the annual CO<sub>2</sub> flux (positive into ocean) and annual export (Figure 2-6d). Large-scale correlation between annual CO<sub>2</sub> fluxes and annual export exists in the subtropical region, but not in the majority of the subpolar region.

As with the seasonal cycle (section 3.1), the large-scale correlation between annual CO<sub>2</sub> fluxes and annual export in the subtropical region does not indicate a first order control of biology in that region; instead it indicates an indirect relationship via temperature. Years of increased mixing bring both cold and nutrient rich waters to the surface. Increased nutrient supply fuels increased biomass growth and export in this nutrient limited region. However, oceanic pCO<sub>2</sub> in the subtropical North Atlantic is largely controlled by temperature [Ullman *et al.*, 2009; Lueger *et al.*, 2008], and it is the anomalously cold temperatures that lead to a reduced pCO<sub>2</sub>. Colder years are therefore years of greater biological production and (indirectly) lower pCO<sub>2</sub> in the region, in agreement with the findings of Bopp *et al.* [2001] and Sarmiento *et al.* [2004]. Annual temperatures and maximum winter mixed layer depth, as defined as the depth at which the



potential density differs from the surface by  $0.125 \text{ kg/m}^3$ , are significantly anti-correlated almost everywhere (not shown).

Thus, we find that years of greater biological production in the subpolar region are years of greater export, but not necessarily years of a greater influx of  $\text{CO}_2$ . In the western subpolar region, where light is seasonally limiting, export is positively correlated to annual SST (Figure 2-6e), indicating that warmer years and years of greater stratification provide more light and less bloom-time mixing, and thus greater biological productivity [Follows and Dutkiewicz [2002]; Ueyama and Monger [2005]]. These are also years of a reduced supply of DIC to the surface. Figure 2-6f illustrates that the air-sea  $\text{CO}_2$  flux is inversely proportional to DIC in the high latitudes. Years of lower surface DIC are years of increased  $\text{CO}_2$  influx in this region, but is the lower DIC due to shallower winter mixing or greater biological drawdown? Using the model, we are able to quantify the change in DIC created by biological production above or below the 25-year daily mean (Supplementary text). We find the day-to-day change in  $\text{pCO}_2$  above or below its mean value due to biological activity amounts to a daily average change in  $\text{pCO}_2$  on the order of  $2 \mu\text{atm}$  or less in the subpolar gyre during summer, consistent with *Le Quéré et al.* [2003], who used a model sensitivity test to determine that biological interannual variability only altered  $\text{pCO}_2$  by a couple of  $\mu\text{atm}$ . Changes in  $\text{pCO}_2$  caused by anomalous winter mixing in the model are larger than those caused by anomalous biological productivity (on the order of  $10 \mu\text{atm}$ , Supplementary Text). Increased wind speeds in winter also cause increased air-sea gas exchange, so winter mixing must be controlling the annual  $\text{CO}_2$  flux variability. These factors combine such that winter flux variability is significantly larger than summer flux variability in the subpolar gyre (Supplementary Figure 2-2).

The small area within the subpolar gyre to the southwest of Iceland that shows a significant correlation between export and CO<sub>2</sub> flux variability (Figure 2-6d) is a region of extremely deep winter mixing. In this region, anomalous biological production is not a first order control of air-sea flux variability, but mixing is highly correlated to biomass here. Deeper mixing in this region increases surface DIC concentrations and decreases the magnitude of the spring bloom by keeping phytoplankton mixed away from the light [Dutkiewicz *et al.*, 2001]. In this way, years of decreased mixing are also years of both increased air-sea CO<sub>2</sub> flux and increased export in this small region, but the correlation is indirect.

Across the basin, years of increased integrated chlorophyll are indeed years of greater export, but years of greater export are not necessarily years of an increased air-sea CO<sub>2</sub> uptake. Export and CO<sub>2</sub> fluxes are correlated in the subtropics, but it is temperature, not biology that controls pCO<sub>2</sub> in this region, so the correlation is indirect. In the subpolar region, anomalies in export do not correlate with air-sea CO<sub>2</sub> flux anomalies. We find that biology is not a first order control on interannual air-sea CO<sub>2</sub> flux variability anywhere in the North Atlantic.

### **2.3.3 Biological Variability**

We have shown that biological productivity in the subpolar region determines the seasonal cycle of pCO<sub>2</sub> (Figure 2-3,2-5), so why is it not a first order control of air-sea CO<sub>2</sub> flux variability (Figure 2-6d)? DIC controls the annual pCO<sub>2</sub> and air-sea CO<sub>2</sub> fluxes in the subpolar region, but

anomalous summertime biomass does not create anomalous annual CO<sub>2</sub> fluxes (Figure 2-6d,f). In this section, we illustrate that large variability in June pCO<sub>2</sub> (Figure 2-5) is driven by bloom timing, not integrated magnitude of the bloom. For our analysis, we define integrated bloom strength as the annually integrated chlorophyll.

The ratio of the standard deviation in daily chlorophyll to the mean between 1998 and 2006 is shown for the model and SeaWiFS in Figure 2-7a,b. Since the model is unable to produce the magnitude of the bloom observed in the subtropical region (Section 2.3), percent variations in less productive regions are unrealistically large, and so areas in which the model integrated annual average chlorophyll is less than 150 mg m<sup>-3</sup> are masked. We consider only the variability in the subpolar North Atlantic. The model does very well at capturing the percent of biological variability throughout the subpolar region, even capturing specific regions of observed greater variability, such as along 30°W. For the area shown in Figure 2-7a,b, the average percent variability is 13.5% in the data and 15.3% in the model. This percent variability agrees reasonably well with *Levy et al.* [2005] who find annually integrated chlorophyll varies by 10% of its mean in a region of the subpolar North Atlantic (16°-22°W, 41°-50°N) using SeaWiFS satellite estimates of chlorophyll for 1998-2002.

The box in Figure 2-7b corresponds to the near-Iceland region introduced in Figure 2-5, and Figure 2-7c depicts the 25 years of model chlorophyll in that region. Though large year-to-year variations in bloom timing exist, the variability in integrated bloom strength (the area underneath each curve) and export are small. This indicates that variations in bloom timing drive a large variability in June pCO<sub>2</sub> (Figure 2-5) but do not translate into significant anomalies in integrated

chlorophyll or export over the course of the year. The percent variation of modeled annual export in this near-Iceland region (4.8%) is much less than the percent variation in modeled yearly chlorophyll (10.9%), since chlorophyll is not a direct measurement of biomass and does not take into account changing community structure. Its variability does not translate to export variability. Between 1998 and 2006, integrated chlorophyll varied by 18% of its mean in SeaWiFS data at this location.

In the subpolar gyre of the North Atlantic, we find that blooms that start earlier also end earlier, an unexpected result for a light-limited region. Further model analysis indicates that tight ecosystem coupling is responsible for limiting interannual variability of integrated bloom strength. An initial diatom bloom begins to reduce silicate and phosphorus availability. At the same time, zooplankton concentrations increase. When silicate is limited, the diatom bloom subsides and small phytoplankton begin to dominate the biomass. When nutrients limit growth, the phytoplankton concentrations decrease. Mixing in late fall relaxes nutrient limitation, but zooplankton are too abundant to allow another bloom. This progression was observed by *Sieracki et al.* [1993] and discussed by *Lochte et al.* [1993] during the North Atlantic Bloom Experiment.

With limited variability in integrated bloom magnitude, there is limited variability in the annual strength of the biological pump. This variability in the biological pump is too weak to be a first order control on the air-sea CO<sub>2</sub> flux variability in the region.

## 2.4 Discussion and Conclusions

We have used a basin scale ocean general circulation model coupled to a medium complexity ecosystem to determine whether variation in biological productivity is a first order control on air-sea CO<sub>2</sub> fluxes in the subpolar North Atlantic. We have shown that large variability in summer pCO<sub>2</sub> exists in the subpolar region and is due to the bloom's control on the seasonal cycle of pCO<sub>2</sub>. However, upon closer inspection, the large variability present in summer is due to bloom timing and not integrated bloom strength. Although no significant causal relationship was found between variations in subpolar biomass and annual subpolar CO<sub>2</sub> fluxes, biology does determine the timing of the seasonal cycle of pCO<sub>2</sub> within the region and is an important driver of the mean air-sea gas exchange [Behrenfeld *et al.*, 2006; Falkowski *et al.*, 2000]. The pattern of annual mean CO<sub>2</sub> fluxes matches the pattern of annual export (Supplementary Figure 2-3), illustrating the importance of biology to the mean air-sea gas exchange.

The model replicates the percent chlorophyll variability observed in SeaWiFS in the subpolar gyre, and the small percent variability in modeled annually integrated export (5-10%) suggests that it is not sufficient to be a first order control of annual CO<sub>2</sub> flux variability. Modeled biological variability alters summertime daily average pCO<sub>2</sub> on the order of a couple  $\mu\text{atm}$ . Light summer winds over the subpolar gyre further also help to limit biological impacts on air-sea CO<sub>2</sub> flux variability.

In the subtropical region, yearly biological production and export are significantly correlated to annual CO<sub>2</sub> fluxes, but the relationship is not causal. Here, SST controls pCO<sub>2</sub> but is related to biology through the vertical supply of nutrients. Colder SSTs decrease oceanic pCO<sub>2</sub>, increase

vertical mixing, and enhance the bloom. Our results agree with *Behrenfeld et al.* [2006] who find a strong correlation between biological production and climate within the permanently stratified regions of the ocean. However, we do not anticipate any effect on the CO<sub>2</sub> fluxes due to the changes in biological production. Even though modeled biological variability in the subtropical region exceeds 100 percent, it is still not a first order control of pCO<sub>2</sub>, because SST controls pCO<sub>2</sub> here [*Ullman et al.*, 2009]. Therefore, we conclude that biology has not been a first order control on the interannual variability of CO<sub>2</sub> fluxes anywhere in the North Atlantic in recent years, barring changes in ecosystem structure that would not be captured in this model.

Despite biology not controlling CO<sub>2</sub> flux interannual variability, interpretation of in situ observations of oceanic pCO<sub>2</sub> need to carefully consider bloom timing in order to properly understand CO<sub>2</sub> cycling, variability, and trends. Model results show that changes in bloom timing can alter monthly pCO<sub>2</sub> values by tens of μatm (Figure 2-5), so sparse observations should be extrapolated to annual timescales with great care.

Recent studies have used SeaWiFS data to understand year-to-year variations and trends in biological productivity on a global scale. Our results suggest SeaWiFS may be very useful for estimating variability in export out of the ocean surface on short timescales, but cannot directly elucidate CO<sub>2</sub> flux variability on annual timescales.

## **Acknowledgments**

We thank Dierk Polzin for assistance with the figures and the computations, Mick Follows for advice, and two anonymous reviewers for their helpful suggestions. We thank NASA for funding (CARBON/04-0300-0228). Ocean color data used in this study were produced by the SeaWiFS Project at GSFC. The data were obtained from the GESDAAC under the auspices of the NASA. Use of this data is in accord with the SeaWiFS Research Data Use Terms and Conditions Agreement. Reynolds and Smith reanalysis data provided by the NOAA/OAR/ESRL PSD, Boulder, Colorado, USA, from their website at <http://www.cdc.noaa.gov/>.

## References

- Anderson, L. A., and J. L. Sarmiento (1994), Redfield ratios of remineralization determined by nutrient data analysis, *Global Biogeochem. Cycles*, 8(1), 65–80.
- Behrenfeld, M.J., O'Malley, R.T., Siegel, D.A., McClain, C.R., Sarmiento, J.L., Feldman, G.C., Milligan, A.J., Falkowski, P.G., Letelier, R.M. and Boss, E.S., (2006), Climate-driven trends in contemporary ocean productivity. *Nature*, 444, 752-755.
- Bopp, L., P. Monfray, O. Aumont, J.-L. Dufresne, H. Le Treut, G. Madec, L. Terray, and J. Orr (2001), Potential impact of climate change on marine export production, *Global Biogeochem Cycles*, 15(1), 81-99.
- Boyer, T. P., Levitus, S., Garcia, H. E., Locarnini, R. A., Stephens, C., and J. Antonov, (2004), Objective analyses of annual, seasonal, and monthly temperature and salinity for the world ocean on a 0.25 degrees grid, *Int. J. Climatol.*, 25(7), 931–945.
- Bretherton, C. S., M. Widmann, V. P. Dymnikov, J. M. Wallace, and I. Bladé, (1999), The effective number of spatial degrees of freedom of a time-varying field, *J. Clim.*, 12, 1990-2009.
- Canadell, J.G., C. Le Quééré, M.R. Raupach, C.B. Field, E.T. Buitenhuis, P. Ciais, T.J. Conway, N.P. Gillett, R.A. Houghton, and G. Marland, (2007), Contributions to accelerating atmospheric CO<sub>2</sub> growth from economic activity, carbon intensity, and efficiency of natural sinks, PNAS:0702737104.
- Doney, S., D. M. Glover, and R. G. Najjar, (1996), A new coupled, one-dimensional biological-physical model for the upper ocean: Applications to the JGOFS Bermuda Atlantic Time-series Study (BATS) site, *Deep Sea Res. II*, 43, 2-3, 591-624.
- Dutkiewicz, S., M. Follows, J. Marshall, and W. W. Gregg, (2001), Interannual variability of phytoplankton abundances in the North Atlantic, *Deep Sea Res. II*, 48, 10, 232-2344.
- Dutkiewicz, S., M. J. Follows, and P. Parekh (2005), Interactions of the iron and phosphorus cycles: A three-dimensional model study, *Global Biogeochem. Cycles*, 19, GB1021, doi:10.1029/2004GB002342.
- Eppley, R. W. (1972), Temperature and phytoplankton growth in the sea, *Fish. Bull.*, 70, 1063 – 1085.
- Falkowski, P.G., W.O. Smith, H. Ducklow, and J.J. McCarthy (2000), Temperature effects on export production in the open ocean, *Global Biogeochem. Cycles*, 14(4), 1231-1246.
- Follows, M. and S. Dutkiewicz, (2001), Meteorological modulation of the North Atlantic spring bloom, *Deep Sea Res. II*, 49, 1-3, 321-344.
- Follows, M., T. Ito, and S. Dutkiewicz (2006), A compact and accurate carbonate chemistry solver for ocean biogeochemistry models, *Ocean Modeling*, 12, 290-301.
- Frouin, R., and R.T. Pinker (1995), Estimating photosynthetically active radiation (PAR) at the Earth's surface from satellite observations, *Remote Sensing of Environment*, 51, 98-107.
- Garcia, H. E., R. A. Locarnini, T. P. Boyer, and J. I. Antonov (2006a), *World Ocean Atlas 2005, Volume 4: Nutrients (phosphate, nitrate, silicate)*. S. Levitus, Ed. NOAA Atlas NESDIS 64, U.S. Government Printing Office, Washington, D.C., 396 pp.
- Garcia, H. E., R. A. Locarnini, T. P. Boyer, and J. I. Antonov (2006b), *World Ocean Atlas 2005, Volume 3: Dissolved Oxygen, Apparent Oxygen Utilization, and Oxygen Saturation*. S. Levitus, Ed. NOAA Atlas



NESDIS 63, U.S. Government Printing Office, Washington, D.C., 342 pp.

- Geider, R.J., H.L. MacIntyre, and T.M. Kana, (1998), A dynamic regulatory model of phytoplanktonic acclimation to light, nutrients, and temperature, *Limnol Oceanogr.*, 43(4), 679-694.
- Gent, P. R., and J. C. McWilliams, (1990), Isopycnal mixing in ocean circulation models, *J. Phys. Oceanogr.*, 20, 150–155.
- Gregg, W.W., and N. Casey, (2004), Global and regional evaluation of the SeaWiFS chlorophyll data set, *Remote Sensing of Environment*, 93, 463-479.
- Kalnay, E., M. Kanamitsu, R. Kistler, W. Collins, D. Deaven, L. Gandin, M. Iredell, S. Saha, G. White, J. Woollen, Y. Zhu, M. Chelliah, W. Ebisuzaki, W. Higgins, J. Janowiak, K. C. Mo, C. Ropelewski, J. Wang, A. Leetmaa, R. Reynolds, R. Jenne, and D. Joseph, (1996), The NCEP/NCAR 40-Year Reanalysis Project. *Bulletin of the American Meteorological Society*, 77 (3), 437–471.
- Keeling, C. D., S. C. Piper, R. B. Bacastow, M. Wahlen, T. P. Whorf, M. Heimann, and H. A. Meijer (2001), Exchanges of atmospheric CO<sub>2</sub> and <sup>13</sup>CO<sub>2</sub> with the terrestrial biosphere and oceans from 1978 to 2000. I. Global aspects, SIO Reference Series, No. 01-06, Scripps Institution of Oceanography, San Diego, 88 pages.
- Key, R.M., A. Kozyr, C.L. Sabine, K. Lee, R. Wanninkhof, J. Bullister, R.A. Feely, F. Millero, C. Mordy, T.-H. Peng (2004). A global ocean carbon climatology: Results from GLODAP. *Global Biogeochemical Cycles*, 18, GB4031.
- Large, W. G., J. C. McWilliams, and S. C. Doney, (1994), Oceanic vertical mixing: a review and a model with a nonlocal boundary layer parameterization. *Rev. Geophys.*, 32, 363-403.
- Lee, K., L. T. Tong, F. J. Millero, C. L. Sabine, A. G. Dickson, C. Goyet, G.-H. Park, R. Wanninkhof, R. A. Feely, and R. M. Key, (2006), Global relationships of total alkalinity with salinity and temperature in surface waters of the world's oceans. *Geophys Res. Letters*, 33, L19605, doi:10.1029/2006GL027207.
- Le Quéré, C., O. Aumont, P. Monfray, and J. Orr (2003), Propagation of climatic events on ocean stratification, marine biology, and CO<sub>2</sub>: Case studies over the 1979-1999 period, *J. Geophys. Res.*, 108(C12), 3375, doi:10.1029/2001JC000920.
- Lévy, M., Y. Lehahn, J.-M. André, L. Mémerly, H. Loisel, and E. Heifetz, (2005). Production regimes in the Northeast Atlantic: a study based on SeaWiFS chlorophyll and OGCM mixed-layer depth, *J. Geophys. Res.*, 110(C7), C07S10, doi:10.1029/2004JC002771.
- Lochte, K., H. W. Ducklow, M.J.R. Fasham, and C. Stienen (1993), Plankton succession and carbon cycling at 47°N 20°W during the JGOFS North Atlantic Bloom Experiment, *Deep-Sea Research II*, 40(1), 91-114.
- Lueger, H., R. Wanninkhof, A. Olsen, J. Triñanes, T. Johannessen, D.W.R. Wallace, and A. Körtzinger (2008): The sea-air CO<sub>2</sub> flux in the North Atlantic estimated from satellite and ARGO profiling float data, NOAA Tech. Memo. OAR AOML-96, NOAA/Atlantic Oceanographic and Meteorological Laboratory, 28 pp.
- Lutz, M.J., K. Caldeira, R.B Dunbar, and M. Behrenfeld (2007), Seasonal rhythms of net primary production and particulate organic carbon flux to depth describe the efficiency of biological pump in the global ocean, *J. Geophys Res.*, 112, C10011, doi:10.1029/2006JC003706.
- Marshall, J., A. Adcroft, C. Hill, L. Perelman, and C. Heisey (1997a), A finite volume, incompressible Navier-Stokes model for studies of the ocean on parallel computers, *J. Geophys. Res.*, 102, 5753-5766.
- Marshall, J., C. Hill, L. Perelman, and A. Adcroft (1997b), Hydrostatic, quasi-hydrostatic, and nonhydrostatic ocean modeling, *J. Geophys. Res.*, 102, 5733-5752.

- McGillicuddy, D., L. Anderson, N. Bates, T. Bidy, K. Buesseler, C. Carlson, C. Davis, C. Ewart, P. Falkowski, S. Goldthwait, D. Hansell, W. Jenkins, R. Johnson, V. Kosnyrev, J. Ledwell, Q. Li, D. Siegel, and D. Steinberg, (2007), Eddy/wind interactions stimulate extraordinary mid-ocean plankton blooms, *Science*, 316(5827), 1021-1026, doi:10.1126/science.1136256.
- Millero, F.J., (1995), The thermodynamics of the carbonic acid system in the oceans, *Geochimical and Cosmochimical Acta*, 59, 661-67.
- Najjar, R. G. and J. C. Orr, Biotic-HOWTO. Internal OCMIP Report, LSCE/CEA Saclay, Gif-sir-Yvette, France, 15 pp., 1999.
- Olofsson, P., P.E. Van Laake, and L. Eklundh (2007), Estimation of absorbed PAR across Scandinavia from satellite measurements, Part I: Incident PAR, *Remote Sens. Env.* 110, 252-261.
- Oschlies, A., and V. Garçon, (1998), Eddy-induced enhancement of primary production in a model of the North Atlantic Ocean, *Nature* 394, 266-269, doi:10.1038/28373.
- Raupach, M., G. Marland, P. Ciais, C. Le Quéré, J. Canadell, G. Klepper, and C. B. Field, (2007), Global and regional drivers of accelerating CO<sub>2</sub> emissions, *PNAS*, 104(24), 10288-10293.
- Sarmiento, J. L. and T. M. C. Hughes, (1999): Keynote Perspective: Anthropogenic CO<sub>2</sub> uptake in a warming ocean. *Tellus*, 51B(2), 560-561.
- Sarmiento, J. L., et al. (2004), Response of ocean ecosystems to climate warming, *Global Biogeochem. Cycles*, 18, GB3003, doi:10.1029/2003GB002134.
- Schuster, U., and A. J. Watson (2007), A variable and decreasing sink for atmospheric CO<sub>2</sub> in the North Atlantic, *J. Geophys. Res.*, 112, C11006, doi:10.1029/2006JC003941.
- Sieracki, M., P. Verity, and D. Stoecker (1993), Plankton community response to sequential silicate and nitrate depletion during the 1989 North Atlantic spring bloom, *Deep-Sea Research II*, 40(1), 213-225.
- Takahashi, T., Olafsson, J., Goddard, J., Chipman, D. W. and Sutherland, S. C., (1993). Seasonal variation of CO<sub>2</sub> and nutrients in the high-latitude surface oceans: A comparative study. *Global Biogeochem. Cycles*, 7, 843-878.
- Takahashi, T., Sutherland, S. C., Sweeney, C., Poisson, A., Metzl, N., Tillbrook, B., Bates, N., Wanninkhof, R., Feely, R. A., Sabine, C., Olafsson, J. and Nojiri, Y., (2002), Global sea- air CO<sub>2</sub> flux based on climatological surface ocean pCO<sub>2</sub>, and seasonal biological and temperature effects, *Deep-Sea Res. II*, 49, 1601-1622.
- Ueyama, R. and B. C. Monger, (2005), Wind-induced modulation of seasonal phytoplankton blooms in the North Atlantic derived from satellite observations, *Limnol. Oceanogr.*, 50(6), 1820-1829.
- Ullman, D. J., G. A. McKinley, V. Bennington, and S. Dutkiewicz (2009), Trends in the North Atlantic carbon sink: 1992 - 2006, *Global Biogeochem. Cycles*, 23, GB4011, doi:10.1029/2008GB003383.
- Wanninkhof, R. (1992), Relationship between wind speed and gas exchange over the ocean, *J. Geophys Res*, 97, C5, 7373-7382.

## Figure Captions

**Figure 2-1.** Model and data (Reynolds and Smith) annual average SST (left) and seasonal cycle of SST (right). Model and data climatology from 1982-2006. Seasonal cycle of SST defined as difference between summer/early fall (JAS) mean SST and winter (FMA) mean SST.

**Figure 2-2.** Climatology of bloom peak day in SeaWiFS satellite data (1998-2006) and in the model (1982-2006).

**Figure 2-3.** Model surface (55 meters) and SeaWiFS climatology and root mean square (RMS) of June chlorophyll  $\text{mg/m}^3$ . Modeled climatology and standard deviation between 1998 and 2006. SeaWiFS data from 1998-2006.

**Figure 2-4.** Maps of the seasonal amplitude (ASO – JFM) of  $\text{pCO}_2$ ,  $\text{pCO}_2\text{-T}$ , and  $\text{pCO}_2\text{-nonT}$  in the North Atlantic for the model and observational data of *Takahashi et al.* [2002]. Amplitudes shown are in units of  $\mu\text{atm}$ . The dark line is zero seasonal change.

**Figure 2-5. (a)** Standard deviation of 25 years of June  $\text{pCO}_2\text{-nonT}$  in  $\mu\text{atm}$ . The large variability in June  $\text{pCO}_2$  (not shown) in the subpolar region is due to  $\text{pCO}_2\text{-nonT}$  variability. The boxed region corresponds to the Icelandic region depicted in b. **(b)** Twenty-five year climatology of the  $\text{pCO}_2$  seasonal cycle and root mean square of weekly  $\text{pCO}_2$  and each of its

components near Iceland (57.5°N 17.5°W). Summertime variability in pCO<sub>2</sub> is driven by variability in pCO<sub>2</sub>-nonT.

**Figure 2-6.** (a) Significant correlations between the day of the year of the bloom peak and the day of the year of the minimum oceanic pCO<sub>2</sub> value. (b) Significant correlations between the annual maximum mixed layer depth and surface DIC concentrations. (c) Significant correlations between annual biomass and annual export. (d) Significant correlations between annual export and detrended annual air-sea CO<sub>2</sub> flux. (e) Significant correlations between annual average SST and annual export. (f) Significant correlations between annual surface DIC concentrations and the annual air-sea CO<sub>2</sub> flux.

All correlations presented take into account the temporal autocorrelation between the two time series as in [Bretherton *et al.*, 1999] and are considered significant at the 95% confidence level. Dashed and labeled contour lines indicate a negative correlation. The thick black lines are lines of zero correlation.

**Figure 2-7.** (a,b) The percent the standard deviation is of the mean daily chlorophyll between fall 1998 and 2006 in SeaWiFS (a) and the model (b). Eight-day weeks 10 through 37 of the year are used in this analysis, because SeaWiFS data in the subpolar region is too sparse during the omitted weeks. To compare the model to SeaWiFS satellite data, a daily average chlorophyll value for each year was calculated in both the data and model. Due to cloud cover and other satellite issues, not all grid points have observational data every 8-day period, so area-weighted averages for 5° x 5° regions were used with observational data. Within a 5° x 5° area, the available data for each 8-day record is assumed representative of the entire area and an area-

weighted average is created, ignoring missing data points. The model is able to capture the percent variability observed and much of the pattern of variability magnitude.

(c) 25 years of modeled chlorophyll at region near Iceland boxed in (b). Thick black line is modeled climatology. Annually integrated chlorophyll varies by only 10.9% of the mean, and annual export varies by only 4.8% of the mean between 1982 and 2006. SeaWiFS daily average chlorophyll (1998-2006) varies by 18% of its mean in this region.

Figure 2-1.

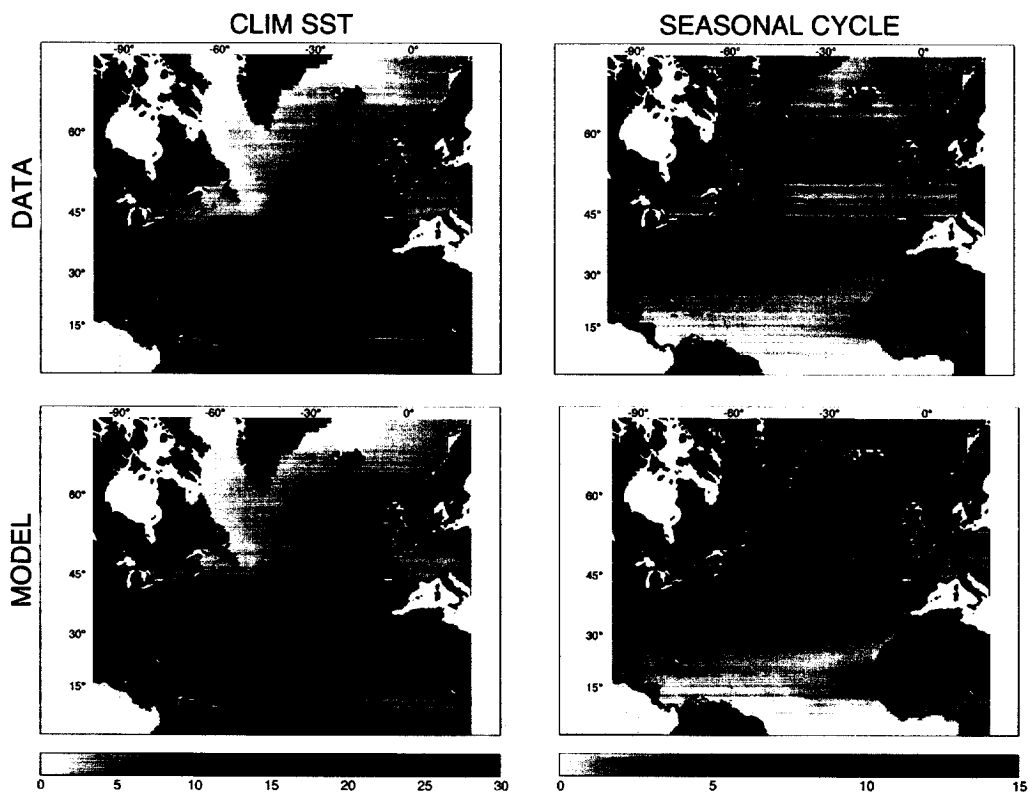


Figure 2-2.

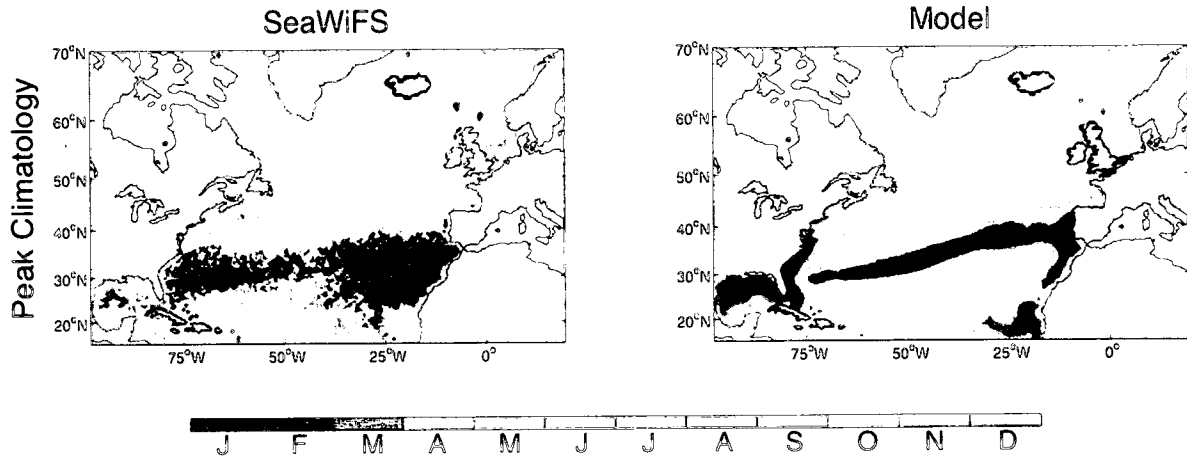


Figure 2-3.

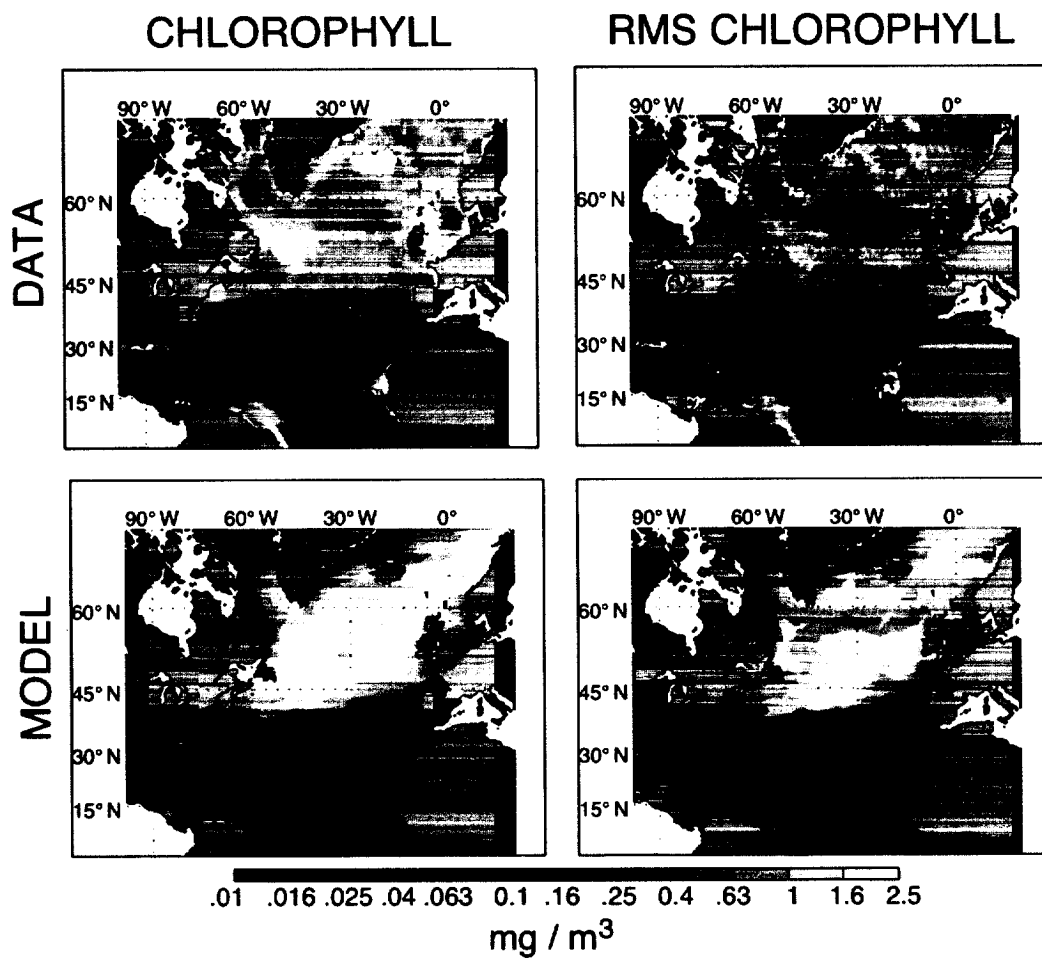




Figure 2-4.

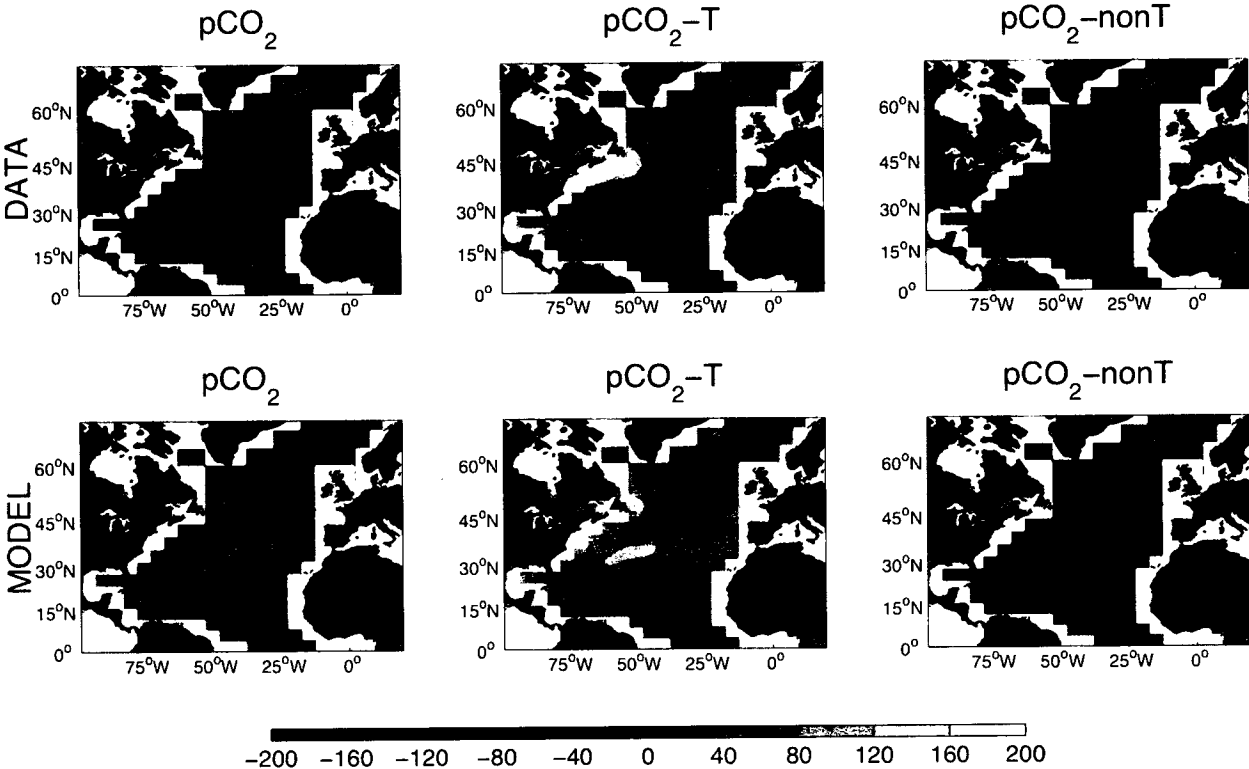


Figure 2-5.

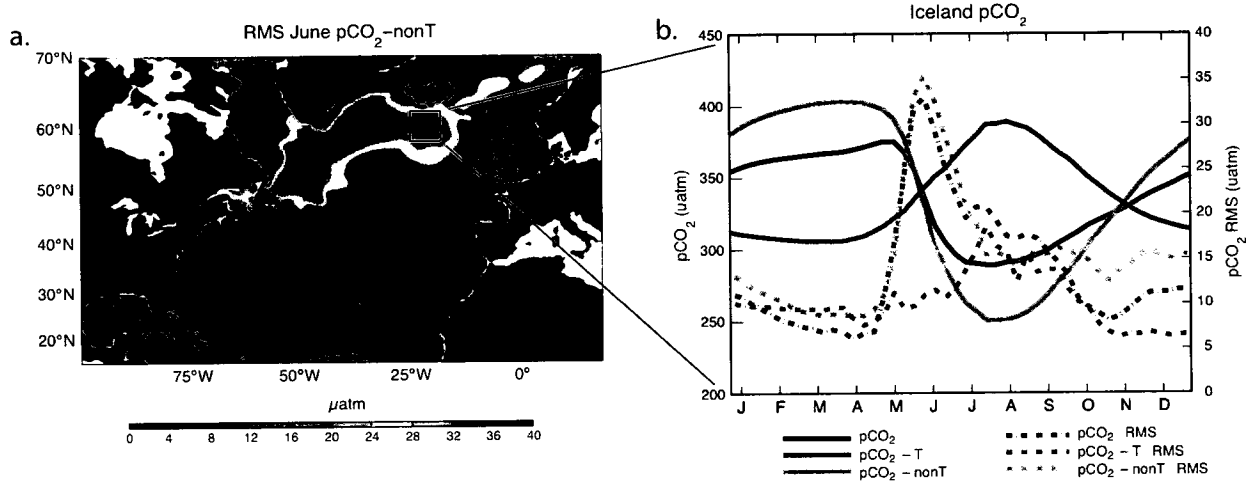


Figure 2-6.

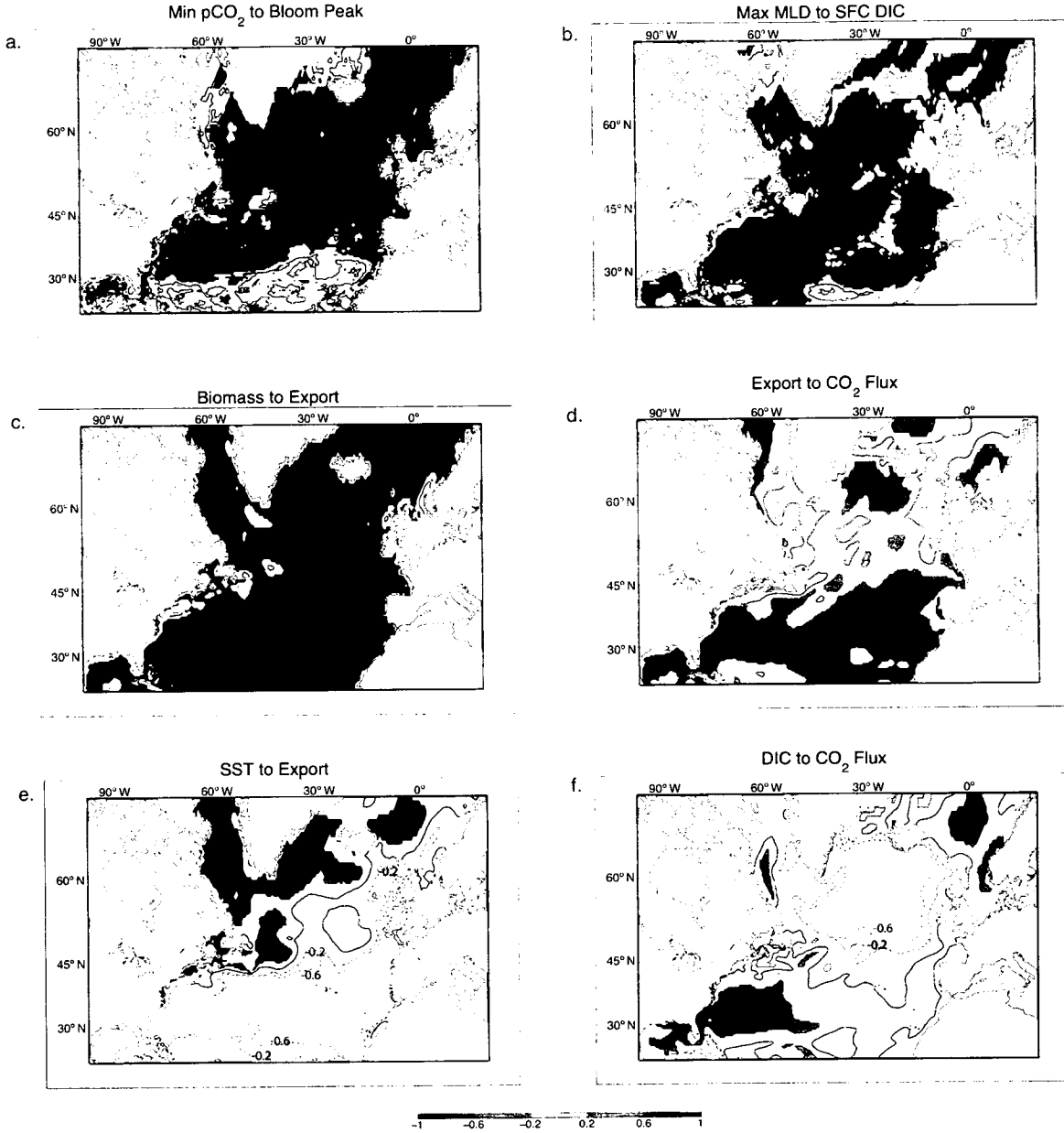
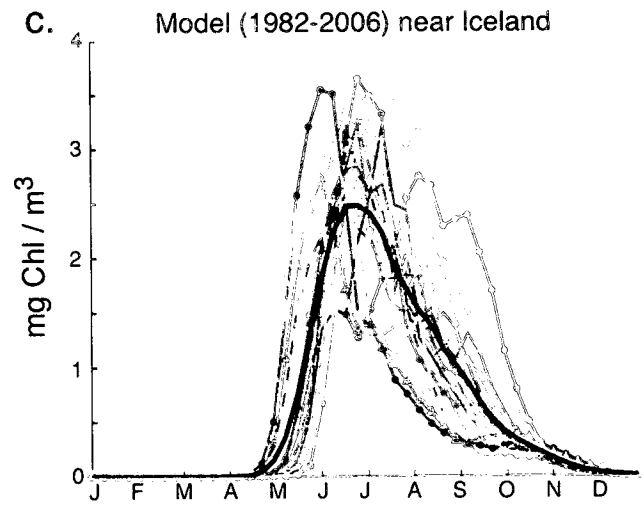
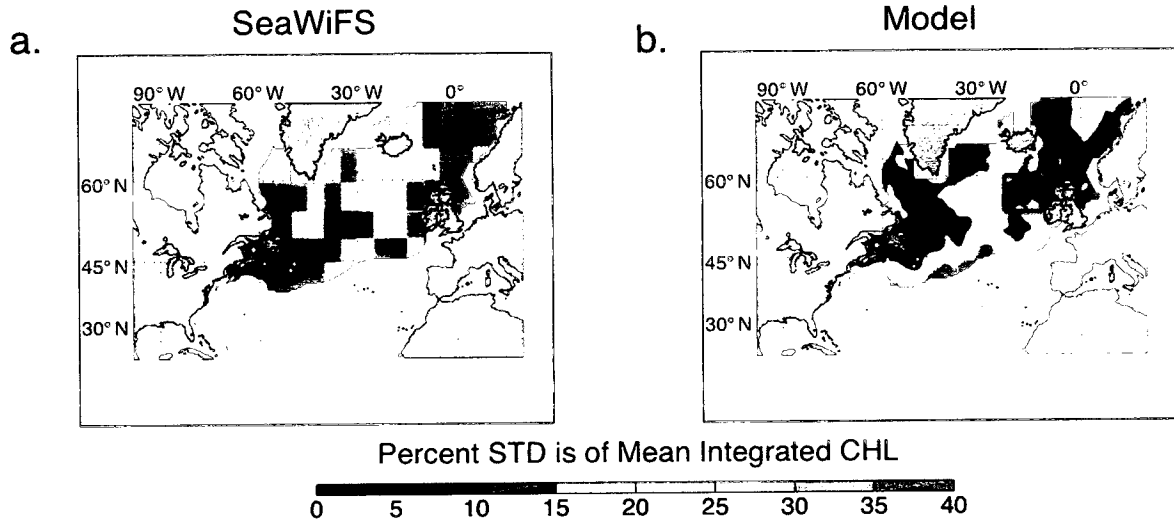


Figure 2-7.



## 2.5 Supplementary Text

The effect of the anomalous biological drawdown of DIC on pCO<sub>2</sub> is estimated offline at daily resolution using model results. We calculate the mean effect of biology on DIC for each day of the year from the 25 years of model diagnostic output. Biology, for this analysis, is considered to be the sum of the drawdown of DIC for photosynthesis and the remineralization of organic matter into DIC. For all 25 years, the daily anomalous effect of biology on DIC ( $BIO_{anom}$ ) is considered to be the total drawdown from model diagnostic output less the 25-year mean (Equation 1). We then estimate the DIC that would be present if biological drawdown of DIC were average for that day (Equation 2). pCO<sub>2</sub> is a function of DIC, so the anomalous biological effect on DIC creates a change in oceanic pCO<sub>2</sub>. The model outputs pCO<sub>2</sub> resulting from total biological drawdown ( $pCO_{2-output}$ ), so we estimate  $pCO_{2-meanbio}$ , the pCO<sub>2</sub> that would have resulted from mean biological drawdown, on a given day. This is done by plugging in  $DIC_{meanbio}$  into the equation for pCO<sub>2</sub> (Equation 3), keeping all other variables unchanged from model output. The difference between model output pCO<sub>2</sub> and  $pCO_{2-meanbio}$  (Equation 4) is the daily effect of anomalous biology on pCO<sub>2</sub> ( $\Delta pCO_{2-anombio}$ ). Anomalous biological drawdown results in a daily average change in pCO<sub>2</sub> of 2 $\mu$ atm.

$$BIO_{anom} = BIO_{output} - \overline{BIO} \quad (S2-1)$$

$$DIC_{meanbio} = DIC_{output} - BIO_{anom} \quad (S2-2)$$

$$pCO_{2-meanbio} = f(DIC_{meanbio}) \quad (S2-3)$$

$$\Delta pCO_{2-anombio} = pCO_{2(output)} - pCO_{2-meanbio} \quad (S2-4)$$

The effect of anomalous mixing on  $p\text{CO}_2$  is quantified using the same technique. The model outputs a diagnostic quantifying how much DIC is supplied to the ocean surface through mixing (MIX). To determine how anomalous mixing affects oceanic  $p\text{CO}_2$ , the equations 1-4 were used with BIO replaced by MIX. Anomalous mixing results in a daily average change in  $p\text{CO}_2$  of the order of  $10\mu\text{atm}$ .

## Supplementary Figure Captions

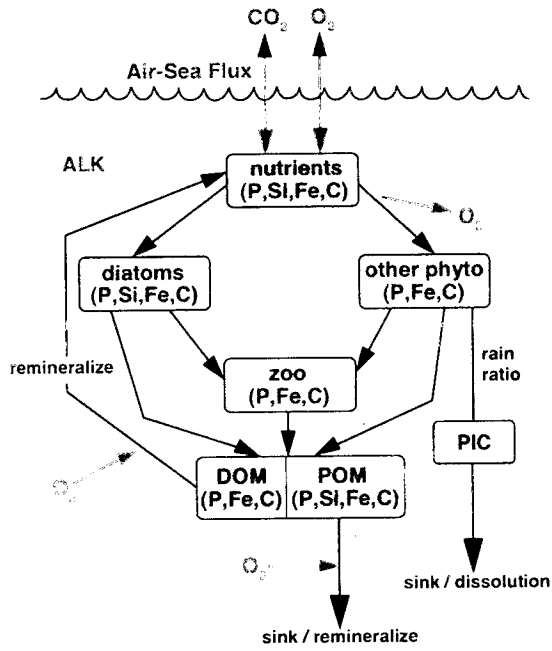
**Supplementary Figure 2-1.** Ecosystem model schematic [Dutkiewicz *et al.*, 2005] showing movement of iron, phosphorus, silicon, and carbon through the nutrient, plankton, particulate, and dissolved matter pools. The figure also shows the ecosystem's contribution to the air-sea exchange of carbon dioxide and oxygen, and the use and production of oxygen within the water column.

**Supplementary Figure 2-2.** Winter (Dec-Apr) (top) and summer (May-Sep) (bottom) average wind speed, root mean square (RMS) of  $p\text{CO}_2$ , and RMS of  $\text{CO}_2$  flux. Winter has significantly faster winds and greater flux variability than summer.

**Supplementary Figure 2-3.** Modeled 25-year mean annual (D-N) export and mean annual (D-N)  $\text{CO}_2$  flux. Positive fluxes are ones into the ocean.

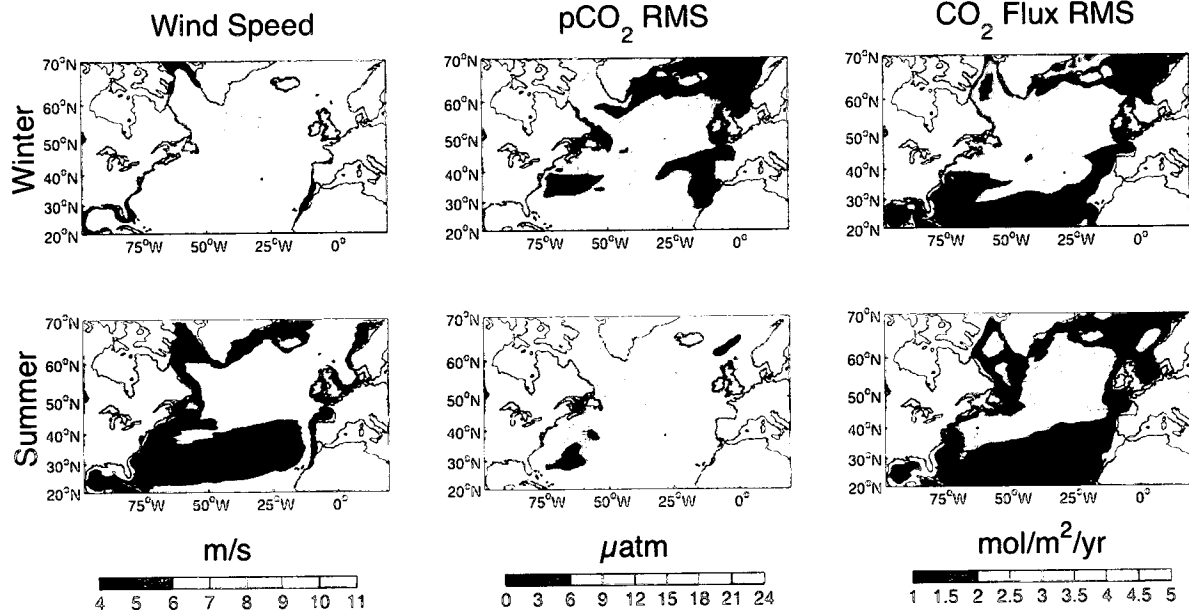
Supplementary Figures

Supplementary Figure 2-1

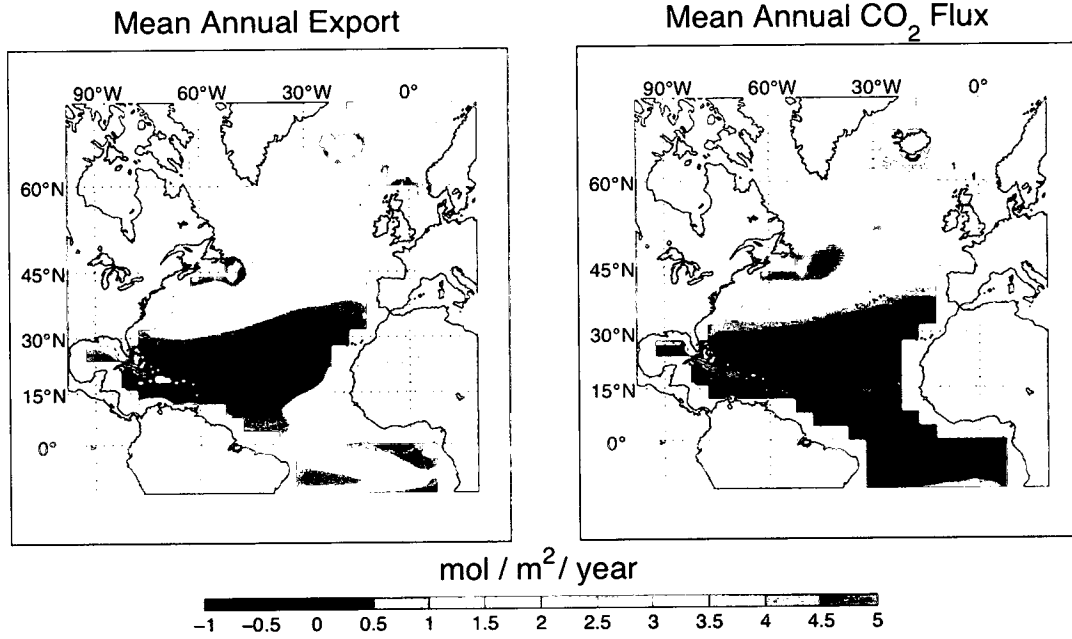




## Supplementary Figure 2-2



Supplementary Figure 2-3



## **Chapter 3.**

### **The General Circulation of Lake Superior:**

#### **Mean, Variability, and Trends from 1979-2006**

This chapter appears in full as Bennington, V., G.A. McKinley, N. Kimura, and C. Wu (in press), The general circulation of Lake Superior: mean, variability, and trends from 1979-2006, *Journal of Geophysical Research–Oceans*. Reproduced by permission of American Geophysical Union.

## Abstract

Previous observations and modeling studies of Lake Superior have only partly elucidated its large-scale circulation, in terms of both the climatological state and interannual variability. We use an eddy resolving, three-dimensional hydrodynamic model to bridge this gap. We simulate Lake Superior circulation and thermal structure from 1979 to 2006 and consider the mechanisms responsible for the flow. Model results are compared to available direct observations of temperature and currents. Circulation in the lake is primarily cyclonic during all seasons, and a two gyre structure is sometimes present. Surface circulation patterns in winter mimic wind directions, but become organized in summer by the presence of thermal gradients. On the annual mean, near-shore currents are controlled by thermal gradients, while offshore flow is primarily determined by the wind. From a uniform bathymetry simulation, we determine that topographic variations cause small-scale structures in the open lake flow and are critical to the development of near shore-offshore temperature gradients. The lake exhibits significant variability in current speed and direction on synoptic timescales, but coherent patterns of interannual variability are not found. Long-term trends due to changing meteorological forcing are found. Model results suggest the increase in lake surface temperature ( $0.37^{\circ}\text{C}/\text{decade}$ ) is significantly correlated to increases in wind speed above the lake ( $0.18\text{ m/s}/\text{decade}$ ), increased current speeds ( $0.37\text{ cm/s}/\text{decade}$ ), and declining ice coverage ( $-886\text{ km}^2/\text{yr}$ ).

### 3.1 Introduction

Understanding of the mean and variability of the large-scale circulation in Lake Superior is of critical importance to environmental problems such as contaminant and invasive species transport, water quality, and ecosystem analysis and prediction. Mixing, circulation, and temperature determine the availability of light and nutrients for primary productivity, and changes in the thermal structure of the lake should alter locations and timing of phytoplankton blooms. Observations of surface lake partial pressure of carbon dioxide ( $p\text{CO}_2$ ) also suggest the carbon cycle cannot be understood without accounting for spatial heterogeneity in the Lake Superior's physical system [Atilla *et al.*, 2010; Urban *et al.*, 2005]. Lakes are subject to the atmospheric conditions and anthropogenic changes of their larger watersheds, and lake ecosystems may respond more rapidly to changes in the climate system than their terrestrial counterparts [Williamson *et al.*, 2009]. Lake Superior is no exception. Its summer heat content is increasing twice as rapidly as regional atmospheric temperatures [Austin and Colman, 2007]. Wind speeds above the lake are also increasing due to a decrease in the lake-atmosphere temperature gradient and are expected to continue to change in warming conditions [Desai *et al.*, 2009].

Lake Superior is the largest lake in the world by surface area and its volume is large enough to hold all of the other Great Lakes combined. The deepest part of the lake exceeds 400 m [Schwab and Seller, 1996], its mean depth is ~150 m, and its water residence time is 178 yrs [Quinn, 1992]. The lake turns over twice yearly, and the entire water column must warm (or cool in winter) to 3.98°C before stratification, because freshwater is densest at 3.98°C. Due to its

northern location and great depth, Lake Superior is the coldest of the Great Lakes and often does not stratify until June near shore and later in the open waters. The lake is completely ice covered about once every ten years [Assel, 2003, 2005], but each year ice forms throughout the near shore zone. The presence of near shore ice and otherwise harsh winters have generally precluded wintertime observations of temperature and currents.

There have been a few observations and modeling studies of the mean circulation and interannual variability of circulation in Lake Superior, but overall the system is poorly understood. Published studies on its circulation are based on data that is restricted in space and/or time. The first map of Lake Superior's summer circulation was put together by *Harrington* [1895] from a bottle drift experiment. He released bottles within the lake and inferred a curved path between the bottle's starting point and where it washed ashore. *Harrington's* [1895] results exhibited a cyclonic flow around the basin during summer with many bottle paths following the bathymetry. The Federal Water Pollution Control Administration (FWPCA) collected current meter data at point locations throughout the lake during 1966 and 1967. These observations are the most recent lake-wide current observations for Lake Superior. *Sloss and Saylor* [1976] analyzed this data and organized the results into monthly maps of currents at the sixteen summer and nine winter locations. *Beletsky et al.* [1999] summarized the analysis of *Sloss and Saylor* [1976] into two maps, one of mean depth-average summer circulation in the lake and one of the mean depth-average winter circulation. Neither map is intended to represent a long-term mean. Large areas of these maps are empty, particularly in winter, because no current observations exist. Intensive current observations were also taken during the Keweenaw Interdisciplinary Transect Experiments (KITES). Spring through fall currents and temperatures were measured

along the Keweenaw Peninsula during the late 1990s using Acoustic Doppler Current Profilers (ADCP). Current measurements from the KITES project have high temporal and depth resolution but are limited in space to three locations within 21 km (8 km for one transect) of the southern shore.

Given the limited long-term, lake-wide observations, numerical models are valuable tools to fill in the gaps of both time and space. Hydrodynamic modeling of Lake Superior began in the 1970s when *Lam* [1978] simulated the lake-wide currents from June through September of 1973 using a 10 km horizontal grid resolution, prescribed model temperatures, and meteorological winds as forcing. The depth-average large-scale flow of *Lam* [1978] largely agrees with the summer map presented in *Beletsky et al.* [1999], suggesting that depth-average summer flow during 1973 was similar to the summer circulation of 1966 and 1967. *Zhu et al.* [2001] and *Chen et al.* [2001] developed a hydrodynamic model to study the development of the currents along the Keweenaw Peninsula and the effects of heat fluxes on the jet intensification. Their model was lake-wide, but the simulations were for summer periods and their analyses focused on currents along the Keweenaw Peninsula. NOAA's Great Lakes Coastal Forecasting System (GLCFS) [*Schwab and Bedford*, 1999] simulates the daily circulation and temperature for each of the Great Lakes, Lake Superior at 10km resolution. The GLCFS is an excellent tool for water quality predictions. Plots of lake surface temperatures, surface currents, temperature transects, temperature profiles, and water levels for the current date are available online at: <http://www.glerl.noaa.gov/res/glcfs/>. It is unknown by these authors if the many years of hydrodynamic modeling done at GLCFS have been done with a single, internally consistent model. The accumulated years of simulated currents have not been analyzed in the literature. Although hydrodynamic models have been

utilized for Lake Superior, studies have not considered the climatological large-scale circulation of the lake or its long-term variability.

In the other Great Lakes, there have been numerical studies that have focused primarily on describing the mean circulation. Lake Michigan's large-scale circulation is best studied. *Beletsky and Schwab* [2008] simulated ten years of lake hydrodynamics in Lake Michigan during 1998-2007 and found a stable cyclonic depth-integrated circulation during both winter and summer. Weak anticyclonic circulations exist in the far northern and southern regions of the lake. *Schwab and Beletsky* [2003] analyzed the generation of vorticity in Lake Michigan and determined that wind stress curl during winter and heat fluxes during summer are primarily responsible for the pattern of large-scale circulation in the lake. Bathymetry also has an impact on current patterns, but its effect is not as important as wind curl or heat fluxes. Recently, models have been developed for other Great Lakes. *Sheng and Rao* [2006] simulated the circulation of Lake Huron for 1974-1975 using a high resolution, nested grid hydrodynamic model and presented monthly mean circulation and thermal structure of the lake during that time. *Schwab et al.* [2009] present simulated summer currents in Lake Erie for 1994, and *Prakash et al.* [2007] used a hydrodynamic model to simulate mean circulation patterns and pollutant transport in Lake Ontario.

In this paper, we simulate the thermal structure and circulation of Lake Superior from 1979 to 2006. This is the longest single Great Lake simulation to date. Modeled temperatures and currents are compared to available observations. Seasonal maps of the climatological circulation are created for surface, depth-average, and below 50 m depths. Variability in depth-average



currents at nine open lake stations is examined and summarized in current rose plots. We address the following questions. What are the climatological patterns of the lake's circulation? How much does the current direction change from year to year? Do winds and heat fluxes control Lake Superior's circulation, as in Lake Michigan, or does the bathymetry have a greater control on flow? How has the lake circulation and thermal structure changed over the last three decades?

The paper is organized as follows. Section 2 includes a description of the hydrodynamic model and a comparison of model results to observations. The climatology of Lake Superior's circulation is presented in Section 3.1, and mechanisms of the lake circulation are examined in Section 3.2. We discuss lake-wide trends in Section 3.3. Discussion and conclusions are presented in Section 4.

## **3.2 Model**

### **3.2.1 Physical Model**

Lake Superior's large volume and long residence time (178 years) [Quinn, 1992] make it an appropriate water body to study with a fixed volume numerical model. We use the MIT general ocean circulation model (MITgcm) [Marshall *et al.*, 1997a, 1997b] configured to the bathymetry of Lake Superior [Schwab and Seller, 1996]. The MITgcm has been used to simulate circulation in water bodies of all sizes [e.g. Dutkiewicz *et al.*, 2005; Doronstkar *et al.*, 2010; Liu *et al.*, 2010; Querin *et al.*, 2006]. The model resolves eddies and has a uniform horizontal resolution of 2 km x 2 km. The model uses a z-coordinate system of 28 vertical layers. The top 50 meters have

finest vertical resolution, with layer thicknesses of 5 meters. Vertical resolution gradually becomes coarser with depth to a thickness of 33.7 meters at 322 meters depth. The model setup uses the hydrostatic approximation. The *Smagorinsky* [1963] horizontal diffusivity scheme and the K Profile Parameterization (KPP) vertical mixing scheme [*Large et al.*, 1994] simulate the effects of sub-grid scale processes.

A bulk formula atmospheric module is used to calculate momentum exchange and heat fluxes between the atmosphere and lake, dependent on atmospheric stability. Model evaporation is a function of local winds, lake surface temperature, and atmospheric humidity. The rate of evaporation is modified by the atmospheric stability. We do not include precipitation in the model. Ice cover data from NOAA [*Assel*, 2003; 2005] is applied as a fractional mask to each grid cell at daily resolution, as done in the oceanographic work of *McKinley et al.*, [2004] and *Dutkiewicz et al.*, [2005]. The presence of ice alters lake albedo and prohibits a fraction of the evaporation, heat, and momentum exchange. This fraction is equal to the fraction of the grid cell that is ice-covered. If a grid cell is 40% ice covered, 60% of the ice-free heat fluxes and momentum exchange is assumed. Temporal increases/decreases in fractional ice coverage create a heat flux to/from the lake. For this purpose, lake ice is assumed to have a constant thickness of 0.25 meters when present.

The model is forced with 3-hourly winds, downward shortwave and longwave radiation at the surface, air temperature, and specific humidity from the North American Regional Reanalysis (NARR) [*Mesinger et al.*, 2006] between 1979 and 2006. This forcing product has a uniform horizontal resolution of 32 km. NARR is the only dynamically consistent, historical, and freely

available public dataset that provides meteorological conditions over all of North America at 3-hourly and 32 km spatial resolution between 1979 and the present (Supplementary Section 1).

The time step of numerical integration is 200 seconds. The physical model is spun up for five years using 1979 forcing before the model is run for 1979-2006. After the first year of the spin up, the next four years are identical, indicating model drift is insignificant. For the entirety of the analysis, summer is June through September (JJAS), to be consistent with the circulation maps presented in *Beletsky et al.* [1999].

### **3.2.2 Model - Observation Comparisons**

To evaluate the model simulation, we utilize the available temperature and current observations throughout the lake.

#### **3.2.2.1 Model-Observation Temperature Comparisons**

The National Data Buoy Center (NDBC) observes surface water and meteorological conditions on Lake Superior between April and November at the three open lake buoy stations shown in Figure 3-1. Buoys 45001, 45004, and 45006 became operable in 1979, 1980, and 1981 respectively. In Figure 3-2, we show model surface temperature at the three buoy locations during 2000 and 2004. Modeled surface temperatures capture both the seasonal cycle and synoptic variability in surface temperatures observed at the three buoys during 2000. In 2000, root mean square error (RMSE) at buoys 45001, 45004, and 45006 are 1.14, 1.14, and 1.54 °C respectively. During 2004, modeled surface temperatures are higher than observed because the model stratifies earlier than in the data. In 2004, the RMSE at buoys 45001, 45004, and 45006 are 2.78, 3.05, and 2.9°C, respectively. The model generally warms too early in spring and does

not cool as rapidly as observed; however, the shapes of the seasonal cycles at the three buoys are consistent with the spatial and temporal heterogeneity seen in the observations. The model captures cooling and warming events on synoptic time scales recorded by the buoys, suggesting the model adequately represents physical processes but has a warm bias. During 2004, temperatures during August and September were below the 28-year mean of 12.1, 12, and 14.3°C at buoys 45001, 45004, and 45006, respectively. The summer of 2000 was warmer than average.

For the entire 28-year period, model RMSE at buoys 45001, 45004, and 45006 are 3.2, 3.0, and 3.4°C. During years with above average temperatures during August and September (warm years), model RMSE are 2.7, 2.4, and 3.1°C; RMSE during colder years (August and September temperatures below mean) are 3.7, 3.7, and 3.8°C. Although modeled temperatures are generally warmer than observed at the buoys, interannual variability in modeled summer temperatures at the buoys are highly correlated with observations ( $r^2=0.73$ ). The RMSE for all years at the buoy locations is provided in Supplementary Table 1, and summer average temperatures at buoy locations in the model and data are shown in Supplementary Figure 3-1.

The Environmental Protection Agency (EPA) has been sampling the physical and chemical characteristics at ~8 depths within the water column at nineteen open lake stations in Lake Superior (Figure 3-1) twice each year since 1992, usually in April and August. The sampling depths are not consistent from year to year or between stations, so we compare model temperatures to EPA observations (Figure 3-3) at the EPA depths closest to two depths (surface, below 75m) in April and at three depths (10m, 20m, below 75m) in summer, using all available

years on GLENDA, the EPA's searchable data archive website:

([http://www.epa.gov/glnpo/monitoring/data\\_proj/glenda/glenda\\_query\\_index.html](http://www.epa.gov/glnpo/monitoring/data_proj/glenda/glenda_query_index.html)).

During April, the model overestimates surface temperatures with a root mean square error (RMSE) of 1.06°C at the surface and 0.77°C below 75m. Station to station and year-to-year variability in modeled temperatures correlate to observations with  $r^2=0.6$  at the surface and  $r^2=0.42$  and below 75 m in April. The model is better able to capture observations above 2°C, so the scatter plot is overall flatter than the one-to-one reference line. Modeled lake surface temperatures are warmer than observations during summer (RMSE=3.2°C), but the model captures the spatial and interannual variability present in EPA observations with an  $r^2=0.83$ . The modeled thermocline is not as sharp as observed, thus modeled temperatures are too warm within the thermocline at 20 m (RMSE=5.1°C). Water in the hypolimnion (below 75 m) is captured well in the model, with a RMSE of 0.3°C and  $r^2$  of 0.97. The model warm bias may be partially explained by a warm bias in the 10 m air temperature forcing described below. Even with the known bias, the model captures observed variability, with colder observed years being colder modeled years, just not as cold as observed.

### **3.2.2.2 Warm Bias in NARR Forcing**

The North American Regional Reanalysis Project is a long-term, 32 km horizontal resolution climate product for the North American region. Air temperatures above Lake Superior have a warm bias in NARR. When compared to air temperatures observed at the NDBC buoy locations, NARR forcing has a RMSE of 2.4°C during April. NARR 10m air temperatures at the NDBC buoy locations on Lake Superior have large RMSE (4-7°C) and a warm bias during May through

July (Supplementary Figure 3-2). NARR air temperatures above the lake are biased warm except during the warmest years.

To determine atmospheric conditions above the Great Lakes, the North American Regional Reanalysis Project sets lake surface temperatures to a spatially heterogeneous climatology of its seasonal cycle (personal communication F. Mesinger, D. Schwab, 2009). Interannual variability in observed lake surface temperatures are not utilized. Once lake temperature reaches 3.98°C, the lake stratifies and surface temperatures rapidly increase. Due to averaging, the climatology of lake surface temperatures is significantly warmer than observed during the spring and early summer of the cooler years; thus, boundary conditions for the atmospheric product are too warm during cooler years. A lake that is warmer than observed will cause air temperature above the lake to be warmer than observed in the atmospheric product. The warmer waters may also decrease the atmospheric stability above the lake in spring, when lake temperatures are cooler than air above the lake. Boundary layer parameterizations in the NARR atmospheric model may also cause spring and summer air temperatures to be too warm.

The warm bias in NARR air temperatures causes the model to be too warm in spring and summer. The larger summer heat content means that the heat loss from the lake during winter must be greater than observed for the lake to cool to observed temperatures. This effect and the lack of an explicit lake-ice model contribute to model error during April. If the model does not cool to zero degrees in all years before the ice mask is applied, the presence of ice impedes lake cooling and traps some heat over winter. This can modify local surface temperatures by up to one degree during spring.

Although the product has a known warm bias, winds in NARR are similar to winds in an alternative forcing, interpolated from meteorological observations (not shown). NARR winds produce currents in agreement with observations (Section 2.2.3) and result in the same large-scale circulation as when using the alternative forcing. The trend in wind speed above Lake Superior (0.18 m/s/decade) is comparable to buoy and satellite observations (0.51 m/s 1985-2008 [Desai *et al.*, 2009]). The trend in atmospheric temperatures above the lake is also present in the NARR product. Thus, model results will be warmer than observations but are responding to realistic changes in atmospheric conditions.

### 3.2.2.3 Model-Observation Current Comparisons

No lake-wide multi-year current observations exist in Lake Superior. Modeled surface circulation during summer is qualitatively similar to the lake-wide circulation deduced by *Harrington's* [1895] bottle drifter experiment. Lake-wide depth-average currents were observed by the FWPCA during the late 1960s. We determine the speed and direction of depth-average flow at nine locations around the lake, consistent with current observation locations depicted in *Sloss and Saylor* [1976]. We average to 150 m, because FWPCA instrumentation did not exceed this depth. Figure 3-4 depicts the daily speed and direction of depth-average flow at the nine stations during summers of 1979-2006. Subplots A through I correspond to the locations shown in Figure 3-1. Daily depth-average current direction and speed are depicted in the current roses for each location A-I. Bar direction indicates direction *toward* which current flows. Length of bar indicates percentage of summer days (1979-2006) that daily average flow is in that direction. Color of bar indicates speed of flow. Flow in one direction may have many colors, indicating percentage of days that daily average flow was both in that direction *and* with that speed.

Separate arrow indicates direction *toward* which current flow was observed by the FWPCA, as summarized by *Beletsky et al.* [1999]. Color and number at end of arrow indicate mean speed of the observed flows [*Sloss and Saylor, 1976*]. Due to instrumentation failures, FWPCA data does not span the entire depth and season at all nine selected locations. Exact latitude and longitude coordinates are also not available for the direct observations, so we selected the model grid cell of the observations by matching the bathymetry to published figures in *Sloss and Saylor* [1976].

We first note that modeled flows are generally in good agreement with current speed and direction observed by the FWPCA in summer. At locations A, B, C, E, F, and H, modeled currents are in the same direction as observed. At location D, modeled current direction is highly variable and mean observed flow suggests currents toward the northwest. At location G, the model shows a bimodal distribution of direction, and so only agrees with the observed mean for about half of the days of summer. Just east of Isle Royale, at location I, simulated currents are generally more southward than those observed. Modeled flows are highly variable, and only at locations A and C are daily-average currents consistently in one direction for more than 20% of the summer. When considering both direction and speed, less than 5% of summer days have the same direction ( $\pm 5^\circ$ ) and speed ( $\pm 0.5$  cm/s) at every location except C (<10% of summer days at C).

Current observations with high temporal resolution are only available near shore during the late 1990s. In spring through winter of 1998 and 1999 during the Keweenaw Interdisciplinary Transport Experiments (KITES), Acoustic Doppler Current Profilers (ADCP) were stationed offshore along the Keweenaw Peninsula (Figures 1,5). The instruments recorded zonal and



meridional velocities and temperature throughout the water column. In Figure 3-5, we compare modeled and observed current velocities and temperature through the water column at station H3 from May to December 1998. The model is able to capture the seasonal cycle of temperature, cooling events, and the magnitude and direction of horizontal velocities unique to the station. The model is able to replicate the observed spatial and temporal heterogeneity, and captures temperature and velocity patterns. Modeled currents rapidly change from baroclinic to barotropic (and back) and are able to completely reverse direction on daily time scales as observed, capturing the transient nature of local flow in Lake Superior. It is also able to capture station-to-station and year-to-year variations (Supplementary Figures 3,4). The model over predicts maximum summer surface temperatures and begins to stratify prematurely in spring, consistent with NARR's warm bias (Section 2.2.2). Heat also penetrates deeper in the model than in the data because the thermocline is too deep, in part due to lack of colored dissolved material in the model, which has been found to increase the attenuation of light within the water column in the global ocean [Anderson *et al.*, 2007].

In summary, although the model has a warm bias due to a biased meteorological forcing product, the model captures the spatial and temporal (daily, seasonal, and interannual) variability in the thermal structure and circulation seen in observations. Warming and cooling events driven by the passing weather systems occur in the correct locations and at the correct time, as seen in the buoy measurements of lake surface temperature. The model is unable to capture the coldest temperatures during the coldest years but replicates warmer years well, and modeled surface temperatures correlate well with EPA observations ( $r^2=0.83$ ) and lake surface temperatures at the open lake buoys ( $r^2=0.73$ ). Under influence of a warming climate, as experienced between 1979

and 2006, trends in temperature should be dampened in our results given the enhanced warm bias during cold years. However, the trend in NARR wind speed above the lake (0.18 m/s/decade) is comparable to observations (0.51 m/s 1985-2008, [Desai *et al.*, 2009]). Thus, the model should capture trends in thermal structure and circulation due to this increase. The directions and magnitudes of daily and seasonal observed currents are captured by the model, and we believe the model is an adequate tool to analyze the circulation and long term changes in lake thermal structure.

### **3.3 Results**

#### **3.3.1 General Circulation**

Figure 3-6 shows model results for the general circulation averaged over 1979-2006 during winter (DJFM) and summer (JJAS) in the top 15 m, below 50 m, and throughout the entire water column. Colors depict the average water temperature within the same columns. Supplementary Animation 1 provides daily resolution of temperature and currents for these three layers.

During winter, winds are primarily from the north, and horizontal gradients in water temperature are small. Temperature increases with depth to just under four degrees below 50 m. The water column can stratify, with coldest water at the surface, but currents are primarily barotropic during winter, indicated by the similarity of surface currents to those at depth. Currents are southward in the western arm of the lake. There is a return flow toward the northeast along the Keweenaw Peninsula. A temperature gradient exists from near to offshore along the peninsula

with colder waters near shore. This alone would support a flow toward the southwest if the resulting pressure gradient force was balanced by the Coriolis force (thermal wind). Thus, the northeast flow indicates dominance by the wind. Some northward flow exists in the eastern and central parts of the lake during winter, where there are two rough cyclonic cells just east and north of the Keweenaw Peninsula. When the model is run at coarser (10km) horizontal resolution, the circulation pattern is smoothed and the gyres can be more easily viewed by the reader (Figure 3-7).

During summer, there are significant near to offshore temperature gradients and winds from the southwest (Figure 3-6). Warmer waters are along the coastlines, since shallower water heats more rapidly. We choose to separate the flow above 15 m and below 50 m so that flow in the variable depth of the thermocline zone does not confuse the interpretation. In contrast to winter surface circulation, summer flows above 15 m do not mimic winds. The circulation is largely cyclonic, i.e. the flow pattern is counterclockwise along the eastern coastlines. Flow diverges when it reaches Isle Royale, and there is a southward flow to the Keweenaw Peninsula. The flow east of Isle Royale may be viewed as a single cyclonic surface gyre. The western arm is warmer than the eastern arm. Circulation is still primarily counterclockwise along the coastlines, but the southwestern-most region of the lake, by the mouth of the St. Louis River, is anticyclonic. Summer circulation is baroclinic, and small-scale structures are omnipresent below the thermocline. Two cyclonic cells follow along the isobaths. A cell exists just east of the Keweenaw Peninsula, and a second, smaller, cell exists north of the Keweenaw Peninsula and east of Isle Royale. Summer depth-average flows are strong and counterclockwise along the

coastlines. Flow is cyclonic everywhere except in the far southwestern arm, and there is weaker flow along the 200 m isobaths within the two cyclonic gyres.

### ***Current Speed***

Lake-wide mean current speeds peak in October and November (2.8 cm/s) and decay over winter, reaching a minimum during late May (0.7 cm/s). Current speeds are relatively constant between March and May. Although wind speeds are greatest in winter, thermal gradients within the lake decrease and increased ice coverage decreases the transfer of momentum to the lake. The annual average of lake-wide depth-average current speed is 1.5 cm/s. Fast coastal currents begin to develop in June after slowing throughout winter and spring, and coastal currents reach maximum mean velocities of over 5 cm/s during October and November (>15 cm/s in top 15 m). Open-lake current speeds are weakest during May and June and strongest in October and November (2.5 cm/s), when an ice-free lake begins to experience increasing winds. Offshore flows remain above 2 cm/s until January, when they begin to significantly slow because of ice coverage. (Supplementary Figure 3-5). Surface velocities (top 15 m) show the same seasonal cycle and structure as depth-average velocities throughout the lake, but reach a maximum lake-wide speed of 7.4 cm/s in October and weakest velocities (2-3 cm/s) from March through May.

### ***Variability***

In Figure 3-4, we depict direction and speed of summer currents for all years on a single plot. Selecting any individual year during the model simulation results in current roses with nearly identical distributions of current direction at all nine locations; thus interannual variability in

summer depth-average currents appears to be minimal. However, variability on daily and synoptic time scales is significant, as all current roses exhibit spread in current speed and direction. These distributions are also robust to alternative choices of “summer” months. Daily variability of currents is therefore more significant than interannual variability, and when considering speed, each location can be understood as having a probability distribution function of currents during summer.

We conclude that the mean current direction depicted in *Beletsky et al.* [1999] are generally representative of the flow for nearly all days of summer at locations A, B, F, and H. Current directions at locations C, D, E, and G are best understood as probability distributions. While flow at location C is most often toward the northeast, twenty percent of the time currents are weaker and toward the southwest. Here, flows may enter the cyclonic cell when going toward the northeast. Near the eastern part of the same cell, depth-average currents at location D are best described as weak and frequently westward. Significant spread in direction near Sault Saint Marie at location E is also present. In the far western arm, at location G, currents are bimodal and stronger than averaging observations would suggest. Flows are toward the southwest just as often as toward the northeast, so mean currents only tell part of the story. Even currents along the Keweenaw Peninsula (location A) can weakly reverse direction when winds are able to overcome the temperature gradient [*Zhu et al.*, 2001].

### 3.3.2 Current Mechanisms

What controls the current speed and direction? In Lake Michigan, *Schwab and Beletsky* [2003] find that lake-wide vorticity is primarily generated by vorticity in wind stress during winter and

baroclinic effects during summer. Vorticity generated by the bottom topography is a second order effect. Are the mechanisms similar in Lake Superior?

For wind-driven currents we expect that transport within the Ekman layer to be 90° from wind stress. For thermally driven flows, we expect currents to be geostrophic and thus along isotherms, with colder water to the left. To determine how much thermal gradients contribute to both the direction and speed of currents, we correlate daily anomalies of local temperature gradients in the zonal direction with daily anomalies in current speed in the meridional direction ( $r_{mt}$ ). We correlate daily anomalies of the local temperature gradient in the meridional direction with daily anomalies in the current speed in the zonal direction ( $r_{zt}$ ). We present the spatial distribution of the geometric mean ( $r_g$ ) of these correlations (Equation 3-1) in the top of Figure 3-8.

$$r_g = \sqrt{|r_{zt} \times r_{mt}|} \quad \text{Equation (3-1)}$$

A geometric mean of 1 indicates a perfect correlation of wind stress anomalies and currents in both zonal and meridional directions. Correlations between temperature gradients and currents may be underestimated due to the use of local temperature gradients.

Similarly, we would like to know how significant an effect wind stress has on local currents. We compute the geometric mean of correlations between daily anomalies in wind stress in the zonal direction with daily current anomalies in the meridional direction and correlations between daily anomalies in wind stress in the meridional direction with daily current anomalies in the zonal

direction. The resulting geometric mean of these correlations is shown in the bottom of Figure 3-8. We integrate to 25 m, because the Ekman depth is dependent on the eddy flux of momentum and varies in both time and space. Integrating to 50 m does not significantly alter the results or conclusions.

Figure 3-8 clearly shows that near surface flows in the open lake and immediately onshore are significantly correlated with the wind stress, but currents within the coastal jets are steered along isotherms and are faster flowing when temperature gradients increase. A change in winds is accompanied by a change in surface flows during the same day in the open lake and within a couple kilometers of the shore. Similarly, if a temperature gradient from near to offshore is observed, the pattern and speed of the coastal jets may be inferred. We show summer correlations, because they are strongest, but annual correlations show the same pattern. The correlations were computed for lags up to one week, but correlations were strongest for both wind and temperature gradients with a lag of zero. Thus, changes in wind or temperature gradient translate into a change in surface currents on the same day.

We cannot decompose depth-average flows in the same manner, since we do not expect a change in winds to result in currents to change at a  $90^\circ$  angle below the Ekman Layer. However, the pattern is identical when we correlate daily anomalies in wind speed and depth-average current speeds and the magnitude of the thermal gradient and depth-average current speeds. Winds are the dominant current mechanism in the open lake and immediately onshore, and temperature gradients control flows near shore. This finding is consistent with sensitivity studies in a model of 10 km horizontal resolution, in which the model is run without wind, without heat fluxes

(barotropic), and with a spatially-averaged wind field (no curl). (Supplementary Section 2, Supplementary Figure 3-6). Thus, wind is a first order control of circulation patterns all year, but temperature gradients in summer are the first order control of near-coastal flows.

Although it is apparent winds are important to the circulation pattern, the cyclonic gyres are also coincident with lake bottom topography. We would like to know if the wind-induced pattern would differ without the topographic gradients. To consider this effect, we run the model with a uniform, flat bathymetry of the mean lake depth, such that lake volume is the same as in real-bathymetry simulations. Lake coastlines remain unchanged. In Figure 3-9, we present monthly average flows and vorticity for January and June of 2006 from the flat bottom and realistic topography runs. Bathymetry significantly changes the horizontal temperature structure of the lake. Shallower water near shore cools to lower temperatures during winter and heats more rapidly during spring and summer. While temperature gradients control lake flow patterns near the coast in summer, these temperature gradients are primarily created by variations in lake bathymetry. In the open lake, wind is the largest driver of lake flow patterns and speeds. However, bathymetry creates small-scale structures in the open lake flow pattern as a result of a barotropic response to changes in depth, and local currents are not homogeneous as in the uniform bathymetry model run. The large gyre that encompasses the central and eastern basin in the uniform bathymetry run is split into two cyclonic gyres by the presence of bottom topography (Figure 3-9). In summary, winds are an important mechanism to circulation patterns year round, and baroclinic effects alter nearshore currents during summer. Topographic gradients enhance horizontal temperature gradients during summer, split a single cyclonic gyre into two cyclonic gyres, and create small-scale structures in local flows throughout the year.



### 3.3.3 Trends

Figure 3-10 shows annual average modeled depth-average temperature (analogous to heat content from zero degrees), surface temperature, depth-average and surface current speeds, and modeled summer mixed layer depths. The Figure 3-also shows model forcing of air temperature, ice cover, and wind speed (10 m) over the lake during the same period. Slopes of trend lines and their p-values are presented in Table 1. Modeled annual average depth-average temperature increased from 5.2°C (mean 1979-2003) to 5.5°C (mean 2002-2006). Lake surface temperatures increased from 7.4 to 8.1°C, forced by an increase in annual atmospheric temperature above the lake of 3.7 to 5.7°C. Modeled temperature trends likely underestimate realistic trends, given the warm bias in the forcing that causes the model to fail to capture the coldest observed temperatures but capture temperatures during the warmest years.

As above-lake air temperatures have increased [*Austin and Colman, 2007*], so have observed wind speeds above the open lake [*Desai et al., 2009*]. Wind speeds increased from 4.9 (1979-1983) to 5.5 m/s (2002-2006) in the NARR forcing over the 28-year period, a rate comparable to observations. The increase in wind speed and lake surface temperature drives an increase in the wind stress on the lake, resulting in increased current speeds. Surface current speeds (15m) increased from 4.1 to 5.2 m/s. Mixed layer depths are determined by surface heating and turbulent mixing, often driven by the winds. The increase in lake temperatures could result in a shallowing of the thermocline, but an increase in wind stress should work to deepen the mixed layer. These two drivers appear to work against each other during the 28-year period; although wind speed is increasing over the lake, so is lake surface temperature, and the modeled result is no statistically significant trend in mixed layer depth.

Decreases in ice cover are significantly correlated to increases in air temperature ( $r^2 = 0.52$ ) and modeled evaporation ( $r^2 = 0.55$ ) (Table 2). Lake ice coverage is decreasing by 886 km<sup>2</sup>/yr, but evaporation has no significant trend. Increases in wind speed also appear to contribute to increases in evaporation ( $r^2 = 0.30$ ).

### 3.4 Discussion and Conclusions

In this study, we use an eddy-resolving model to simulate and analyze the circulation of Lake Superior for 1979-2006. We find that summer surface circulation is highly organized with strong counterclockwise flows around the coastlines. This pattern is in agreement with the first map of Lake Superior circulation created by *Harrington* [1895] after a bottle drifter experiment. Flows are baroclinic during summer, and open-lake subsurface flows follow along the isobaths, causing depth-average currents to consist of two cyclonic cells, strong coastal currents, and weak anticyclonic rotation near the St. Louis River. Circulation during winter is more barotropic, and depth-average flows consist of two rough cyclonic cells in the central and eastern basin and weaker coastal currents.

By correlating anomalies in wind stress to anomalies in lake currents, we show that winter lake-wide circulation is primarily controlled by wind. Temperature gradients control currents near shore in summer, while changes in open lake currents are wind-driven all year. It has long been conjectured why medium to large-sized lakes are consistently cyclonic. This study agrees with the findings in Lake Michigan of *Schwab and Beletsky* [2003] that curl in the wind stress field is

the dominant source of lake-wide positive vorticity. Lake Superior is warmer than the surrounding land during winter, causing a mesoscale low pressure system over the lake [Petterssen and Calabrese, 1959], which creates positive vorticity in the wind stress and promotes the cyclonic lake circulation. Due to the effect of lake surface temperatures on atmospheric stability and the presence of horizontal temperature gradients in the lake, even a spatially uniform wind field exerts wind stress with positive vorticity during summer. This effect, proposed by *Emery and Csanady* [1973], enhances thermally driven currents and captures the pattern of lake-wide circulation, but not speed (Supplementary Section 2 and Supplementary Figure 3-6). The winter pattern of the circulation cannot be generated without spatially heterogeneous winds.

From a uniform bathymetry run, we determine that lake bathymetry causes significant near to offshore temperature gradients that drive coastal currents during summer. Lake topography creates local heterogeneities in flow and confuses the depth-average large-scale circulation pattern year-round. East of Isle Royal, lake topography divides the single cyclonic gyre of the uniform bathymetry simulation into two, more complex cyclonic cells. While side-by-side gyres have been observed in Lake Ontario [*Pickett and Richards*, 1975] and many small lakes, the gyres were wind-driven and counter-rotating, not both cyclonic. Such counter-rotating cells are sometimes present in the southwestern arm of Lake Superior. Both cells in central and eastern Lake Superior are cyclonic and are the result of a single cyclonic gyre divided by the spatially variable topography.

We have shown that depth-average currents vary significantly within the summer season in both direction and speed, but that year-to-year changes in circulation at nine locations throughout the lake are minimal. *Waples and Klump* [2002] determined that wind directions have shifted over all of the Great Lakes except for Superior, so the lack of significant year-to-year variability during the modeled time period may not hold true in other Great Lakes. Still, Lake Superior is undergoing significant changes. Due to an increase in above-lake temperature, modeled annual lake surface temperatures increase 1°C during the 28-year simulation, despite a known underestimate due to warm biases in the model forcing that are pronounced during cold years. *Austin and Colman* [2007] analyzed spring through summer buoy temperatures and determined that Lake Superior surface temperatures during this time of year are warming ( $1.21 \pm 0.68$  °C decade<sup>-1</sup>), twice as rapidly as regional air temperatures. For the lake to freeze, the entire water column must first cool to 3.98°C, and then the surface layer may begin to cool. Strong winter winds often make this surface layer very deep. Winter air temperatures determine lake ice coverage and spring lake heat content. A warmer winter leads to a larger spring heat content and an earlier onset of stratification, because less heat needs to be added to warm the entire water column to 3.98°C. This earlier onset of stratification leads to warmer lake surface temperatures throughout summer, causing a significant correlation between winter ice coverage and summer surface temperatures. Our findings are in agreement with *Austin and Colman* [2007].

While *Hanrahan et al.* [2010] find an increasing trend in evaporation from GLERL modeling results in Lake Michigan and Lake Huron beginning in the 1980s, we do not find a statistically significant increase in evaporation in Lake Superior. The model indicates that ice cover is the dominant mechanism controlling annual evaporation. Lake surface temperatures and wind

speeds are also increasing above the lake, but these changes are not large enough to cause a significant change in annual evaporation during this period.

*Desai et al.*, [2009] utilize observations and an atmospheric boundary layer model to show that wind speeds above Lake Superior increased during the model time period. They attribute this increase to the reduced air-lake surface temperature gradient observed by *Austin and Colman* [2007] that reduces atmospheric stability above the lake. The model responds to the increase in above-lake wind speeds, causing an increase in modeled current speed. While an increase in wind speed alone would cool lake surface temperatures, [*Huang et al.*, 2010], here, consistent with observations, the increasing air temperature dominates. If the air-surface lake temperature gradient continues to decrease due to anthropogenic climate warming in the coming decades, we expect an increase in above lake wind speed, faster lake currents, and a decreased lake mixing time. These changes could spread pollutants and invasive species (mussels) more rapidly around the lake. Increased lake temperatures may also allow sea lampreys to begin feeding earlier in spring and thus to grow larger and more deadly to host fish [*Kitchell and Breck*, 1980] and may require updated management techniques. Increased and systematic year-round monitoring of lake thermal structure throughout the lake began in 2009 by investigators at the University of Minnesota-Duluth and the Large Lakes Observatory (J. Austin, personal communication) and will increase our understanding of the current, and likely future, physical state of the lake. These data and further numerical simulations can shed light on Lake Superior's physical and ecological response to climate change.

## **Acknowledgments**

The authors would like to thank NSF for funding (NSF OCE 0628560) and David Schwab at GLERL for providing meteorological observations over the lake for the five years (1997-2001) of alternative forcing. Noel Urban at Michigan Technological University graciously provided ADCP data from the KITES experiment for model evaluation. The authors also acknowledge Dierk Polzin at the University of Wisconsin-Madison for help with figures and two anonymous reviewers for their insightful comments. North American Regional Reanalysis data provided by NOAA/NESDIS/NCDC, Ashville, NC, from their website at <http://nomads.ncdc.noaa.gov/>.

## References

- Anderson, W.G., Gnanadesikan, A., Hallberg, R.W., Dunne, J.P., and B.L. Samuels (2007), Impact of ocean color on the maintenance of the Pacific Cold Tongue, *Geophysical Research Letters*, *34*, L11609, doi:10.1029/2007GL03011.
- Assel, R.A. (2003), *An Electronic Atlas of Great Lakes Ice Cover: NOAA Great Lakes Ice Atlas*, Great Lakes Environ. Res. Lab., Ann Arbor, Michigan. (<http://www.glerl.noaa.gov/data/ice/atlas/>)
- Assel, R.A. (2005), Classification of annual Great Lakes ice cycles: Winters of 1973-2002, *J. Climate*, *18*(22), 4895-4905.
- Atilla, N., G.A. McKinley, V. Bennington, M. Baehr, N. Urban, M. DeGrandpre, A. Desai, and C. Wu, Observed Variability of Lake Superior  $p\text{CO}_2$ , submitted to *Limnology and Oceanography*.
- Austin, J.A. and S.M. Colman (2007), Lake Superior summer water temperatures are increasing more rapidly than regional air temperatures: A positive ice-albedo feedback, *Geophys. Res. Lett.*, *34*(6), L06604, doi: 10.1029/2006GL029021.
- Chen, C.S., J.R. Zhu, E. Ralph, S.A. Green, J.W. Budd, and F.Y. Zhang (2001), Prognostic modeling studies of the Keweenaw current in Lake Superior. Part I: Formation and evolution, *J. Phys. Oceanog.*, *31*(2), 379-395.
- Beletsky, D., J.H. Saylor, and D.J. Schwab (1999), Mean Circulation in the Great Lakes, *J. Great Lakes Res.*, *25*(1), 78-93.
- Beletsky, D. and D. Schwab (2008), Climatological circulation in Lake Michigan, *Geophys Res Lett*, *35*, L21604, doi:10.1029/2008GL035773.
- Desai, A.R., J.A. Austin, V. Bennington, and G.A. McKinley (2009), Stronger winds over a large lake in response to weakening air-to-lake temperature gradient, *Nature Geoscience*, *2*(12), 855-858.
- Dorostkar, A., L. Boegman, P.J. Diamessis, and A. Pollard (2010), Comparison of hydrostatic and non-hydrostatic modeling of internal wave fields in Cayuga Lake, presented at the 53<sup>rd</sup> International Association of Great Lakes Research Conference, Toronto, ON.
- Dutkiewicz, S., M. Follows, and P. Parekh (2005), Interactions of the iron and phosphorus cycles: a three-dimensional model study. *Global Biogeochemical Cycles*, *19*, GB1021, doi:10.1029/2004GB002342
- Emery, K. O., and G.T. Csanady (1973) Surface circulation of lakes and nearly locked seas. *Proc. Natl. Acad. Sci. U.S.A.* 70:93-97.
- Hanrahan, J.L., S.V. Kravtsov, and P.J. Roebber (2010), Connecting past and present climate variability to water levels of Lakes Michigan and Huron, *Geophys. Res. Lett.*, *37*, L01701, doi:10.1029/2009GL041707.
- Harrington, M.W. (1895) Surface currents of the Great Lakes. *Weather Bureau Bulletin*, U.S. Department of Agriculture.
- Kitchell, J.F. and J.E. Breck (1980), Bioenergetics Model and Foraging Hypothesis for Sea Lamprey (*Petromyzon marinus*), *Can. J. Fish. Aquat. Sci.* *37*(11): 2159-2168, doi:10.1139/f80-258.
- Lam, D. C. (1978), Simulation of water circulations and chloride transports in Lake Superior for summer 1973, *J. Great Lakes Res.*, *4*, 343-349.

- Large, W. G., J. C. McWilliams, and S. C. Doney, (1994), Oceanic vertical mixing: a review and a model with a nonlocal boundary layer parameterization. *Rev. Geophys.*, *32*, 363-403.
- Liu, W. and K.G. Lamb (2010), Internal Kelvin Waves in Lake Erie, presented at the 53<sup>rd</sup> International Association of Great Lakes Research Conference, Toronto, ON.
- Marshall, J., A. Adcroft, C. Hill, L. Perelman, and C. Heisey (1997a), A finite volume, incompressible Navier-Stokes model for studies of the ocean on parallel computers, *J. Geophys. Res.*, *102*, 5753-5766.
- Marshall, J., C. Hill, L. Perelman, and A. Adcroft (1997b), Hydrostatic, quasi-hydrostatic, and nonhydrostatic ocean modeling, *J. Geophys. Res.*, *102*, 5733-5752.
- McKinley, G.A., M. J. Follows, and J. Marshall (2004) Mechanisms of CO<sub>2</sub> air-sea flux variability in the Equatorial Pacific and North Atlantic with implications for atmospheric inversions, *Global Biogeochem. Cycles* *18*, GB2011, doi:10.1029/2003GB002179.
- Mesinger, F., G. DiMego, E. Kalnay, K. Mitchell, P.C. Shafran, W. Ebisuzaki, D. Jovic, J. Woollen, E. Rogers, E.H. Berbery, M.B. Ek, Y. Fan, R. Grumbine, W.Higgins,
- H. Li, Y. Lin, G. Manikin, D. Parrish, and W. Shu (2006), North American regional reanalysis, *Bull. of the Amer. Met. Soci.*, *87*(3), doi: 10.1175/BAMS-87-3-343.
- Querin, S., A. Crise, D. Deponte, and C. Solidoro (2006), Numerical study of the role of wind forcing and freshwater buoyancy input on the circulation in a shallow embayment (Gulf of Trieste, Northern Adriatic Sea), *J. Geophys. Res.*, *111*, C03S16, doi:10.1029/2006JC00361.
- Quinn, F.H. (1992), Hydraulic residence times of the Laurentian Great Lakes, *J. Great Lakes Res.*, *18*(1), 22-28.
- Petterssen, S., and P.A. Calabrese (1959), On some weather influences to warming of the air by the Great Lakes in winter, *J. Meteor.*, *16*, 646-652.
- Pickett R.L., and F.P. Richards (1975), Lake Ontario mean temperatures and mean currents in July 1972, *J. Phys. Oceanogr.*, *5*, 775-781.
- Prakash, S., Atkinson, J. F., and M. L. Green (2007) A semi-lagrangian study of circulation and transport in Lake Ontario, *J. Great Lakes Res.*, *33*(4), 774-790.
- Schwab, D.J. and K. W. Bedford (1999), The great lakes forecasting system. In: Moores, C. (Ed.), Coastal and Estuarine Studies. D.C. American Geophysical Union, Washington, pp. 157-173.
- Schwab, D. and D. Beletsky (2003), Relative effects of wind stress curl, topography, and stratification on large-scale circulation in Lake Michigan, *J. Geophys. Res.*, *108*(C2), 3044, doi:10.1029/2001JC001066.
- Schwab, D. J., Beletsky, D., DePinto, J., and D.M. Dolan (2009), A hydrodynamic approach to modeling phosphorus distribution in Lake Erie, *J. Great Lakes Res.*, *35*(1), 50-60.
- Schwab, D.J., and D.L. Sellers (1996), *Computerized bathymetry and shorelines of the Great Lakes*. Ann Arbor MI, NOAA Data Report ERL GLERL-16, 8pp.
- Sheng, J. Y., and Y. R. Rao (2006), Circulation and thermal structure in Lake Huron and Georgian Bay: Application of a nested-grid hydrodynamic model, *Continental Shelf Resesarch*, *26*(12-13), 1496-1518.
- Sloss, P.W., and J. H. Saylor (1976) *Large-scale current measurements in Lake Superior*. NOAA Tech. Rep. ERL 363 GLERL 8.
- Smagorinsky, J. (1963) General circulation experiments with the primitive equations. I. The basic experiments, *Mon. Weather Rev*, *91*, 99-164.



- Urban, N. R., M. T. Auer, S. A. Green, X. Lu, D. S. Apul, K. D. Powell, and L. Bub (2005), Carbon cycling in Lake Superior, *J. Geophys. Res.*, 110, C06S90, doi:10.1029/2003JC002230.
- Waples J.T., and J.V. Klump (2002), Biophysical effects of a decadal shift in summer wind direction over the Laurentian Great Lakes, *Geophys Res. Lett.*, 29(8), 1201, doi:10.1029/2001GL014564.
- Williamson, C.E., J.E. Saros, and D.W. Schindler (2009) Lakes and reservoirs provide key insights into the effects and mechanisms of climate change, *Science*, 323 (5916), 887-888, doi: 10.1126/science.1169443.
- Zhu, J.R., C.S. Chen., E. Ralph, S.A. Green, J.W. Budd, and F.Y. Zhang (2001), Prognostics modeling studies of the Keweenaw current in Lake Superior. Part II: Simulation, *J. Phys. Oceanog.*, 31(2), 396-410.

## Figure Captions

Figure 3-1. Locations of observations in Lake Superior used for model evaluation. Solid circles indicate the 19 open lake EPA stations (SU1-SU19). Three crosses show locations of three surface buoys operated by NOAA. A through I are locations of current measurements from *Sloss and Saylor* [1976]. E3, E4, and H4 are ADCP locations during the KITES experiment. Shaded contours every 100 m. Inset of boxed region along the Keweenaw Peninsula. Isobaths within inset every 50 m.

Figure 3-2. Daily average modeled and observed lake surface temperatures at the three NDBC buoy locations during 2000 (left) and 2004 (right). 2000 was a year of above-average lake temperatures, and 2004 temperatures were below the 28-year average.

Figure 3-3. Model daily average temperature plotted against instantaneous temperature measured at the 19 EPA stations between 1992 and 2006 during April (a) and summer (b). Model results when forced with alternative forcing (See Supplementary) are included on the scatter plots. Summer sampling primarily done during the month of August. Model temperatures compared to sample temperature at depths nearest the surface and below 75m in April. In summer, model temperatures compared to sampled temperatures nearest the depths of 10m, 20m, and below 75m. One-to-one line shown on both (a) and (b) for ease of comparison.  $R^2$  and RMSE are shown for modeled temperatures when forcing the model with atmospheric conditions of the NARR product.

Figure 3-4. Subplots A through I correspond to the locations shown in Figure 3-1. Daily depth-average current direction and speed are depicted in the current roses for each location A-I. Bar direction indicates direction *toward* which current flows. Length of bar indicates percentage of summer days (1979-2006) that daily average flow was in that direction. Color of bar indicates speed of flow. Flow in one direction may have many colors, indicating percentage of days that daily average flow was both in that direction *and* with that speed. Separate arrow indicates direction *toward* which current flow was observed at that location during two years during the 1960s, as summarized by *Beletsky et al.* [1999]. Color and number at end of arrow indicates mean speed of the observed flows [*Sloss and Saylor, 1976*].

Figure 3-5. Zonal velocity (U), meridional velocity (V), and temperature (T) at ADCP location H3 during the summer of 1998. Data in left column, model on right. Data and model plotted versus depth (m) and time (day). Month denoted on first day of the month. Data averaged within model layers. For ease of comparison, model layers with no ADCP measurements are left blank for both data and model.

Figure 3-6. (a,b) Depth-average currents and column temperature during winter (DJFM) (1979-2006) (a) and summer (JJAS) (1979-2006) (b). (c,d) Mean currents and column temperature within the top 15 m of the water column during winter (c) and summer (d). (e,f) Mean currents and temperature of the water column below 30 m during winter (e) and summer (f). Note change in current scale for surface flows.

Figure 3-7. Depth-average currents during winter (DJFM) and summer (JJAS) of 1997-2001 from model simulation with a 10km horizontal grid resolution. Current speed indicated by arrow length.

Figure 3-8. (a) Geometric mean of: 1) correlation between daily summer zonal temperature gradient anomalies and meridional current anomalies (depth-average to 25m) and 2) correlation between daily meridional temperature gradient anomalies and zonal current (depth-average to 25 m) anomalies during summer. A geometric mean of 1 corresponds to a correlation of 1 for both 1 and 2. (b) Geometric mean of: 1) correlation between daily summer zonal wind stress anomalies and meridional current (depth-average to 25 m) anomalies and 2) correlation between daily summer meridional wind stress anomalies and zonal current (depth-average to 25 m) anomalies.

Figure 3-9. (a,b) Lake-wide depth-average currents and temperature in January 2006 for model simulations with and without realistic bathymetry. Color indicates temperature. (c,d) Depth-average vorticity during January for the uniform and realistic topography runs. (e,f) Depth-average currents and temperature during June and (g,h) vorticity for the uniform and realistic topography simulations.

Figure 3-10. Lake-wide annual average modeled lake surface temperature, column-average temperature, surface current speed, depth-average current speed, and NARR 10 m above-lake air temperature and wind speed from 1979-2006.

## Tables

**Table 3-1.** Lake Trends and p-values

lake characteristic	trend	p-value
lake surface temperature	0.34°C per decade	0.027
heat content	0.12°C per decade	0.13
ice cover (JFMA)	-886 km <sup>2</sup> /yr	0.007
speed (15m)	0.37 cm/s per decade	0.0001
speed (depth-average)	0.13 cm/s per decade	0.0002
above-lake air temperature	0.8°C per decade	0.001
wind speed	0.18 m/s per decade	0.002
mixed layer depth	0.4 m shallower / decade	0.33
evaporation	1.3 cm per decade	0.38
buoy temperatures (AMJJASON)	0.7°C per decade	0.13

Table 3-2.  $r^2$  Values of lake variables of interest

Variable 1	Variable 2	$R^2$
speed (15m)	wind speed	0.77
speed (15m)	speed (depth-average)	0.98
lake surface temp	air temp	0.81
lake surface temp	ice cover	0.37 (r = -0.58)
lake surface temp	heat content	0.88
air temp	ice cover	0.52
air temp	wind speed	0.26
evaporation	ice cover	0.55 (r = -0.78)
evaporation	wind speed (10m)	0.30
evaporation	lake surface temp	0.33
lake surface temp	mixed layer depth	0.28
wind speed	mixed layer depth	0.06 (r = -0.25)

# Figures

Figure 3-1

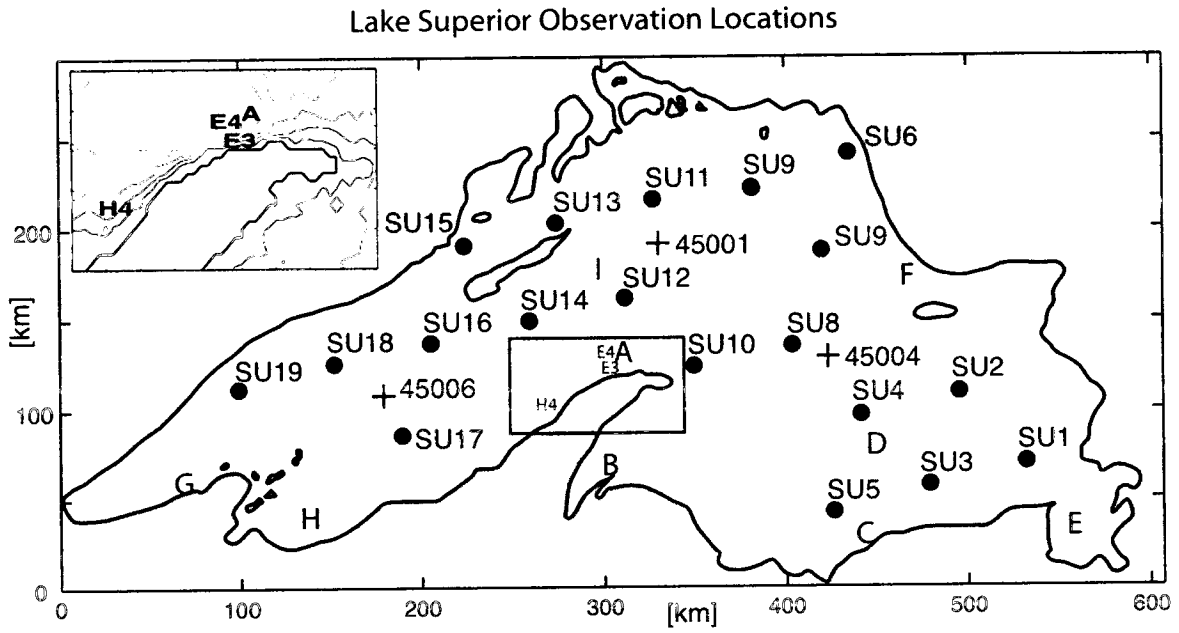


Figure 3-2.

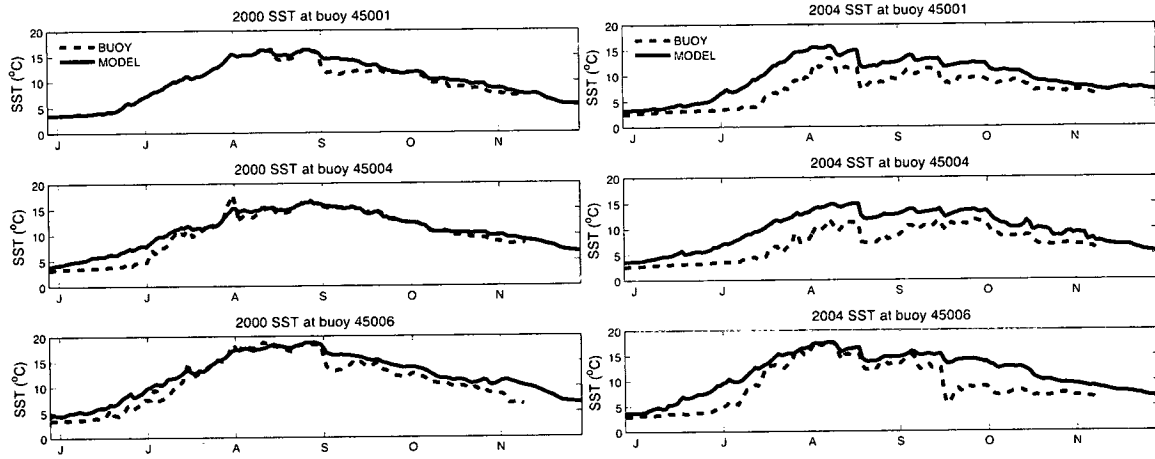
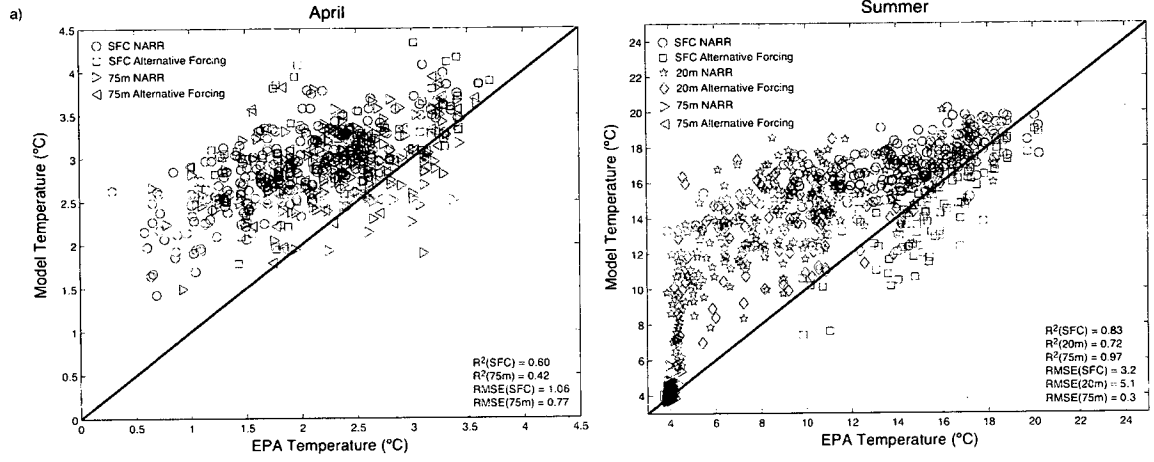




Figure 3-3.



**Figure 3-4.**

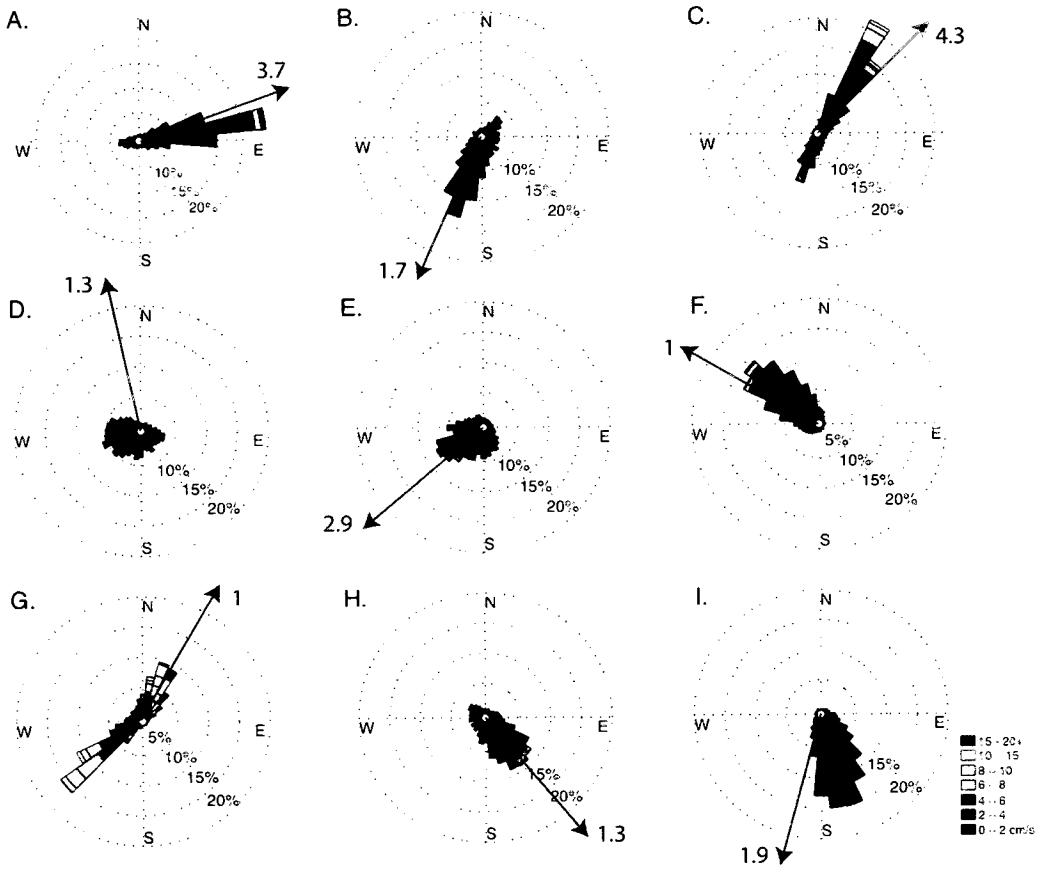


Figure 3-5.

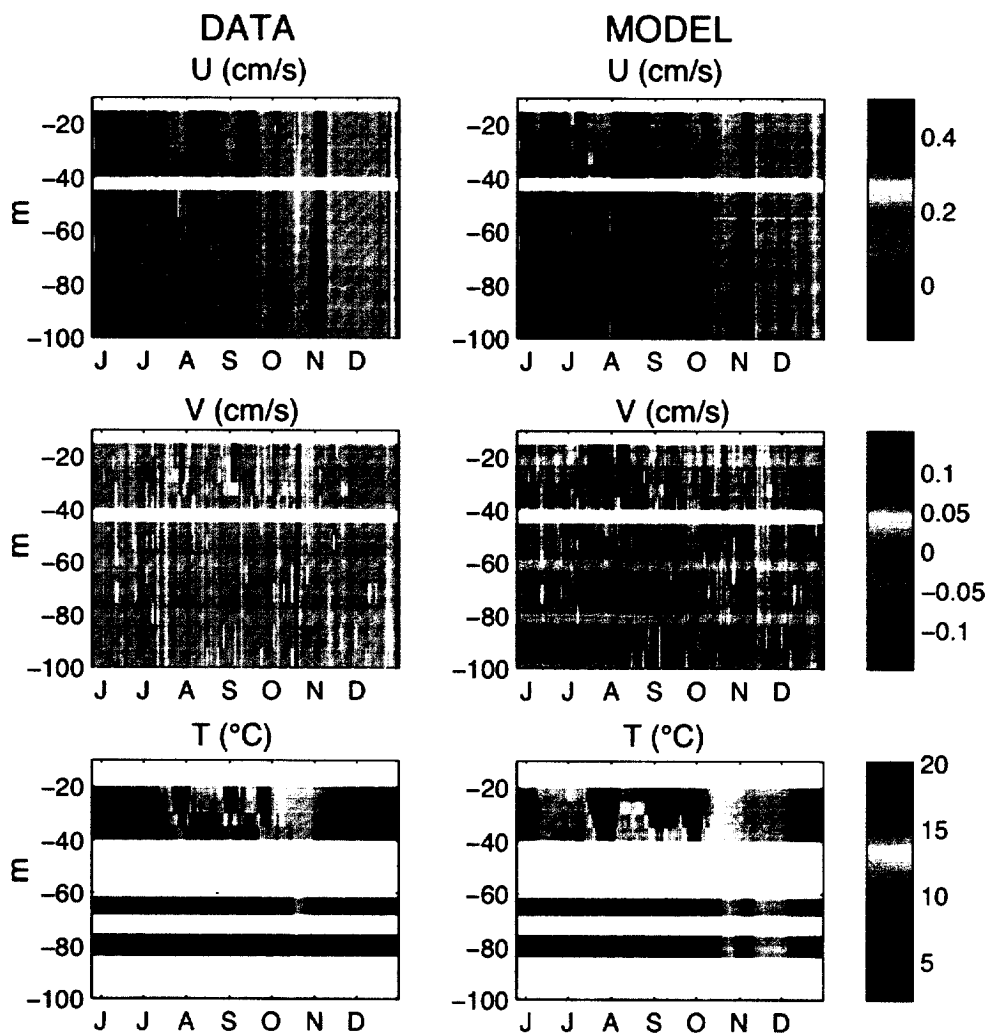


Figure 3-6.

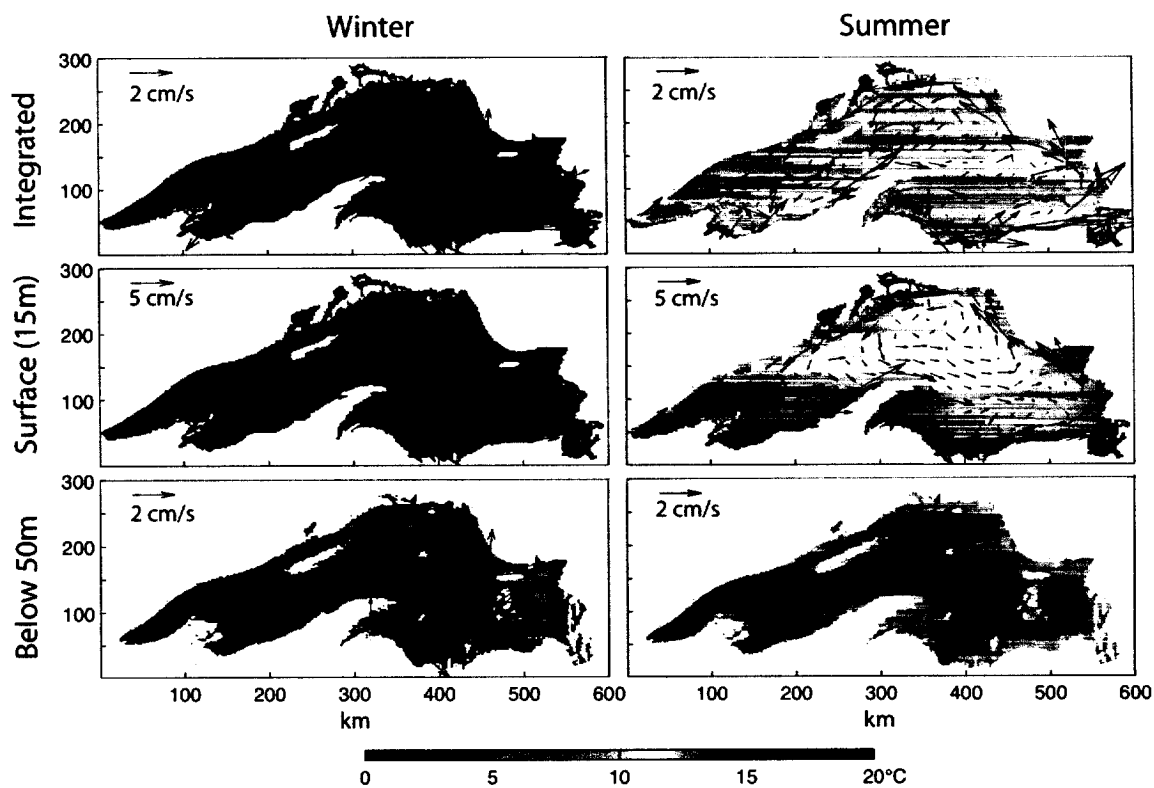


Figure 3-7.

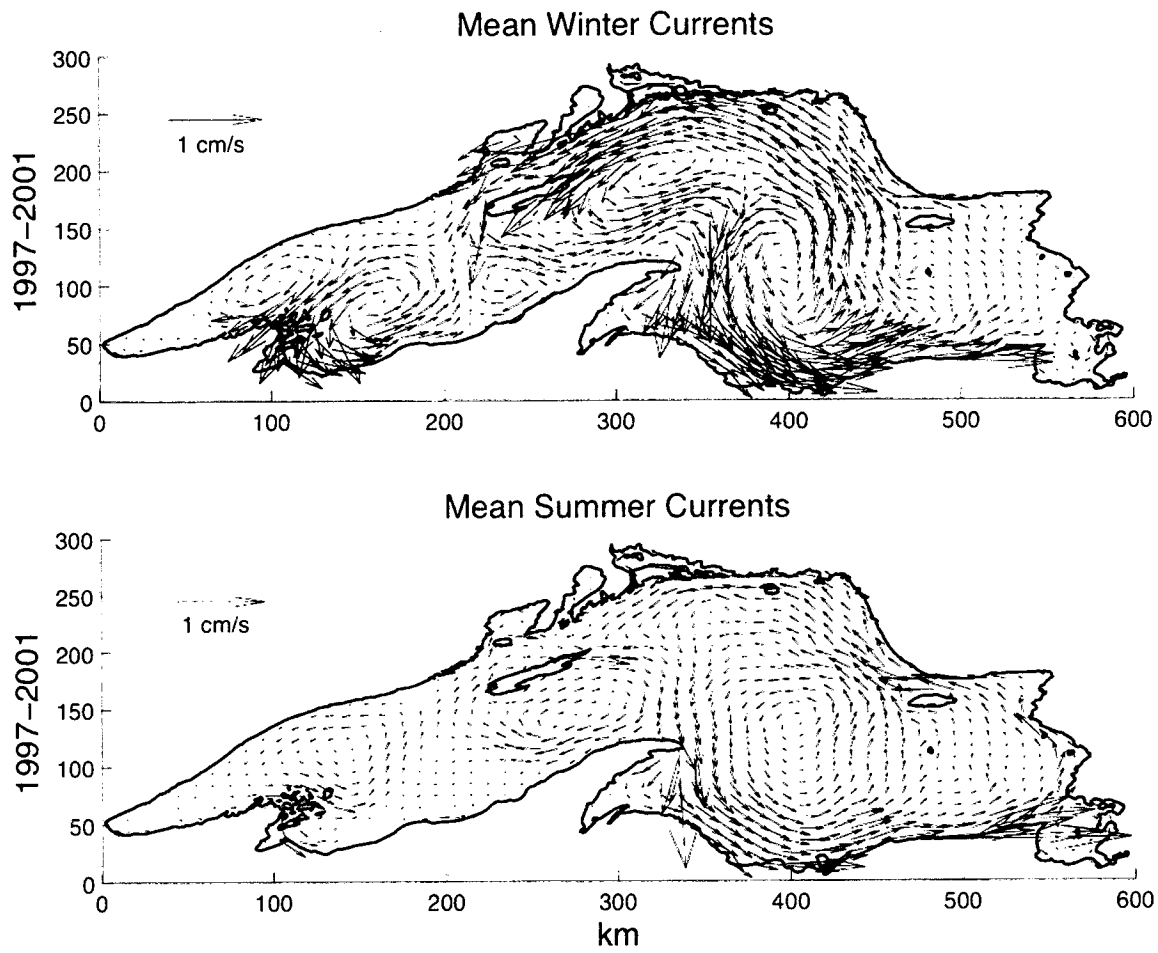


Figure 3-8.

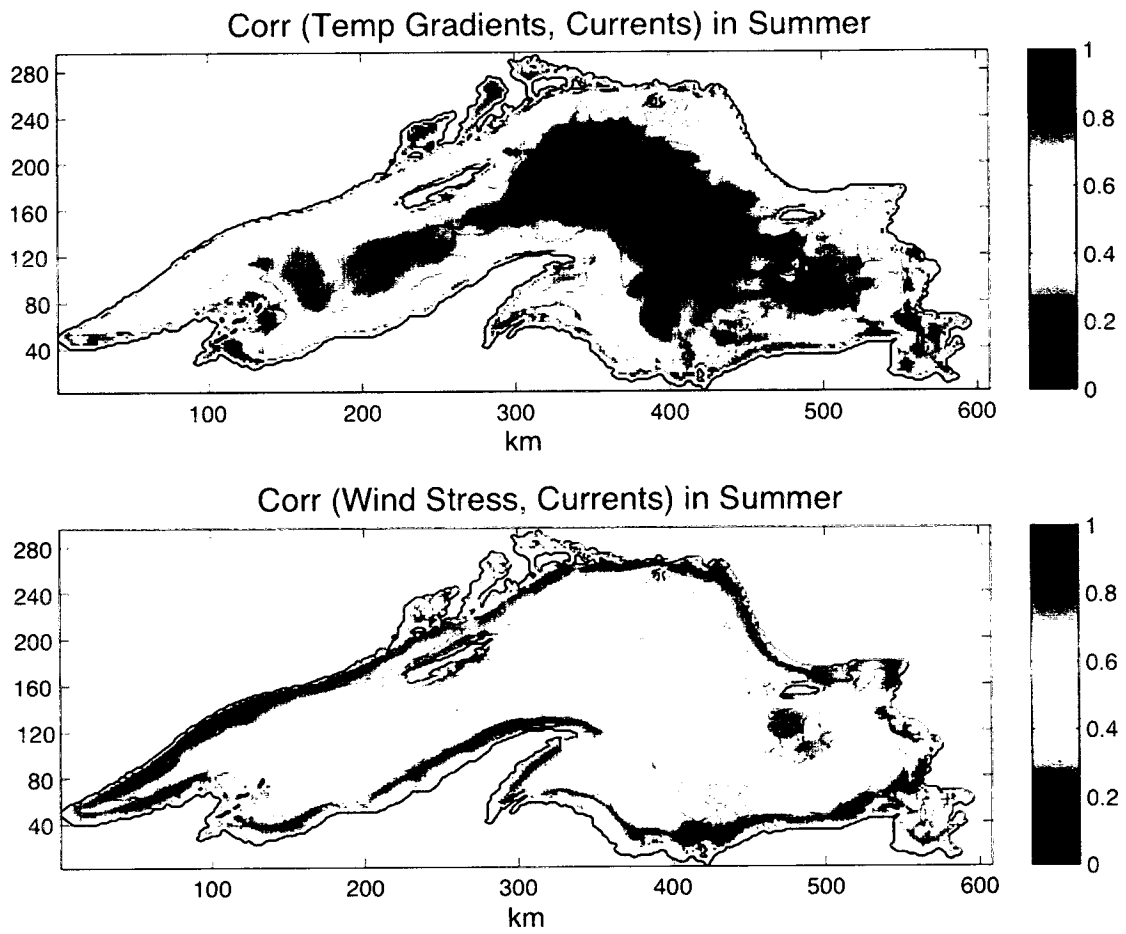


Figure 3-9.

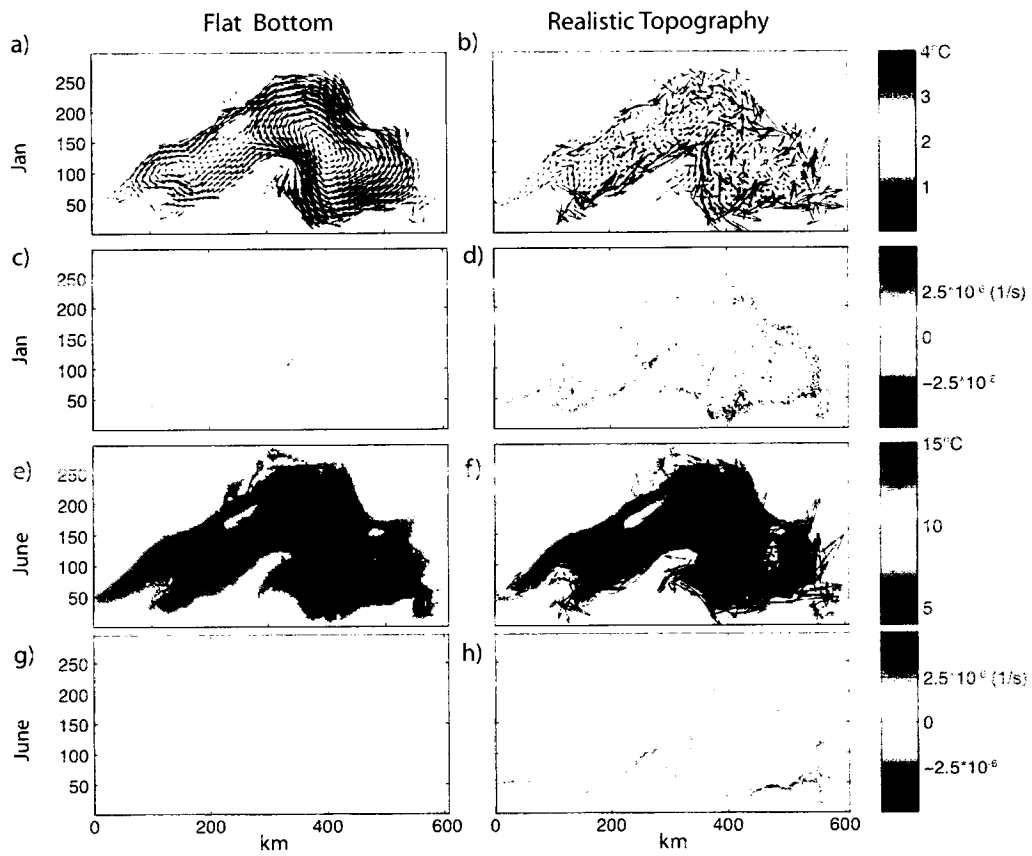
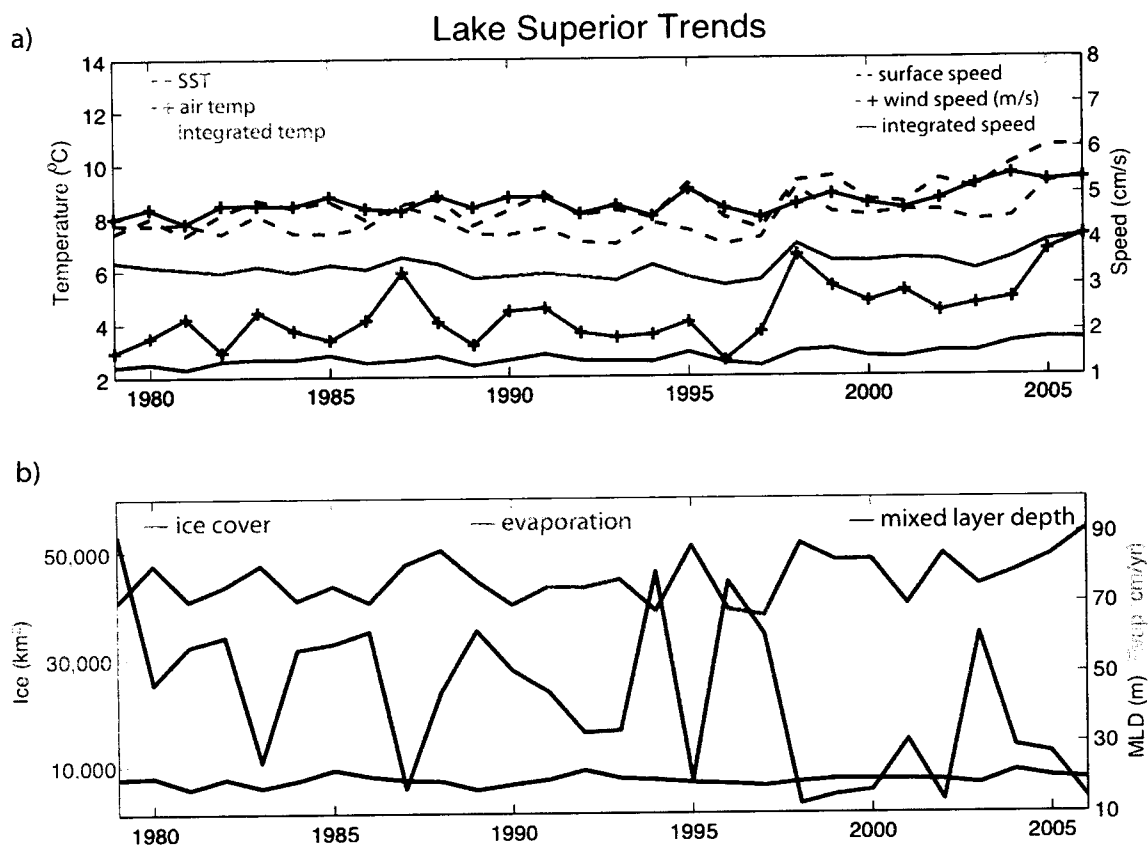


Figure 3-10.





## Supplementary

### Section 1: Model Forcing

The model was run for 1997-2001 using both the NARR atmospheric conditions and over-lake conditions interpolated from meteorological observations from over and around the lake using an empirical method [Schwab, 1978; Hsu, 1986]. Model results from these simulations were compared to observed lake surface temperatures at the three open-lake buoys, thermal profiles at the 19 EPA stations, and ADCP measurements off the Keweenaw Peninsula. In Supplementary Table 1, we show root mean square error (RMSE) at the three buoy locations for model simulations with both types of forcing. The model simulation using NARR forcing has lower RMSE at all buoy locations during 1998, a warm El Niño year, and 2000. During 1999, running the model using NARR forcing results in a lower RMSE at one of the three buoys. At other times, the alternative forcing results in lower RMSE. During the five years, warmer years were better simulated using NARR forcing, and colder years were better captured using interpolated forcing. Summer and winter large-scale circulation patterns produced by the forcing products are comparable. Neither forcing product is clearly better than the other for these years. The North American Regional Reanalysis Project uses well-documented, internally consistent methods and a uniform horizontal resolution of 32km to create their product. Buoyed meteorological stations are only present in the lake from April through November. Meteorological observations above the lake are often more than 100 km apart and as one goes back in time, fewer and fewer direct atmospheric observations over the lake exist, which makes this method more suspect for earlier years. We opted to use NARR atmospheric conditions to force the model for 1979-2006.

## **Supplementary Section 2: Circulation Sensitivity Studies**

To assess the importance of heat fluxes, winds, and vorticity in the wind field, we simulated lake circulation for 1997-2001 in three sensitivity runs using the model at 10km horizontal resolution. The model was run without any wind, without heat fluxes, and with a spatially uniform wind field (Supplementary Figure 6).

### *Supplementary Section 2.1: No Wind Experiment*

For the no wind experiment, absolutely no lake momentum is generated by winds. To determine heat fluxes, the model assumes a minimum wind speed of 0.5 m/s at all times.

In the no wind experiment, winter flows are extremely weak compared to the control simulation. Only one gyre is present in the central and eastern basins, and the western arm is anticyclonic instead of cyclonic. During the summer, the lack of wind results in negative vorticity in the western arm and weakened flow in the far eastern basin.

### *Supplementary Section 2.2: No Heat Flux Experiment*

To remove the effects of baroclinicity on lake flow, the model was initialized with uniform temperature and salinity. All heat fluxes were set to zero at all model time steps, creating a barotropic lake. When the model was run without heat fluxes, winter circulation patterns are similar to the control. Summer circulation still has a cyclonic gyre in the eastern basin, but the north-central basin is now anticyclonic. Heat fluxes are crucial to the development of the coastal jet.

*Supplementary Section 2.3: Spatially Uniform Wind Field*

To assess the importance of vorticity in the wind field on lake circulation, the model was run with a spatially uniform wind field between 1997 and 2001. Every hour, each lake grid cell is forced by the lake-wide mean wind, so the wind field is varying in time but not space. A uniform wind results in many small rotating cells without any organized pattern during winter. A spatially varying wind is less important during summer, because horizontal lake temperature gradients generate vorticity. Thus, wind is a first order control of circulation patterns all year. Vorticity in the wind field is crucial for winter circulation patterns, but not summer patterns. Temperature gradients in summer are a first order control of near-coastal flows.

### Supplementary References

Hsu, S. A. (1986), Correction of land-based wind data for offshore application: A further evaluation, *J. Phys. Oceanogr.*, *16*, 390–394.

Schwab, D. J. (1978), Simulation and forecasting of Lake Erie storm surge, *Mon. Weather Rev.*, *106*, 1476–1487.

### Supplementary Table Captions

**Table S3-1.** Root mean square error (RMSE) of lake surface temperature at the three open lake buoys for April through November, 1979-2006. For 1997-2001, RMSE of lake surface temperature when the model is run using the alternate forcing is shown in italics.

## Supplementary Figure Captions

**Supplementary Figure 3-1.** April through November average lake surface temperatures at the three NDBC buoy locations in the model and data for 1979-2006. We use only modeled temperatures on dates with available observational data in each yearly mean.

**Supplementary Figure 3-2.** Daily average 10m air temperature from the North American Regional Reanalysis Project is plotted against observed air temperature at the three NDBC buoy locations in Lake Superior for all days of available observations between April and September of 1979-2006. The one-to-one line is shown for ease of comparison. Correlation between NARR and observed air temperatures and RMSE of NARR air temperatures are provided for each month.

**Supplementary Figure 3-3.** Zonal velocity (U), meridional velocity (V), and temperature (T) at ADCP location E4 during the summer of 1998. Data in left column, model on right. Data and model plotted versus depth (m) and time (day). Month denoted on first day of the month. Data averaged within model layers. For ease of comparison, model layers with no ADCP measurements left blank for both data and model.

**Supplementary Figure 3-4.** Zonal velocity (U), meridional velocity (V), and temperature (T) at ADCP location E4 during the summer of 1999. Data in left column, model on right. Data and model plotted versus depth (m) and time (day). Month denoted on first day of the month. Data

averaged within model layers. For ease of comparison, model layers with no ADCP measurements left blank for both data and model.

**Supplementary Figure 3-5.** Mean integrated current speeds for January through December 1979-2006. Contours of lake bathymetry every 100m in dark blue.

**Supplementary Figure 3-6.** Mean integrated current direction and speed during winter (DJFM) and summer (JJAS) of 1997-2001 when the model with 10km horizontal resolution is run (a) without wind, (b) without heat fluxes, and (c) with a spatially uniform wind field.

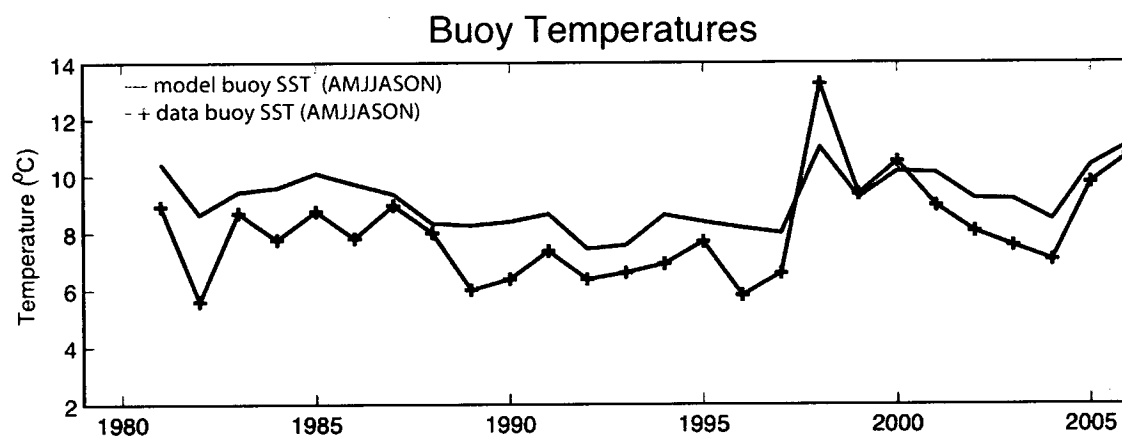
## Supplementary Tables

**Table S3-1.**

	45001	45004	45006
1979	4.5082		
1980	3.5756	2.5732	
1981	3.7915	4.2718	3.5935
1982	5.4451	4.5022	4.9574
1983	2.4466	1.6068	4.4525
1984	4.0385	4.1019	4.3354
1985	2.4047	2.726	4.2665
1986	2.8465	4.535	4.1424
1987	2.2235	2.0794	2.1706
1988	2.6615	2.1022	3.5757
1989	4.0683	4.3834	4.1086
1990	4.3419	3	3.4372
1991	3.3568	2.5224	4.0829
1992	2.5011	1.7406	3.6119
1993	2.521	1.9331	3.0029
1994	3.764	4.9212	3.3687
1995	2.5437	2.3191	3.372
1996	4.5001	4.8658	5.184
1997	3.4097	3.6615	3.4197
	<i>1.8151</i>	<i>1.4631</i>	<i>3.1339</i>
1998	1.3876	1.384	1.7344
	<i>2.5361</i>	<i>2.6029</i>	<i>2.4237</i>
1999	2.3692	1.5753	2.7883
	<i>1.4283</i>	<i>1.8666</i>	<i>2.4588</i>
2000	1.1368	1.1375	1.5381
	<i>1.6578</i>	<i>1.7724</i>	<i>1.745</i>
2001	3.6243	2.9643	3.6337
	<i>1.8729</i>	<i>1.2522</i>	<i>1.6036</i>
2002	3.2555	3.0885	3.6036
2003	4.2235	4.2601	3.3339
2004	2.7758	3.0501	2.8943
2005	2.6097	2.6712	3.0289
2006	2.9359	2.9911	1.9877

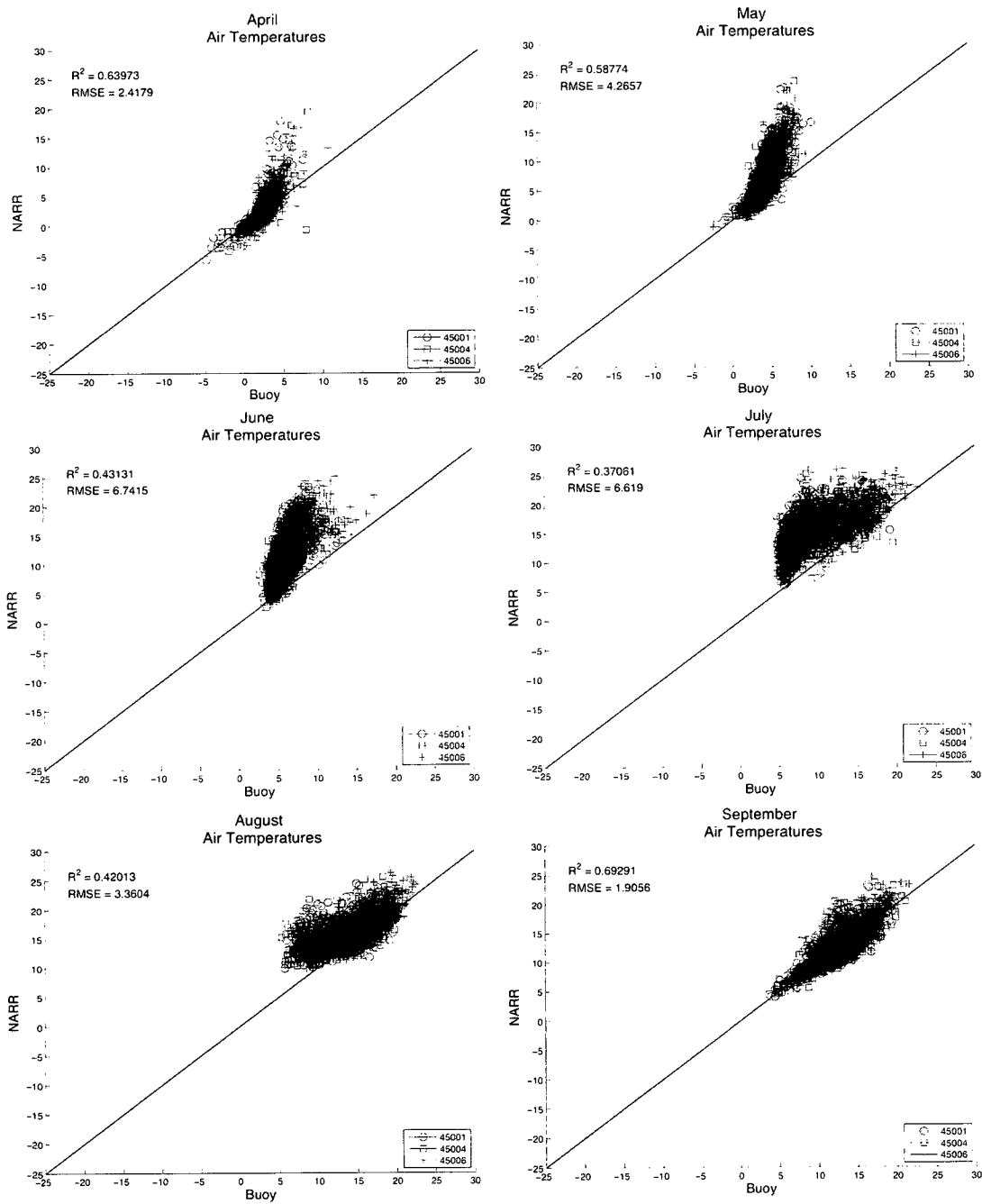
## Supplementary Figures

### Supplementary Figure 3-1.

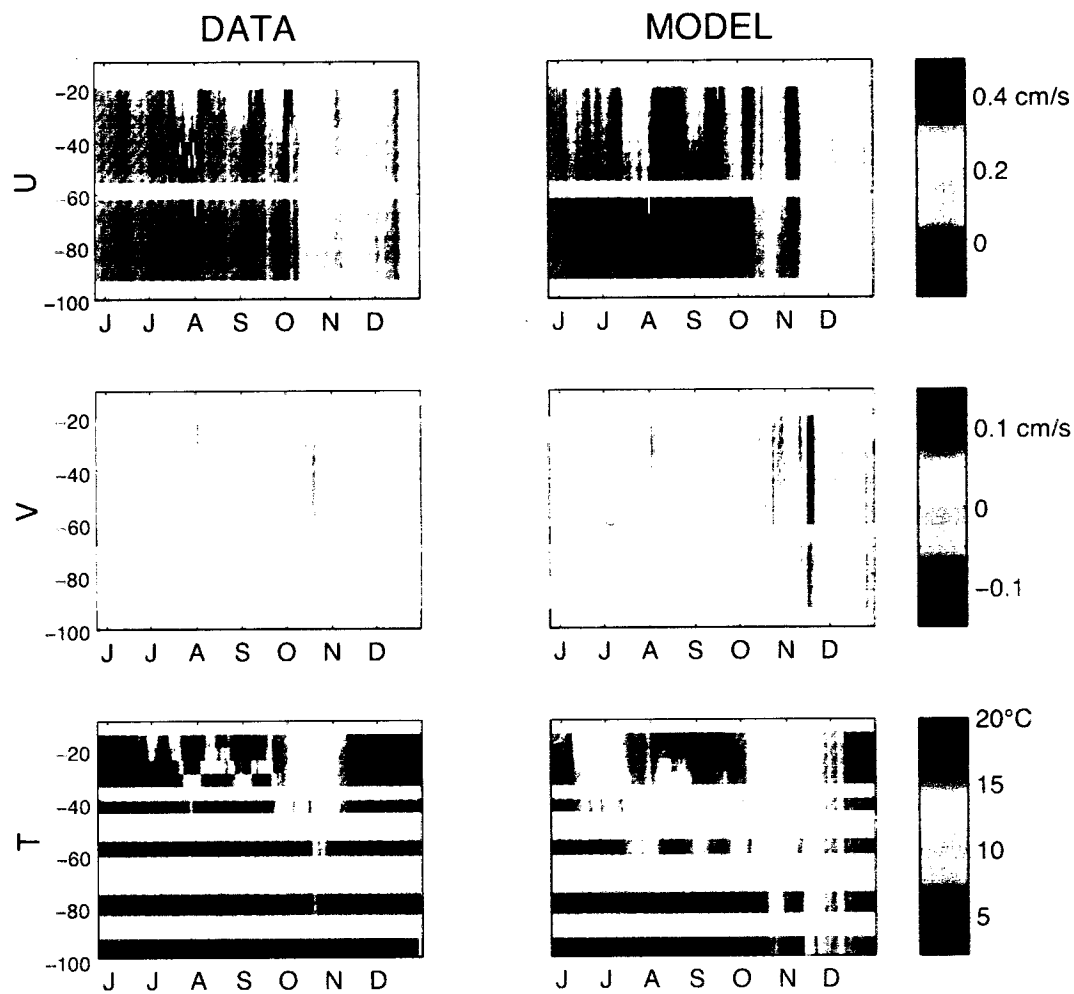




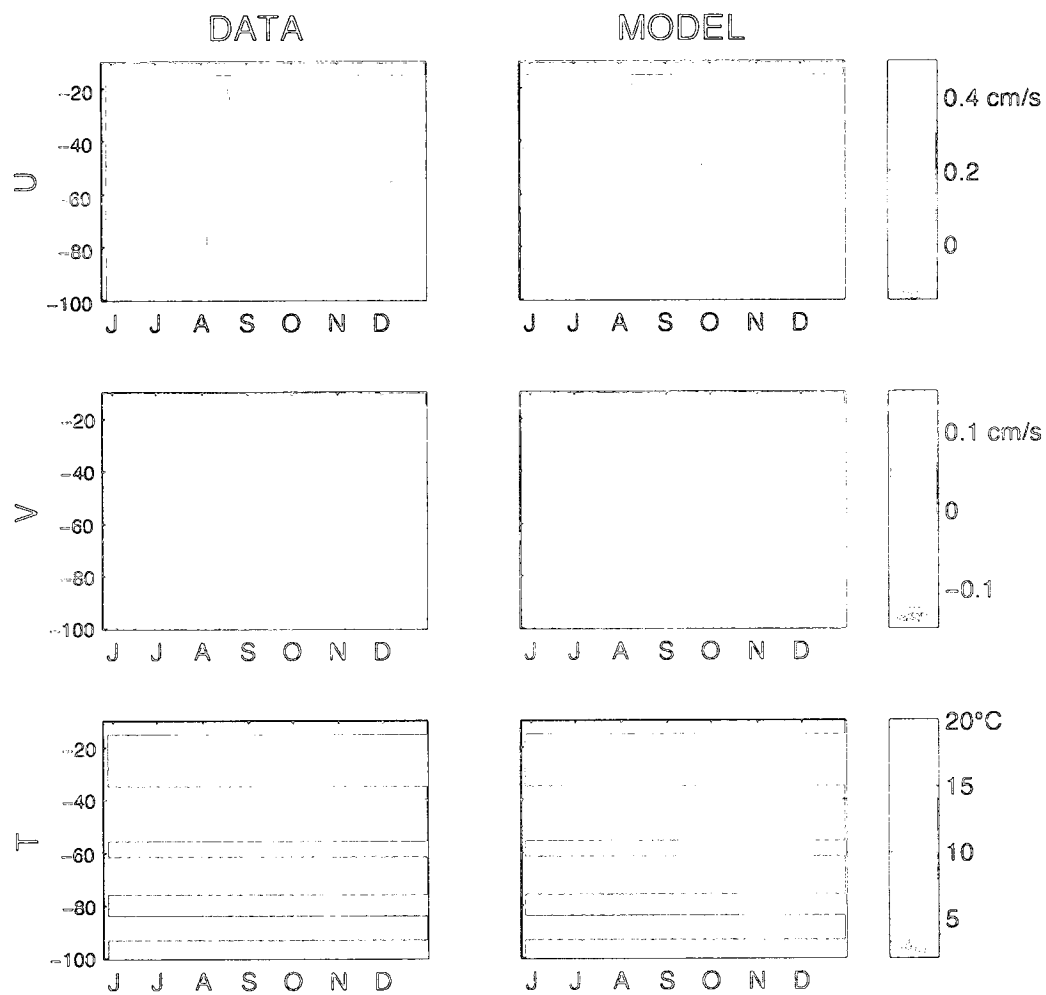
Supplementary Figure 3-2.



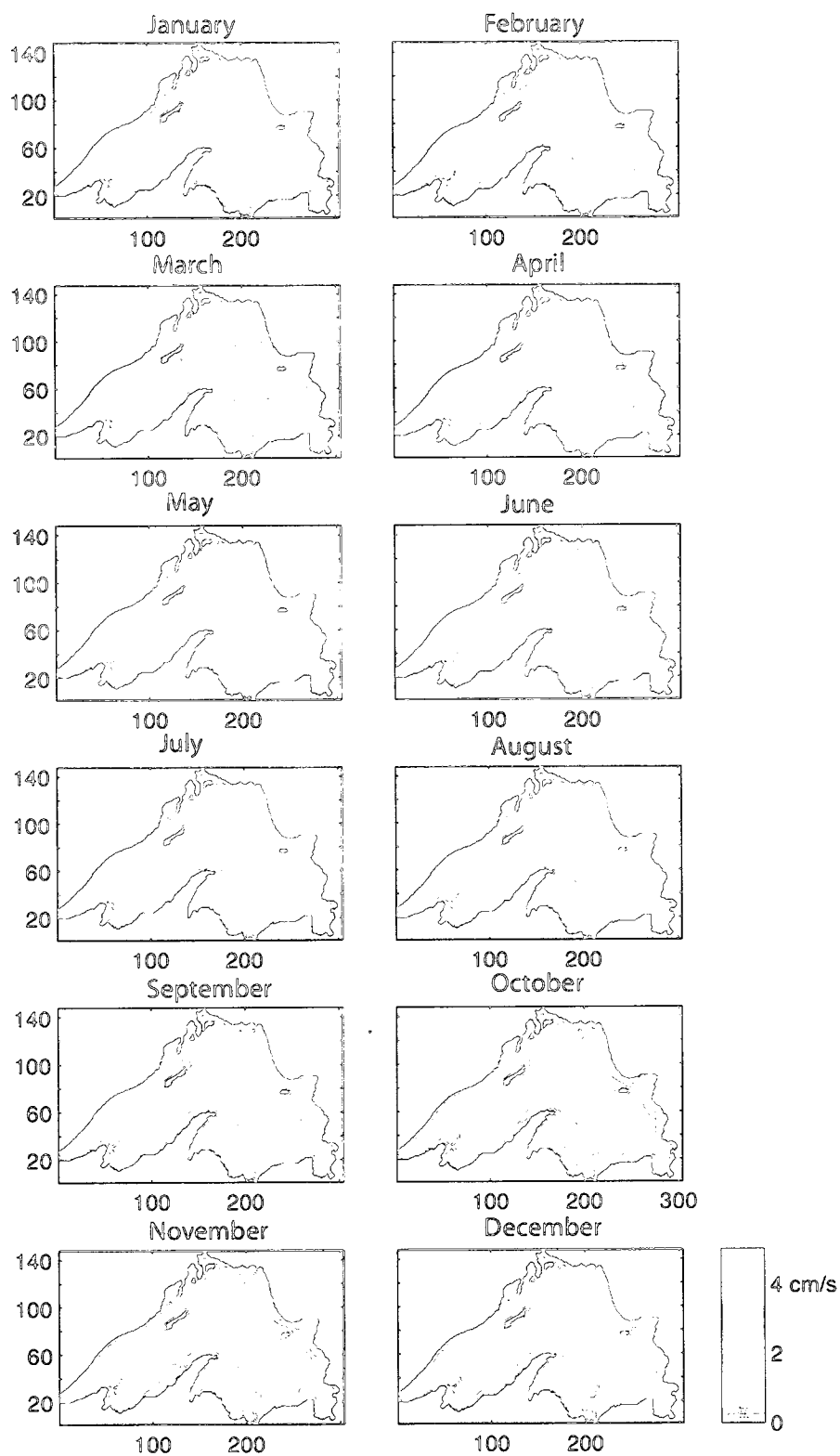
Supplementary Figure 3-3.



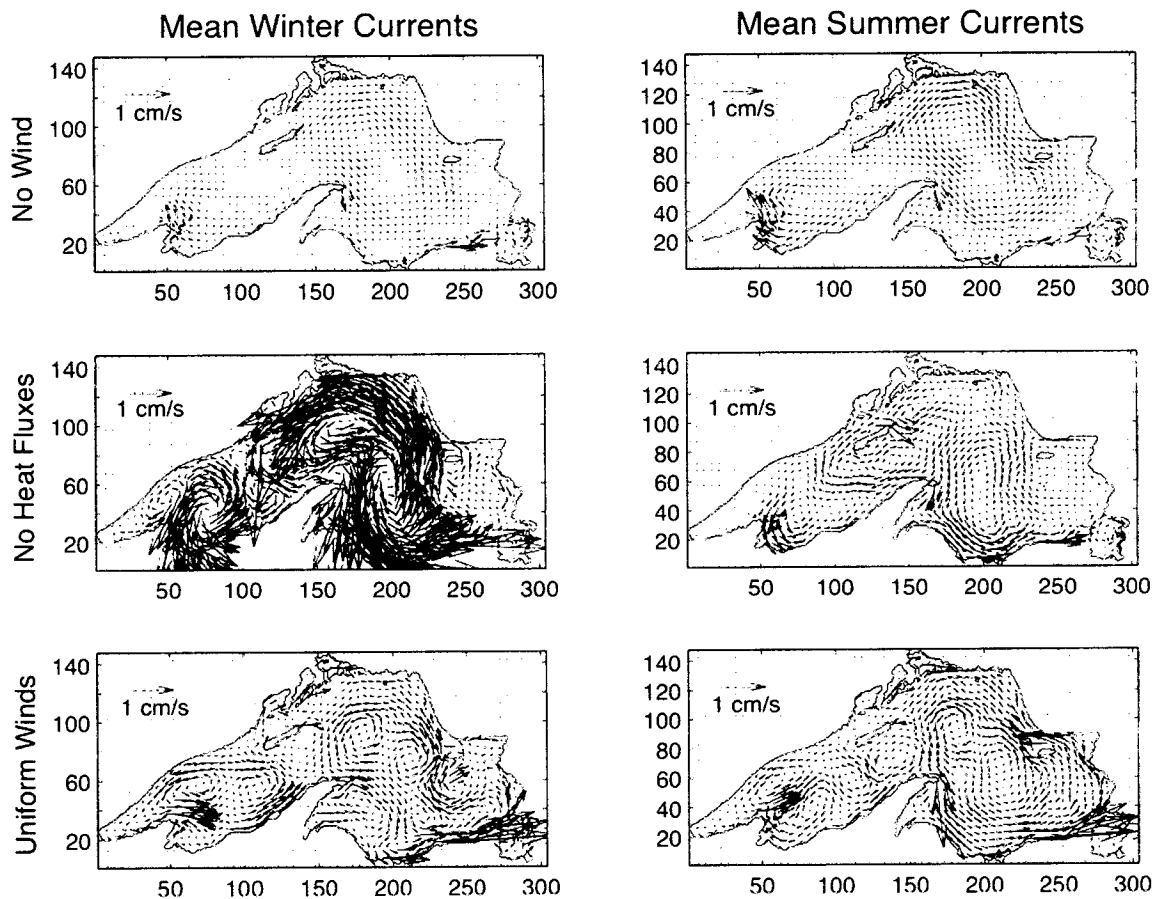
Supplementary Figure 3-4.



Supplementary Figure 3-5.



Supplementary Figure 3-6.



## Chapter 4

# Internal Carbon Cycling in Lake Superior

### 4.1 Introduction

The terrestrial biosphere is a natural sink of anthropogenic carbon dioxide, removing about one quarter of annual emissions. Inverse models are used to pinpoint carbon sink and source locations and suggest the North American continent is currently a large sink of carbon dioxide (although anthropogenic emissions from the continent far exceed this sink). The North American Carbon Program (NACP) uses a combination of observations and models in an attempt to mechanistically understand this sink. This sink has been attributed largely to forest re-growth and reduction in forest fires [*Field et al.*, 2007] but to date, inverse models have set Great Lakes (and coastal oceans) carbon fluxes to zero, thus carbon fluxes from these water bodies are aliased to the land. This may either exaggerate or suppress the natural variability and seasonality of true air-land fluxes, confounding our understanding of probable future changes to this sink.

Inland water bodies have historically been neglected by global and regional inverse modelers, simply because the air-water CO<sub>2</sub> fluxes were unknown or assumed to be insignificant. Inland water bodies were viewed simply as closed pipes, moving carbon and other nutrients from the land to the ocean where they are processed. However, using direct observations and indirect

techniques to estimate partial pressure of carbon dioxide ( $p\text{CO}_2$ ) of global inland water bodies, *Cole et al.* [1994] found that most lakes are supersaturated with carbon dioxide and later concluded that all inland water bodies are a significant source to the global atmosphere (*Cole et al.*, [2007]; 0.75 Pg C/yr). Thus, much of the carbon sunk into the terrestrial biosphere runs off into inland water bodies where it is respired and released back into the atmosphere. Only about half of the carbon entering this “pipe” makes it to the ocean. *Tranvik et al.* [2009] updated *Cole et al.*'s [2007] estimate, suggesting that inland water bodies efflux 1.4 PgC/yr. Thus, inland water bodies are a globally significant source of atmospheric carbon dioxide and should be considered in regional carbon budgets.

*Vollenweider et al.* [1974] estimated primary productivity in the Great Lakes to be 60-300 g C m<sup>-2</sup> yr<sup>-1</sup>, the same order of magnitude as the surrounding terrestrial system, suggesting they may be a significant component of the regional carbon budget. Lake Superior is the largest freshwater lake in the world by surface area and contains approximately 10% of the Earth's freshwater. Situated within Michigan, Minnesota, Wisconsin, and Ontario, Lake Superior is the coldest and deepest of the Laurentian Great Lakes. Its average depth is 150 m, and its deepest point is over 400 m. Surface temperatures rarely exceed 4°C near shore before mid April, and the open lake often does not stratify until late June or July [*Bennett, 1978; Austin and Colman, 2007*].

Small lakes with large ratios of drainage basin to lake surface area are dominated by external inputs. They receive far more carbon from their watershed than they can produce in their small volume, and thus, respiration in these lakes can be dominated by the decomposition of externally

produced (allochthonous) carbon. As you move to larger lakes and those with smaller ratios of drainage basin to lake surface area, the lake produces more carbon internally than is supplied from the surrounding watershed. In these cases, internal processes should dominate the lake carbon budget [*Hanson et al.*, 2004]. Lake Superior has a small watershed to lake surface area ratio (1.55) compared to even the other Great Lakes (Michigan – 2; Erie, Ontario > 3), suggesting that internal processes dominate in Lake Superior.

*Alin and Johnson* [2007] show that low latitude large lakes are more likely to be a sink of atmospheric carbon dioxide, due to their permanent stratification and high rates of primary production. As you move to higher latitudes, this sink changes to a source. Lake Superior is situated within this transitional zone, suggesting it may be either a source or sink of carbon dioxide. Observational studies [*Cotner et al.*, 2004; *Urban et al.*, 2005] have suggested that Lake Superior is a source of carbon dioxide to the atmosphere, but are unable to account for the source of carbon being respired in the lake. Observations from the nearby eddy flux tall tower in Park Falls, WI suggest that Lake Superior is either a source of carbon dioxide during summer, or a smaller sink than the nearby forests [*Desai et al.*, 2008].

The carbon budget of Lake Superior has remained imbalanced, likely due to data being sparse in space and time, and to heterogeneity in the physical system that make extrapolation from a small area of the lake to the entire lake difficult. Harsh winters also prevent observations, and to date, no wintertime measurements of primary productivity or pCO<sub>2</sub> have been made in Lake Superior. Thus, extrapolation over an entire year is a source of significant uncertainty. From measurements primarily taken in the western arm of Lake Superior, *Cotner et al.*, [2004] estimated the lake



ecosystem creates 5.3-8.2 Tg of organic carbon each year via photosynthesis and respire 13-39 TgC/yr. They estimated river and atmospheric inputs of 0.52-0.62 and 0.16-0.41 TgC/yr, respectively. Thus, even without considering outflow (0.08-0.1 TgC/yr) and burial losses (0.48 TgC/yr [McManus et al., 2003]), the lake appears to be respiring far more organic carbon than supplied to the lake each year [Cotner et al., 2004]. Urban et al. [2005] also estimated sources and sinks of carbon in Lake Superior from measurements of respiration and photosynthesis. Their study area was just off the Keweenaw Peninsula, within 20 km of shore in southern Lake Superior, but their findings were similar to Cotner et al.'s, [2004]. Urban et al. [2005] estimated a net efflux from Lake Superior of 3 TgC/yr from pCO<sub>2</sub> observations and estimates, but again, no known source of carbon to the lake is large enough to support this magnitude of heterotrophy.

The Environmental Protection Agency (EPA) samples the water column at 19 stations throughout Lake Superior twice per year, once in April or May, and again in August or September (Figure 3-1). Using EPA measurements of surface alkalinity, temperature, and pH, Atilla et al. [2010] determine that Lake Superior is likely supersaturated with CO<sub>2</sub> during April and in near equilibrium during summer. Thus, Lake Superior is likely a source to the atmosphere in April and neutral in August, although pCO<sub>2</sub> resulting from these estimates may be biased high. Indirect techniques of pCO<sub>2</sub> estimation have large uncertainty (approximately 130 μatm in April and 80 μatm in summer) due to a bias in measuring pH in freshwater using an electrode [French et al., 2002] and the extreme sensitivity of pCO<sub>2</sub> estimates to pH in freshwater. Even without any uncertainty in indirect estimates of pCO<sub>2</sub>, EPA data provide only two moments in time each year. What is occurring throughout the lake during the rest of the year? What is the entire seasonal cycle of pCO<sub>2</sub>?

There are only two available time series of direct measurements of  $p\text{CO}_2$  in Lake Superior. Data collected by M. Baehr and M. DeGrandpre at a single mooring in the far western arm during spring and summer of 2001 and summarized in *Atilla et al.*, [2010] and in Thunder Bay by *Kelly et al.* [2001] are consistent with *Atilla et al.*, [2010] in suggesting  $\text{CO}_2$  uptake during the stratified period. Although these measurements are limited in space and time, *Atilla et al.*, [2010] show that changes in  $p\text{CO}_2$  are driven by the annual cycle of biological export of organic carbon to depth and its return to the surface by mixing in the winter un-stratified period.

New estimates of primary production [*Sterner*, 2010] suggest that annual primary production (9.73 TgC/yr) is larger than previously estimated ((5.3-8.2 TgC/yr), *Cotner et al.*, [2004]; (3-8 TgC/yr), *Urban et al.*, [2005]; (~5 TgC/yr), *Hecky* [2000]). This would still not balance the carbon budget if respiration estimates (42 TgC/yr, *Urban et al.*, [2005]; 13-39 TgC/yr, *Cotner et al.*, [2004]) are correct. It is unlikely that river inputs or primary production are orders of magnitude larger than previously estimated, and more likely that spatial heterogeneity in a lake larger than the state of South Carolina accounts for the imbalance in the carbon budget.

In this chapter, I use two ecosystem models coupled to the three dimensional hydrodynamic model of Lake Superior (Chapter 3) to determine whether a closed lake system (no river, precipitation, or sedimentation) can capture the observed seasonal variations in lake surface  $p\text{CO}_2$ . Is Lake Superior's carbon budget really out of balance, or can spatial and temporal heterogeneity in the system explain the apparent imbalance? What is the full seasonal cycle of  $p\text{CO}_2$  and  $\text{CO}_2$  fluxes in Lake Superior? What mechanisms control Lake Superior's  $p\text{CO}_2$ ?

## 4.2 Methods

To determine the seasonal cycle of  $p\text{CO}_2$  within the internal carbon cycle of Lake Superior, I couple two separate ecosystem models to the three dimensional hydrodynamic model of Lake Superior, configured at 10 km horizontal resolution.

The first model, called the phosphorus model (PM), is a phosphorus-based ecosystem, in which primary productivity is limited by light, phosphorus, and temperature (Figure 4-1; see 4.3). Model parameters were taken from the literature or tuned to best capture observations of net primary production (NPP) and respiration within Lake Superior. The second model, termed the no-phosphorus model (NPM) does not include phosphorus or its effect on photosynthesis (Figure 4-2; see 4.4). Instead, NPP is completely determined by available light and temperature after *Sterner* [2010], who found that variability in NPP could be explained using only temperature and light with an  $r^2=0.93$ . Complete descriptions for each of these models are provided in Sections 4.4 (PM) and 4.5 (NPM).

The ecosystem is initialized with an alkalinity of  $838 \text{ meq/m}^3$  everywhere, and a DIC of  $860 \text{ mmol/m}^3$ . The only dissolved organic carbon (DOC) and particulate organic carbon (POC) in the model are created by the ecosystem, since there are no inputs from the land or atmosphere. The model is run for 5 years using 1979 ice [*Assel*, 2003, 2005] and atmospheric forcing from the North American Regional Reanalysis (NARR) [*Mesinger et al.*, 2006], until the lake has out-gassed all excess  $\text{CO}_2$  (10 years) and is in equilibrium with the atmosphere over the course of a year. After the spin up, model DIC stabilizes around  $863 \text{ mmol/m}^3$ , and lake pH between 8.1 and 8.18 (spatial heterogeneity). The model is then run between 1979 and 2006 using NARR

atmospheric forcing and estimates of 8-day average atmospheric pCO<sub>2</sub> at Park Falls, WI from Carbon Tracker [*Peters et al.*, 2007]

(<http://www.esrl.noaa.gov/gmd/ccgg/carbontracker/co2timeseries.php>). I output daily average concentrations of model tracers, surface pCO<sub>2</sub>, and air-lake CO<sub>2</sub> fluxes over the 28-year period.

### **4.3 Physical Model**

We use the MIT general ocean circulation model (MITgcm) [*Marshall et al.*, 1997a, 1997b] configured to the bathymetry of Lake Superior [*Schwab and Seller*, 1996] at 10 km horizontal resolution. The model uses a z-coordinate system of 29 vertical layers. The top 50 meters have finest vertical resolution, with layer thicknesses of 5 meters. Vertical resolution gradually becomes coarser with depth to a thickness of 11.2 m at 100 m depth, 20.6 m at 200 m depth, and 31 meters at 300 meters depth. The circulation of Lake Superior is simulated well by the model at 2 km horizontal resolution [*Bennington et al.*, 2010], and this coarser version captures the major features of Lake Superior's circulation. Near shore flows are weaker, however, in the 10 km version. For a complete description of the physical model configuration, refer to Chapter 3. The coupled physical/ecosystem model is spun up for five years using 1979 forcing until the lake equilibrates to atmospheric CO<sub>2</sub> before the model is run for 1979-2006.

### **4.4 Ecosystem Model 1 – Phosphorus Based Model**

We use a medium-complexity ecosystem model within a three dimensional lake circulation model. The explicit pelagic ecosystem consists of two phytoplankton classes (pico and large) and one zooplankton class. The model includes an implicit microbial loop. Carbon, alkalinity, and phosphorus cycling are fully coupled within the entire water column.

#### 4.4.1 Nutrient Cycling

The model includes fully prognostic cycles of carbon, alkalinity, oxygen, and phosphorus (Figure 4-1). Nitrogen and silicate do not limit growth in Lake Superior (*Sterner et al.*, [2004]) and are therefore not included. No external inputs (runoff, precipitation) of carbon, alkalinity, or phosphorus to Lake Superior are included. Thus, to conserve mass, there is no sedimentation, which is observed to be small (0.4 TgC/yr) [*Heinen and McManus*, 2004]. Organic phosphorus and carbon remineralize at the bottom of the lake and become available for photosynthesis after mixing back to the epilimnion.

Soluble reactive phosphorus (SRP) and dissolved inorganic carbon (DIC) are transformed into organic matter by the explicit ecosystem (see below) and are transported out of the epilimnion as dissolved or particulate organic matter. The matter is remineralized by the implicit microbial loop with a maximum remineralization rate of  $0.2 \text{ d}^{-1}$  [*Urban et al.*, 2005], which is modified by temperature according to *Moore et al.* [2002].

$$rate_{remin} = remin_p * tfunc$$

Equations 4-4-1 and 4-4-2

$$tfunc = \exp(tbase * [(1/TempK) - (1/tnorm)])$$

Although we do not include the nitrogen cycle in the model, we assume that for each mol of phosphorus consumed by the phytoplankton that 16 moles of  $\text{NO}_3$  are also consumed (Redfield Ratio). This is used to calculate alkalinity in the model. However, *Kumar et al.* [2008] determined the uptake ratio of C:N in Lake Superior is significantly higher than the Redfield Ratio (6.6), suggesting the N:P ratio in biomass in Lake Superior is closer to 30. The biomass of

Lake Superior prefers to consume ammonium, which requires less energy to utilize. The impact of this preference on alkalinity is ignored in the model. *Urban et al.* [2009b] suggest an uptake ratio of NO<sub>3</sub>:P of 13 (C:P~205, C:NO<sub>3</sub>~13), but still, the impacts of ammonium uptake on alkalinity should be evaluated and the alkalinity parameterization improved if necessary.

$$\frac{dAlk}{dt} = -R_{np} * \frac{dPO_4}{dt}$$

Equations 4-4-3 and 4-4-4

$$\frac{dPO_4}{dt} = \text{remineralization} - \text{uptake}$$

Lake pH is calculated from alkalinity, dissolved inorganic carbon (DIC), and temperature according to CO<sub>2</sub>sys and is used to calculate the partial pressure of carbon dioxide (pCO<sub>2</sub>) in the lake surface waters [*Lewis and Wallace*, 1998]. The flux of carbon dioxide across the lake-air interface is determined by wind speed and the difference in pCO<sub>2</sub> between the atmosphere and the lake according to *Wanninkhof* [1992]. Weekly values of atmospheric concentrations of carbon dioxide above Lake Superior are from Carbon Tracker for 1979-2006 [*Peters et al.*, 2007]. We include the effects of atmospheric pressure on atmospheric pCO<sub>2</sub> [*Sarmiento and Gruber*, 2006].

#### 4.4.2 Explicit Ecosystem Model

The medium-complexity ecosystem model (Figure 4-1) of *Dutkiewicz et al.* [2005] is modified for Lake Superior's freshwater system. The ecosystem consists of two phytoplankton classes (picoplankton and diatoms), one zooplankton class, and an implicit microbial loop. The model

includes co-limitation by phosphorus and light. Full ecosystem equations are available in *Dutkiewicz et al.*, [2005].

The simplest model is used in attempt to capture the major features of Lake Superior's productivity and carbon cycle. Phosphorus and carbon are traced in their organic and inorganic forms, as well as alkalinity, a total of twelve tracers. Dissolved inorganic nutrients (P, DIC) are taken up by phytoplankton during photosynthesis and transformed into organic matter (P,C in phytoplankton). The model then recalculates pH based upon the resulting DIC and alkalinity for the given temperature. Rates of photosynthesis are modified by temperature, the availability of photosynthetically active radiation (I), and phosphorus (P), according to a Michaelis-Menton type parameterization [*Sarmiento and Gruber*, 2006]. Small and large phytoplankton have separate growth rates (Table 4-1) (Equations 4-4-5 and 4-4-6).

$$\mu_{phy1} = \mu_{phy1_{max}} * \left(\frac{k_{P1}}{P + k_{P1}}\right) * \left(\frac{k_{I1}}{I + k_{I1}}\right) * tfunc$$

Equations 4-4-5 and 4-4-6

$$\mu_{phy2} = \mu_{phy2_{max}} * \left(\frac{k_{P2}}{P + k_{P2}}\right) * \left(\frac{k_{I2}}{I + k_{I2}}\right) * tfunc$$

The ratio of carbon to phosphorus uptake in phytoplankton is assumed constant (C:P ~ 200) [*Urban*, 2009].

PAR is assumed to be 40% of the incoming shortwave radiation at the lake surface ( $I_0$ ) [*Frouin and Pinker*, 1995] and is attenuated within the water column by water and chlorophyll according to Beer's Law (Equation 4-4-7).

$$I(z) = I_0 e^{-(k_w + k_c)z} \quad \text{Equation 4-4-7}$$

The presence of ice reduces light penetration proportional to its areal coverage, as in the physical model [Bennington *et al.*, 2010]. For example, we assume that when a model grid cell is 40% ice covered, 60% of the PAR penetrates to the lake surface.

Zooplankton graze on both phytoplankton classes at a rate modified by the available phosphorus in phytoplankton, but small phytoplankton are more palpable (Table 4-1). Only a portion of grazed material is assimilated by the zooplankton (*gampn*). Organic nutrients may pass from phytoplankton to zooplankton or are lost to the dissolved and particulate organic matter pools during sloppy grazing and upon mortality of phytoplankton or zooplankton (Equations 4-4-8 through 4-4-12).

$$graz_{phy1} = zoograze * zplat * \left( \frac{phy_1}{zplat * phy_1 + zplat2 * phy_2} \right) * \left( \frac{zoo}{zoo + plim} \right) * tfunc$$

$$graz_{phy2} = zoograze * zplat2 * \left( \frac{phy_2}{zplat * phy_1 + zplat2 * phy_2} \right) * \left( \frac{zoo}{zoo + plim} \right) * tfunc$$

$$\frac{dZoo}{dt} = graz_{phy1} * gampn * zoo + graz_{phy2} * gampn * zoo - mortz * zoo$$

$$\frac{dPhy_1}{dt} = phy_1 * \mu_{phy1} - graz_{phy1} * zoo - mort * tfunc * phy_1$$

$$\frac{dPhy_2}{dt} = phy_2 * \mu_{phy2} - graz_{phy2} * zoo - mort_2 * tfunc * phy_2$$

Dissolved organic matter does not sink but may be transported lower into the water column during a mixing event. Particulate organic matter sinks with a rate of 0.5 m/d [Chai and Urban,



2004] through the water column. All tracers are subject to horizontal diffusion and advection within the three dimensional circulation model. Both dissolved and particulate organic matter are remineralized by the implicit microbial loop at a rate of  $0.2 \text{ d}^{-1}$  modified by temperature (Section 4.4.2) and return to the dissolved inorganic pool.

Chlorophyll concentrations are estimated from biomass and light availability, allowing for photo-adaptation of phytoplankton, according to Equation 4-4-13.

$$Chl = [Chl : P_{\max} - (Chl : P_{\max} - Chl : P_{\min}) * \min(PAR / istar, 1)] * (phy_1 + phy_2) \quad \text{Equation 4-4-13}$$

A full list of model parameters is given in Table 4-1.

The full cycle of oxygen is modeled within the water column. Oxygen is released to the lake during photosynthesis and utilized during the decomposition of organic matter. Thus, the rate of change of oxygen concentration in the subsurface of the lake is modeled as in Equation 4-4-15.

$$\frac{dOxy}{dt} = R_{op} * (\mu_{phy1} * phy_1 + \mu_{phy2} * phy_2 - rate_{remin} * (DOP + POP)) \quad \text{Equation 4-4-15}$$

The ratio of oxygen to phosphorous in the model is the Redfield Ratio of 170 [Sarmiento and Gruber, 2006]. At the lake surface, the air-lake exchange of oxygen impacts surface concentrations. I use the piston velocity parameterization from Wanninkhof [1992] and the saturation oxygen concentration ( $O_2s$ ) from Garcia and Gordon [1992] to calculate the air-lake flux of oxygen (Equations 4-4-16 through 4-4-18).

$$piston\_velocity = 0.28 * wdsp^2$$

$$K_{exch} = piston\_velocity / \sqrt{Schmidt_{O2} / 660} \quad \text{Equations 4-4-16 through 4-4-18}$$

$$Flux_{O2} = K_{exch} * (P_{atmos} * O2s - Oxy)$$

Wdsp is local wind speed at 10 m height. The Schmidt number for oxygen is taken from Wanninkhof [1992],  $P_{atmos}$  is the atmospheric surface pressure, and Oxy is the local model surface oxygen concentration.

As seen above (Equation 4-4-15), for every mol of oxygen consumed during decomposition, 1.2 moles of inorganic carbon (DIC) are returned to the water column (Rcp/Rop). Thus, if all of the DIC were created as  $CO_2$ , the model would be assuming a respiratory quotient greater than 1. However, when the water is supersaturated with  $pCO_2$  with respect to the atmosphere, for each mol of DIC created, ~0.9 moles are  $CO_2$ . At low values of  $pCO_2$ , only ~0.6 moles are in the form of  $CO_2$ , due to readjustment of the carbonate system. Thus, the model respiratory quotient is dependent on ambient conditions (pH), but is generally greater or equal to one. The photosynthetic quotient, or the ratio of moles of oxygen created for each mole of  $CO_2$  consumed is similarly formulated in the model and is generally less than one. For most studies of respiration in Lake Superior (eg. Urban *et al.*, [2004]), a respiratory quotient of 1 is assumed. However, studies now indicate that the respiratory quotient may not be 1 in Lake Superior (personal communication James Cotner). Modeled oxygen concentrations would be improved with in situ measurements of these quotients, but the oxygen cycle does not impact the modeled carbon cycle for this study.

## 4.5 No Phosphorus Model Description

We use a low-complexity ecosystem model within a three dimensional lake circulation model. The ecosystem consists of one phytoplankton class and an implicit microbial loop. Carbon and alkalinity cycling are fully coupled within the entire water column. This model was developed by Cory McDonald as part of his PhD thesis at Michigan Technological University and only literature values are used to extend its purpose here.

### 4.5.1 Nutrient Cycling

The model was developed through a formal optimization procedure within a one-dimensional physical model [McDonald, 2010] and includes fully prognostic cycles of carbon, oxygen, and alkalinity (Figure 4-2). Lake Superior is limited by phosphorus; however, *Sterner* [2010] found that net primary production can be predicted (with  $r^2 = 0.93$ ) using only light and temperature. Soluble reactive phosphorus concentrations are often not detectable, and total phosphorus profiles have no known seasonality. Thus, primary production in the no phosphorus model is a function of only temperature and light.

Dissolved inorganic carbon (DIC) is transformed into organic carbon by phytoplankton (Figure 4-2) during photosynthesis. A fraction of the gross primary production (GPP) is immediately excreted as dissolved organic carbon (DOC) or respired back to DIC. The net primary production ( $NPP = GPP - \text{excretion} - \text{algal respiration}$ ) is assimilated into biomass. The rate of net primary production is determined according to *Sterner* [2010], but adjusted to cover an entire 24 hr period. Phytoplankton die according to a temperature dependent mortality (Equation 4-5-1) rate

that implicitly includes the effects of zooplankton grazing. Live phytoplankton sink with a rate adjusted by water density.

$$\text{sink}_{phy} = \text{tmpsink} * (\text{dens} - \rho_{water}) \quad \text{Equation 4-5-1}$$

A fraction of deceased phytoplankton (fpom) sinks as particulate organic carbon (POC) at a constant rate of 0.1 m/d. A fraction of phytoplankton mortality (fdom) enters the DOC pool, while the remaining fraction (1-fdom-fpom) immediately enters the DIC pool. POC and DOC return to the inorganic pool through implicit bacterial decomposition with a timescale of 100 days that is modified by water temperature according to Equations 4-5-2 and 4-5-3:

$$tfunc_{remin} = \text{thetar}^T$$

$$tfunc_{mort} = \text{thetam}^T$$

Productivity and remineralization alter lake alkalinity throughout the entire water column as in the phosphorus model (Section 4.4.2). Lake chlorophyll, pH, pCO<sub>2</sub>, and CO<sub>2</sub> fluxes are determined as in the phosphorus model (Section 4.4.1).

### 4.5.2 No Phosphorus Ecosystem Model

A schematic of the no phosphorus model is shown in Figure 4-2. The relationship between light, temperature, and production from *Sterner* [2010] is assumed correct (with night correction below), and therefore not put through the optimization process. The model parameters that are optimized in the formal process are referenced as *McDonald* [2010] in Table 4-2 and include mortality and remineralization rates; chlorophyll to carbon ratios; temperature effects on mortality, grazing, and decomposition rates; sinking rates; and fractions of deceased phytoplankton entering the POC and DOC pools. Some literature values (Table 4-2) are used to

connect this ecosystem with the atmosphere via the inclusion of respiration air-lake CO<sub>2</sub> exchange.

Primary production is calculated in moles of carbon according to *Sterner* [2010], adjusted for a 24 hr period according to *McDonald* [2010]. To do this, it is assumed that rates of respiration and excretion remain constant overnight at their daytime rates. Thus, 1/3 of daily respiration and excretion are unaccounted for in *Sterner's* estimate of NPP. Excretion is assumed to be 13% of NPP [*Baines and Pace*, 1991]. C-14 production is estimated to be 45% of GPP measured via O<sub>2</sub> production (GPP\*), according to JGOFS studies [*Bender et al.*, 1999; *Laws et al.*, 2000]. However, O<sub>2</sub> production overestimates GPP of carbon by 15% [*Bender et al.*, 1999] due to photorespiration and Mehler reaction effects. Solving equations 4-5-1 through 4-5-3:

$$NPP = 0.45GPP^* \quad (4-5-4)$$

$$GPP = 0.85GPP^* \quad \text{Equations (4-5-5)}$$

$$Excretion = 0.13NPP \quad (4-5-6)$$

NPP is 53% of GPP, and excretion is 7% of GPP. Respiration is assumed to be the remaining 40% of GPP. *McDonald* [2010] assumes that respiration and excretion continue to occur at their daily rates. Over a 24 hr period, *Sterner's* [2010] net primary production is reduced due to unaccounted for nighttime losses. 24 hr NPP is therefore a fraction of daytime NPP. This fraction is determined through Equations 4-5-7 through 4-5-11 as follows:

$$GPP = (NPP + \text{respiration} + \text{excretion})$$

$$GPP_{day} = 0.53GPP + 0.4GPP_{day} + 0.07GPP_{day}$$

$$GPP_{night} = (1/3)(0.4GPP_{day}) + (1/3)(0.07)GPP_{day} = 0.157GPP_{day}$$

$$NPP = NPP_{Sternier} - GPP_{night}$$

$$NPP/NPP_{Sternier} = (0.53/0.687) = 0.77$$

Thus, net primary is assumed to be 77% of *Sternier's* [2010] estimate:

$$NPP = 0.77 * \text{temp\_func} * \text{light\_func}$$

$$\text{temp\_func} = C_{npp} * \exp\left(\frac{-E_a}{[T_K * T_{coeff}]}\right) \quad \text{Equations 4-5-12 through 4-5-14}$$

$$\text{light\_func} = P_{opt} * (1 - \exp(-\alpha * \frac{PAR}{P_{opt}}))$$

where  $C_{npp}$ ,  $P_{opt}$ ,  $T_{coeff}$ , and  $\alpha$  are constants determined by *Sternier* [2010], listed in Table 4.2.

Light is attenuated within the water column according to Beer's Law including the effects of self-shading (Equation 4-4-7), and 3-hourly light is used for calculating instantaneous NPP.

Respiration and excretion are determined as fractions of NPP to determine GPP:

$$GPP = NPP(1 + f_{res} + f_{exc}) \quad \text{Equation 4-5-15}$$

Chlorophyll is determined as in the phosphorus model, although there is only one phytoplankton type in this case, according to Equation 4-4-13.

Whether this correction to *Sternier's* [2010] production estimate is necessary or not is currently unknown by the author, and further discussion between authors is required.

## 4.6 Main Differences Between Models

Major differences between the two models result in different seasonal cycles of primary productivity and  $p\text{CO}_2$ . Productivity in the phosphorus model was hand tuned to best-fit estimates by *Sterner* [2010] in modeled light conditions by adjusting growth rates, mortality rates, remineralization rates, and fractions of deceased matter entering particulate and dissolved pools. In the no phosphorus model, *McDonald* [2010] uses the results from *Sterner* [2010] to determine model NPP.

The phosphorus model has a lower PAR attenuation coefficient and more rapid remineralization of carbon and phosphorus ( $20\% \text{ day}^{-1}$ ) to increase primary productivity closer to estimates by *Sterner* [2010]. However, in the phosphorus-limited model, the epilimnion becomes depleted in soluble reactive phosphorus during summer, so its productivity peak is earlier than in the NPM. Production in the NPM is dependent only on light and temperature, so production peaks during late summer. Remineralization occurs at a rate of  $1\% \text{ d}^{-1}$ . The lack of phosphorus decouples production from remineralization in the NPM. Annual production in the NPM is actually lower than in the phosphorus model ( $4\text{-}50 \text{ gC/m}^2/\text{yr}$ ), but productivity occurs when the lake is warmest. This reduces summer  $p\text{CO}_2$  in the NPM of Lake Superior, as compared to the PM. The NPM has a higher PAR attenuation coefficient, thereby reducing the depth of the euphotic zone and increasing light limitation in the model, but each model has a different critical light value, so the deep chlorophyll maximum is located at about the same depth in both models.

The phosphorus model is a logical development from the knowledge that Lake Superior is phosphorus-limited. It allows for an interaction between lake dynamics and biology, such as

upwelling and mixing events that boost biological productivity via the supply of nutrients. However, we do not understand phosphorus dynamics in Lake Superior, largely because concentrations are at or under detection limits. Thus, we do not have a good basis on which to develop parameterizations. The NPM neglects any limitation by phosphorus; thus, upwelling and mixing events could actually reduce primary productivity by cooling the surface waters. However, the NPM is the simplest model that can be constrained by available observations and was tuned to best-fit measurements of biological parameters off the Keweenaw Peninsula during the late 1990s [McDonald, 2010].

## 4.6 Model – Observation Comparisons

Modeled chlorophyll at EPA stations (Figure 3.1) during the spring of 1997 is shown against EPA snapshot measurements of chlorophyll in Figure 4.3. Low values of chlorophyll are seen throughout the water column in both models and in observations. Neither model out-performs the other during the spring of 1997 and both models show reasonable spring chlorophyll profiles. During the warm El Niño year of 1998 (not shown), modeled surface chlorophyll during spring in the PM is too high, as production has already taken off. In the spring of 2002 (not shown), observations suggest chlorophyll values of 1 mg/L throughout the water column, which is only captured in the PM. Figure 4.4 shows modeled chlorophyll in the ecosystem models against discrete observations taken by the EPA during the summer of 1999. Both ecosystem models are able to produce a deep chlorophyll maximum (DCM), as observed in Lake Superior [Barbiero and Tuchman, 2004; Sterner, 2010] at 25-35 m. These chlorophyll maxima are not coincident with maxima in primary productivity, consistent with observations [Barbiero and Tuchman,



2004; *Sterner*, 2010]. Surface chlorophyll in the PM is generally too high during summer, even when the value of the deep chlorophyll maximum is captured, as at station SU02. However, during 2006 (not shown), high surface EPA chlorophyll values are captured by the PM. Chlorophyll in the NPM is lower at the surface, as seen in observations, with a deep chlorophyll maximum and compares very well to summer EPA measurements. Both models capture spring and summer chlorophyll profiles as observed by the EPA reasonably well. In summary, the NPM does a better job overall capturing both seasons, but in a few years, the PM out-performs the NPM.

The mean seasonal cycles of productivity in both ecosystem models are shown against estimates of productivity calculated using *Sterner's* [2010] equation, utilizing modeled temperature and light conditions, in Figure 4.5. The phosphorus model captures winter and spring levels of primary productivity estimated by *Sterner* [2010]. However, summer primary productivity is reduced due to the removal of soluble reactive phosphorus within the euphotic zone by spring primary production. Although DOC and POC rapidly remineralize with a time scale of only 5 d to implicitly include the microbial loop, phosphorus is not available fast enough for model phytoplankton to increase NPP during the height of the summer. Phytoplankton may receive a supply of phosphorus from zooplankton migration or terrestrial inputs during summer that would reduce nutrient limitation if added to the phosphorus model. Soluble reactive phosphorus levels are at or near detection level much of the year in Lake Superior; thus, the cycle of SRP is poorly understood.

The seasonal cycle of primary production produced by the no phosphorus model follows temperature and light. Summer growth is not limited by nutrient depletion. Thus, NPP peaks during late summer in the NPM. The NPM has lower levels of annual net primary production (3.4 TgC/yr, GPP = 6.5 TgC/yr), but the bloom occurs when the lake is warmest. Recall that modeled production in NPM includes a night correction factor of 0.77 that is not included in the plot of estimated production according to *Sterner* [2010], and that production itself is determined by *Sterner's* [2010] equation with this correction factor. Further discussion with the authors (*Sterner*, *McDonald*) is required to optimize this comparison. Thus, Figure 4.5 is not an internally consistent method of model-observation comparison, but rather provides the reader with seasonal cycles and magnitudes of productivity in both models.

Modeled rates of gross primary production agree well with the estimates of *Cotner et al.*, [2004] (5.3–8.21 TgC/yr) and *Urban et al.* [2005] (3-8 TgC/yr). The lower level of net primary production is due to the larger PAR attenuation coefficient in the NPM and the strong effect of light on NPP. The PM has higher levels of annual net primary production (65 gC.m<sup>2</sup>/yr; 5.3 TgC/yr), still lower than the most recent estimate of primary production (9.73 Tg C y<sup>-1</sup> *Sterner*, [2010]). It is unable to maintain production through summer, and thus, cannot achieve production estimates of *Sterner* [2010]. Since the same physical model is used in conjunction with both ecosystem models, and the ecosystem does not feed back on lake dynamics, differences in productivity also lead to differences in the cycles of lake surface pCO<sub>2</sub>.

### 4.6.1 Observations of pCO<sub>2</sub>

The EPA visits 19 stations lake-wide twice each year, once in April or May, and again in August or September (Figure 3-1). EPA samples are snapshots, sometimes taken overnight when respiration (no photosynthesis) and cooling occur. *In situ* water temperature at four depths during April and at six depths during August are measured, and water samples are collected and brought back to the lab. Alkalinity and pH are measured after heating the water samples to 25°C. To estimate pCO<sub>2</sub> values at the lake surface, we first correct the measured pH to *in situ* water temperatures, assuming no change in DIC [Atilla *et al.*, 2010]. Then, pCO<sub>2</sub> is estimated using temperature, pH, alkalinity and CO<sub>2</sub>sys with freshwater constants [Lewis and Wallace, 1998].

#### *Uncertainty in Indirect Techniques of Freshwater pCO<sub>2</sub> Estimation*

Uncertainty in estimates of pCO<sub>2</sub> from observations of temperature, pH, and alkalinity is significant and may be biased. pH electrodes have a mean bias of -0.137 pH units in freshwater [French *et al.*, 2002]. Before stratification, an underestimate of pH in Lake Superior would cause an overestimate of pCO<sub>2</sub> by more than 250 µatm (at 3°C, 838 meq/m<sup>3</sup> alk). During summer, this pH bias could cause an overestimate of >100 µatm. From comparison to nearby direct measurements of pCO<sub>2</sub> in 2001, Atilla *et al.*, [2010] conclude that estimates of pCO<sub>2</sub> from EPA data are reasonable without the application of any correction. Year to year changes in accuracy of pCO<sub>2</sub> estimates using EPA pH may exist (1999 for example), and 2001 is potentially a year of less bias, given that estimates of spring time pCO<sub>2</sub> from observations are indistinguishable from the atmosphere and generally lower than other years. Clearly, indirect techniques are an issue when trying to elucidate the lake's surface pCO<sub>2</sub>, and improved methodologies are needed [NOAA, 2010].

Two time series of direct measurements of  $p\text{CO}_2$  are known to exist for Lake Superior, but only one was available for model comparison. A mooring was deployed at 12 m depth in the western arm of Lake Superior from June to September in 2001, 7.5 km offshore from the Split Rock Light House near Duluth (47.19°N, 91.34°W, Figure 3-1). The mooring was equipped with a Submersible Autonomous Moored Instrument for  $\text{CO}_2$  (SAMI- $\text{CO}_2$ ) [DeGrandpre *et al.* 1995; Baehr and DeGrandpre, 2002, 2004] and a temperature sensor. The SAMI collected half hourly data from June 6, 2001 through September 11, 2001.

#### 4.6.2 Model-Observation $p\text{CO}_2$ Comparisons

Figure 4.6 shows model  $p\text{CO}_2$  at the seventeen non-coastal EPA stations against estimates of  $p\text{CO}_2$  from Atilla *et al.*, [2010]. The EPA is unable to reach all stations on the same day or night, and I plot all daily average model  $p\text{CO}_2$  at each station within the month of sampling. For spring and summer sampling months between 1996 and 2006, I use whisker box plots to show the spread in estimated and modeled  $p\text{CO}_2$  values at the 17 lake wide stations. The low end of the box illustrates the lower quartile of values, the median is notched, and the upper quartile is the top of the box. The lines extending from the boxes show the range of non-outlier  $p\text{CO}_2$  values. Outliers are illustrated with crosses.

$p\text{CO}_2$  in the PM (top in magenta) looks reasonable compared to estimates of Atilla *et al.* [2010]. Model predictions of springtime  $p\text{CO}_2$  in Lake Superior are generally lower than observed. August  $p\text{CO}_2$  is often higher than suggested by observations, but never above the highest

estimated value. Neglecting any uncertainty in estimate techniques (see 4.5.1), modeled  $p\text{CO}_2$  is lower than estimates during five of the eleven springs and higher than observational estimates during two springs. Observations suggest a much larger spatial heterogeneity in spring  $p\text{CO}_2$  than the model, although some of this may be due to the comparison between instantaneous measurements and daily average model predictions. Modeled spring  $p\text{CO}_2$  is statistically different from EPA estimates (2-sided t-test, 95% confidence level,  $p = 0.01$ ), but  $p\text{CO}_2$  in the model and observations during the summer are not statistically unique (2-sided t-test, 95% confidence level,  $p=0.27$ ). Assuming a mean pH bias in EPA observations causes observational estimates of  $p\text{CO}_2$  to be lower than modeled during both seasons (t-test,  $p = 0$ ). These comparisons also support the suggestion by *Atilla et al.*, [2010] that observations during the spring of 1999 are erroneous, potentially due to methodological or calibration problems.

$p\text{CO}_2$  from the NPM is shown in the bottom panel in blue of Figure 4.6. Summer  $p\text{CO}_2$  in the NPM is clearly lower than spring values from a biological drawdown of DIC during the height of summer. Modeled summertime  $p\text{CO}_2$  is statistically lower than suggested by observations (t-test,  $p = 0$ ). If pH measurements taken by the EPA have a mean bias of -0.137 pH units, then summer  $p\text{CO}_2$  in Lake Superior is statistically lower than modeled (t-test,  $p=0$ ). The NPM has slightly higher  $p\text{CO}_2$  during spring than the PM, because biological productivity is reduced during this time in the NPM. Modeled spring  $p\text{CO}_2$  cannot be distinguished from observational estimates (t-test,  $p = 0.11$ ). Observations suggest that modeled  $p\text{CO}_2$  is too low during summer in the NPM and too low during spring in the PM. Clearly, model-observation comparisons would be improved with knowledge of the uncertainty in pH measurements taken by the EPA. However, there is also unknown uncertainty in modeled values, including an unknown modeled diurnal

cycle of  $p\text{CO}_2$ . The largest model uncertainties arise from a warm temperature bias in the forcing and errors in ecosystem dynamics. Neither model agrees with EPA estimates of *Atilla et al.* [2010] for both April and August, but both seasons are adequately captured by one model. Both models and data suggest a super-saturation of carbon dioxide during April and a near equilibrium or under-saturation during summer.

Model pH is calculated from modeled alkalinity, DIC, and temperature. Modeled temperatures are warmer than observed due to forcing and model deficiencies (Chapter 3). Modeled alkalinity in the PM varies only by a couple  $\text{meq/m}^3$  within a year at a given location, and root mean square error between the model and EPA surface observations between 1996 and 2006 is 28 and 22  $\text{meq/m}^3$  during spring and summer, respectively. Model alkalinity is impacted by biological production; the impacts of river runoff, precipitation, and evaporation are not included. Thus, the modeled seasonal cycle is weak, leading to error in modeled pH and  $p\text{CO}_2$ . Modeled pH has a root mean square error (RMSE) of 0.20 and 0.11 pH units during spring and summer, respectively. In the NPM, spring RMSE of pH is 0.21, and during summer, the RMSE of pH is 0.18. These errors are larger than the mean freshwater electrode pH measurement bias (-0.137). EPA does not directly measure DIC, so no comparison is done here. Thus, model error in predicting observed  $p\text{CO}_2$  is due to the combination of model errors in temperature, alkalinity, and DIC.

Figure 4.7 shows local modeled grid cell  $p\text{CO}_2$  at the surface and 12.5 m in both models, versus SAMI recorded  $p\text{CO}_2$ . Estimates from the nearest EPA station are shown with red markers. The SAMI data suggests a subsurface super-saturation with respect to the atmospheric value of 364

$\mu\text{atm}$  during spring and a substantial decrease in  $\text{pCO}_2$  during summer. The decrease begins in June, but is dynamic and increases again in July until a substantial local decrease in DIC causes a large under-saturation in August. The large fluctuations were likely caused by internal waves along the thermocline causing the instrument to move in and out of the epilimnion [Atilla *et al.*, 2010]. The NPM shows a decrease in  $\text{pCO}_2$  in the local model grid cell beginning in May when the model warms (NARR forcing bias) and continues to decrease throughout summer as the lake warms and light increases. The PM, however, shows a larger decrease in May from a higher rate of NPP and an increase again to mid June.  $\text{pCO}_2$  throughout summer remains higher than in the NPM. Decreases in  $\text{pCO}_2$  in the PM at 12.5 m occur during increases in the NPM, also suggesting that internal waves bringing up colder water with more nutrients cause phytoplankton growth and DIC consumption in the PM. The NPM instead reduces NPP with the arrival of colder water, because colder water suppresses productivity. Neither model is able to fully capture the localized drawdown observed by the SAMI. The phosphorus model captures the effects of lake dynamics on  $\text{pCO}_2$  and has reasonable values of  $\text{pCO}_2$  for the time-period. The NPM is unaffected by local nutrient changes, and  $\text{pCO}_2$  declines throughout summer as NPP increases.

Two models are used to simulate biological productivity in Lake Superior between 1979 and 2006. While the phosphorus model has higher spring productivity and less skill predicting chlorophyll, dynamic effects on productivity make it a useful mechanistic tool at local levels. Estimates of lake-wide  $\text{pCO}_2$  from EPA observations suggest both models are adequate. The NPM captures chlorophyll profiles well, and provides a nice overview of the large-scale lake productivity. It is inadequate at local scales, where it does not allow variability in nutrient supply

to stimulate productivity. Since both models have their own strength, I will look at annual  $p\text{CO}_2$  cycles and mechanisms in both models.

## 4.7 Results

### **The Seasonal Cycles of $p\text{CO}_2$ and $\text{CO}_2$ Fluxes in Lake Superior**

The seasonal cycles of  $p\text{CO}_2$  for 1997-2000 are shown from both models, EPA estimates, and the atmosphere at Park Falls, WI in Figure 4.8. Atmospheric partial pressure of  $\text{CO}_2$  is shown with green dashed lines. Lake-wide average surface  $p\text{CO}_2$  in the phosphorus model is shown with a thick red line. The thin red dashed line indicates one standard deviation above and below modeled  $p\text{CO}_2$  values lake-wide on that day. The NPM is depicted in blue and blue dashed lines. Both models show a super-saturation of  $\text{CO}_2$  with respect to the atmosphere during winter (NDJ). Both models suggest the twice-yearly lake overturn has significant impacts on the  $p\text{CO}_2$  cycle. The lake outgases during the late fall overturn, ventilating the entire water column, causing a uniform profile of DIC. As the lake reaches its coldest temperatures near February,  $p\text{CO}_2$  decreases and reaches a minimum. The column begins to warm and the weak winter stratification is lost, once again creating a uniform profile of DIC exposed to the atmosphere. This warming again brings the column to an oversaturated state until out-gassing and productivity reduce  $p\text{CO}_2$  in spring.



During all but the warmest of these four years (1998), the lake is under-saturated during late winter (February, March), and into April during one of the coldest years (1997). Productivity decreases  $p\text{CO}_2$  in summer, overwhelming the effects of increasing temperature in the NPM, and the NPM suggests an under-saturation during summer (July-Oct).

Biological productivity decreases springtime  $p\text{CO}_2$  in the PM, but summer production is limited, and the lake is warming. Thus, the PM suggests a lake in near equilibrium with the atmosphere or out-gassing throughout summer. The effect of this lower summer production is a reduced fall/winter  $p\text{CO}_2$  and out-gassing as compared to the NPM (Figure 4.9). The NPM has increased DIC drawdown during summer which increases lake storage of carbon released to the atmosphere during the late fall overturn. EPA data suggests the seasonal cycle in the NPM is more likely, with higher winter and spring  $p\text{CO}_2$ , and a possible under-saturation in summer. The NPM may underestimate summer  $p\text{CO}_2$ , due to the complete lack of nutrient limitation.

The mean monthly cycle of  $\text{CO}_2$  fluxes are shown in the top panel of Figure 4-9. A positive  $\text{CO}_2$  flux is one out of the lake. Both models outgas during fall and early winter and experience an influx when the lake is coldest (end of winter). The phosphorus model suggests the model has almost no efflux during spring, due to increased biological productivity during that season. The lake slowly effluxes throughout summer (rate of  $< 1 \text{ TgC/yr}$ ) and experiences a weak influx at the start of fall cooling. The no phosphorus model effluxes during spring and influxes during summer. Its winter efflux rate ( $2 \text{ TgC/yr}$ ) is twice the rate of the PM winter efflux. Variability in the  $p\text{CO}_2$  and  $\text{CO}_2$  flux cycles result from climatic variability. The daily  $\text{CO}_2$  flux cycles are

shown for both models during 1997 and 1998 in the middle and bottom panes of Figure 4-9, respectively.

1997 was an extremely cold, La Niña year on Lake Superior (although not the coldest), with extensive ice coverage. The ice-free parts of the lake remained a sink of atmospheric carbon into April in both models, since warming and stratification were later than usual. The rest of the year was similar to climatology, with daily flux variations caused by changes in wind speed. In the warm El Niño year of 1998, however, the lake remains neutral or a small source of CO<sub>2</sub> to the atmosphere throughout all of winter. The lake becomes under-saturated with CO<sub>2</sub> earlier in summer in the NPM, due to the effects of temperature on primary productivity out-competing temperature effects on pCO<sub>2</sub>. Primary production in the PM occurred earlier in the year, which is why the NPM is acting as a source during March and April, when the PM model is in near equilibrium with the atmosphere. Therefore, the phosphorus limited system runs out of fuel earlier in the year in the PM and becomes a source of CO<sub>2</sub> to the atmosphere by mid June, as temperatures are still increasing.

The seasonal cycle of pCO<sub>2</sub> in Lake Superior includes a winter super-saturation and efflux and late winter under-saturation and resulting influx of carbon dioxide. The mean CO<sub>2</sub> flux over 1979-2006 suggests a small influx of 0.015 TgC/yr, due to the increase in atmospheric CO<sub>2</sub> over this time period.

Surface waters in Lake Superior are super-saturated with CO<sub>2</sub> during spring. As the lake warms, biological production increases. The two models disagree about summer pCO<sub>2</sub> in the lake,

because of the strength and timing of their blooms. The NPM model suggests an under-saturation and influx throughout summer, while the PM suggests the lake is in equilibrium or a small source to the atmosphere. Thus, seasonal variability in lake temperature alters the thickness of the water column interacting with the atmosphere and the biological production within that column. The cold winters expose an entire lake water column to the atmosphere, but an efflux and low temperatures reduce the column  $p\text{CO}_2$ . Weak stratification and extremely cold temperatures at the end of winter result in an influx. This influx is almost immediately lost back to the atmosphere at the loss of winter stratification, when the entire column is again interacting with the atmosphere and warming. Upon summer stratification, biological productivity modulates the effects of increasing temperatures on lake surface  $p\text{CO}_2$ . Only the mixed layer is interacting with the atmosphere, and a DIC gradient between the surface and subsurface waters is created by biological productivity and reduced subsurface temperatures. It is reasonable to hypothesize that more biological productivity in summer would draw down more DIC and increase the fall/early winter efflux, but productivity is also increased during increasing temperatures. So what really controls year-to-year variability in the lake's  $p\text{CO}_2$  and  $\text{CO}_2$  cycles?

#### **4.7.1 Mechanisms of $\text{CO}_2$ Flux Variability**

Both ecosystem models suggest that over the course of a year, Lake Superior has more than one period of super-saturation. The NPM suggests two periods of under-saturation and two periods of super-saturation. Thus, for determining mechanisms controlling inter-annual variability in the lake's carbon cycle, I divide each year (Nov 1 – Oct 31) into four seasons. Feb 14 – April 15 is the late winter period, when the lake is cold and serves as a sink of atmospheric  $\text{CO}_2$ . During spring (April 16 – June 15), the lake overturns and warms, acting as a source of  $\text{CO}_2$  to the

atmosphere on the mean. Over the summer period, June 15 – October 31, the biological productivity draws down surface DIC, reducing surface  $p\text{CO}_2$ , and causing the lake to take up atmospheric carbon dioxide. The PM suggests the lake may be more neutral during this time period. During winter (Nov 1– Feb 13), Lake Superior effluxes inorganic carbon from its entire water column before cooling (and losing enough carbon to the atmosphere) and once again becoming a sink. I analyze both model results using the same four seasons for consistency. I investigate the mechanisms controlling inter-annual variability in annual and seasonal  $p\text{CO}_2$  and  $\text{CO}_2$  fluxes in Lake Superior.

### **Phosphorus Model**

Figure 4.10 shows the mean  $\text{CO}_2$  flux over each of the four seasons in the top left panel and annual net  $\text{CO}_2$  fluxes over the 1980-2005 period in the top right panel. Panels in Figure 4.10(d-f) show seasonal flux anomalies with seasonal anomalies in lake surface temperature (magenta), net primary production (green dashed), wind speed (black), and annual ice coverage (blue dashed). The seasonal flux anomaly is plotted with the corresponding color from Figure 4.10 (a). Annual fluxes (gray) are correlated with fluxes during early winter (NDJF) ( $r=0.45$ ).

Significant year-to-year variability exists in the annual air-lake  $\text{CO}_2$  exchange. Lake Superior acts as a sink of atmospheric carbon in some years and a source in others. Figure 4.10 (c) show yearly anomalies of seasonal and annual carbon dioxide fluxes between 1980-2005 in the PM. Anomalous fluxes during FMA are anti-correlated with anomalous fluxes during the preceding

NDJF ( $r = -0.4$ ,  $p = 0.04$ ). Larger influxes during the FMA period are followed by larger effluxes during AMJ ( $r = -0.55$ ,  $p = 0.003$ ). No other season is correlated with another in the PM.

#### *November – January*

Fluxes between November and February 14 are not significantly correlated with seasonal lake surface temperature, primary productivity, or annual ice coverage. Seasonal  $p\text{CO}_2$  ( $r=0.68$ ) and wind speed ( $r = 0.34$ ,  $p = 0.09$ ) dominate the year-to-year variability in effluxes during this period. Anomalously high  $p\text{CO}_2$  during this season does not significantly correlate to decreases in NPP or increases in lake surface temperature. It does correlate with the preceding season's  $p\text{CO}_2$  ( $r = 0.64$ ). Anomalously high  $p\text{CO}_2$  during this period indicates that  $p\text{CO}_2$  will be lower than average during the next season (FMA,  $r=-0.40$ ).

#### *February – April*

Ice cover does correlate with flux anomalies during this season ( $r = 0.33$ ,  $p = 0.099$ ), suggesting that colder years are years of a smaller influx during this period. Clearly, temperature is dominating the seasonal variability in  $p\text{CO}_2$  during this season, as colder years are significantly correlated with lower  $p\text{CO}_2$  during this season ( $r = 0.93$ ). However, a lower  $p\text{CO}_2$  does not necessarily indicate a greater influx during this period ( $r=0.2$ ), since the  $\text{CO}_2$  flux is also dependent on wind speed. The correlation between increased wind speeds and increased influxes is weak, however ( $r=-0.2$ ), likely because years of higher  $p\text{CO}_2$  are generally years of greater wind speed during this season ( $r=0.7$ ). Primary production during FMA does correlate with air-lake gas exchange, and more productive years have a larger influx during this time ( $r = -0.35$ ,  $p = 0.08$ ). Anomalies in  $p\text{CO}_2$  during this season correlate with annual  $p\text{CO}_2$  anomalies ( $r=0.77$ ).

Higher pCO<sub>2</sub> during FMA also correlates with higher pCO<sub>2</sub> during JJASO ( $r=0.42$ ) and reduced pCO<sub>2</sub> during the preceding season (NDJ,  $r = -0.40$ ).

#### *April – June*

From April to June, an anomalous efflux is driven by anomalously high pCO<sub>2</sub> ( $r=0.74$ ). Wind speeds are not significantly correlated with changes in the seasonal flux. Years of high pCO<sub>2</sub> during this season are also years of enhanced wind speeds ( $r=0.54$ ), but lake temperature and NPP are not correlated with pCO<sub>2</sub>.

#### *July – October*

During July through October, physical mechanisms dominate year-to-year variations in the flux. Warmer lake surface temperatures during this time indicate a larger efflux in the PM ( $r = 0.67$ ,  $p = 0.0004$ ), and years of less ice coverage (warmer years) indicate that Lake Superior will outgas more carbon dioxide than in a typical year during this period ( $r = -0.74$ ,  $p = 0.0001$ ). Increased pCO<sub>2</sub> ( $r=0.43$ ) and wind speeds ( $r=0.34$ ) are the main drivers of the increased flux. Windier conditions allow the warmer water (higher pCO<sub>2</sub>,  $r=0.43$ ) to efflux CO<sub>2</sub> at a more rapid rate during summer ( $r = 0.61$ ,  $p = 0.0009$ ). Biological variability is not a first order control of CO<sub>2</sub> fluxes during this season, as years of higher NPP are also years of higher pCO<sub>2</sub> ( $r=0.76$ ) and a greater seasonal efflux ( $r = 0.76$ ,  $p = 0.0005$ ). Years with anomalously high pCO<sub>2</sub> during April through June are also years of higher pCO<sub>2</sub> during this season ( $r=0.4$ ).

### *Annual Fluxes*

Years of greater effluxes during FMA or NDJ are years of a greater annual efflux ( $r = 0.48$ ,  $p = 0.012$ ;  $r = 0.41$ ,  $p = 0.035$ , respectively). Anomalous fluxes during JJASO and AMJ provide no information about annual flux anomalies. Increases in annual  $p\text{CO}_2$  indicate a reduced influx ( $r=0.36$ ) and appear to be caused by increased temperatures ( $r=0.56$ ). However,  $\text{CO}_2$  fluxes depend on both wind speed and the air-lake  $p\text{CO}_2$  gradient; thus, annual  $\text{CO}_2$  flux anomalies do not significantly correlate with anomalies in either lake surface temperature or wind speed in the PM.

### **No Phosphorus Model Mechanisms**

Figure 4.11 shows the mean  $\text{CO}_2$  flux over each of the four seasons in the top left panel and annual net  $\text{CO}_2$  fluxes over the 1980-2005 period in the top right panel. Significant year-to-year variability exists in the annual air-lake  $\text{CO}_2$  exchange. Lake Superior acts as a sink of atmospheric carbon in some years and a source in others. Figure 4.11 (c) shows yearly anomalies of seasonal and annual carbon dioxide fluxes between 1980-2005 in the NPM. Annual fluxes (gray) are correlated with fluxes during early winter (NDJF) ( $r=0.45$ ). Panels in Figure 4.11(d-f) show seasonal flux anomalies with seasonal anomalies in lake surface temperature (magenta), net primary production (green dashed), wind speed (black), and annual ice coverage (blue dashed). The seasonal flux anomaly is plotted with the corresponding color from Figure 4.11 (a).

### *February – April*

Lake Superior acts as a sink of atmospheric  $\text{CO}_2$  from mid February to mid April in the NPM. Anomalously high  $p\text{CO}_2$  reduces this influx ( $r=-0.66$ ).  $p\text{CO}_2$  increases during this period are driven by increases in lake temperature ( $r=0.96$ ). Net primary production increases in warmer

temperatures. NPP is not strong enough to overcome the effect of temperature on  $p\text{CO}_2$  during this season, as years of higher NPP are also years of increased  $p\text{CO}_2$  ( $r=0.79$ ). Years of warmer lake surface temperature from February-April are also years of faster winds ( $r=0.72$ ) and an increased efflux ( $r=0.64$ ).

#### *April-June*

On the mean, this period acts as a source of  $\text{CO}_2$  to the atmosphere in the NPM. When wind speeds and  $p\text{CO}_2$  are increased, this efflux is also increased ( $r = 0.44$ ;  $r=0.87$ ), but temperature and ice coverage do not significantly correlate with inter-annual variability in this spring efflux. No single mechanism controls anomalies in seasonal  $p\text{CO}_2$  in the NPM model. A larger influx of carbon dioxide during February through April does correlate with a larger efflux between April and June ( $r=-0.55$ ). A larger efflux during this period also indicates an anomalous efflux over the entire year ( $r = 0.525$ ,  $p = 0.006$ ).

#### *July-October*

In the NPM, biological productivity peaks during this period, and although temperatures peak as well, the biological drawdown of DIC dominates the mean flux during this period (influx). Greater biological productivity indicates a season of a larger influx than a typical year ( $r = -0.48$ ,  $p = 0.013$ ). Anomalous influxes during this period are driven by decreases in  $p\text{CO}_2$  ( $r=0.66$ ). Although anomalous warmth would alone increase  $p\text{CO}_2$ , it is a driver of biological productivity in the NPM. Warmer years are in fact years of a larger influx between July and October, due to this increase in biological productivity ( $r = -0.48$   $p = 0.014$ ).  $p\text{CO}_2$  does not correlate with lake



surface temperatures during this season. Anomalous wind speed does not significantly correlate with increases or decreases in the mean seasonal flux.

#### *November – Feb 14*

The yearly winter efflux that occurs between November and mid February is increased by anomalously high (de-trended) pCO<sub>2</sub> (r=0.5) and increased wind speeds (r=0.43). The increased pCO<sub>2</sub> is not caused by any single mechanism during the same season. A larger efflux during this season correlates with a larger annual efflux (r = 0.54).

#### *Annual Fluxes*

Decreases in the annual net sink are significantly correlated with increased annual pCO<sub>2</sub> (r=0.65) and increased wind speeds (r=0.34). This increase in annual pCO<sub>2</sub> is due to increased lake surface temperatures (r=0.43). Warmer years are also years of increased net primary production (r=0.85), thus years of higher productivity are also years of increased pCO<sub>2</sub> and a reduced influx.

### **El Niño, Southern Oscillation**

Lake Superior's temperature is significantly impacted by significant ENSO events. For example, 1998 is one of Lake Superior's warmest years. Thus, it is reasonable to hypothesize that global climate indices such as the Southern Oscillation Index (SOI) may impact the carbon cycle of Lake Superior. Since ENSO is a northern hemisphere winter phenomenon, I correlate annual anomalies in the SOI as averaged July-June with the model results (Nov-October). Correlations between annual and seasonal anomalies in pCO<sub>2</sub>, CO<sub>2</sub> fluxes, wind speed, lake surface temperature, and net primary production are shown in Table 4-8.

The Southern Oscillation Index is significantly correlated (90% confidence level) with annual  $p\text{CO}_2$  ( $r=-0.37$ ) and  $\text{CO}_2$  fluxes ( $r=-0.34$ ) in the phosphorus via a significant correlation with February-April lake surface temperatures ( $r=-0.36$ ) and  $p\text{CO}_2$  ( $r=-0.38$ ). A positive SOI indicates a cool, La Niña year, thus temperatures in February through April are reduced. In the no phosphorus model, the SOI is significantly correlated with FMA  $p\text{CO}_2$  ( $r=-0.33$ ) and NDJ  $p\text{CO}_2$  ( $r=0.4$ ) but not with annual  $p\text{CO}_2$  or annual  $\text{CO}_2$  fluxes.

#### **4.7.2 Empirical Orthogonal Function (EOF) Analysis**

To determine the dominant patterns of variability in the carbon cycle of Lake Superior and its physical drivers, I perform EOF analysis on annual and seasonal anomalies. EOF analysis determines the spatial pattern that explains the maximum percentage of variance of the variable, and its principal component tells us how the magnitude of that pattern varies over time. The first EOF for each season for lake surface temperature, wind speed, NPP,  $p\text{CO}_2$ , and  $\text{CO}_2$  flux and the corresponding principal components are shown in Figures 4-12 through 4-19. The fraction of variance explained by the first EOF for each variable, season, and model are shown in Table 4.9. In Tables 4.10 through 4.14, the first principal components for  $p\text{CO}_2$ ,  $\text{CO}_2$  flux, lake surface temperature, net primary production, and wind speed are correlated with each other and the annual Southern Oscillation Index. I do this for each of the four seasons and for annual anomalies.

## Physical Model Principal Components

### *Lake Surface Temperature (Figure 4-12)*

The first EOF of annual lake surface temperature explains 70% of the variance in annual surface temperature. The entire lake experiences a warming or a cooling, although the warming is strongest where the lake is deepest and in the eastern arm. The western arm has the least annual surface temperature variability. The first EOF of lake surface temperature during FMA explains 69% of the variance. Similar to the first EOF of annual temperatures, warming is greatest in the regions of the lake with lowest ice coverage. Coastal and shallow regions experience the smallest temperature variability in this season, and the deep and open waters of the lake warm the most. Temperature variability during spring (AMJ) shows a larger southern coastal warming and a smaller offshore cooling. This EOF explains 69% of the variance and reflects the near-to-offshore gradient in stratification timing. During summer (JJASO), the western arm warms (cools) the least, and the deepest portion of the lake warms (cools) the most. This EOF explains 88% of the variance in surface temperature during this season. The first EOF of NDJ lake surface temperature explains 66% of the variability and shows a decreased warming (cooling) in the deepest and ice covered parts of the lake, although temperature variability during this season is less than in other seasons.

### *Wind Speed (Figure 4-13)*

82% of the variability in annual wind speed is explained by the first EOF and shows a lake-wide increase (decrease) in wind speeds. Wind speed variance during FMA is significant and greatest over the central basin. During AMJ, the first EOF (69% variance) shows a lake-wide increase or decrease in wind speed. Wind speed variability is largest in magnitude during this season. In

summer (JJASO), wind speed variance is weakest in the western arm and greatest in the eastern arm, although speeds increase or decrease over the entire lake in sync. Early winter (NDJ) wind speeds increase (decrease) the most in the western arm, and this EOF explains 85% of the variance.

## **Phosphorus Model Principal Components**

### *Annual Anomalies*

In the phosphorus model, the first EOF of  $p\text{CO}_2$  explains 52% of the variance. It is significantly correlated with the first principal components of NPP ( $r=0.75$ ),  $\text{CO}_2$  flux ( $r=0.55$ ), the Southern Oscillation Index ( $r=-0.40$ ), and lake surface temperatures ( $r=0.63$ ). The EOF pattern indicates that the largest spatially coherent annual flux anomalies occur in the deep, open waters of Lake Superior, where observations are most inadequate. The principal component of the first EOF of the annual  $\text{CO}_2$  flux in the PM is also significantly correlated to the principal component of the first EOF of NPP ( $r=0.48$ ), lake surface temperature ( $r=0.69$ ), wind speed ( $r=0.45$ ), and the Southern Oscillation Index ( $r=-0.44$ ). The pattern of annual  $\text{CO}_2$  flux variability is most similar to the anomalous  $p\text{CO}_2$  pattern. The first EOF implies that warmer years are years of a greater efflux. This anomalous warming and efflux occur in the deepest portions of the lake, with coastal regions actually experiencing an anomalous, weaker influx. Negative anomalies in biological production are also present in the deepest waters of Lake Superior in the first EOF of NPP, while NPP has a positive anomaly everywhere else.

The greatest anomalies in the CO<sub>2</sub> flux implied by EOF analysis occur during February, March, and April. At this time, the lake is a sink during an average year. However, if the lake is warmer than normal, the lake begins to stratify sooner. Thus, the entire water column must first warm to 3.98°C, and the deepest parts of the lake overturn sooner. The combination of warmer temperatures and an earlier overturn in the deeper portions of the lake causes anomalously high pCO<sub>2</sub> in the open lake. NPP can be reduced here, because the overturn keeps phytoplankton out of the light. Very near shore, some regions experience a reduction in pCO<sub>2</sub>, as biological production begins sooner. The patterns are similar in both models (Figures 4.14, 4.17), although flux and anomaly magnitudes are larger in the NPM during FMA. This pattern of pCO<sub>2</sub> is significantly correlated with the SOI index in both models (Table 4-11) but fluxes only correlate with pCO<sub>2</sub> in the NPM, perhaps because mean productivity in the PM is higher.

Although November through February is a season of large mean efflux and anomalies, the SOI does not significantly correlate with NPP, pCO<sub>2</sub>, CO<sub>2</sub> flux, LST, or wind speed during this time (Table 4-14). Perhaps this is because the first EOF of pCO<sub>2</sub> only explains 32-35% of its variance (Table 4-9, Figure 4-15), since pCO<sub>2</sub> in the NPM is almost significantly correlated with the SOI ( $r=0.33$ ).

The first EOF's of pCO<sub>2</sub>, CO<sub>2</sub> flux, net primary production, and lake surface temperature suggest contrasting behavior between the near shore and deep, open waters of the lake. For seasonal anomalies, some of this behavior is likely due to the long lag between coastal and deep-water stratification and overturn.

## No Phosphorus Model Principal Components

### *Net Primary Production (Figure 4-17)*

Net primary production either increases or decreases lake wide and is significantly correlated with anomalies in lake surface temperature during all seasons (Tables 4-10 through 4-14, ***bold italics***). The first EOF of annual net primary production (Figure 4-17) explains 87% of the variance and shows an increase (decrease) in NPP that is strongest near shore and in the southern part of the lake. Very little year-to-year variability exists in NPP during FMA, but is strongest in the western arm of the lake, as explained (81%) by the first EOF. The first EOF of NPP during AMJ (66% variance) is significantly correlated with the first EOFs of lake surface temperature, pCO<sub>2</sub>, and CO<sub>2</sub> fluxes. Warmer years have increased NPP along the southern coastline, due to an earlier stratification and warming. During summer (JJASO), 83% of NPP variability in the NPM can be explained by the first EOF and shows a larger increase (decrease) in the eastern arm of the lake. The principal component of JJASO NPP in the NPM does not significantly correlate with the first EOF of pCO<sub>2</sub> or CO<sub>2</sub> fluxes. Increased lake cooling in the shallower, coastal regions of the lake during NDJ causes the greatest variability in NPP there (EOF 1, 79% variance), with smaller year-to-year changes in western arm productivity during the early winter. The principal component of this EOF is only significantly correlated with the principal component of the first EOF of lake surface temperatures. This strong relationship between temperature and production is expected in the NPM, as modeled production is only a function of temperature and light.

### *pCO<sub>2</sub> (Figure 4-18)*

The first EOF (48% variance) of annual pCO<sub>2</sub> in the NPM is dominated by variability during late winter and early spring (FMA, AMJ). The EOFs of these two seasons have opposite sign,

agreeing with previous analysis (4.6.1) that suggests timing of the lake overturn has a significant impact of pCO<sub>2</sub> during the early part of the year. Variability in summer (JJASO) pCO<sub>2</sub> explained by the first EOF (65% variance) shows weaker year-to-year anomalies in pCO<sub>2</sub> during summer, with the greatest anomalies along the upwelling region along northwestern coast (north of Duluth). pCO<sub>2</sub> anomalies during NDJ are larger than in summer and greatest in the open lake.

### *Fluxes of Carbon Dioxide*

The EOFs of carbon dioxide fluxes in the NPM show an opposing relationship between near shore and offshore fluxes. During all seasons except summer, an increase in near shore effluxes would suggest a decrease in offshore fluxes, as suggested by EOF analysis. The FMA EOF suggests that warmer years have reduced ice, warmer water, and larger CO<sub>2</sub> flux anomalies occurring in the deep open waters of the lake. Small flux anomalies, some of opposite sign, occur near shore. This pattern just changes sign for the months of AMJ, when positive flux anomalies near shore would indicate negative flux anomalies offshore, according to the first EOF (50% variance). The first EOF of summer CO<sub>2</sub> fluxes has the same pattern as the first EOF of summer pCO<sub>2</sub>. The northwestern coast experiences large CO<sub>2</sub> flux anomalies during this season, of the same sign as most of the lake and all of the open lake. The first pattern of spatial variability of CO<sub>2</sub> fluxes during NDJ is similar to the first EOF of annual CO<sub>2</sub> fluxes, explaining 58% of the variance.

## 4.8 Discussion and Conclusions

I have coupled two unique ecosystem models to a hydrodynamic model of Lake Superior. One model, the phosphorus model (PM) has higher rates of productivity as suggested by *Sterner* [2010], but the inclusion of phosphorus and inadequate phosphorus recycling or mechanisms of supply to the euphotic zone causes summer production rates to be lower than observed. The second model, the no-phosphorus model, determines productivity from light and temperature conditions; thus, productivity is maximized during summer as suggested by observations. However, the lack of the lake's limiting nutrient may cause the NPM to respond contrary to expectations during a mixing event that brings nutrients to the surface. Both models predict spring and summer chlorophyll reasonably well, although the no phosphorus model generally does a better job predicting surface chlorophyll values in summer. Both models predict a single season of pCO<sub>2</sub> within the uncertainty of estimating lake surface pCO<sub>2</sub> from EPA observations of alkalinity, pH, and temperature. Model setup constrains Lake Superior to remain in equilibrium with the atmosphere over long time scales; thus, the lake does not act as a significant source of atmospheric carbon dioxide on annual time scales in either model. However, both models suggest periods of influx and efflux, most significant in the NPM, which may be significant during winter.

Both models agree with *Atilla et al.*, [2010] that Lake Superior is super-saturated with carbon dioxide during April due to warming of the water column, and the phosphorus model suggests August lake surface pCO<sub>2</sub> is near equilibrium with the atmosphere. The NPM suggests that without any external inputs to the lake, Lake Superior should be a sink of CO<sub>2</sub> during summer, when primary production is at its peak. This model is in better agreement with the pCO<sub>2</sub>



estimates of *Atilla et al.*, [2010] between 1997 and 2000 (Figure 4-7) but in disagreement during summer when including all 11 years of observations (1996-2006). Currently, the two models can only provide possible realities of Lake Superior's carbon cycle and include unquantified error. The seasonal cycles of productivity in the two models are unique, yet the resulting pCO<sub>2</sub> cycles are similarly shaped, suggesting a physical dominance in the annual cycle.

Lake Superior is a source of carbon dioxide to the atmosphere during the beginning of winter (N-J), as the lake begins to overturn and the entire water column interacts with the atmosphere.

When the lake reaches its coldest temperatures, it can be weakly stratified with colder waters at the surface, and it acts as a sink of CO<sub>2</sub> between February and March, sometimes into April. As the lake begins to warm again, the entire water column must reach 3.98°C before stratification can occur. Thus, the entire water column is again in contact with the atmosphere as it begins to warm. During this period, the lake outgases carbon dioxide to the atmosphere at a rate of nearly 0.5 Tg C/yr. In the phosphorus model, this efflux is tempered by the start of coastal primary production. Once the lake stratifies, temperatures in the surface waters rapidly increase.

However, due to large variations in the lake's depth and a need to warm the entire water column before stratification, there is significant spatial variability in stratification timing. In the phosphorus model, spring primary production decreases the availability of soluble reactive phosphorus, and summer production is less than during spring. This allows the increase in lake surface temperatures to cause an increase in pCO<sub>2</sub> and a small net efflux during summer on the mean. Productivity is just getting started in the no phosphorus model and peaks at the height of summer. The biological drawdown of DIC overcomes the temperature effect on pCO<sub>2</sub> during summer, and the lake is under-saturated with CO<sub>2</sub>, causing a significant influx at the rate of

nearly 0.5 TgC/yr (Figure 4-11). The summer influx in the NPM allows for a larger net efflux during winter when the lake cools and overturns, as compared to the phosphorus model. Lacking external inputs, both models must equilibrate with the atmosphere over the long term, so between 1979 and 2006, the modeled lake acts as a small sink of CO<sub>2</sub> (0.015 TgC/yr), driven by anthropogenic increases in atmospheric CO<sub>2</sub>. The models show that spring and summer observations of pCO<sub>2</sub> are insufficient to elucidate the full annual cycle of pCO<sub>2</sub> and CO<sub>2</sub> fluxes in Lake Superior. EPA sampling likely misses a period of significant efflux and another of significant influx.

Day to day variability in the CO<sub>2</sub> flux is primarily driven by changes in wind speed, but year to year changes in the flux are harder to understand mechanistically. Annual anomalies in pCO<sub>2</sub> cause anomalies in the CO<sub>2</sub> flux. Both models show that warmer years are years of a reduced sink. Winter anomalies in CO<sub>2</sub> flux (N-J) are most indicative of annual anomalies, suggesting that the observations now available are inadequate for determining inter-annual variability in air-lake CO<sub>2</sub> exchange. Lake Superior open lake surface temperatures increased at a rate of 1.1°C/decade between 1980 and 2005 [*Austin and Colman, 2007*]. The model captures some, but not all of this temperature trend (Chapter 3); thus, the model may underestimate the magnitude of year-to-year variability of the CO<sub>2</sub> flux. If biological production were a first order control on lake-wide CO<sub>2</sub> flux anomalies, years of increased production would be years of an increased sink, because phytoplankton draw down lake DIC concentrations and reduce lake surface pCO<sub>2</sub>. However, in both models, years of increased biological production are years of increased pCO<sub>2</sub>, likely because warmer years are years of increased production in both models.

Global climate indices can also be used to gain insight about Lake Superior's carbon cycle. The Southern Oscillation Index (a positive anomaly being an indicator of a La Niña year) correlates with a reduction in annual  $p\text{CO}_2$  and  $\text{CO}_2$  fluxes in the PM. However, it does not correlate with flux anomalies during any particular season in the phosphorus model, even though lake surface temperature and  $p\text{CO}_2$  are reduced during FMA of a La Niña year. In the NPM, a La Niña winter correlates to an increase in N-J  $p\text{CO}_2$  ( $r=0.40$ ). However, since it does not correlate with temperature, wind, or productivity anomalies during this season, I am uncertain whether there is a true mechanistic cause of this correlation. No other seasonal  $p\text{CO}_2$  or  $\text{CO}_2$  flux anomaly correlates with the SOI in the NPM.

I used principal component analysis to determine anomalous patterns that explain the most variance in each of the relevant carbon cycle components and seasons. Spatially coherent variability in the annual  $\text{CO}_2$  flux is largest in the deep, open waters of Lake Superior, where observations are most rare, and ice coverage least common. This pattern of contrasting behavior from near to offshore waters persists in the other variables, indicating that we must observe both near shore and open waters to fully understand the lake's carbon cycle. To observationally estimate lake-wide  $\text{CO}_2$  fluxes and anomalies, observation stations would best be situated in the deep, open waters of the lake.

The open waters of Lake Superior do not appear to be a significant source or sink of atmospheric  $\text{CO}_2$ , since large seasonal variability in surface  $p\text{CO}_2$  suggested by the observations is captured using only the lake's internal carbon cycle. The significantly earlier and larger net primary production in the phosphorus model only tempers the spring efflux and brings summer  $p\text{CO}_2$  to

slightly supersaturated levels. Even though primary production in the NPM is smaller than most recently estimated by *Sterner* [2010] and *Cotner et al.* [2004], if the summer NPP maximum actually occurs when the lake is warmest, the open waters of Lake Superior may act as a sink of carbon dioxide during summer.

The model is poorly constrained by observational data. Indirect estimates of  $p\text{CO}_2$  are highly and variably uncertain. The carbon budget cannot be brought closer to balanced using EPA data [Atilla et al., 2010]. Frequent indirect estimates of  $p\text{CO}_2$  will do little to close the carbon budget of Lake Superior until the pH bias is known. We are interested in lake  $p\text{CO}_2$ , and instruments are available to directly measure this lake property with an uncertainty of less than  $1 \mu\text{atm}$ . Thus, direct estimates of  $p\text{CO}_2$  are the best method forward. Efforts are currently underway to directly measure  $p\text{CO}_2$  in Lake Michigan, using an automated sensor attached to the ferry [Bootsma et al., 2009]. Automated sensors at the three open lake buoys would provide coincident measurements of temperature and  $p\text{CO}_2$  in the open waters, which make up the vast majority of Lake Superior.

The most poorly measured property of Lake Superior is its respiration rate. All of the currently available respiration observations are from near shore stations in summer and sporadic. It is most likely that respiration is largely over-estimated in previous estimates of the carbon cycle, from a seasonal and spatial bias. I return to this issue in Chapter 6. The models cover a wide range of net primary production estimates and even timing. Both models still capture spring supersaturation and lower summer values suggested by EPA data.

This model includes only the internal carbon cycling of Lake Superior and neglects all external inputs of carbon (e.g. runoff). Thus, it is most likely representative of the open lake carbon cycling, where coastal runoff likely has less of an impact. Observations of  $p\text{CO}_2$  near the southern coast and just off the Keweenaw Peninsula suggest that the lake surface waters may be supersaturated with  $\text{CO}_2$  throughout the summer, although uncertainty in these indirect methods is unknown [*Urban*, unpublished data]. The model is unable to capture such high  $p\text{CO}_2$  in these regions, which may be due to the lack of river inputs and sediment re-suspension in the model. I explicitly include riverine inputs and evaluate impacts on the carbon cycle in the next chapter (Chapter 5).

## Table Captions

- Table 4-1** Model parameter values used in the phosphorus model ecosystem and relevant references.
- Table 4-2** Model parameter values used in the no phosphorus model ecosystem and relevant references.
- Table 4-3** Correlations of seasonal anomalies for FMA for NPP, pCO<sub>2</sub>, CO<sub>2</sub> flux, lake surface temperature, wind speed, and ice for both ecosystem models. Values for the non-phosphorus model are given in parentheses. Correlations significant at the 90% confidence level are italicized and bolded.
- Table 4-4** Correlations of seasonal anomalies for AMJ for NPP, pCO<sub>2</sub>, CO<sub>2</sub> flux, lake surface temperature, wind speed, and ice for both ecosystem models. Values for the non-phosphorus model are given in parentheses. Correlations significant at the 90% confidence level are italicized and bolded.
- Table 4-5** Correlations of seasonal anomalies for JJASO for NPP, pCO<sub>2</sub>, CO<sub>2</sub> flux, lake surface temperature, wind speed, and ice for both ecosystem models. Values for the non-phosphorus model are given in parentheses. Correlations significant at the 90% confidence level are italicized and bolded.
- Table 4-6** Correlations of seasonal anomalies for NDJ for NPP, pCO<sub>2</sub>, CO<sub>2</sub> flux, lake surface temperature, wind speed, and ice for both ecosystem models. Values for the non-phosphorus model are given in parentheses. Correlations significant at the 90% confidence level are italicized and bolded.
- Table 4-7** Correlations of annual anomalies for N-O for NPP, pCO<sub>2</sub>, CO<sub>2</sub> flux, lake surface temperature, wind speed, and ice for both ecosystem models. Values for the non-phosphorus model are given in parentheses. Correlations significant at the 90% confidence level are italicized and bolded.
- Table 4-8** Correlations between annual and seasonal anomalies in NPP, pCO<sub>2</sub>, CO<sub>2</sub> flux, lake surface temperature, and wind speed and the Southern Oscillation Index (SOI) for both models. Correlations significant at the 90% confidence level are italicized and bolded.
- Table 4-9** Fraction of variance explained by the first EOF of annual and seasonal anomalies in NPP, pCO<sub>2</sub>, CO<sub>2</sub> flux, lake surface temperature (LST), and wind speed for both models.
- Table 4-10** Correlations between the principal components of the first EOFs of annual NPP, pCO<sub>2</sub>, CO<sub>2</sub> flux, lake surface temperature, wind speed, and the Southern Oscillation Index (SOI) in both models. Correlations significant at the 90% confidence level are italicized and bolded.

**Table 4-11** Correlations between the principal components of the first EOFs of FMA NPP, pCO<sub>2</sub>, CO<sub>2</sub> flux, lake surface temperature, wind speed, and the Southern Oscillation Index (SOI) in both models. Correlations significant at the 90% confidence level are italicized and bolded.

**Table 4-12** Correlations between the principal components of the first EOFs of AMJ NPP, pCO<sub>2</sub>, CO<sub>2</sub> flux, lake surface temperature, wind speed, and the Southern Oscillation Index (SOI) in both models. Correlations significant at the 90% confidence level are italicized and bolded.

**Table 4-13** Correlations between the principal components of the first EOFs of JJASO NPP, pCO<sub>2</sub>, CO<sub>2</sub> flux, lake surface temperature, wind speed, and the Southern Oscillation Index (SOI) in both models. Correlations significant at the 90% confidence level are italicized and bolded.

**Table 4-14** Correlations between the principal components of the first EOFs of NDJF NPP, pCO<sub>2</sub>, CO<sub>2</sub> flux, lake surface temperature, wind speed, and the Southern Oscillation Index (SOI) in both models. Correlations significant at the 90% confidence level are italicized and bolded.

## Figure Captions

**Figure 4-1** Schematic of the phosphorus ecosystem model, adapted from *Dutkiewicz et al.*, [2005].

**Figure 4-2** Schematic of no phosphorus ecosystem model, adapted from *McDonald* [2010].

**Figure 4-3** Modeled and observed chlorophyll profiles at six EPA stations (Figure 3-1) are shown for May of 1997. Model results from the phosphorus model (PM) are in red, and chlorophyll from the no phosphorus model (NPM) are in black. Discrete measurements taken by the EPA are shown with blue crosses.

**Figure 4.4** Modeled and observed chlorophyll profiles at eight EPA stations (Figure 3-1) are shown for August of 1999. Model results from the phosphorus model (PM) are in red, and chlorophyll from the no phosphorus model (NPM) is in black. Discrete measurements taken by the EPA are shown with blue crosses.

**Figure 4-5.** Daily average net primary productivity (1979-2006) in the phosphorus (solid black) and non-phosphorus (solid blue) models. Estimates of NPP based on the relationship between light, temperature, and NPP from *Sterner* [2010] are shown with a black dashed line for light conditions in the PM and with a blue dashed line for light conditions in the NPM. Note that production in the NPM is determined by the relationship between light, temperature, and production in *Sterner* [2010], with correctional factor (0.77). *Sterner's* [2010] (blue dashed line) estimate of NPP is not adjusted by that factor here.

**Figure 4-6** Estimates of  $p\text{CO}_2$  at 17 non-coastal EPA stations [*Atilla et al.*, 2010] are shown in black. The boxes have lines at the lower quartile, median, and upper quartile values. The notched boxes provide an estimate of uncertainty about the median from spatial heterogeneity. The dotted lines (whiskers) extend from the boxes to show the extent of the estimates. Outliers are shown in red crosses. Modeled  $p\text{CO}_2$  at the 17 EPA station locations for the sampled month from the phosphorus model are shown in magenta (top) and from the non-phosphorus model in blue (bottom).

**Figure 4-7** Local model grid-cell daily average  $p\text{CO}_2$  is compared to daily averaged direct measurements from SAMI of  $p\text{CO}_2$  [*Atilla et al.*, 2010]. The submersible was deployed at 14 m. Results from the phosphorus model (PM) are shown in blue at 15 m and blue dashed lines for the surface. Modeled  $p\text{CO}_2$  from the NPM are show in green and green dashed lines (surface). Estimates of  $p\text{CO}_2$  from EPA observations at the nearest EPA station are shown with red markers.

**Figure 4-8.** The modeled lake-wide mean seasonal cycles of  $p\text{CO}_2$  are show for 1997-2000. Phosphorus model results shown in red, with one standard deviation from the mean shown in red dashed lines. NPM  $p\text{CO}_2$  is shown in blue, and one standard deviation is shown with blue dashed lines. Estimates from EPA data [*Atilla et al.*, 2010] are shown with black box plots. Atmospheric  $p\text{CO}_2$  at Park Falls, WI is shown with green dashed lines [*Peters et al.*, 2009].



**Figure 4-9.** The mean seasonal (monthly) cycles of CO<sub>2</sub> (top) fluxes for both models are depicted in black (PM) and black dashed lines (NPM). Months are indicated by the month's first letter. Two years with contrasting climates, 1997 (middle) and 1998 (bottom) are also shown. A positive CO<sub>2</sub> flux is one *out* of the lake. The divisions of four seasons for analysis of the pCO<sub>2</sub> and CO<sub>2</sub> flux cycles are shown in shading. Start of each month is indicated by the month's first letter.

**Figure 4.10** Mean seasonal CO<sub>2</sub> fluxes (a) and net annual fluxes for 1980-2005 in the PM (b). All seasonal flux anomalies are plotted in (c) for a visual of how one season's flux alters another. (d)-(g) show seasonal flux *anomalies* for each individual season plotted against the corresponding seasonal anomalies in wind speed (black), lake surface temperature (magenta), net primary production (green dashed), and annual ice cover (blue dashed). There are no units, as the anomalies are normalized to a common scale for visualization. Seasonal colors from (a) are continued throughout the figure.

**Figure 4.11** Mean seasonal CO<sub>2</sub> fluxes (a) and net annual fluxes for 1980-2005 in the NPM (b). All seasonal flux anomalies are plotted in (c) for a visual of how one season's flux alters another. (d)-(g) show seasonal flux *anomalies* for each individual season plotted against the corresponding seasonal anomalies in wind speed (black), lake surface temperature (magenta), net primary production (green dashed), and annual ice cover (blue dashed). There are no units, as the anomalies are normalized to a common scale for visualization. Seasonal colors from (a) are continued throughout the figure.

**Figure 4-12** The first EOFs of lake surface temperature for annual (top left), FMA (top right), AMJ (middle left), JJASO (middle right), and NDJ (bottom left). Units are °C. The principal components for each of the EOFs are show at the bottom right.

**Figure 4-12** The first EOFs of lake surface temperature for annual (top left), FMA (top right), AMJ (middle left), JJASO (middle right), and NDJ (bottom left). Units are °C. The principal components for each of the EOFs are show at the bottom right.

**Figure 4-13** The first EOFs of wind speed for annual (top left), FMA (top right), AMJ (middle left), JJASO (middle right), and NDJ (bottom left). Units are m/s. The principal components for each of the EOFs are show at the bottom right.

**Figure 4-14** The first EOFs of NPP in the phosphorus model for annual (top left), FMA (top right), AMJ (middle left), JJASO (middle right), and NDJ (bottom left) seasons, in TgC/yr. The principal components for each of the EOFs are show at the bottom right.

**Figure 4-15** The first EOFs of pCO<sub>2</sub> in the PM for annual (top left), FMA (top right), AMJ (middle left), JJASO (middle right), and NDJ (bottom left) seasons. Units are µatm. The principal components for each of the EOFs are show at the bottom right.

**Figure 4-16** The first EOFs of CO<sub>2</sub> flux in the PM for annual (top left), FMA (top right), AMJ (middle left), JJASO (middle right), and NDJ (bottom left) seasons. Units are gC/m<sup>2</sup>/yr. The principal components for each of the EOFs are show at the bottom right.

**Figure 4-17** The first EOFs of net primary production in the NPM for annual (top left), FMA (top right), AMJ (middle left), JJASO (middle right), and NDJ (bottom left) seasons. Units are TgC/yr. The principal components for each of the EOFs are show at the bottom right.

**Figure 4-18** The first EOFs of lake surface pCO<sub>2</sub> in the NPM for annual (top left), FMA (top right), AMJ (middle left), JJASO (middle right), and NDJ (bottom left) seasons. Units are µatm. The principal components for each of the EOFs are show at the bottom right.

**Figure 4-19** The first EOFs of CO<sub>2</sub> fluxes in the NPM for annual (top left), FMA (top right), AMJ (middle left), JJASO (middle right), and NDJ (bottom left) seasons. Units are gC/m<sup>2</sup>/yr. The principal components for each of the EOFs are show at the bottom right.

**Table 4-1** PM Parameter Values

Parameter	Description	Value	Reference
$k_0$	Water light extinction coefficient	$0.1 \text{ m}^{-1}$	as in [Chen et al., 2002]
$k_c$	Light extinction coefficient (chl)	$0.02 \text{ m}^{-1}$	
$\mu_{phy1_{max}}$	Max small phyto growth rate	$12 \text{ d}^{-1}$	
$\mu_{phy2_{max}}$	Maximum diatom growth rate	$10 \text{ d}^{-1}$	
zoograz	maximum zoo grazing rate	$0.5 \text{ d}^{-1}$	similar to [Chen et al., 2002]
mort	Small phyto mortality rate	$1/30 \text{ d}^{-1}$	
mort <sub>2</sub>	Diatom mortality rate	$1/30 \text{ d}^{-1}$	
mortz	Zooplankton mortality rate	$1/30 \text{ d}^{-1}$	
$k_{I_1}$	phy <sub>1</sub> light half saturation constant	$15 \text{ W/m}^2$	Dutkiewicz et al., [2005]
$k_{I_2}$	diatom light half saturation constant	$10 \text{ W/m}^2$	similar to Dutkiewicz et al., [2005]
$k_{P_1}$	Small phytoplankton phosphorus half saturation constant	$1.8 \text{ mmol/m}^3$	tuned for NPP, size class fraction
$k_{P_2}$	diatom phosphorus half saturation constant	$3 \text{ mmol/m}^3$	tuned for NPP, size class fraction
zplat	palatability of small phyto	0.9	
zplat <sub>2</sub>	Palatability of diatoms	0.4	
$k_{P_z}$	Zooplankton phytoplankton half saturation constant	$0.094 \text{ mmol/m}^3$	
reminp	Remineralization rate of organic matter	$1/5 \text{ d}^{-1}$	similar to [Chen et al., 2002]
gampn	Zooplankton assimilation coefficient	0.3	[Jorgensen et al., 1991]
donfracmn <sub>1</sub>	Fraction of small phytoplankton mortality going to DOP	0.95	Tuned for implicit microbial pool
donfracmn <sub>2</sub>	Fraction of diatom mortality going to DOP	0.8	Tuned for implicit microbial pool
Rcp	Ratio of C to P in algae	200	[Urban, 2009]
Rop	Ratio of oxygen to phosphorus	70	[Sarmiento and Gruber, 2006]
Rnp	N:P in algal production	16	[Sarmiento and Gruber, 2006]
Chl:P <sub>max</sub>	Maximum ratio of Chl:P	$28 \text{ mg/mmol}$	[Dutkiewicz et al., 2005; Parsons et al., 1984]
Chl:P <sub>min</sub>	Minimum ratio Chl:P	$20 \text{ mg/mmol}$	[Dutkiewicz et al. 2005; Parsons et al., 1984]
wn_sink	Sinking rate of POP / POC	$0.5 \text{ m/d}$	[Urban et al., 2004]
tbase	temp function base coefficient	-3400	[Moore et al., 2002]
tnorm	temp function normal coefficient	280.15	[Moore et al., 2002]
istar		$70 \text{ W/m}^2$	[Dutkiewicz et al., 2005]

**Table 4-2** NPM Parameter Values

Parameter	Description	Value	Reference
$k_0$	Light attenuation coefficient (water)	$0.15 \text{ m}^{-1}$	various
$k_c$	Light attenuation coefficient (chl)	$0.0149 \text{ m}^{-1}$	[ <i>McDonald, 2010</i> ]
mort	Phytoplankton death rate	$1/34.5 \text{ d}^{-1}$	[ <i>McDonald, 2010</i> ]
reminc	Carbon remineralization rate	$0.01 \text{ d}^{-1}$	[ <i>McDonald, 2010</i> ]
Rcp	Ratio of C to P	200	[ <i>Urban, 2009</i> ]
Rnp	Ratio of N to P	16	[ <i>Sarmiento and Gruber, 2006</i> ]
Rop	Ratio of O to P	170	[ <i>Sarmiento and Gruber, 2006</i> ]
O <sub>2</sub> crit	Critical oxygen concentration	4.d-6 mmol/m <sup>3</sup>	[ <i>Dutkiewicz et al., 2005</i> ]
thetam	Coefficient for temperature effect on mortality and grazing	1.0568	[ <i>McDonald, 2010</i> ]
thetar	Coefficient for temperature effect on Remineralization	1.06	[ <i>McDonald, 2010</i> ]
f <sub>res</sub>	Fraction of NPP that is respired	0.75	[ <i>McDonald, 2010</i> ]
f <sub>exc</sub>	Fraction of NPP that is excreted	0.13	[ <i>Baines and Pace, 1991</i> ]
f <sub>dom</sub>	Fraction of dead phytoplankton that enters DOM pool	0.14	[ <i>McDonald, 2010</i> ]
f <sub>pom</sub>	Fraction of dead phytoplankton that enters POM pool	0.5	[ <i>McDonald, 2010</i> ]
dens	Density of phytoplankton	$1.027 \text{ kg/m}^3$	
diam2	Phytoplankton diameter squared	$734.73 \text{ }\mu\text{m}^2$	
tm <sub>psink</sub>	Unadjusted phytoplankton sinking rate (adusts to ~0.7 m/d)	24.7 m/d	[ <i>McDonald, 2010</i> ]
E <sub>a</sub>	Activation energy	0.2816 eV	<i>Sterner [2010]</i>
P <sub>opt</sub>	Rate of NPP in optimal conditions	838 mgC/m <sup>3</sup> /day	<i>Sterner [2010]</i>
C <sub>npp</sub>	Dimensional fit with unit adustment	$96.5 \text{ d}^{-1}$	<i>Sterner [2010]</i>
$\alpha$		499 (for W/m <sup>2</sup> )	<i>Sterner [2010]</i>
wc sink	Sinking rate of POC	0.1 m/d	[ <i>Urban et al., 2004</i> ]
chl <sub>c</sub> <sub>max</sub>	Maximum Chl:C ratio in phytoplankton	0.2193 mg/mmol	[ <i>McDonald, 2010</i> ]
chl <sub>c</sub> <sub>min</sub>	Minimum Chl:C ratio in phytoplankton	0.0756 mg/mmol	[ <i>McDonald, 2010</i> ]
istar	Critical light for chlorophyll	$11.06 \text{ W/m}^2$	[ <i>McDonald, 2010</i> ]

**Table 4-3** Correlations of Seasonal Anomalies: FMA

	NPP	$p\text{CO}_2$	$\text{CO}_2$ Flux	LST	WDSP	ICE
NPP		<b>0.74</b> (0.79)	<b>-0.35</b> (0.27)	<b>0.88</b> (0.86)	<b>0.66</b> (0.56)	<b>-0.94</b> (-0.95)
$p\text{CO}_2$			0.19 (0.66)	<b>0.93</b> (0.96)	<b>0.75</b> (0.77)	<b>-0.61</b> (-0.73)
$\text{CO}_2$ Flux				0.04 (0.64)	-0.20 (0.3)	<b>0.33</b> (-0.23)
LST					<b>0.72</b>	<b>-0.8</b>
WDSP						<b>-0.53</b>

**Table 4-4** Correlations of Seasonal Anomalies: April - June

	NPP	$p\text{CO}_2$	$\text{CO}_2$ Flux	LST	WDSP	ICE
NPP		0.22 (-0.14)	0.29 (-0.08)	<b>-0.5</b> (0.96)	0.01 (0.27)	-0.18 (-0.31)
$p\text{CO}_2$			<b>0.74</b> (0.87)	0.23 (-0.12)	<b>0.54</b> (0.25)	0.17 (0.36)
$\text{CO}_2$ Flux				-0.12 (-0.05)	0.14 (0.43)	-0.15 (0.27)
LST					0.32	-0.31
WDSP						-0.25

**Table 4-5** Correlations of Seasonal Anomalies: JJASO

	NPP	$p\text{CO}_2$	$\text{CO}_2$ Flux	LST	WDSP
NPP		<b>0.48</b> (0.04)	<b>0.76</b> (-0.48)	<b>0.61</b> (0.96)	0.24 (0.38)
$p\text{CO}_2$			<b>0.43</b> (0.66)	<b>0.43</b> (0)	<b>0.34</b> (0.33)
$\text{CO}_2$ Flux				<b>0.67</b> (-0.5)	<b>0.61</b> (0)
LST					0.2

**Table 4-6** Correlations of Seasonal Anomalies NDJ

	NPP	$p\text{CO}_2$	$\text{CO}_2$ Flux	LST	WDSP	ICE
NPP		-0.33 (-0.13)	-0.25 (-0.23)	<b>0.68</b> ( <b>0.77</b> )	0.02 (0.13)	<b>-0.84</b> ( <b>-0.87</b> )
$p\text{CO}_2$			<b>0.68</b> ( <b>0.5</b> )	0.04 (0.12)	0.30 (0.09)	0.32 (0.26)
$\text{CO}_2$ Flux				0 (0.1)	<b>0.34</b> ( <b>0.43</b> )	0.28 (0.3)
LST					0.21	<b>-0.64</b>
WDSP						0.14

**Table 4-7** Correlations of Annual Anomalies

	NPP	$p\text{CO}_2$	$\text{CO}_2$ Flux	LST	WDSP	ICE
NPP		<b>0.62</b> ( <b>0.63</b> )	-0.21 (0.17)	<b>0.62</b> ( <b>0.85</b> )	<b>0.35</b> (0.31)	<b>-0.97</b> ( <b>-0.9</b> )
$p\text{CO}_2$			<b>0.36</b> ( <b>0.65</b> )	<b>0.56</b> ( <b>0.43</b> )	<b>0.4</b> ( <b>0.67</b> )	<b>-0.61</b> ( <b>-0.65</b> )
$\text{CO}_2$ Flux				0.30 (0.06)	0.26 ( <b>0.34</b> )	0.17 (0.17)
LST					0.25	<b>-0.62</b>
WDSP						<b>-0.34</b>

**Table 4-8** Correlations with the Southern Oscillation Index (SOI)

Model	SOI (PM)	SOI (NPM)
Annual $p\text{CO}_2$	<b>-0.37</b>	-0.25
Annual $\text{CO}_2$ Flux	<b>-0.34</b>	-0.20
Annual LST	-0.25	-0.25
Annual NPP	-0.28	-0.27
Annual WDSP	-0.03	-0.03
NDJ $p\text{CO}_2$	0.2	<b>0.40</b>
NDJ $\text{CO}_2$ Flux	0.17	0.20
NDJ LST	0.04	0.04
NDJ NPP	0.11	-0.04
NDJ WDSP	0	0
FMA $p\text{CO}_2$	<b>-0.38</b>	<b>-0.33</b>
FMA $\text{CO}_2$ Flux	-0.1	-0.30
FMA LST	<b>-0.36</b>	<b>-0.36</b>
FMA NPP	-0.24	-0.26
FMA WDSP	-0.20	-0.20
AMJ $p\text{CO}_2$	-0.15	0.08
AMJ $\text{CO}_2$ Flux	-0.09	0.06
AMJ LST	-0.06	-0.06
AMJ NPP	-0.27	-0.2
AMJ WDSP	0.06	0.06
JJASO $p\text{CO}_2$	-0.11	-0.08
JJASO $\text{CO}_2$ Flux	-0.20	-0.07
JJASO LST	-0.20	-0.20
JJASO NPP	-0.22	-0.21
JJASO WDSP	-0.04	-0.04

**Table 4-9** Fraction of Variance Explained by First EOF

	PM	NPM
NPP	0.68	0.87
$p\text{CO}_2$	0.52	0.48
CO <sub>2</sub> Flux	0.36	0.47
LST	0.70	0.70
WDSP	0.82	0.84
NPP – FMA	0.68	0.81
$p\text{CO}_2$ – FMA	0.57	0.57
CO <sub>2</sub> Flux – FMA	0.43	0.51
LST – FMA	0.69	0.69
WDSP – FMA	0.82	0.82
NPP – AMJ	0.29	0.66
$p\text{CO}_2$ – AMJ	0.31	0.38
CO <sub>2</sub> Flux – AMJ	0.30	0.50
LST – AMJ	0.69	0.69
WDSP – AMJ	0.65	0.65
NPP – JJASO	0.57	0.83
$p\text{CO}_2$ – JJASO	0.60	0.65
CO <sub>2</sub> Flux – JJASO	0.52	0.44
LST – JJASO	0.88	0.88
WDSP – JJASO	0.82	0.82
NPP – NDJF	0.61	0.79
$p\text{CO}_2$ – NDJF	0.35	0.32
CO <sub>2</sub> Flux – NDJF	0.53	0.58
LST – NDJF	0.66	0.66
WDSP – NDJF	0.85	0.85



**Table 4-10** Correlations of First Principal Components -- Annual

	NPP	<i>p</i> CO <sub>2</sub>	CO <sub>2</sub> Flux	LST	WDSP	SOI
NPP		<b>0.75</b> (0.67)	<b>0.48</b> (0.26)	<b>0.71</b> (0.92)	<b>0.38</b> (0.38)	-0.29 (-0.27)
<i>p</i> CO <sub>2</sub>			<b>0.55</b> (-0.73)	<b>0.63</b> (0.51)	<b>0.42</b> (0.59)	<b>-0.40</b> (-0.30)
CO <sub>2</sub> Flux				<b>0.45</b> (-0.14)	<b>0.45</b> (-0.42)	<b>-0.44</b> (0.25)
LST					0.28	-0.25
WDSP						0.04

**Table 4-11** Correlations of Principal Components --- FMA

	NPP	<i>p</i> CO <sub>2</sub>	CO <sub>2</sub> Flux	LST	WDSP	SOI
NPP		<b>0.87</b> (0.84)	0.19 (0.59)	<b>0.93</b> (0.87)	<b>0.69</b> (0.58)	-0.26 (-0.27)
<i>p</i> CO <sub>2</sub>			<b>0.52</b> (0.78)	<b>0.97</b> (0.97)	<b>0.75</b> (0.74)	<b>-0.39</b> (-0.35)
CO <sub>2</sub> Flux				<b>0.46</b> (0.77)	0.14 (0.46)	-0.25 (-0.36)
LST					<b>0.73</b>	<b>-0.37</b>
WDSP						-0.21

**Table 4-12** Correlations of Principal Components AMJ

	NPP	<i>p</i> CO <sub>2</sub>	CO <sub>2</sub> Flux	LST	WDSP	SOI
NPP		0.25 (0.09)	<b>0.45</b> (0.04)	0.15 (0.95)	0.23 (0.35)	-0.16 (-0.20)
<i>p</i> CO <sub>2</sub>			<b>0.78</b> (0.84)	-0.11 (0.12)	<b>0.54</b> (-0.23)	0.12 (-0.05)
CO <sub>2</sub> Flux				0.23 (0.08)	0.17 (-0.45)	0.05 (-0.05)
LST					<b>0.35</b>	-0.05
WDSP						-0.05

**Table 4-13** Correlations of Principal Components --- JJASO

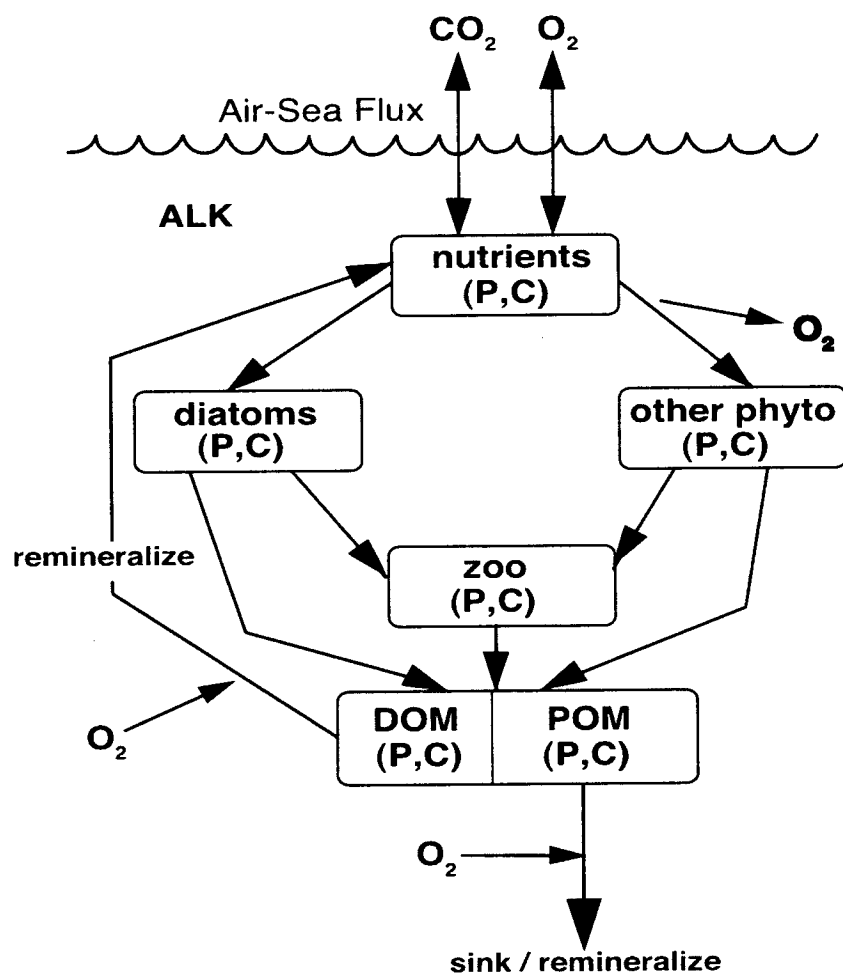
	NPP	$p\text{CO}_2$	$\text{CO}_2$ Flux	LST	WDSP	SOI
NPP		<b>0.53</b> (0.1)	<b>0.85</b> (0.2)	<b>0.68</b> <b>(0.95)</b>	0.15 (0.17)	-0.2 (-0.22)
$p\text{CO}_2$			<b>0.51</b> <b>(-0.70)</b>	<b>0.45</b> (0.02)	0.03 <b>(0.79)</b>	-0.11 (-0.08)
$\text{CO}_2$ Flux				<b>0.69</b> <b>(0.42)</b>	0.21 <b>(-0.4)</b>	-0.18 (0.02)
LST					0.11	-0.20
WDSP						-0.04

**Table 4-14** Correlations of Principal Components --- NDJF

	NPP	$p\text{CO}_2$	$\text{CO}_2$ Flux	LST	WDSP	SOI
NPP		0.21 (0.23)	-0.03 (-0.06)	<b>0.79</b> <b>(0.82)</b>	0.23 (0.27)	0.15 (-0.05)
$p\text{CO}_2$			0 (0.18)	0.23 (0.33)	0.17 (-0.05)	0.15 (0.33)
$\text{CO}_2$ Flux				0.15 (0.08)	<b>-0.52</b> <b>(-0.4)</b>	-0.20 (-0.22)
LST					<b>0.34</b>	0.03
WDSP						0

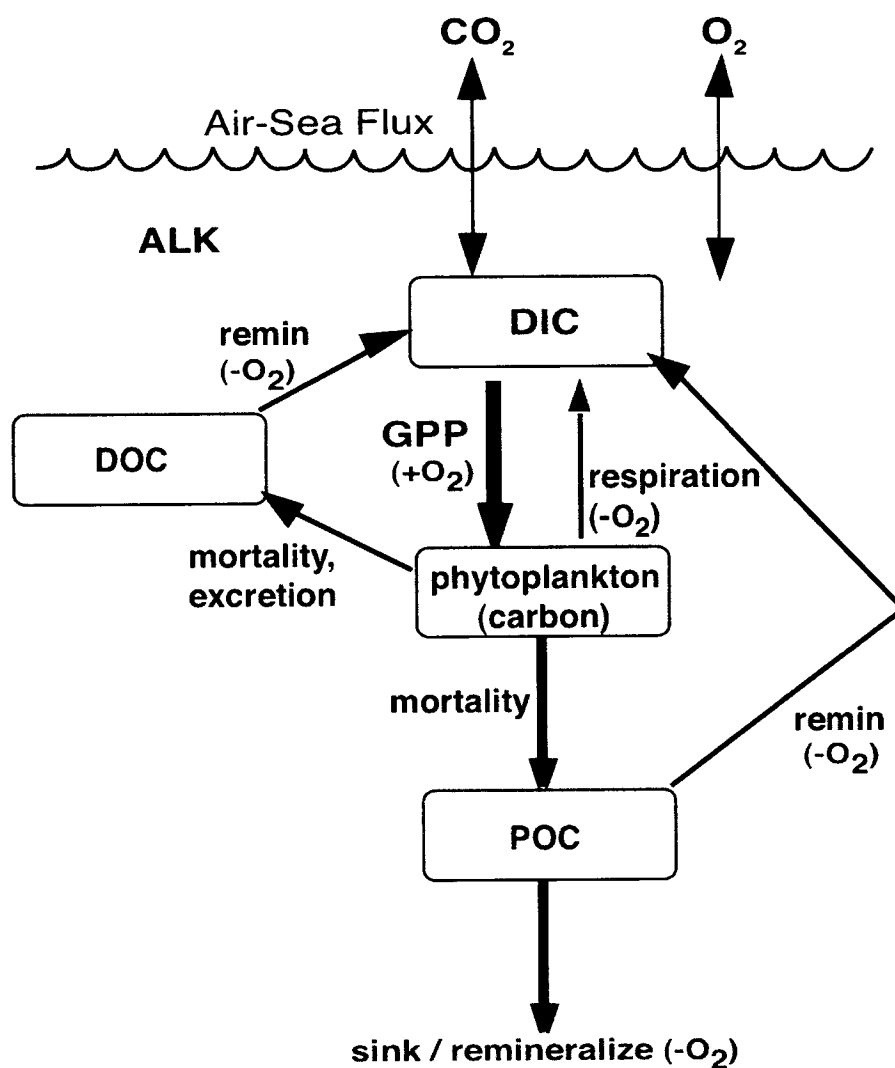
## Figures

**Figure 4-1** Schematic of Phosphorus Ecosystem

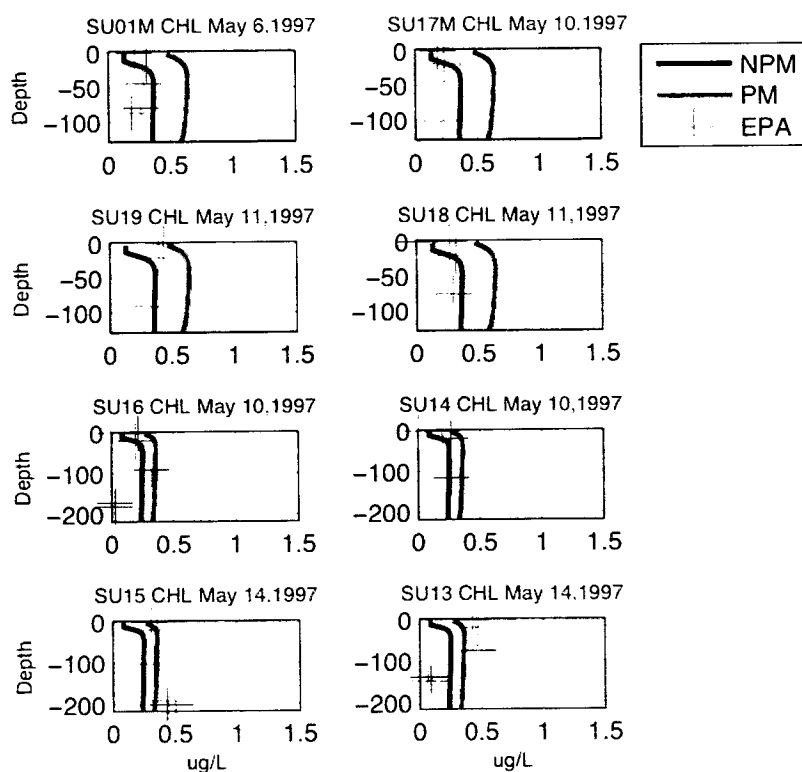


**Figure 4-1** Ecosystem schematic for the phosphorus model. Modified from *Dutkiewicz et al.*, [2005].

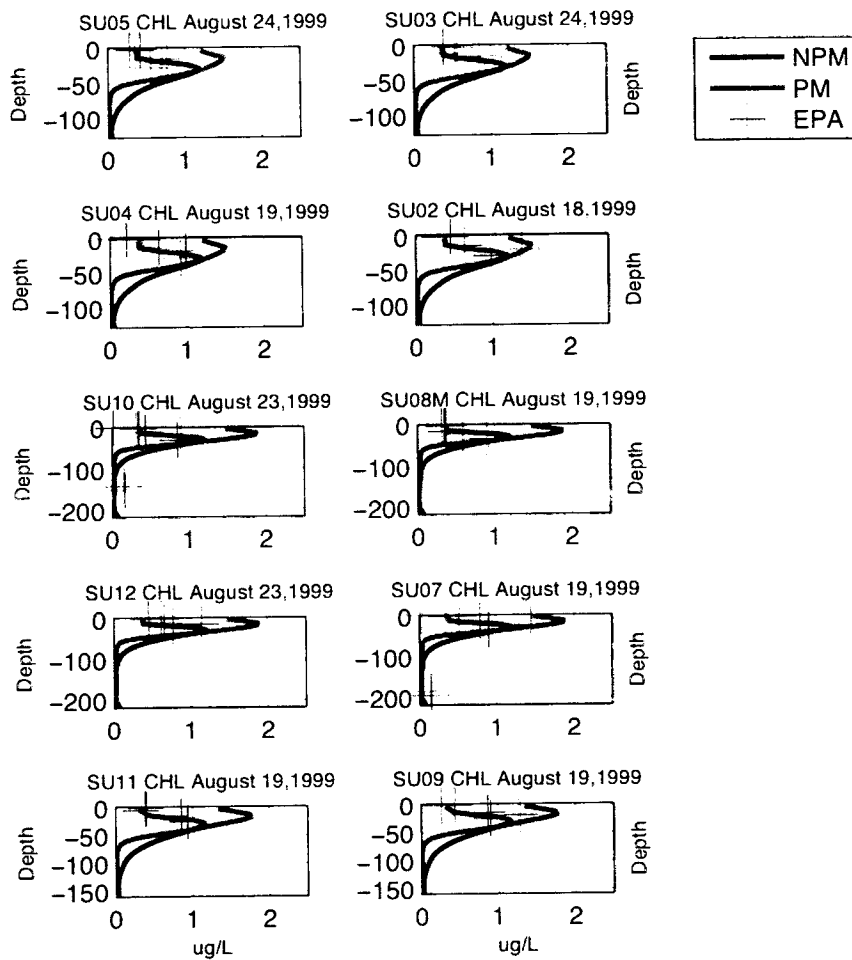
**Figure 4-2** Schematic of No Phosphorus Model



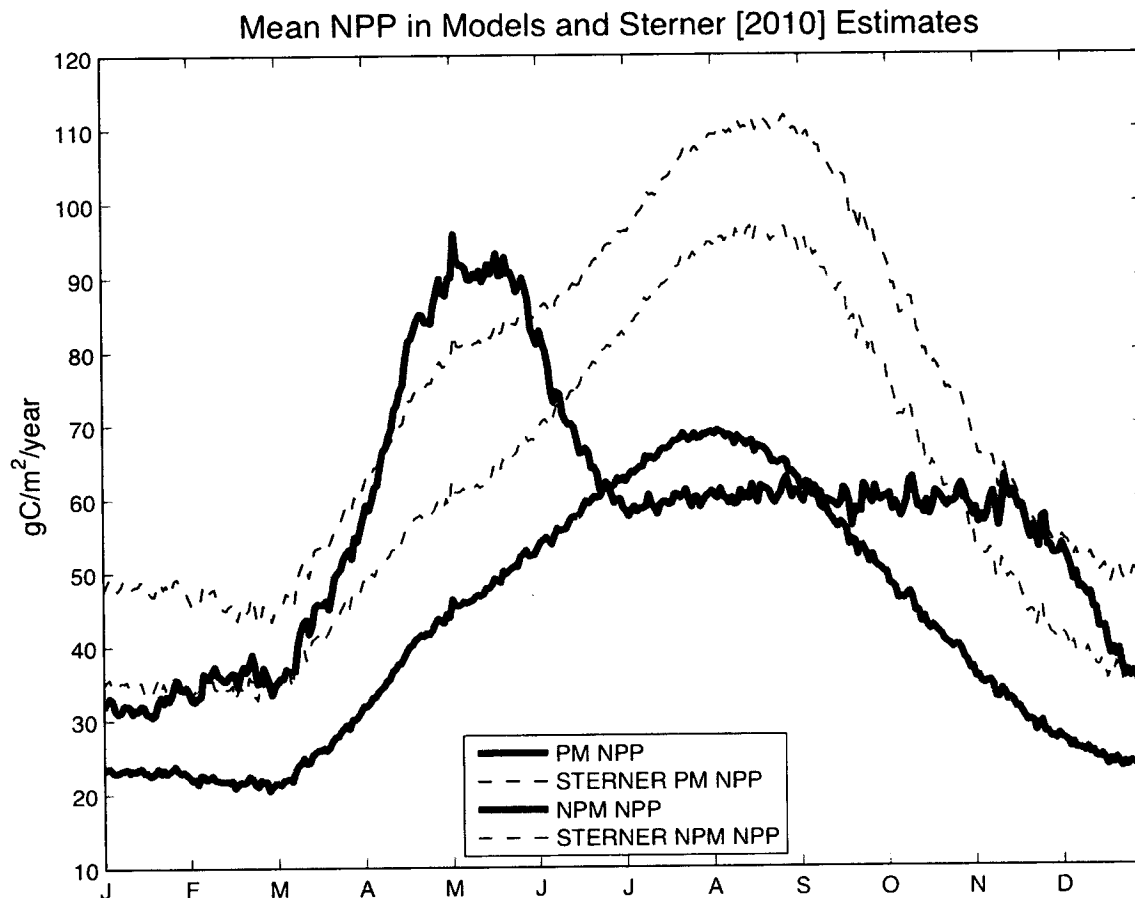
**Figure 4-2** Schematic of no-phosphorus model from *McDonald* [2010].

**Figure 4-3**

**Figure 4-3.** Modeled and observed chlorophyll profiles at six EPA stations (Figure 3-1) are shown for May of 1997. Model results from the phosphorus model (PM) are in red, and chlorophyll from the no phosphorus model (NPM) is in black. Discrete measurements taken by the EPA are shown with blue crosses.

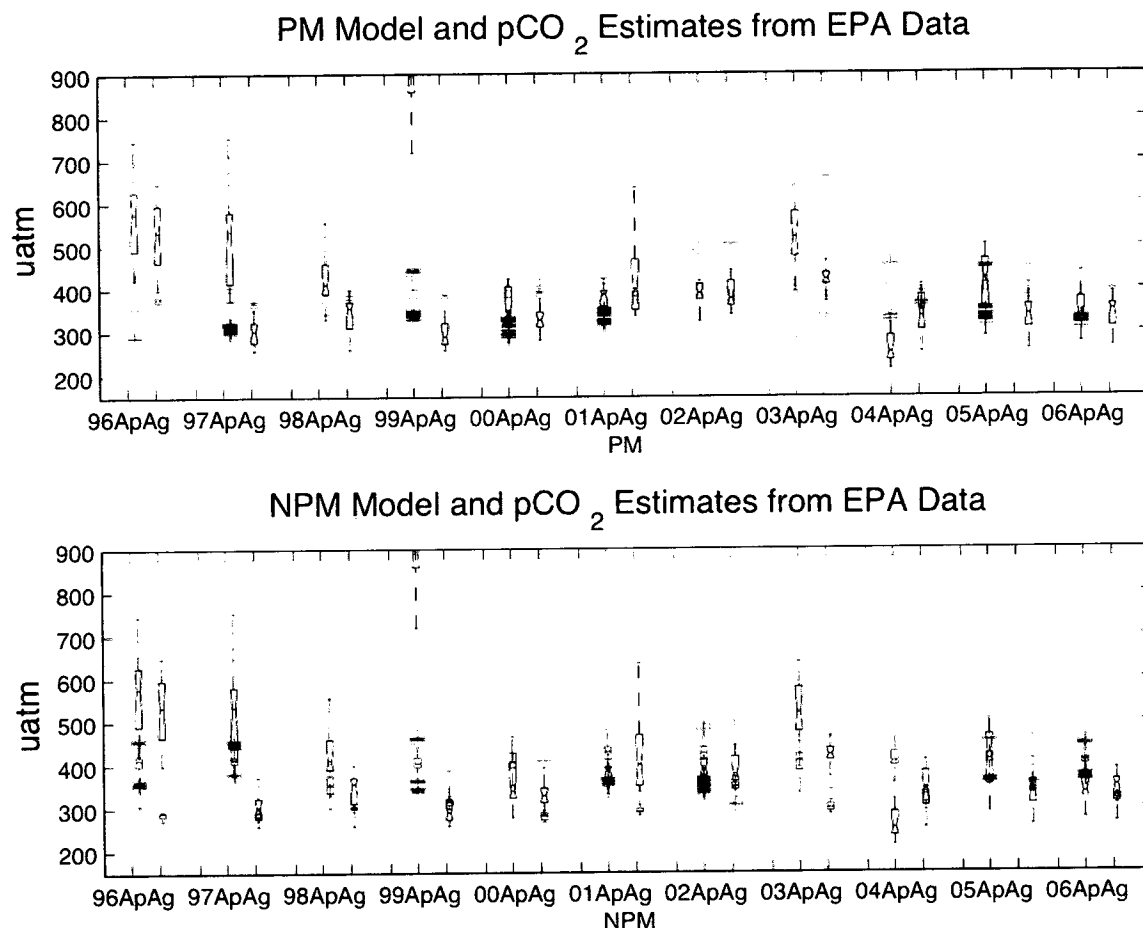
**Figure 4-4.**

**Figure 4.4.** Modeled and observed chlorophyll profiles at eight EPA stations (Figure 3-1) are shown for August of 1999. Model results from the phosphorus model (PM) are in red, and chlorophyll from the no phosphorus model (NPM) is in black. Discrete measurements taken by the EPA are shown with blue crosses.

**Figure 4-5**

**Figure 4-5.** Daily average net primary productivity (1979-2006) in the phosphorus (solid black) and non-phosphorus (solid blue) models. Estimates of NPP based on the relationship between light, temperature, and NPP from *Sterner* [2010] are shown with a black dashed line for light conditions in the PM and with a blue dashed line for light conditions in the NPM. Note that production in the NPM is determined by the relationship between light, temperature, and production in *Sterner* [2010], with correctional factor (0.77). *Sterner's* [2010] (blue dashed line) estimate of NPP is not adjusted by that factor here

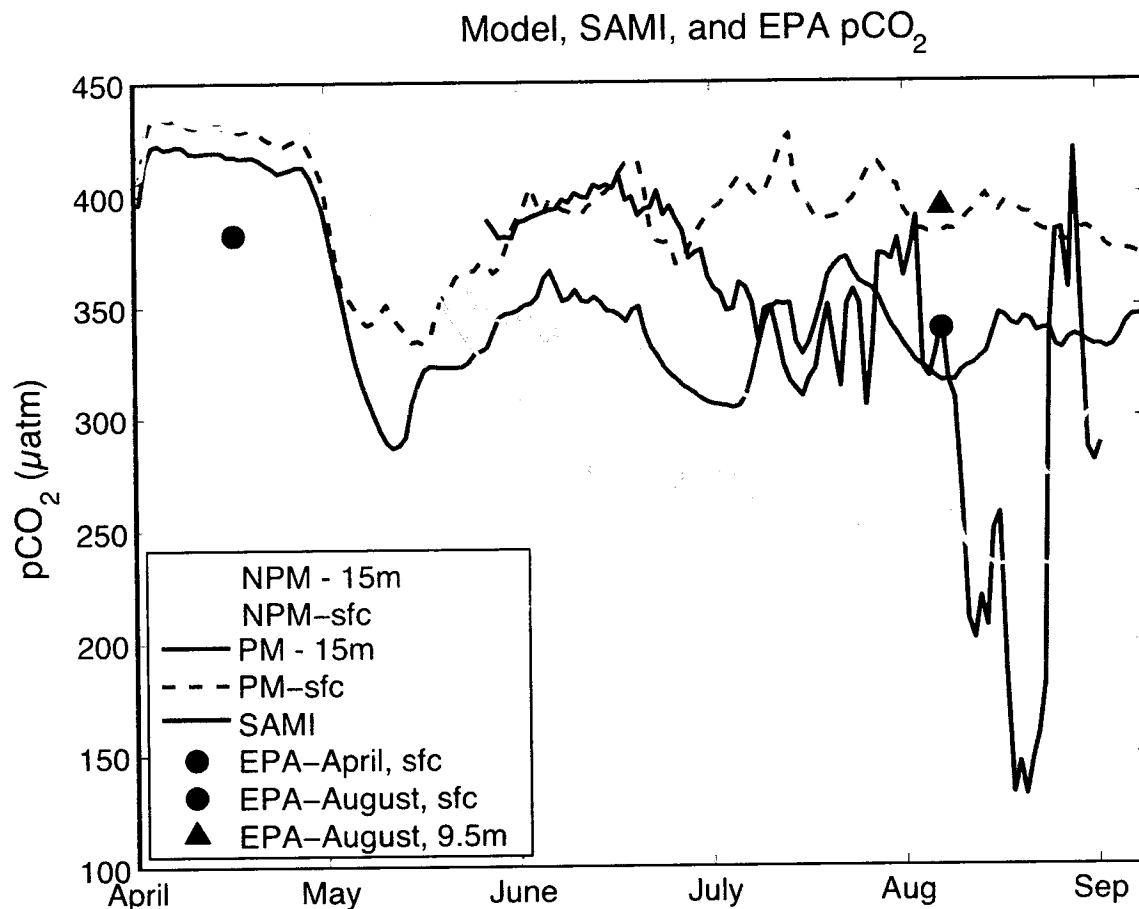
Figure 4-6



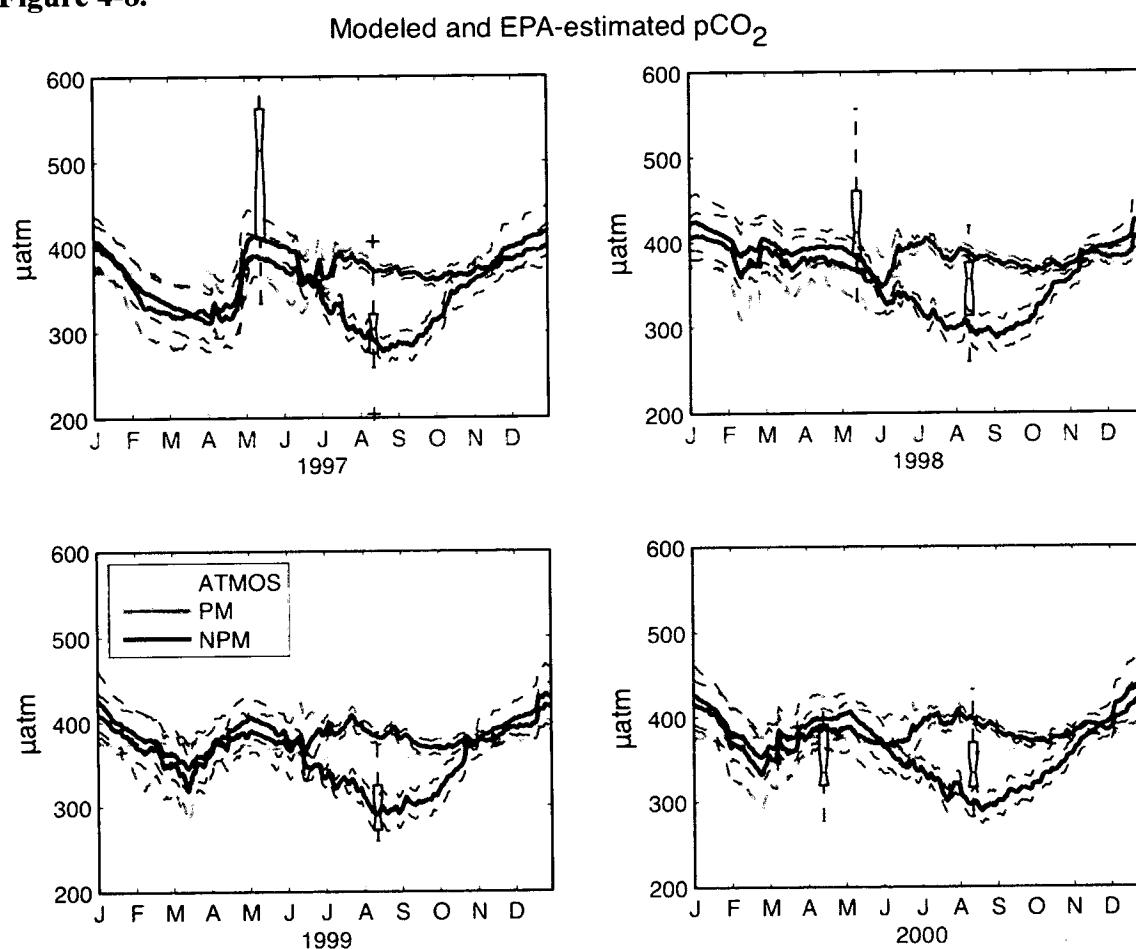
**Figure 4-6.** Estimates of  $p\text{CO}_2$  at 17 non-coastal EPA stations [Atilla *et al.*, 2010] are shown in black. The boxes have lines at the lower quartile, median, and upper quartile values. The notched boxes provide an estimate of uncertainty about the median from spatial heterogeneity. The dotted lines (whiskers) extend from the boxes to show the extent of the estimates. Outliers are shown in red crosses. Modeled  $p\text{CO}_2$  at the 17 EPA station locations for the sampled month from the phosphorus model are shown in magenta (top) and from the non-phosphorus model in blue (bottom).



Figure 4-7

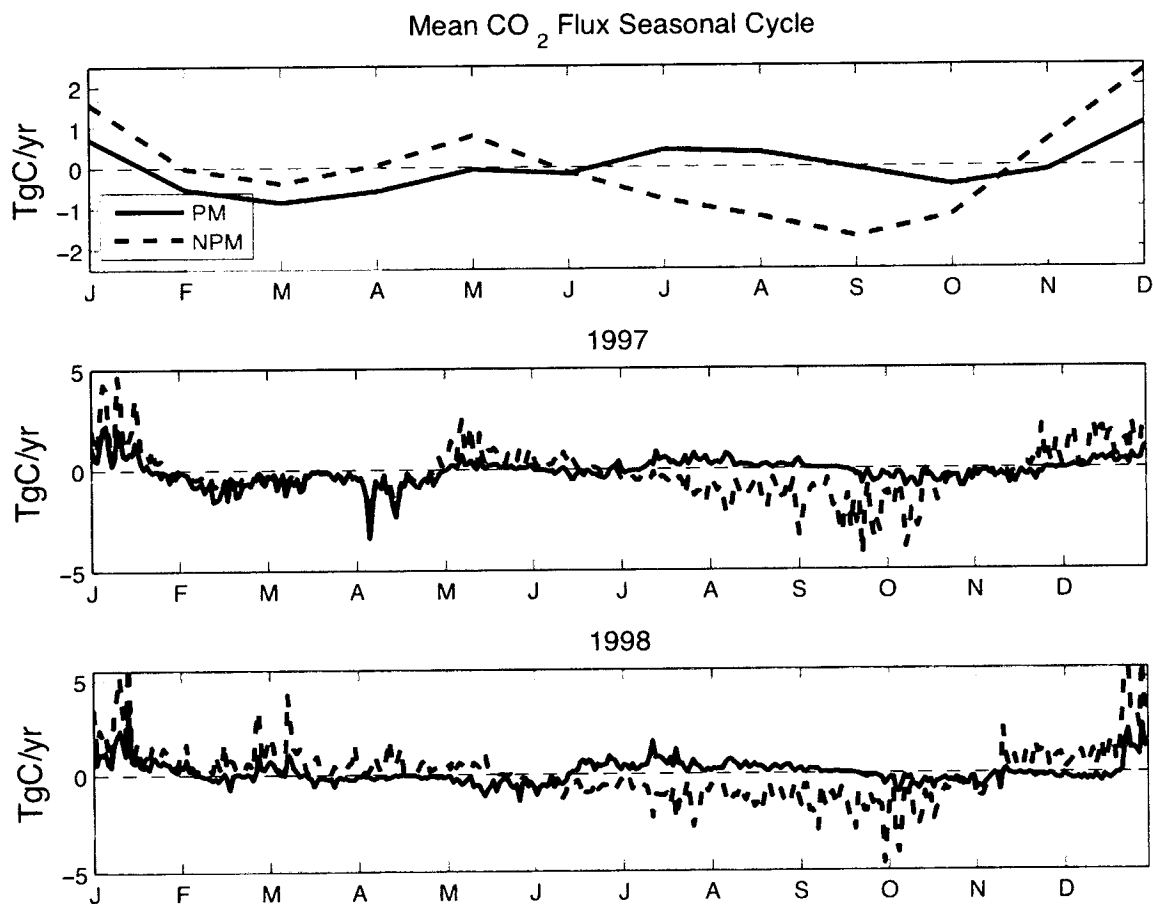


**Figure 4-7** Local model grid-cell daily average  $p\text{CO}_2$  is compared to daily averaged direct measurements from SAMI of  $p\text{CO}_2$  [Atilla *et al.*, 2010]. The submersible was deployed at 14 m. Results from the phosphorus model (PM) are shown in blue at 15 m and blue dashed lines for the surface. Modeled  $p\text{CO}_2$  from the NPM are shown in green and green dashed lines (surface). Estimates of  $p\text{CO}_2$  from EPA observations at the nearest EPA station are shown with red markers.

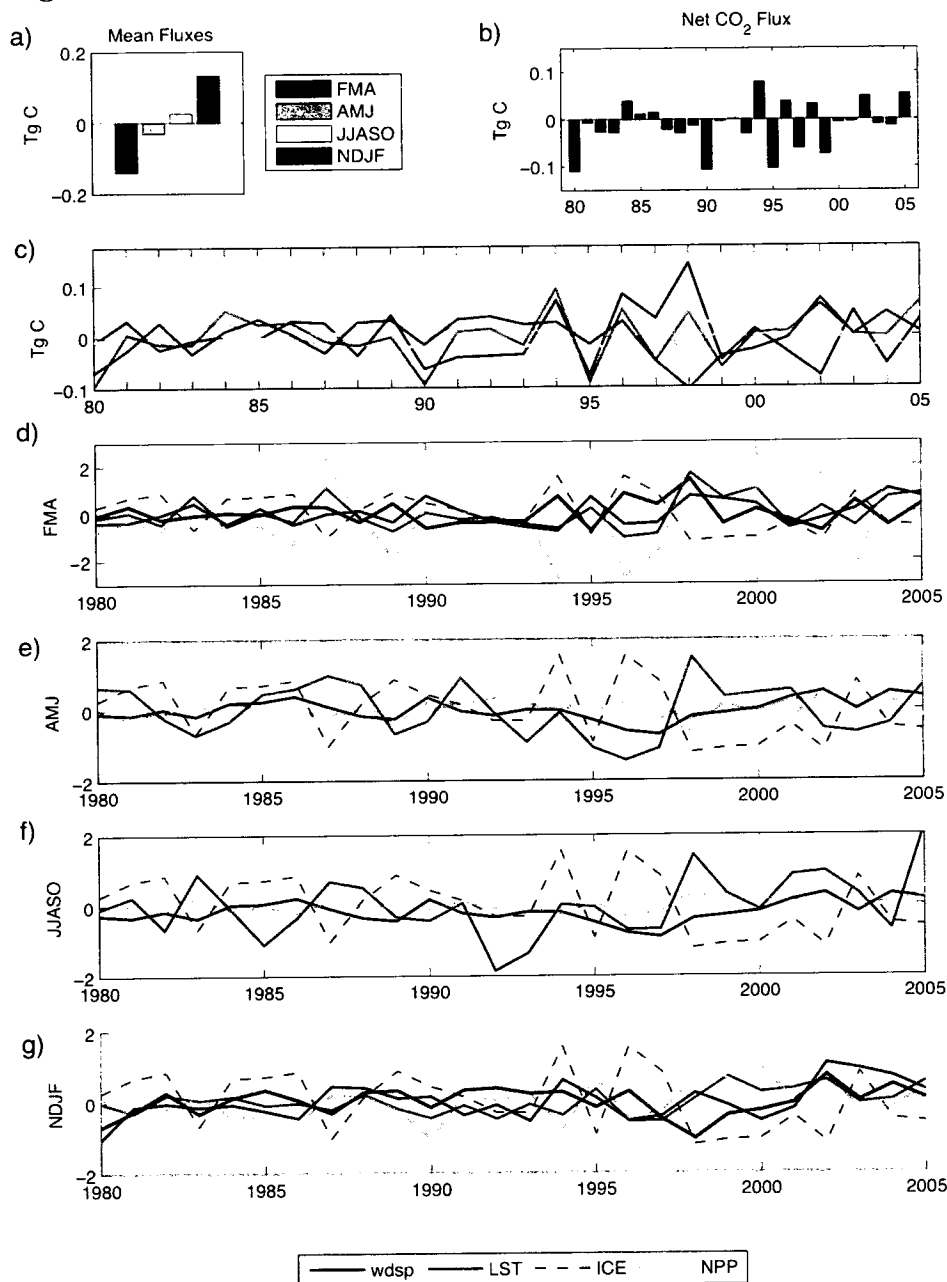
**Figure 4-8.**

**Figure 4-8.** The modeled lake-wide mean seasonal cycles of  $p\text{CO}_2$  are shown for 1997-2000. Phosphorus model results shown in red, with one standard deviation from the mean shown in red dashed lines. NPM  $p\text{CO}_2$  is shown in blue, and one standard deviation is shown with blue dashed lines. Estimates from EPA data [Atilla *et al.*, 2010] are shown with black box plots. Atmospheric  $p\text{CO}_2$  at Park Falls, WI is shown with green dashed lines [Peters *et al.*, 2007].

Figure 4-9.

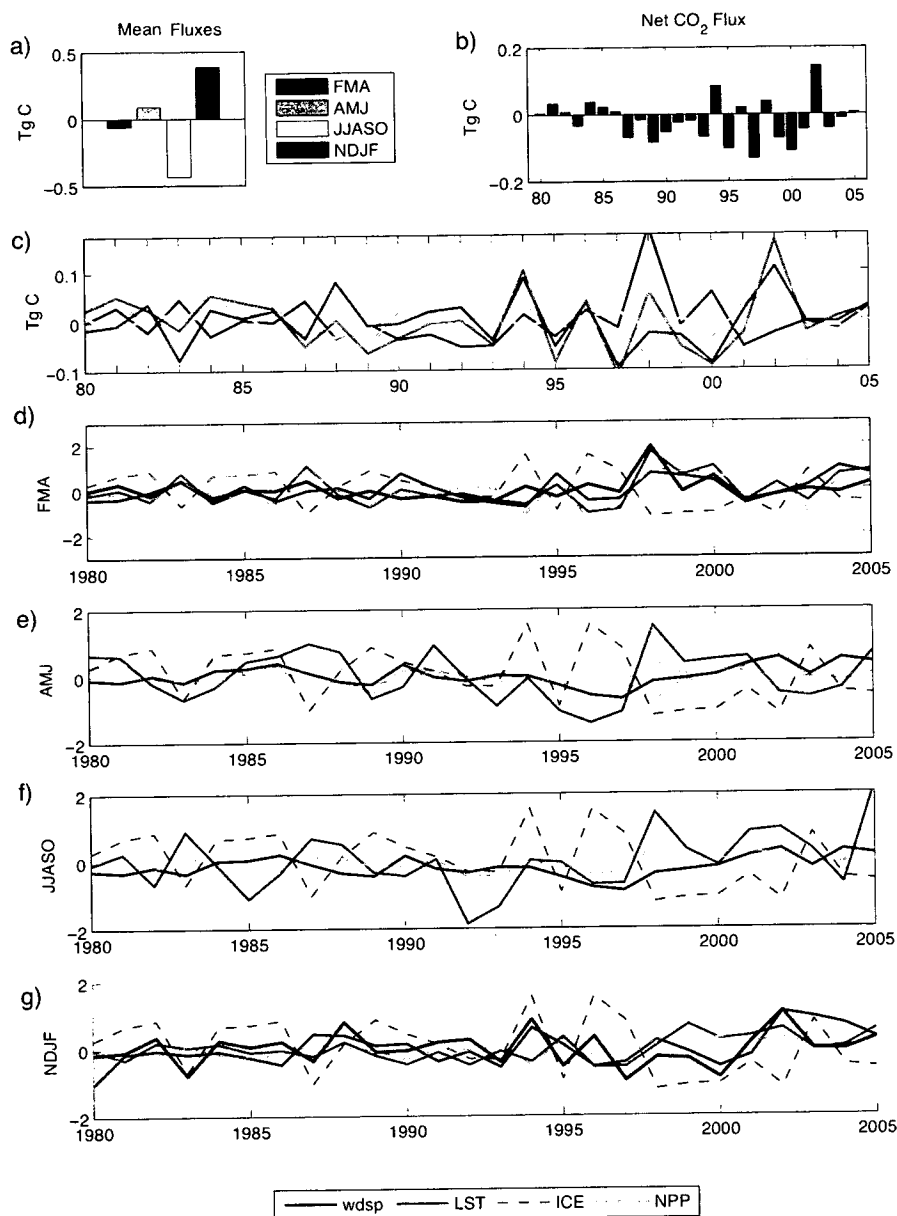


**Figure 4-9.** The mean seasonal (monthly) cycles of CO<sub>2</sub> (top) fluxes for both models are depicted in black (PM) and black dashed lines (NPM). Months are indicated by the month's first letter. Two years with contrasting climates, 1997 (middle) and 1998 (bottom) are also shown. A positive CO<sub>2</sub> flux is one *out* of the lake. The divisions of four seasons for analysis of the pCO<sub>2</sub> and CO<sub>2</sub> flux cycles are shown in shading. Start of each month is indicated by the month's first letter.

**Figure 4-10**

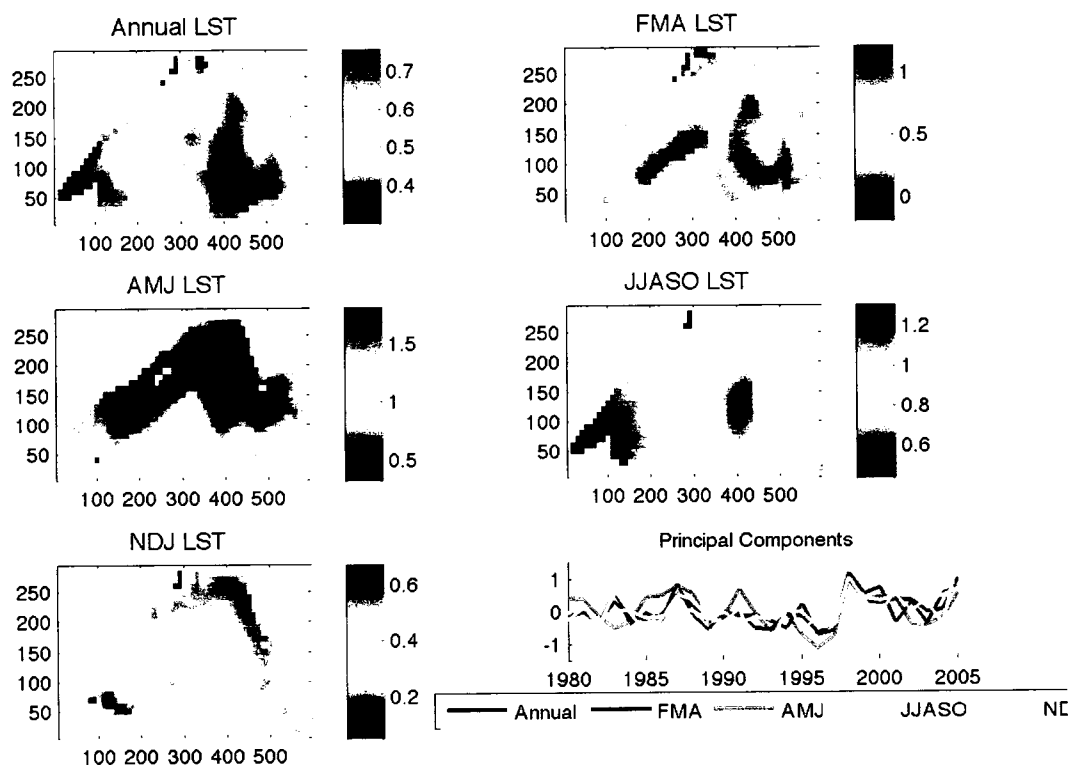
**Figure 4-10** Mean seasonal CO<sub>2</sub> fluxes (a) and net annual fluxes for 1980-2005 in the PM (b). All seasonal flux anomalies are plotted in (c) for a visual of how one season's flux alters another. (d)-(g) show seasonal flux *anomalies* for each individual season plotted against the corresponding seasonal anomalies in wind speed (black), lake surface temperature (magenta), net primary production (green dashed), and annual ice cover (blue dashed). There are no units, as the anomalies are normalized to a common scale for visualization. Seasonal colors from (a) are continued throughout the figure.

Figure 4-11



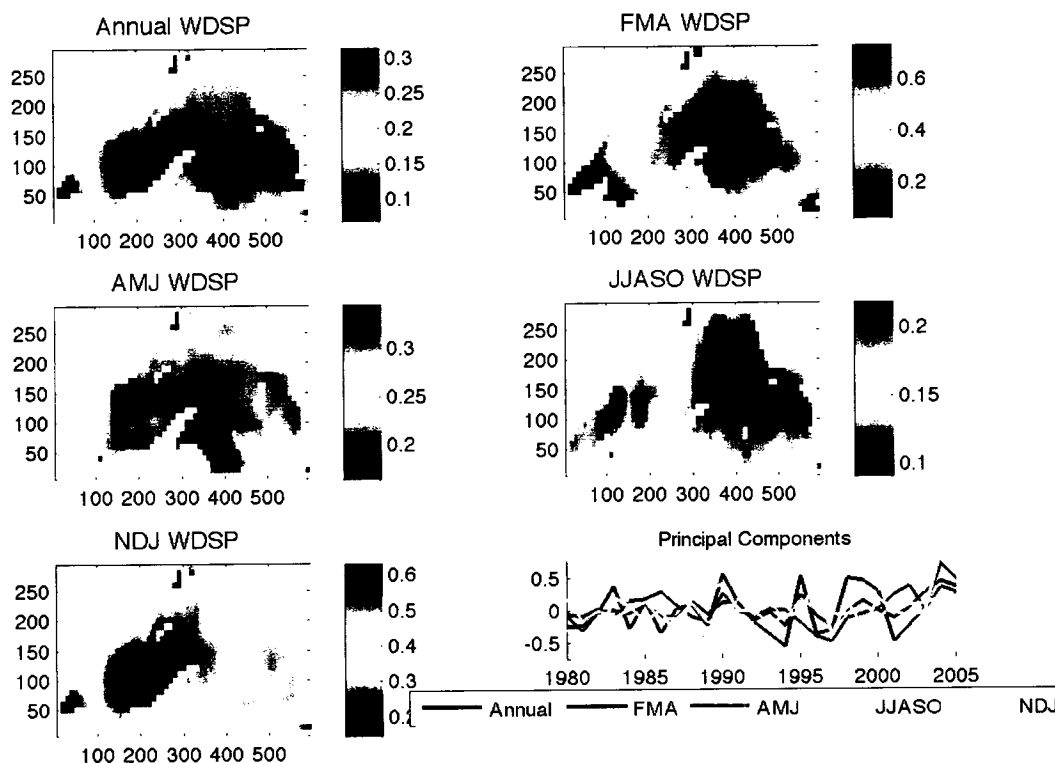
**Figure 4-11** Mean seasonal CO<sub>2</sub> fluxes (a) and net annual fluxes for 1980-2005 in the NPM (b). All seasonal flux anomalies are plotted in (c) for a visual of how one season's flux alters another. (d)-(g) show seasonal flux *anomalies* for each individual season plotted against the corresponding seasonal anomalies in wind speed (black), lake surface temperature (magenta), net primary production (green dashed), and annual ice cover (blue dashed). There are no units, as the anomalies are normalized to a common scale for visualization. Seasonal colors from (a) are continued throughout the figure.

Figure 4-12



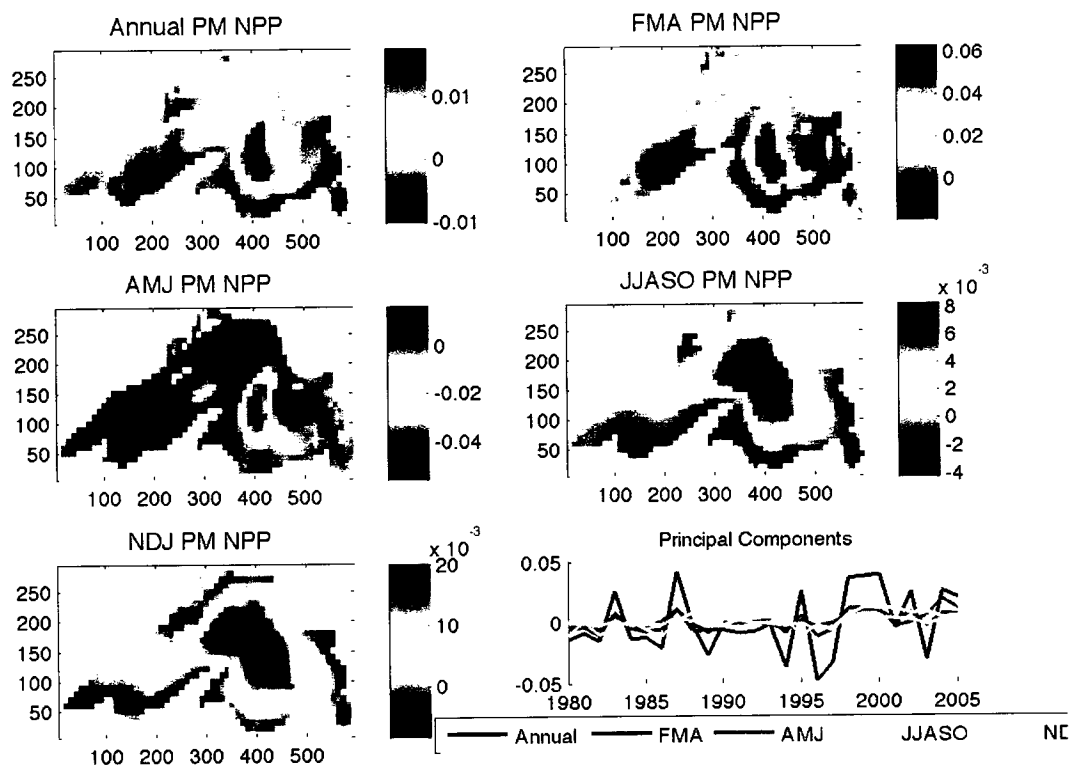
**Figure 4-12** The first EOFs of lake surface temperature for annual (top left), FMA (top right), AMJ (middle left), JJASO (middle right), and NDJ (bottom left). Units are  $^{\circ}\text{C}$ . The principal components for each of the EOFs are show at the bottom right. Note different temperature anomaly scales between seasons.

Figure 4-13



**Figure 4-13** The first EOFs of wind speed for annual (top left), FMA (top right), AMJ (middle left), JJASO (middle right), and NDJ (bottom left). Units are m/s. The principal components for each of the EOFs are show at the bottom right. Note that scale of wind speed anomalies is unique for each season.

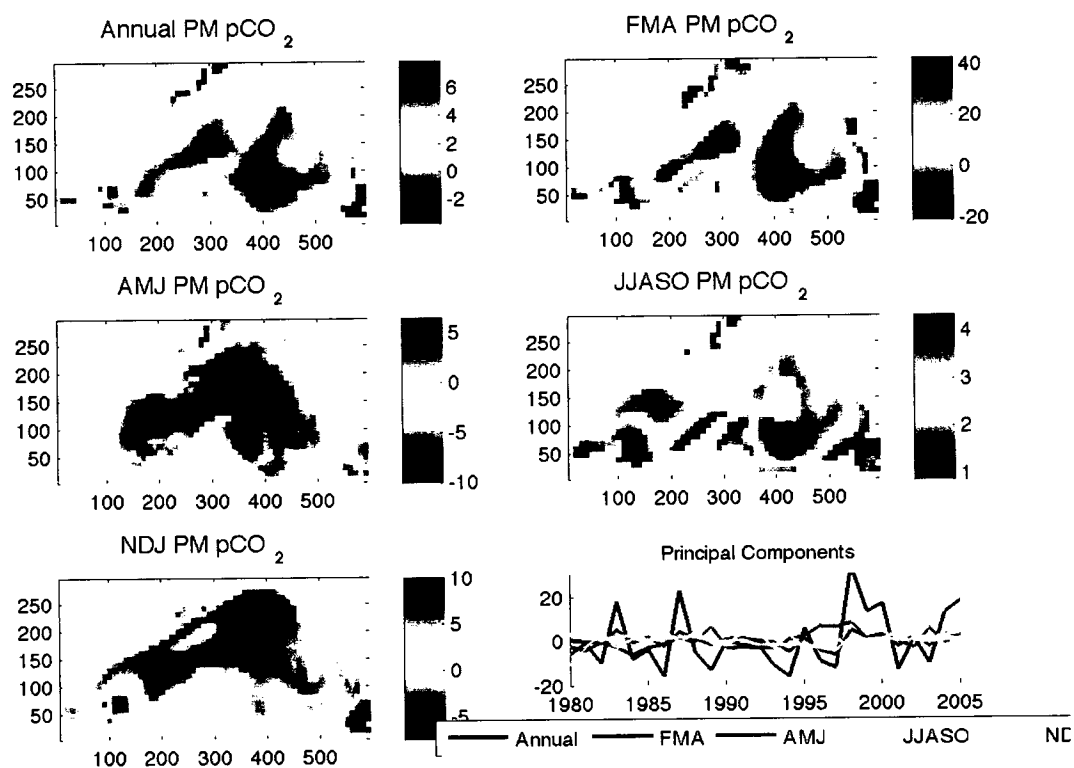
Figure 4-14



**Figure 4-14** The first EOFs of NPP in the phosphorus model for annual (top left), FMA (top right), AMJ (middle left), JJASO (middle right), and NDJ (bottom left) seasons, in TgC/yr. The principal components for each of the EOFs are show at the bottom right. Note that the scale of NPP anomalies varies according to season.

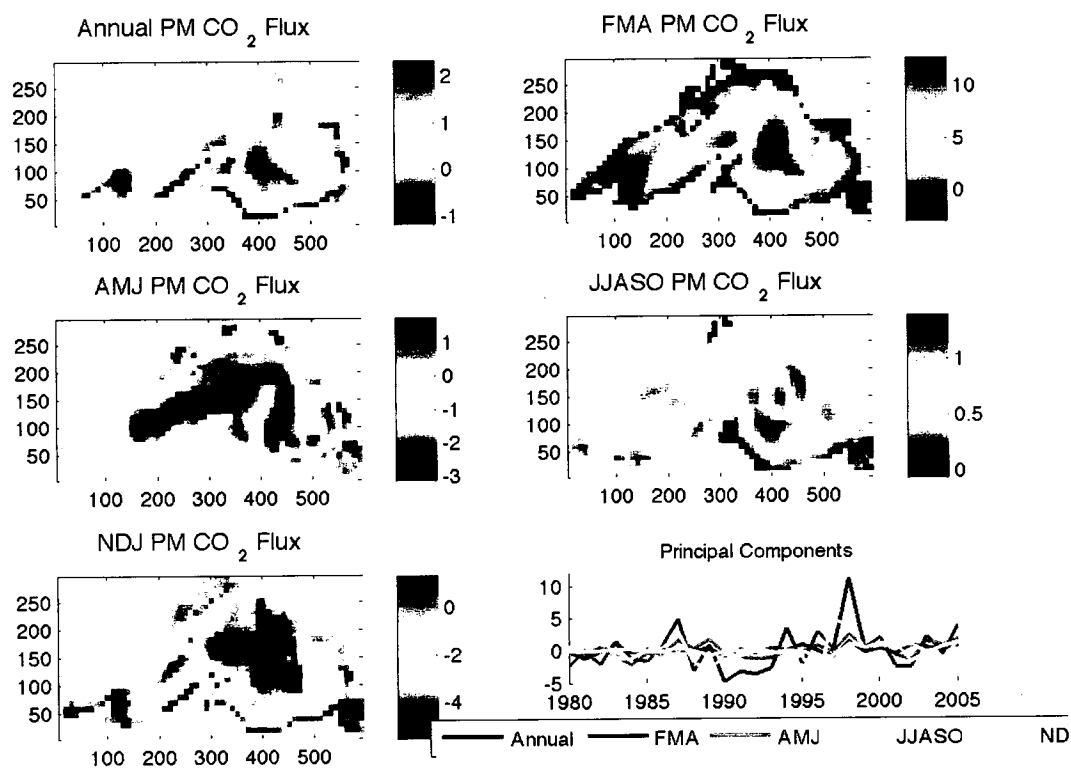


Figure 4-15

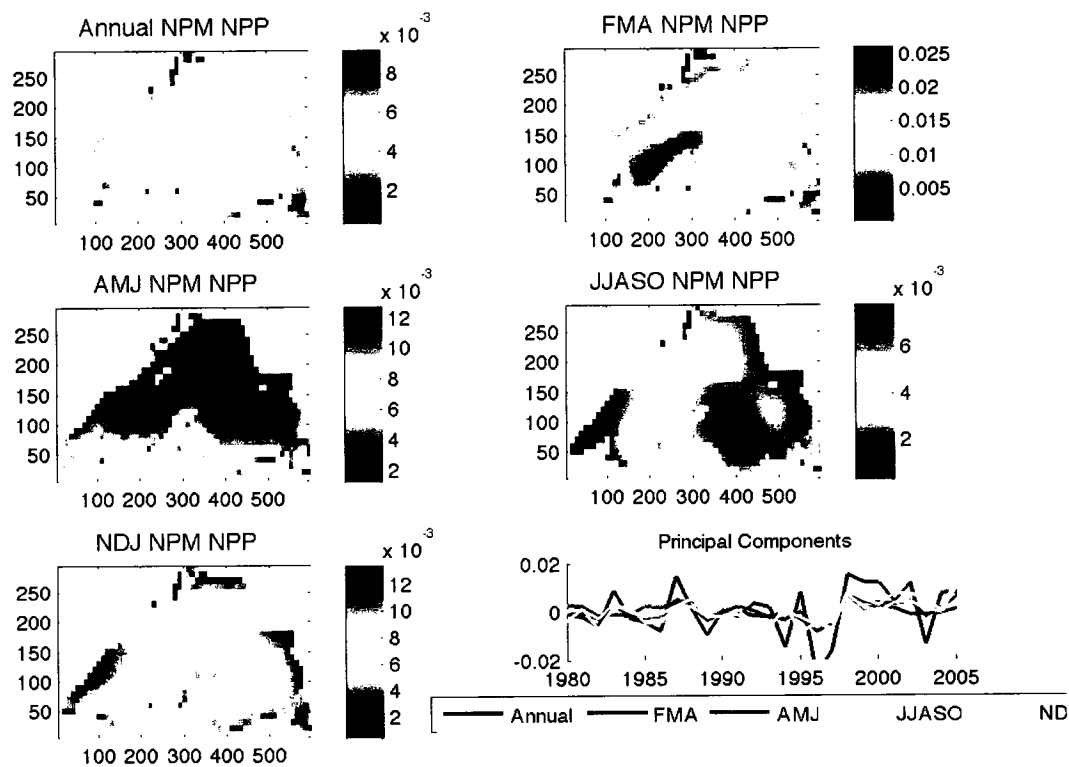


**Figure 4-15** The first EOFs of pCO<sub>2</sub> in the PM for annual (top left), FMA (top right), AMJ (middle left), JJASO (middle right), and NDJ (bottom left) seasons. Units are  $\mu\text{atm}$ . The principal components for each of the EOFs are show at the bottom right. Note the change of scale between seasons.

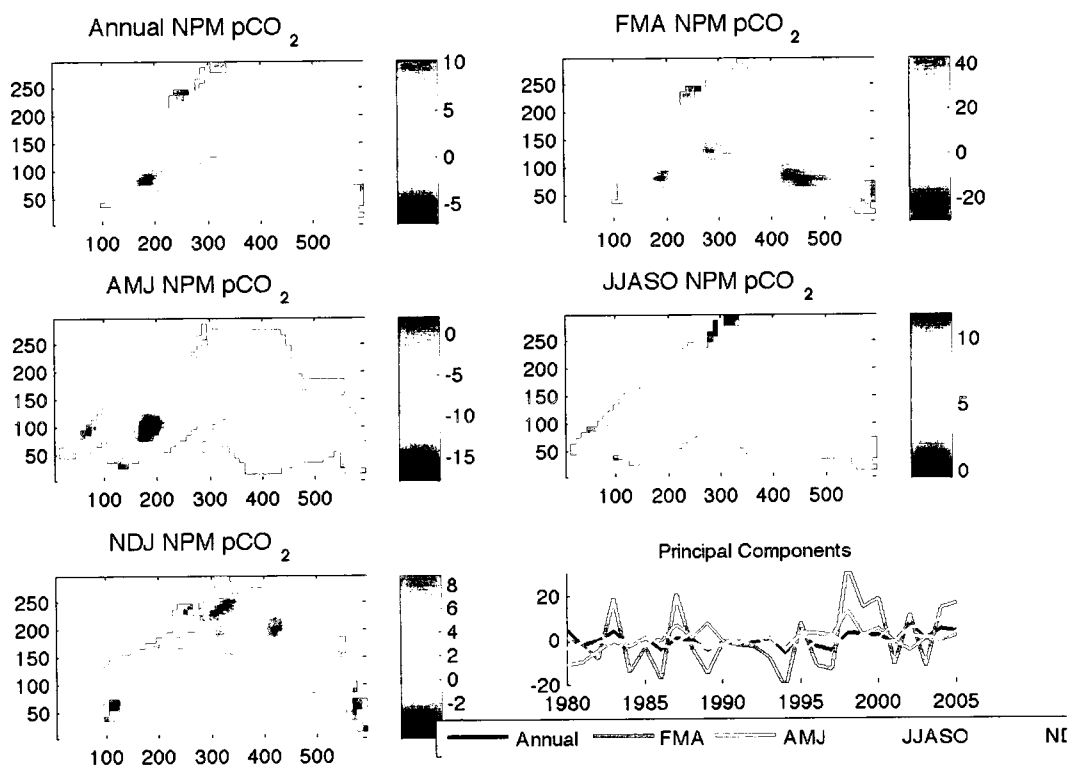
Figure 4-16



**Figure 4-16** The first EOFs of CO<sub>2</sub> flux in the PM for annual (top left), FMA (top right), AMJ (middle left), JJASO (middle right), and NDJ (bottom left) seasons. Units are gC/m<sup>2</sup>/yr. The principal components for each of the EOFs are show at the bottom right. Note the change in scale between seasons.

**Figure 4-17**

**Figure 4-17** The first EOFs of net primary production in the NPM for annual (top left), FMA (top right), AMJ (middle left), JJASO (middle right), and NDJ (bottom left) seasons. Units are TgC/yr. The principal components for each of the EOFs are show at the bottom right. Note the change in scale between seasons.

**Figure 4-18**

**Figure 4-18** The first EOFs of lake surface pCO<sub>2</sub> in the NPM for annual (top left), FMA (top right), AMJ (middle left), JJASO (middle right), and NDJ (bottom left) seasons. Units are  $\mu\text{atm}$ . The principal components for each of the EOFs are show at the bottom right. Note the change in scale of pCO<sub>2</sub> anomalies between seasons.

Figure 4-19

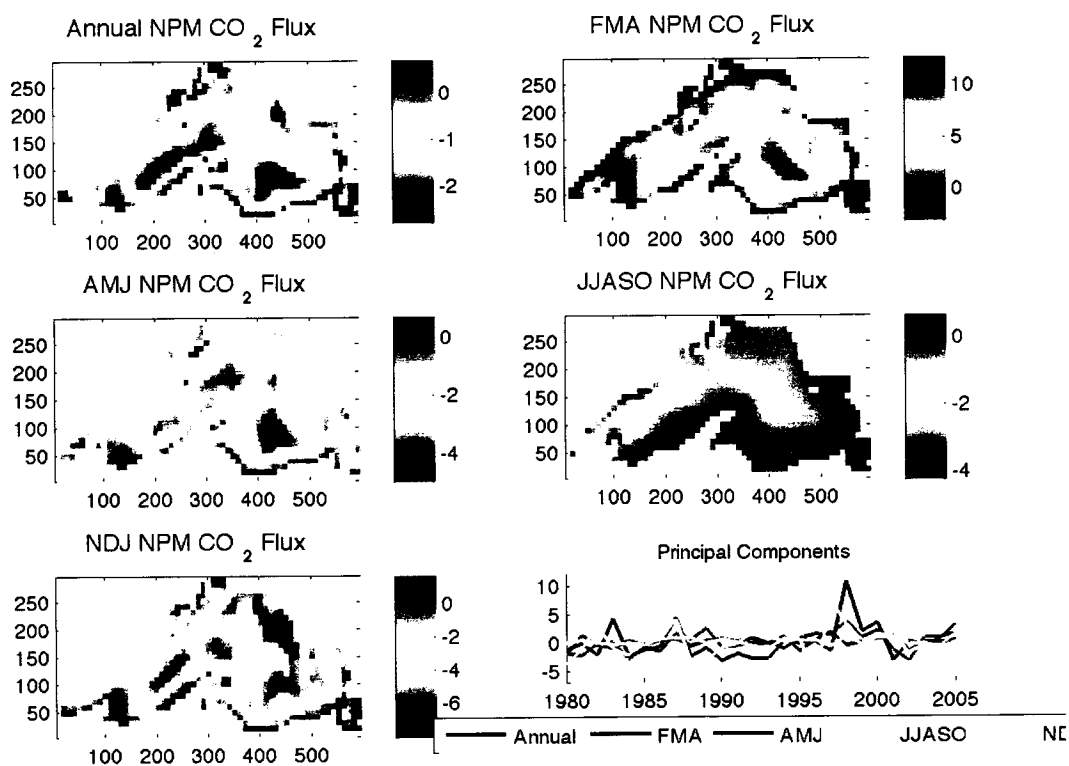


**Figure 4-19** The first EOFs of CO<sub>2</sub> fluxes in the NPM for annual (top left), FMA (top right), AMJ (middle left), JJASO (middle right), and NDJ (bottom left) seasons. Units are gC/m<sup>2</sup>/yr. The principal components for each of the EOFs are show at the bottom right. Note the change in scale between seasons.

## Chapter 5.

# Impact of River Runoff on the carbon cycle of Lake Superior

### 5.1 Introduction

Carbon budgets elucidated from observations sparse in space and time, and biased near shore, are largely imbalanced [Cotner *et al.*, 2004; Urban *et al.*, 2005]. Estimates of respiration far exceed those of photosynthesis, but no known source of carbon can account for such a discrepancy.

Rivers supply an estimated 0.9 TgC/yr [Urban *et al.*, 2005] to Lake Superior, and thus, have been disregarded as a possible explanation for the magnitude of respiration estimates. However, observations have been limited to primarily near shore locations and the far western arm of Lake Superior during spring and summer.

In Chapter 4, I show that a hydrodynamic model coupled to two unique ecosystem models are able to capture the chlorophyll and pCO<sub>2</sub> observed in the open waters of Lake Superior. The

model carbon budget is forced to be in balance, and the model suggests that the open lake may be in near equilibrium with the atmosphere over the year. Is it possible that river inputs of DOC, DIC, and alkalinity elevate near shore observations of respiration and create a near to offshore gradient in lake  $p\text{CO}_2$ ?

River inputs of DOC were previously believed to be recalcitrant and of little impact on the carbon cycle of the Arctic Ocean. However, recent studies suggest that significant amounts of labile DOC reach the Arctic Ocean via rivers and likely impact coastal carbon cycling on the Arctic shelf [Raymond *et al.*, 2007; Holmes *et al.*, 2008]. Decreases in river alkalinity are present during high flow conditions [Cooper *et al.*, 2008] and are thus likely in the tributaries of Lake Superior. Seasonal cycles of pH in Lake Superior tributaries are observed [Keller, 1983]. River DOC increases with flow in the arctic [McClelland *et al.*, 2007; Raymond *et al.*, 2007; Holmes *et al.*, 2008] and has been shown to increase with river flow in tributaries to Lake Superior [Urban *et al.*, 2005]. Such seasonality may cause an influx of low alkalinity, high DOC, and high DIC waters during the spring melt. Due to the strong near to offshore temperature gradient in Lake Superior and the coastal circulation pattern during summer (Chapter 3), it is reasonable to hypothesize that river inputs of carbon and alkalinity cause a significantly larger impact on the carbon cycle of near shore Lake Superior. Excess river DIC and the majority of labile river DOC may be respired within the coastal regions of Lake Superior, explaining large efflux estimates from near shore observations [Cotner *et al.*, 2004; Urban *et al.*, 2005] and a possible near equilibrium in the open waters (Chapter 4). In this chapter, river inputs of DOC, alkalinity, and DIC from the nine rivers of greatest flow into Lake Superior are added to determine whether a significant near to offshore gradient in  $p\text{CO}_2$  is possible in Lake Superior.

## 5.2 Methods

To access the lake-wide impact of river runoff on the carbon cycle of Lake Superior, the 2 km horizontal resolution circulation model is coupled to both the phosphorus and no phosphorus ecosystem models. I add river inputs of DIC, DOC, and alkalinity to the model at river mouth local grid cells. The nine largest rivers, chosen by drainage basin area, are used to assess impacts of runoff on the seasonal cycle and spatial heterogeneity of the lake's carbon cycle. Full descriptions of the nine rivers are given in Appendix A.1-A.9. River mouth locations are shown in Figure 5-1. To determine local effects of the river runoff, the 2 km horizontal resolution circulation model is coupled to both ecosystems. In order to include inputs of river DOC, I replace the original model tracer for autotrophic DOC with three separate tracers: highly labile DOC, background DOC, and refractory DOC. Autotrophic DOC, produced by the ecosystem of Lake Superior is considered to be 100% highly labile. All types of DOC move into the DIC pool once decomposed. All other tracers and parameters in the two ecosystem models are unchanged (Tables 4-1 and 4-2).

The nine rivers chosen comprise ~56% of the annual flow into Lake Superior [*Thompson, 1978*]. The impacts of river momentum and vorticity on lake momentum are ignored. There is no sedimentation in the model, nor is there outflow. Sedimentation is estimated to be small and located mainly offshore, where sediment re-suspension is less frequent [*McManus et al., 2003*]. Outflow from Lake Superior only occurs through St. Mary's River, a region somewhat cutoff from the rest of the lake in the 10 km model, and removing mass from the local model grid cell would result in an unrealistic localized loss of mass. Instead, river inputs of carbon and alkalinity are treated as local mixing events that increase or decrease local concentrations. I add all river



inputs to the model surface layer (top 5 m). Lake Superior is densest at 4°C. In summer, river water is warmer than lake water and less dense. During the spring thaw, the snowmelt brings nearly 0°C water to the lake. The lake is still unstratified, and the warmest water is at the lake bottom, with water near freezing at the surface. River temperature data from USGS indicated that for nearly all days of the year, river water is less dense than local lake water. Additionally, on the days when river water is denser than lake water, model sensitivity tests indicate that within four days, lake water mixes to the bottom during the spring mix.

The addition of river dissolved inorganic carbon (DIC) is treated as a mixing event at the surface of the model grid cell containing the river mouth. I use the daily average river flow from United States Geological Survey (USGS), Environment Canada (EC), or the Ontario Power Generation (OPG) (Appendix A) in combination with river DIC concentration to determine the change in local grid cell DIC concentration according to Equation 5-1.

$$\frac{\partial DIC}{\partial t} = \frac{flow}{volume} * DIC_{river} + (1 - \frac{flow}{volume}) * DIC_{lake} \quad \text{Equation 5-1}$$

Flow is the river flow rate in m<sup>3</sup>/s. Volume is the local grid cell volume. The concentration of DIC in river water is assumed to be a function of river flow. I use measurements of river temperature, pH, and alkalinity to estimate river DIC [Lewis and Wallace, 1998]. I use LOADEST, a USGS modeling tool, [Runkel et al., 2004] to determine the most likely relationship between river flow and river DIC concentrations based on the available observations. Thus, daily average DIC concentration is a function of the daily average river flow (see Appendix A).

I treat the addition of river alkalinity in the same manner. A unique relationship between river alkalinity and river flow is determined for the nine major rivers using LOADEST (Appendix A), and each river mouth has a different flow rate and alkalinity on any given day. Over time, excess DIC supplied by the rivers can be emitted via air-lake gas exchange, and thus, there should be little long-term DIC accumulation. Alkalinity cannot be removed in this way. Since I am neglecting the impact of precipitation on lake DIC and alkalinity, lake alkalinity would continuously increase over time with the addition of the nine largest river inputs. This is not simply a result of the surrounding geology, as watershed basins chosen for river inputs are not dramatically different from those not included. Rainwater has a very low alkalinity ( $<10 \text{ mg/L CaCO}_3 = 200 \text{ mmol/m}^3$ ), whereas river water draining to Lake Superior has alkalinity in the range of  $600 - >2000 \text{ mmol/m}^3$ . Rainwater provides an average of  $1605 \text{ mm/yr}$  ( $815$  over land and  $799$  over lake) to the lake while river flow brings  $610 \text{ mm/yr}$  to Lake Superior (<http://www.glerl.noaa.gov/data/arc/hydro/mnth-hydro.html>) between 1979 and 2006. The highly alkaline river water is diluted by rainwater and concentrated by evaporation ( $630 \text{ mm/yr}$ ) while in the lake. Thus, the mean lake alkalinity is relatively stable at  $838 \text{ mmol/m}^3$ . Neglecting these effects in the model would cause a significant increase in the lake's buffering capacity, which is not observed [Cotner *et al.*, 2004]. To correct for this, I relax lake surface alkalinity to  $838 \text{ mmol/m}^3$  with a time scale of 2 months. This allows for some local alkalinity effects, but prevents the model from drifting.

In contrast to alkalinity, rainwater DIC concentrations vary between  $50\text{-}2500 \text{ mmol/m}^3$  depending on its temperature ( $0\text{-}10^\circ\text{C}$ ), pH ( $5\text{-}6$ ), and alkalinity ( $10\text{-}200 \text{ mmol/m}^3$ ). The more alkaline the rainwater is, the greater its concentration of DIC for a given pH. I am neglecting the

impacts of precipitation and evaporation on the lake's carbon cycle, implicitly assuming those impacts would be uniformly distributed throughout the lake.

Dissolved organic carbon is deposited by the rivers into Lake Superior. During its estimated 30-35 yr residence time [Cotner *et al.*, 2004], this DOC may be remineralized into DIC and fluxed out of the lake; coagulate and sink; or flow out of the lake at St. Mary's. In the model, river DOC is added to the local model grid cell in the same manner as alkalinity and DIC. There are insufficient measurements of river DOC to vary the concentration of DOC as a function of individual river flow. Urban *et al.* [2005] found that the relationship between flow and DOC concentration is river specific; thus, I use a unique mean DOC concentration for each of the nine rivers (Appendix A) during all flow conditions. The lability of riverine DOC deposited into Lake Superior is unknown [Cotner *et al.*, 2004]. For both models, 15% of riverine DOC is assumed to be highly labile and remineralizes at the same rate as autochthonous (internal) DOC. This rate of remineralization is in fact different in the two models (Chapter 4, Tables 4-1 and 4-2). I assume that 84% of the river DOC is semi-labile and remineralizes with a time scale equal to the residence time for DOC in the lake (30 yr). I assume only 1% of the river DOC to be completely refractory, and its remineralization time scale is set at the lake water's residence time of 180 yr.

In fact, it is highly likely that the lability of DOC varies by season. DOC supplied to the Arctic Ocean via river inputs was believed to be refractory during its residence time in the Beaufort Gyre [Cooper *et al.*, 2005]. However, recent work has suggested that during the spring freshet, when there were no previous estimates, highly labile carbon is transported to the ocean where it is decomposed [Holmes *et al.*, 2008]. During the spring melt, cold temperatures, the scouring of

surface terrain, and rapid river flows allow for labile DOC to reach the ocean before being remineralized [Holmes *et al.*, 2007]. Lake Superior is also situated in a very cold environment where the maximum river flows occur during the spring melt. As I do not vary the percentages of highly labile, semi-labile, and refractory carbon over the year, I assume a relatively high percentage of highly-labile DOC in the rivers at all times. Frazer *et al.*, [2006] show a 15-25% loss in DOC over a 1 month period from three arctic rivers during the snowmelt period. Elizabeth Minor at the Large Lakes Observatory is currently researching how labile river DOC is in Lake Superior. My numbers are reasonable (personal communication, Prosper Zigah, 2010) given limited data constraints, but these are highly uncertain model parameters.

The impact of these model parameters will be seen near the river mouth. A higher fraction of highly labile material would cause more decomposition near the river mouth and thus, a higher pCO<sub>2</sub> and local efflux. A higher fraction of semi-labile material will cause the effect to be more lake-wide. In fact, the impact of semi-labile DOC is small, as remineralization rates are low and there is a high background concentration of semi-labile DOC. The two ecosystem models have different remineralization rates for highly labile DOC, so if model results were sensitive to small changes in the highly labile fraction, it could also be seen as a difference in local carbon cycle effects between the two ecosystem model runs.

To understand localized river effects and the extent of river impacts, I run both ecosystem models at 2 km horizontal resolution between 1996 and 1999, using 1996 as a spin up year. Tracer concentrations are initialized from the end of 1995 in the corresponding model runs from Chapter 4 (1979-2006 coupled runs); tracer concentrations are interpolated onto the 2 km grid.

Background DOC is added to the models, and it is initialized at  $115 \text{ mmol/m}^3$  everywhere, consistent with estimates of the DOC pool in Lake Superior [17 TgC, *Urban et al.*, 2005].

To assess the relative importance of inorganic carbon inputs to the lake, I run the models with river inputs, but do not include river inputs of DOC. I also run the models while only including the effects of organic material to the lake. In this case, I neglect any effects due to river alkalinity or river DIC. Only DOC is added to the lake. I determined 10 km model resolution to be adequate for lake-wide  $\text{pCO}_2$  effects and sensitivity experiments after a 2 km model run for the same time-period. Thus, inorganic/organic carbon sensitivity analyses are run at 10 km model resolution between 1996 and 2001.

### 5.3 Model-Observation Comparison

*Urban* [unpublished data] indirectly estimated  $\text{pCO}_2$  near shore during 2007 and 2008 at the Marquette Water Treatment Plant's intake and just northwest of the Ontonagon River (Figure 5-1). In Figures 5-2 (Ontonagon) and 5-3 (Marquette), I show *Urban's*  $\text{pCO}_2$  with blue asterisks by day of year, ignoring the fact that observations occurred during two separate years. In black crosses, I show estimates of  $\text{pCO}_2$  (1996-2006) from the nearest EPA station, offshore from *Urban's* observation locations. EPA station 5 is closest to Marquette, and EPA station 17 is closest to Ontonagon. I average the spring EPA  $\text{pCO}_2$  values and *Urban*  $\text{pCO}_2$  estimates from the first half of the year. Mean values for the spring season are show in red, crosses for EPA estimates and asterisks for *Urban* estimates. I use the same procedure for the remainder of the year in which observations were taken. The data suggest a significant difference between near

shore and open water  $p\text{CO}_2$  during both seasons and at both locations, with  $p\text{CO}_2$  higher near shore. The observations, although sparse and from differing years, suggest that the near to offshore surface  $p\text{CO}_2$  gradient is larger in summer.

Using the 2 km model run, I show model  $p\text{CO}_2$  differences between the two observation locations of Urban and the corresponding EPA locations in Figure 5.4. I also show the daily river flow from the Ontonagon River ( $\text{m}^3/\text{s}$ ). Contrary to suggestions by the observations, the modeled near to offshore gradient (positive indicates higher  $p\text{CO}_2$  near shore) is larger in the spring of 1997 and often negative. LOADEST predicts high alkalinity in the Ontonagon River, causing a reduction in local  $p\text{CO}_2$  at the river mouth part of the year. Although the observations suggest alkalinity as high as  $3000 \text{ meq}/\text{m}^3$  at the river mouth, the observations are from the 1970s.

Alkalinity observations are used to estimate DIC, and thus, could significantly alter estimated river effects. DIC concentrations in the river are significantly higher than in the lake, except for a short period at the start of summer. Thus, the lack of a large near to offshore gradient may be due to the alkalinity, and resulting DIC, values used. As there are no rivers near Marquette in the model, near shore values of  $p\text{CO}_2$  will be low during the start of the coastal bloom (April, May) when the open waters have not yet stratified. Only minimal river impacts would be expected.

The general result is not sensitive to the ecosystem model used (NPM / PM).

Due to the fact the Ontonagon River is the only river to lower local  $p\text{CO}_2$  in the model frequently, which may be due to forcing error, I look at the near to offshore gradient in  $p\text{CO}_2$  by the Black Sturgeon River. The drainage basin of the Black Sturgeon River is closest in size to the Ontonagon River, although slightly smaller. Figure 5-5 shows the near (within 4 km of shore) to

offshore gradient of  $p\text{CO}_2$  in blue near the mouth of the Black Sturgeon River for 1996-1999. River flow ( $\text{m}^3/\text{s}$ ) is shown in green. Note the differing scales for each year. Before the spring melt and high flow, there is a large (hundreds of  $\mu\text{atm}$ ) near to offshore gradient. This is likely compounded by the presence of ice. After the melt and ice breakup, the gradient is large following high flow conditions, but extremely variable, suggesting areas impacted by rivers must be observed with high frequency over the year to estimate  $p\text{CO}_2$  and gradients. Outside of the spring-melt, the gradient is largest in early summer and fall. The model is capturing huge near to offshore gradients. The gradient is sensitive to season and flow conditions, suggesting that if rivers near Marquette were included and recent alkalinity observations from the Ontonagon made available, the model might be able to capture the magnitude of  $p\text{CO}_2$  observed by Urban.

The model shows significant near to offshore  $p\text{CO}_2$  gradients driven by river inputs. How do these inputs affect the whole lake carbon cycle?

## 5.4 Results

Figures 5-6 and 5-7 show the annual mean difference in  $p\text{CO}_2$  due to river and allochthonous DOC throughout the lake between 1997 and 2001. Figure 5-6 shows the results from the NPM, and Figure 5-7 shows river effects in the PM. Rivers negligibly affect open lake  $p\text{CO}_2$  in the NPM, likely due to the slowly remineralizing semi-labile DOC pool ( $\tau = 30 \text{ yr}$ ). The phosphorus model shows a slightly larger river influence lake-wide. The difference between the two models is due to the rapidly remineralizing highly labile pool in the PM (20%/day) versus in NPM

(1%/day) that allows the deposited DOC to remineralize away from the river mouth, but before mixing throughout the lake. This is confirmed by the larger river influence in the western arm, which is not present in the NPM. Both models have unique seasonal cycles of primary productivity (Chapter 4), allowing river inputs to have a larger impact on the PM and its seasonal cycle (Figure 5-9).

In Figures 5-8, I show the seasonal cycles of  $p\text{CO}_2$  at the 17 non-coastal EPA stations for the non-phosphorus model for 1996-2001. I include results from the model run including all river effects (purple) and for no river effects (black). Dashed lines indicate the standard deviation among stations for the corresponding model run. I show the same for PM in Figure 5-9. The rivers increase summer  $p\text{CO}_2$  only slightly in the NPM and occasionally decrease winter  $p\text{CO}_2$ . In the PM, summer  $p\text{CO}_2$  is more increased, as biological productivity peaks in spring and increases the autochthonous DOC pool in May. Productivity in the NPM is just getting going, so river effects are not compounded by decaying phytoplankton. Overall agreement with  $p\text{CO}_2$  estimates from EPA data remains the same with the addition of rivers.

When including the rivers from the nine largest drainage basins, the net air-lake  $\text{CO}_2$  flux increases by an order of magnitude. The models must be in equilibrium with the atmosphere on long time scales when river inputs are neglected. Thus, the modeled net efflux is determined by the magnitude of river DOC and the  $p\text{CO}_2$  of river water entering the lake. The lake goes from being a small sink of atmospheric carbon dioxide due to an increase in anthropogenic atmospheric  $\text{CO}_2$  when neglecting river inputs to a net source. The models disagree as to the exact value of this efflux, but the mean is 0.2 TgC/yr to the atmosphere (Figure 5-10). The model



disagreement is due to a summer influx in the no phosphorus model (Figure 5-11) that is not present in the phosphorus model (Chapter 4).

The relative impacts of DIC and DOC can be seen in a sample year in Figures 5-12 (PM) and 5-13 (NPM). I plot the lake-wide mean seasonal cycle of  $p\text{CO}_2$  for the model test runs: no rivers (black), all river effects (blue), no DIC (red), and no DOC (green). Dashed lines indicate one standard deviation of  $p\text{CO}_2$  (spatial) for any given day. Including all model grid cells makes it possible to distinguish seasonal cycles for model test runs including any river effects (not shown). Both models are most impacted by the inclusion of river DOC. This impact is largest during the spring melt, when lake-wide  $p\text{CO}_2$  is increased by 2-5  $\mu\text{atm}$  by including terrestrial DOC. More spatial variability exists in the PM when only including the effects of DOC (red). Due to a more rapid rate of remineralization in the PM, highly labile material deposited at river mouths moves ~200 km before decomposing, whereas this material would move an average of 1000 km in the NPM before decomposition. Thus, material moves away from the mouth, but not lake-wide, before becoming DIC in the PM.

## 5.4 Discussion and Conclusions

I have added river inputs of DIC, alkalinity, and DOC to two ecosystem models coupled to a hydrodynamic model of Lake Superior. Both models suggest that these nine rivers cause an annual efflux on the order of 0.1 TgC/yr from Lake Superior. The largest river effects can be seen during the spring melt and resulting high stream flows. The rivers do not significantly

impact the seasonal cycle of  $p\text{CO}_2$  at the 17 open lake EPA stations.  $p\text{CO}_2$  is increased there slightly (6-15  $\mu\text{atm}$ ) due to the inclusion of a background DOC pool and river inputs.

The model is able to capture a large near-to-offshore  $p\text{CO}_2$  gradient near the mouth of the Black Sturgeon River. The magnitude of this gradient is comparable to crudely estimated near to offshore surface  $p\text{CO}_2$  gradients from the Ontonagon River and offshore from Marquette. The model does not capture such a large gradient from the mouth of the Ontonagon River, which may be due to the highly uncertain DIC and alkalinity values used as river inputs there. The model suggests that huge near to offshore gradients can be caused by river effects and are largest during high flow conditions. The exact magnitude of these effects are dependent on river concentrations of alkalinity, DIC, and DOC. For most rivers, alkalinity is the best known solute. DIC was estimated from pH, temperature, and alkalinity for any day that all three measurements exist. pH was measured with an electrode and therefore subject to the same uncertainties as the EPA data (Chapter 4.6.1). This can easily cause an overestimate of river DIC. For some rivers, such as the Ontonagon River, data had to be used from separate river branches and from more than thirty years ago. However, with all of the uncertainty in river constituent concentrations, the models show that even with varying remineralization rates and seasonal cycles of primary productivity, the rivers cause an elevation of near shore  $p\text{CO}_2$  and a net efflux of  $\text{CO}_2$  near shore.

River DOC was the most important river solute impacting Lake Superior  $p\text{CO}_2$  by 3-6  $\mu\text{atm}$  at the 17 open lake EPA stations, with significantly larger impacts near river mouths. DIC impacts the mouth and its immediate neighbors, with a smaller lake-wide effect (1-2  $\mu\text{atm}$ ). DOC is rarely measured in the rivers, and only a mean estimate of its concentration was available. In

reality, this concentration varies with flow and is higher during high flow conditions [Raymond *et al.*, 2007; Urban *et al.*, 2005]. The relationship with flow is river specific, so a large number of observations would be necessary to improve this aspect of the model. The fraction of river DOC that is labile also varies by time of year [Holmes *et al.*, 2008] and is unconstrained in Lake Superior [Cotner *et al.*, 2004]. The work of Elizabeth Minor at LLO will prove to be useful in constraining estimates of lability.

Lake Superior has more than 200 tributaries, and thus, the results found here should be extrapolated lake-wide. Coastal regions near river mouths will experience a local increase in pCO<sub>2</sub>. Dependent on the rate of remineralization in the lake and the fraction of labile carbon in river DOC, the effects will be seen for tens to hundreds of kilometers downstream. This downstream effect is on the order of 1-10 µatm, dependent on the stream size. The model includes an estimated 56% of annual river flow to Lake Superior; thus, it is reasonable to assume that the modeled efflux is only half of the actual efflux. This efflux (0.2-0.4 Tg C/yr) is still an order of magnitude lower than suggested by previous studies [3 Tg C/yr, Urban *et al.*, 2005], supporting the conclusion that annual, lake-wide respiration rates have been overestimated for Lake Superior.

The models show that rivers likely create a strong near to offshore gradient in pCO<sub>2</sub>. This effect is largest in the western arm in the PM, and likely exists around the lake wherever river mouths or runoff from land are present. The model produces a large gradient of pCO<sub>2</sub> while still capturing pCO<sub>2</sub> estimates by EPA, within the large uncertainty. Lake Superior does not appear to be a large source of atmospheric CO<sub>2</sub>, and I would estimate its net annual efflux as < 1 TgC/yr.

Most observations used to create a carbon budget for Lake Superior have been within the reaches of river and land influence, and this study clearly illustrates the need for observations further offshore.

## Figure Captions

**Figure 5-1** Map of Lake Superior. The largest drainage basins to Lake Superior are depicted in light gray. The mouths of the nine rivers used in this study are depicted with X's and names are shown in the top left legend. EPA biannual survey station locations are shown with circles. Observation locations for *Urban* [unpublished data] are labeled ONT for Ontonagon and MQT for Marquette.

**Figure 5-2** Indirect estimates of surface pCO<sub>2</sub> [*Urban*, unpublished] at station ONT (Ontonagon) for 2007 and 2008 are shown with blue astericks. Indirect estimates of pCO<sub>2</sub> from EPA observations (1996-2006) offshore from ONT at station SU17 are shown with black crosses. Mean values of spring (MAMJ) and summer (JASO) pCO<sub>2</sub> for near and offshore locations are shown in red with the corresponding marker. Crudely estimated near to offshore pCO<sub>2</sub> gradients are shown with a purple line and labeled for both seasons.

**Figure 5-3** Indirect estimates of surface pCO<sub>2</sub> [*Urban*, unpublished] at station MQT (Marquette) for 2007 and 2008 are shown with blue astericks. Indirect estimates of pCO<sub>2</sub> from EPA observations (1996-2006) offshore from ONT at station SU05 are shown with black crosses. Mean values of spring (MAMJ) and summer (JASO) pCO<sub>2</sub> for near and offshore locations are shown in red with the corresponding marker. Crudely estimated near to offshore pCO<sub>2</sub> gradients are shown with a purple line and labeled for both seasons.

**Figure 5-4** Daily modeled near to offshore pCO<sub>2</sub> gradient from MQT to SU05 (blue) and from ONT to SU17 (black) for 1996-1999. Ontonagon river flow is shown in green.

**Figure 5-5** Daily modeled near to offshore pCO<sub>2</sub> gradient from 3 km offshore to 20 km offshore from the mouth of the Black Sturgeon River for 1996-1999. Black Sturgeon river flow (m<sup>3</sup>/s) is shown in green.

**Figure 5-6** Annual mean difference in surface pCO<sub>2</sub> between the NPM model run with rivers and the NPM model run without rivers. Open lake pCO<sub>2</sub> differs by less than 5 μatm over the course of the year, on the mean. River mouth locations show significant river effects of over 100 μatm in some locations.

**Figure 5-7** Annual mean difference in surface pCO<sub>2</sub> between the PM model run with rivers and the PM model run without rivers. Open lake pCO<sub>2</sub> differs by less than 20 μatm over the course of the year. River mouth locations show significant river effects of over 100 μatm in some locations.

**Figure 5-8** Seasonal cycles of modeled pCO<sub>2</sub> at the 17 open lake EPA stations between 1996 and 2001 in the NPM. Model runs including river inputs are shown in purple, and control runs are shown in black. One standard deviation of modeled pCO<sub>2</sub> at the 17 stations for each day is shown with dashed lines in respective colors. Estimates of pCO<sub>2</sub> at the EPA stations [Atilla *et al.*, 2010] are shown with whisker box plots.

**Figure 5-9** Seasonal cycles of modeled  $p\text{CO}_2$  at the 17 open lake EPA stations between 1996 and 2001 in the PM. Model runs including river inputs are shown in purple, and control runs are shown in black. One standard deviation of modeled  $p\text{CO}_2$  at the 17 stations for each day is shown with dashed lines in respective colors. Estimates of  $p\text{CO}_2$  at the EPA stations [Atilla *et al.*, 2010] are shown with whisker box plots.

**Figure 5-10** Annual net fluxes (positive to the atmosphere) of carbon dioxide from Lake Superior when including the nine major rivers. Circles are results from the phosphorus model, and crosses indicate results from the no phosphorus model.

**Figure 5-11** Modeled seasonal cycles of lake-wide  $p\text{CO}_2$  for 1997-2001 in the phosphorus model (black) and no phosphorus model (red).

**Figure 5-12** Lake-wide mean  $p\text{CO}_2$  in PM river test runs for 1997. Black line is model run including no river effects. The blue line indicates  $p\text{CO}_2$  cycle for model run including all river effects. Red and green lines indicate model runs without DIC and DOC, respectively. Dashed lines indicate lake-wide standard deviation of  $p\text{CO}_2$  for the corresponding model run.

**Figure 5-13** Lake-wide mean  $p\text{CO}_2$  in NPM river test runs for 1997. Black line is model run including no river effects. The blue line indicates  $p\text{CO}_2$  cycle for model run including all river effects. Red and green lines indicate model runs without DIC and DOC, respectively. Dashed lines indicate lake-wide standard deviation of  $p\text{CO}_2$  for the corresponding model run.

## Figures

**Figure 5-1**

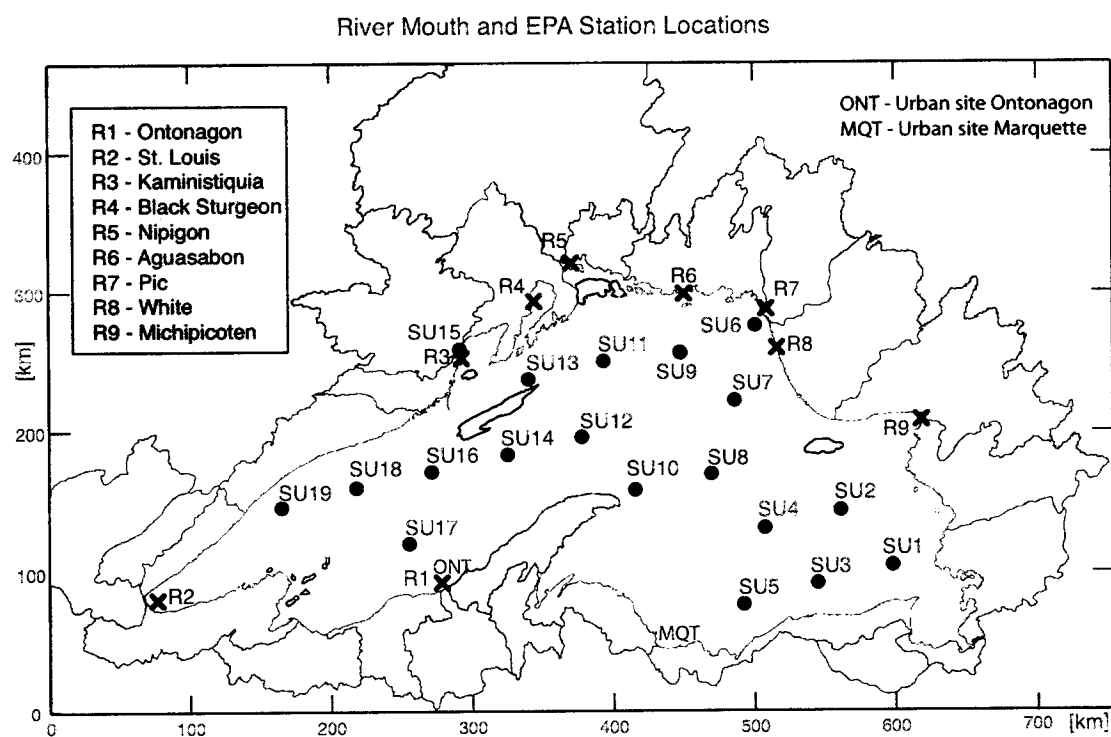


Figure 5-1 Map of Lake Superior. The largest drainage basins to Lake Superior are depicted in light gray. The mouths of the nine rivers used in this study are depicted with X's and names are shown in the top left legend. EPA biannual survey station locations are shown with circles. Observation locations for *Urban* [unpublished data] are labeled ONT for Ontonagon and MQT for Marquette.

Figure 5-2.

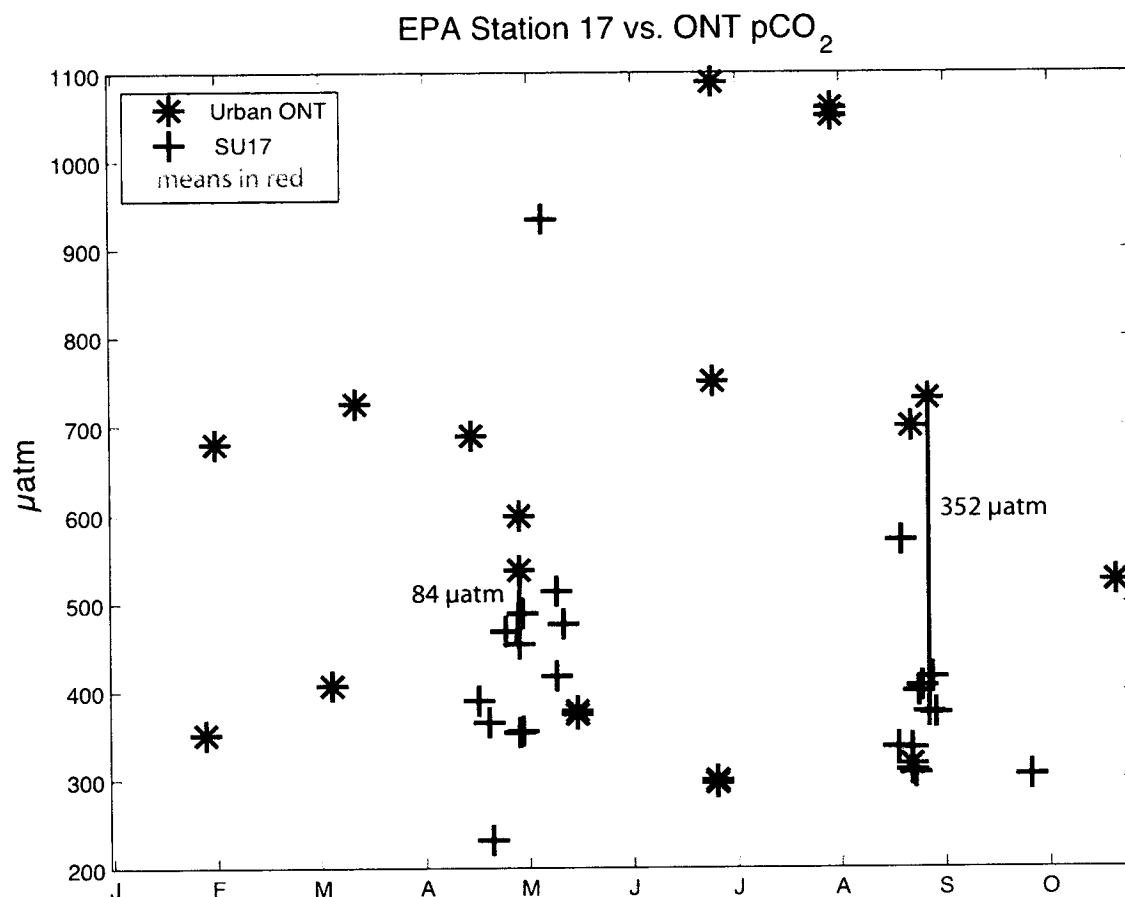


Figure 5-2 Indirect estimates of pCO<sub>2</sub> [*Urban*, unpublished data] at station ONT (Ontonagon) for 2007 and 2008 are shown with blue astericks. Indirect estimates of pCO<sub>2</sub> from EPA observations (1996-2006) offshore from ONT at station SU17 are shown with black crosses. Mean values of spring (MAMJ) and summer (JASO) pCO<sub>2</sub> for near and offshore locations are shown in red with the corresponding marker. Crudely estimated near to offshore pCO<sub>2</sub> gradients are shown with a purple line and labeled for both seasons.



Figure 5-3

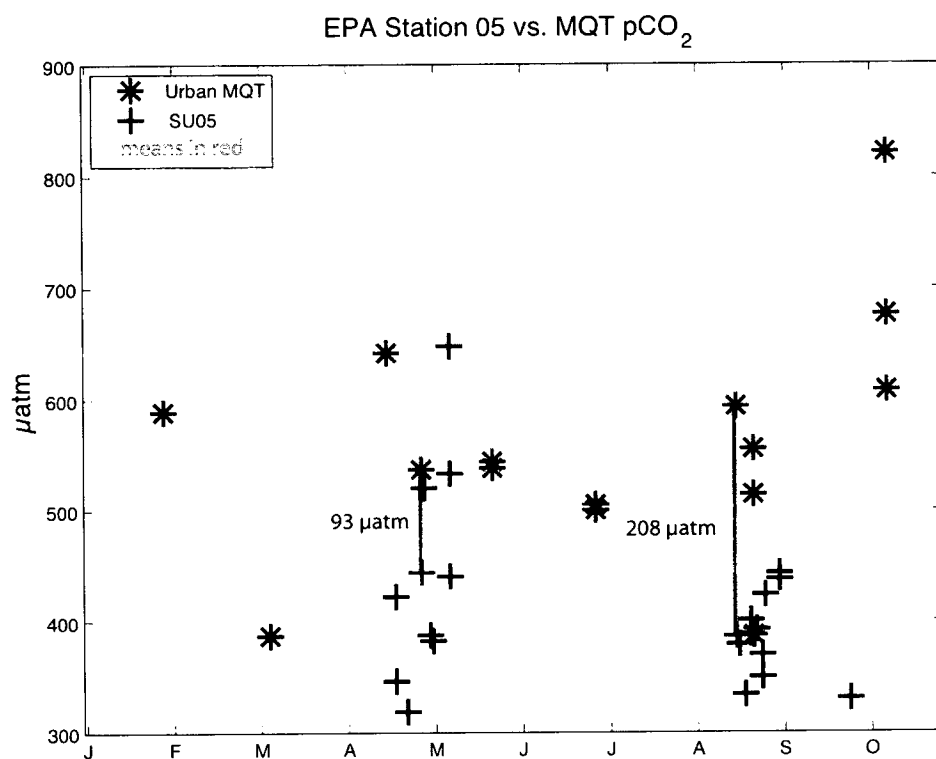


Figure 5-3 Indirect estimates of surface pCO<sub>2</sub> [*Urban, unpublished*] at station MQT (Marquette) for 2007 and 2008 are shown with blue asterisks. Indirect estimates of pCO<sub>2</sub> from EPA observations (1996-2006) offshore from ONT at station SU05 are shown with black crosses. Mean values of spring (MAMJ) and summer (JASO) pCO<sub>2</sub> for near and offshore locations are shown in red with the corresponding marker. Crudely estimated near to offshore pCO<sub>2</sub> gradients are shown with a purple line and labeled for both seasons.

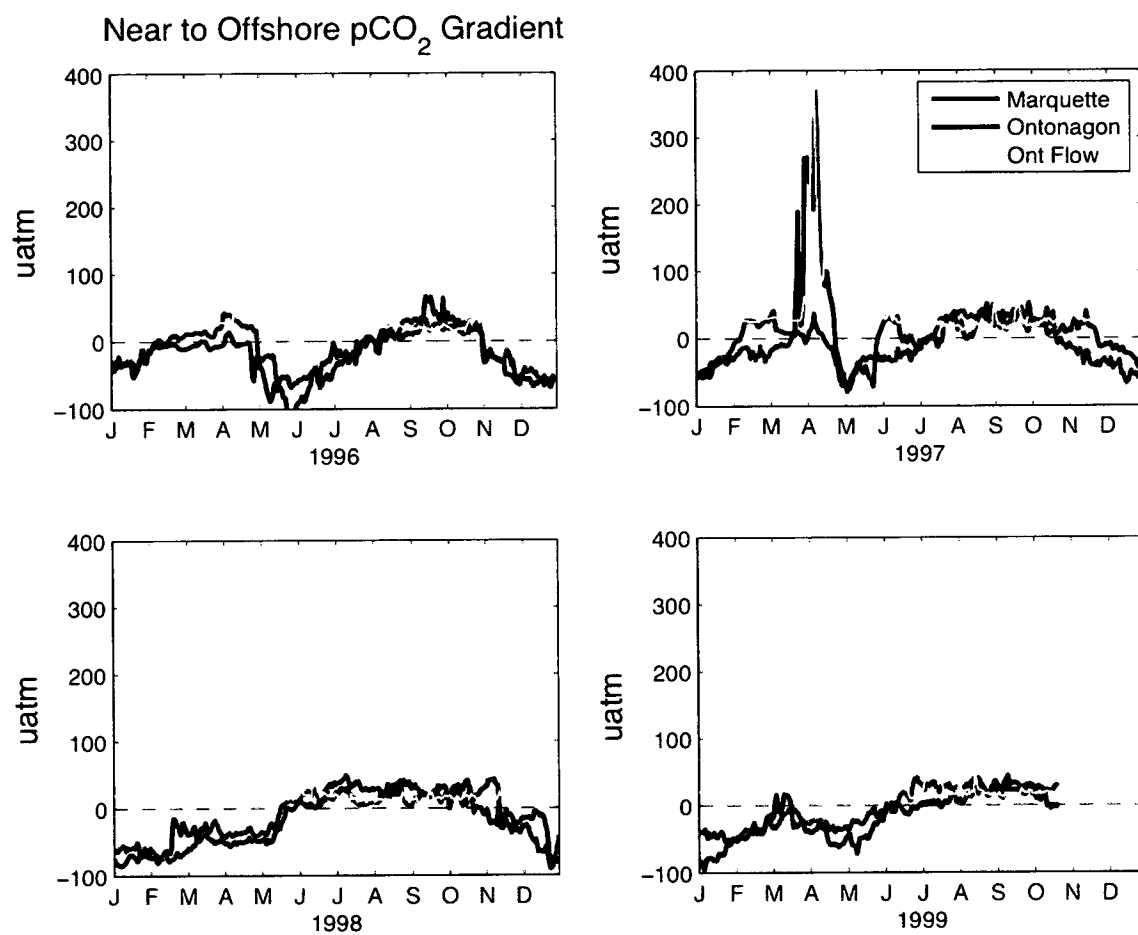
**Figure 5-4**

Figure 5-4 Daily modeled near to offshore pCO<sub>2</sub> gradient from MQT to SU05 (blue) and from ONT to SU17 (black) for 1996-1999. Ontonagon river flow is shown in green.

Figure 5-5

Near to Offshore near Black Sturgeon River

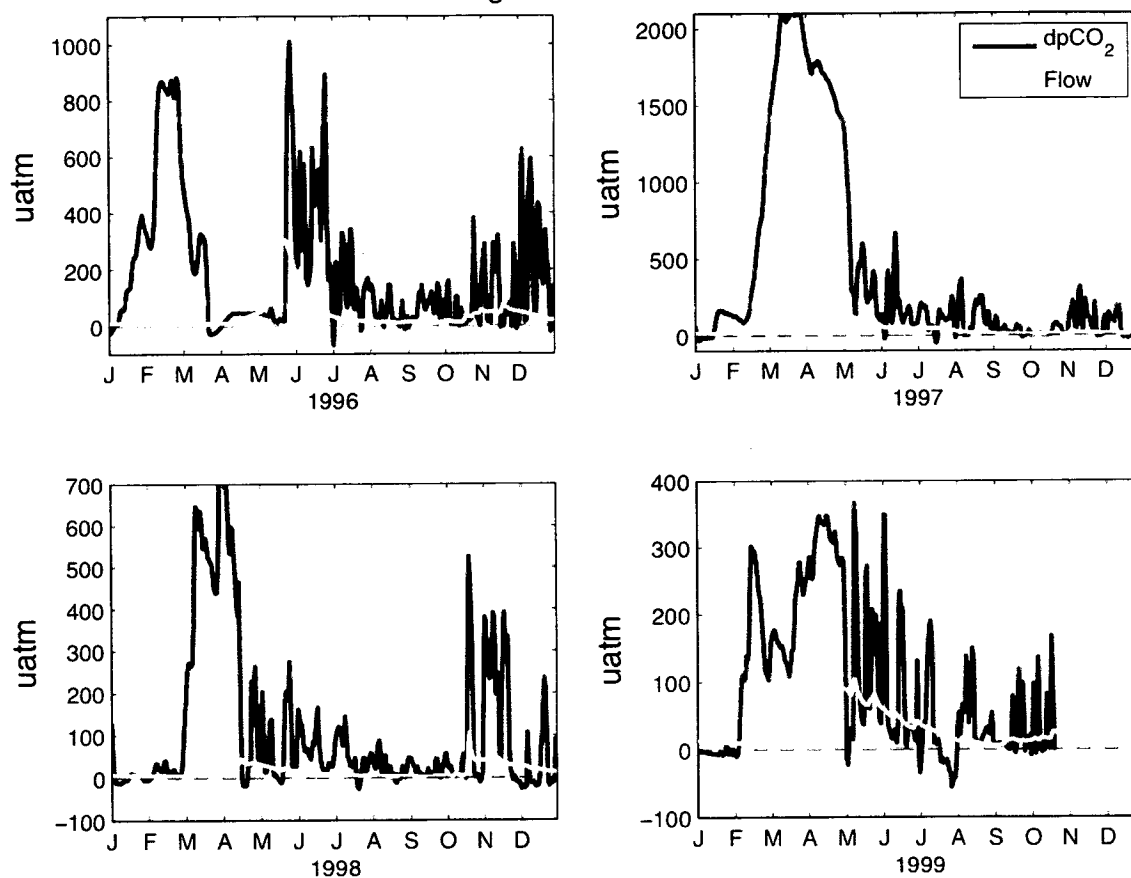


Figure 5-5 Daily modeled near to offshore pCO<sub>2</sub> gradient from 3 km offshore to 20 km offshore from the mouth of the Black Sturgeon River for 1996-1999. Black Sturgeon river flow (m<sup>3</sup>/s) is shown in green.

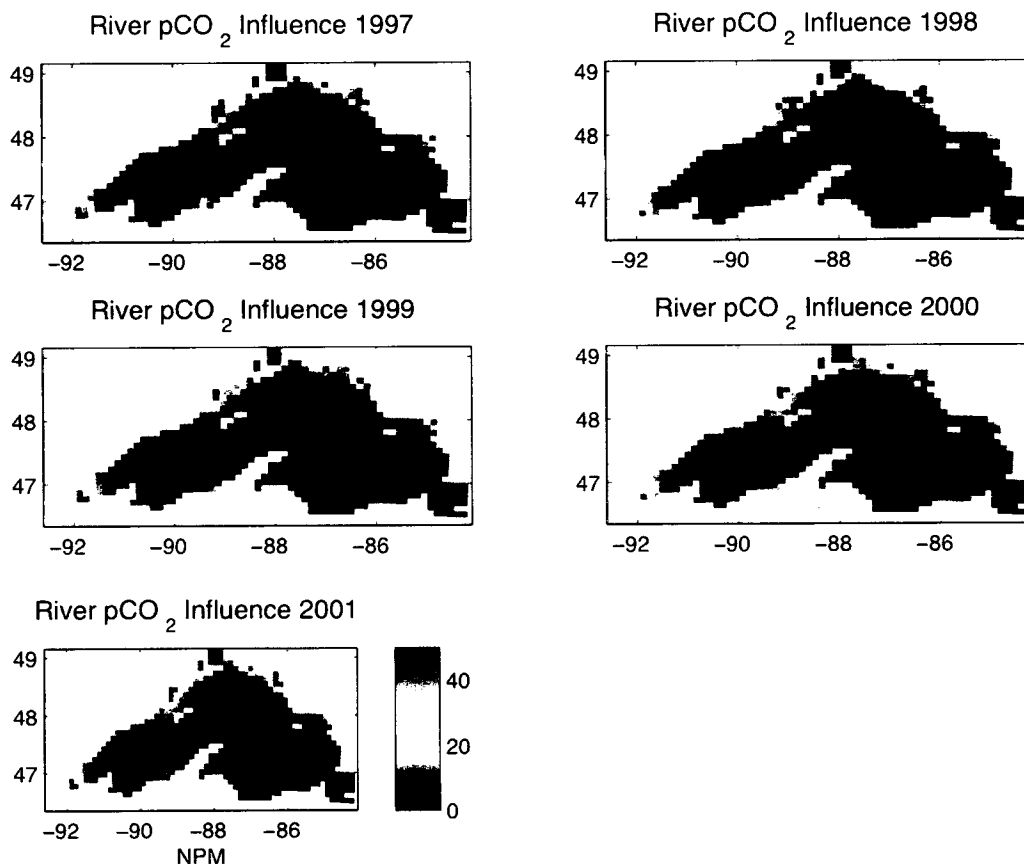
**Figure 5-6**

Figure 5-6 Annual mean difference in surface pCO<sub>2</sub> between the NPM model run with rivers and the NPM model run without rivers. Open lake pCO<sub>2</sub> differs by less than 5  $\mu$ atm over the course of the year, on the mean. River mouth locations show significant river effects of over 100  $\mu$ atm in some locations.

Figure 5-7

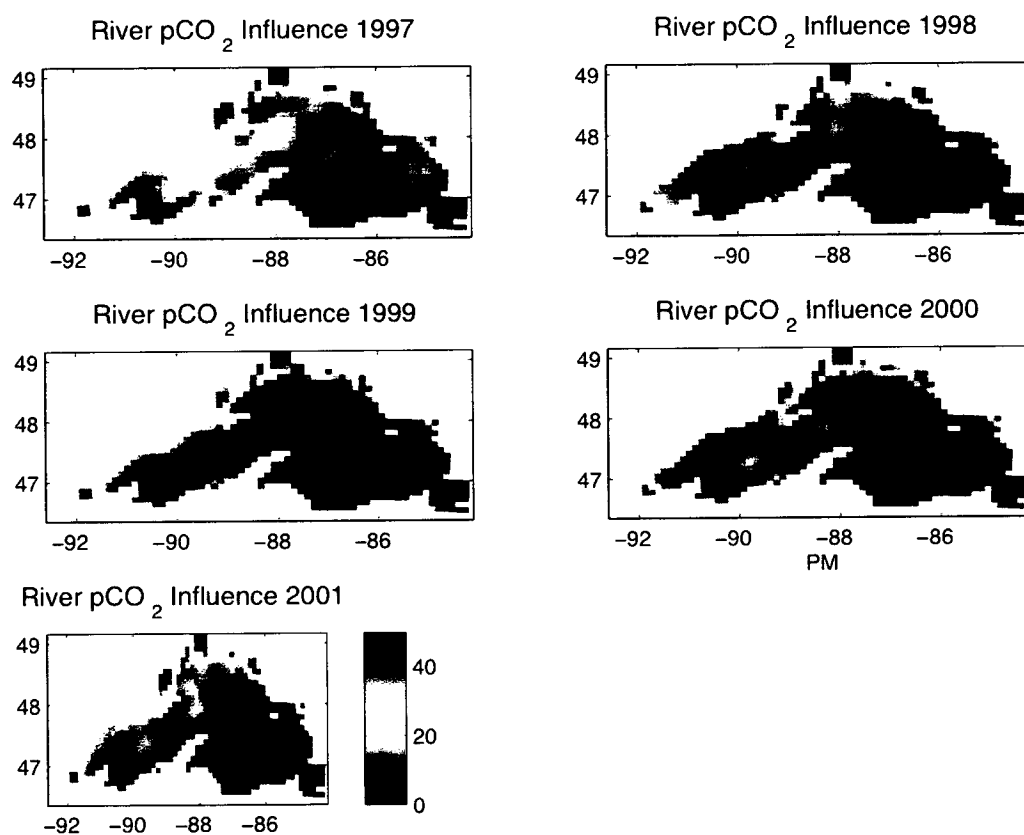


Figure 5-7 Annual mean difference in surface pCO<sub>2</sub> between the PM model run with rivers and the PM model run without rivers. Open lake pCO<sub>2</sub> differs by less than 20 μatm over the course of the year. River mouth locations show significant river effects of over 100 μatm in some locations.

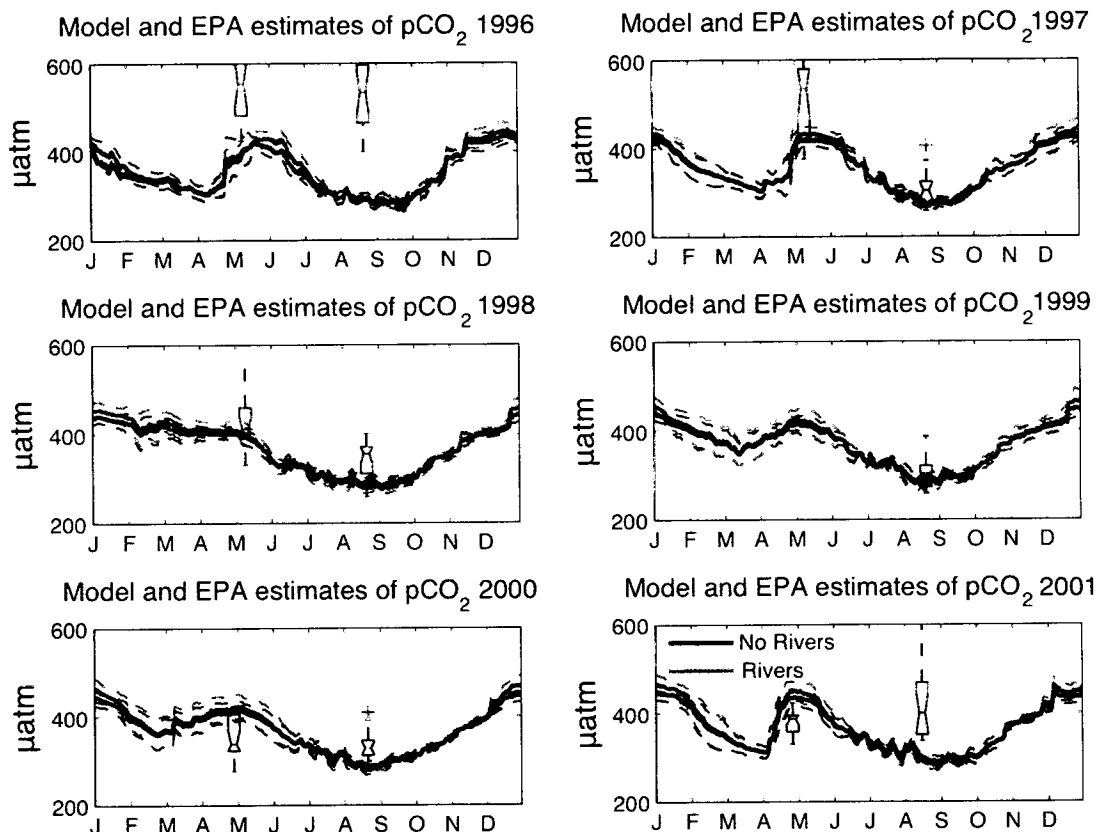
**Figure 5-8**

Figure 5-8 Seasonal cycles of modeled pCO<sub>2</sub> at the 17 open lake EPA stations between 1996 and 2001 in the NPM. Model runs including river inputs are shown in purple, and control runs are shown in black. One standard deviation of modeled pCO<sub>2</sub> at the 17 stations for each day is shown with dashed lines in respective colors. Estimates of pCO<sub>2</sub> at the EPA stations [Atilla *et al.*, 2010] are shown with whisker box plots.

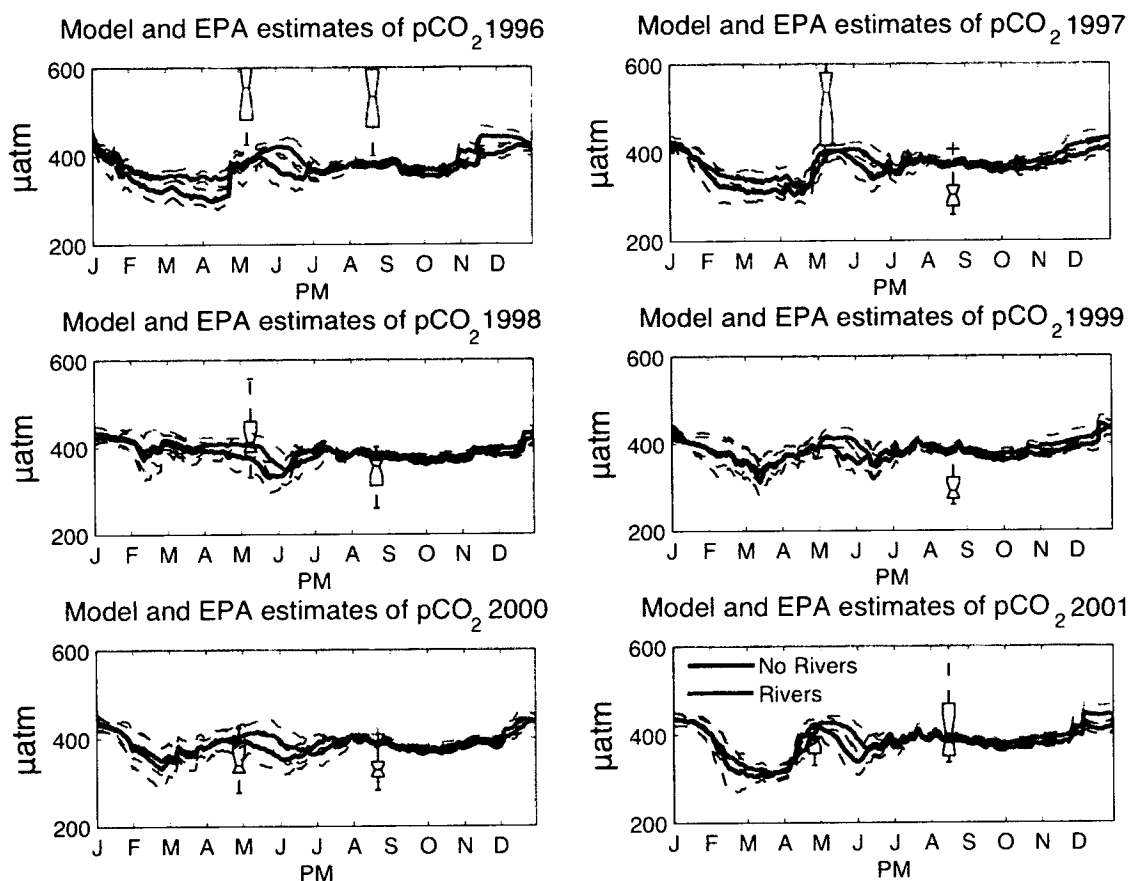
**Figure 5-9**

Figure 5-9 Seasonal cycles of modeled pCO<sub>2</sub> at the 17 open lake EPA stations between 1996 and 2001 in the PM. Model runs including river inputs are shown in purple, and control runs are shown in black. One standard deviation of modeled pCO<sub>2</sub> at the 17 stations for each day is shown with dashed lines in respective colors. Estimates of pCO<sub>2</sub> at the EPA stations [Atilla *et al.*, 2010] are shown with whisker box plots.

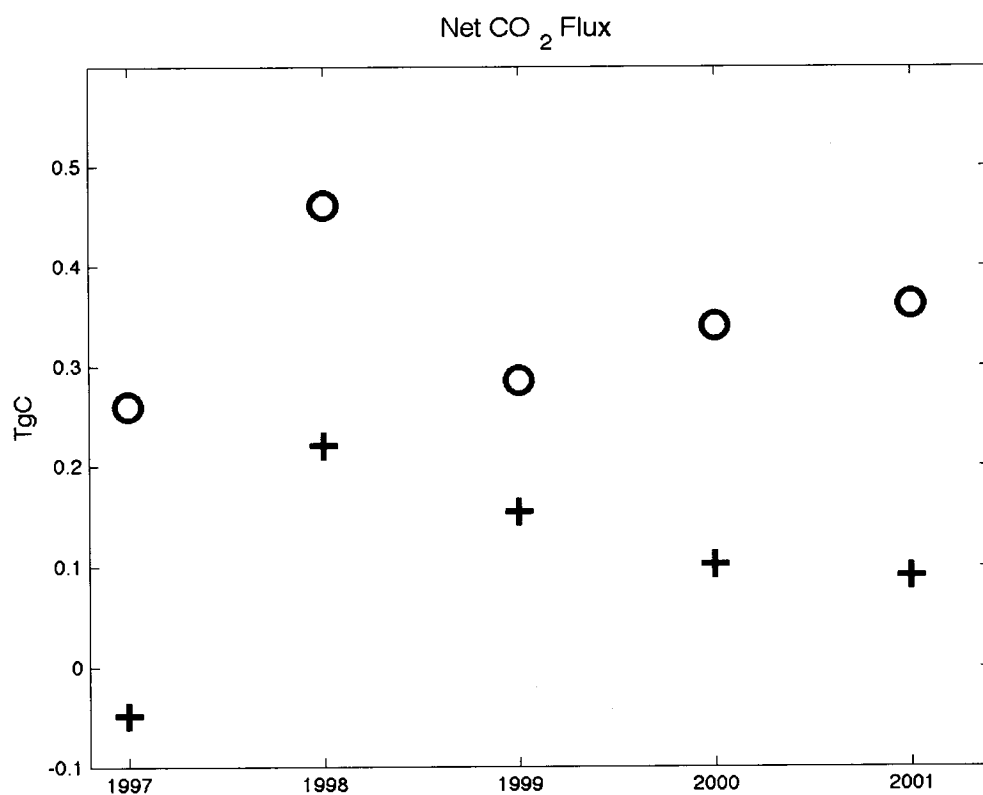
**Figure 5-10**

Figure 5-10 Annual net fluxes (positive to the atmosphere) of carbon dioxide from Lake Superior when including the nine major rivers. Circles are results from the phosphorus model, and crosses indicate results from the no phosphorus model.



Figure 5-11

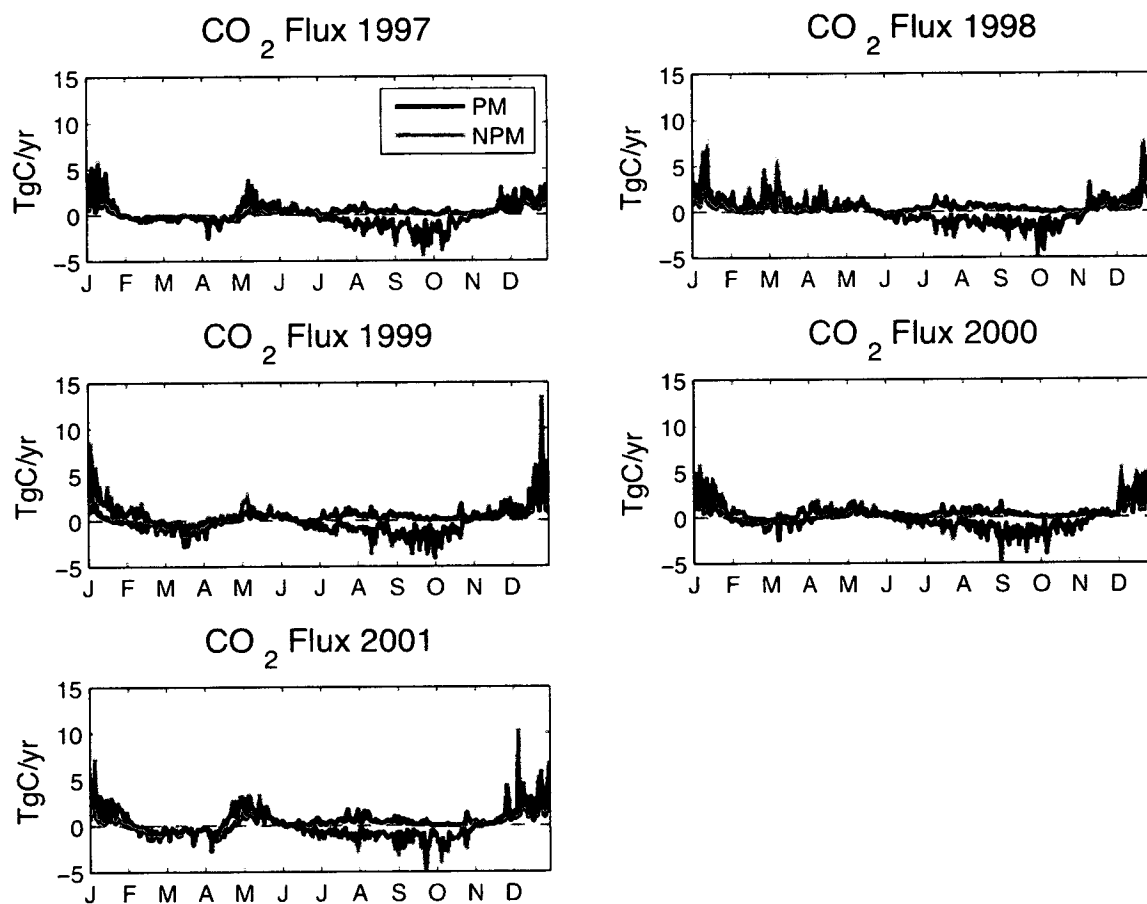


Figure 5-11 Modeled seasonal cycles of lake-wide pCO<sub>2</sub> for 1997-2001 in the phosphorus model (black) and no phosphorus model (red).

Figure 5-12

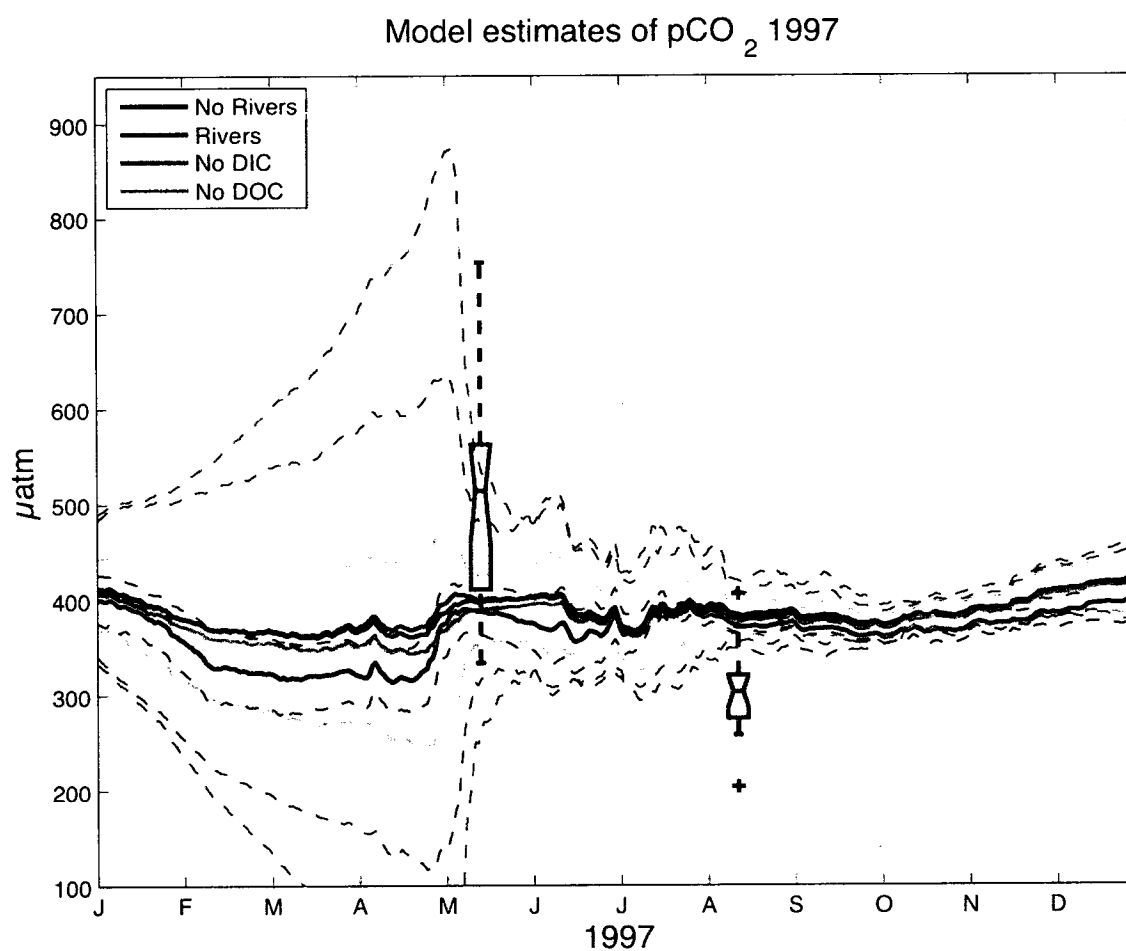


Figure 5-12 Lake-wide mean  $p\text{CO}_2$  in PM river test runs for 1997. Black line is model run including no river effects. The blue line indicates  $p\text{CO}_2$  cycle for model run including all river effects. Red and green lines indicate model runs without DIC and DOC, respectively. Dashed lines indicate lake-wide standard deviation of  $p\text{CO}_2$  for the corresponding model run.

Figure 5-13

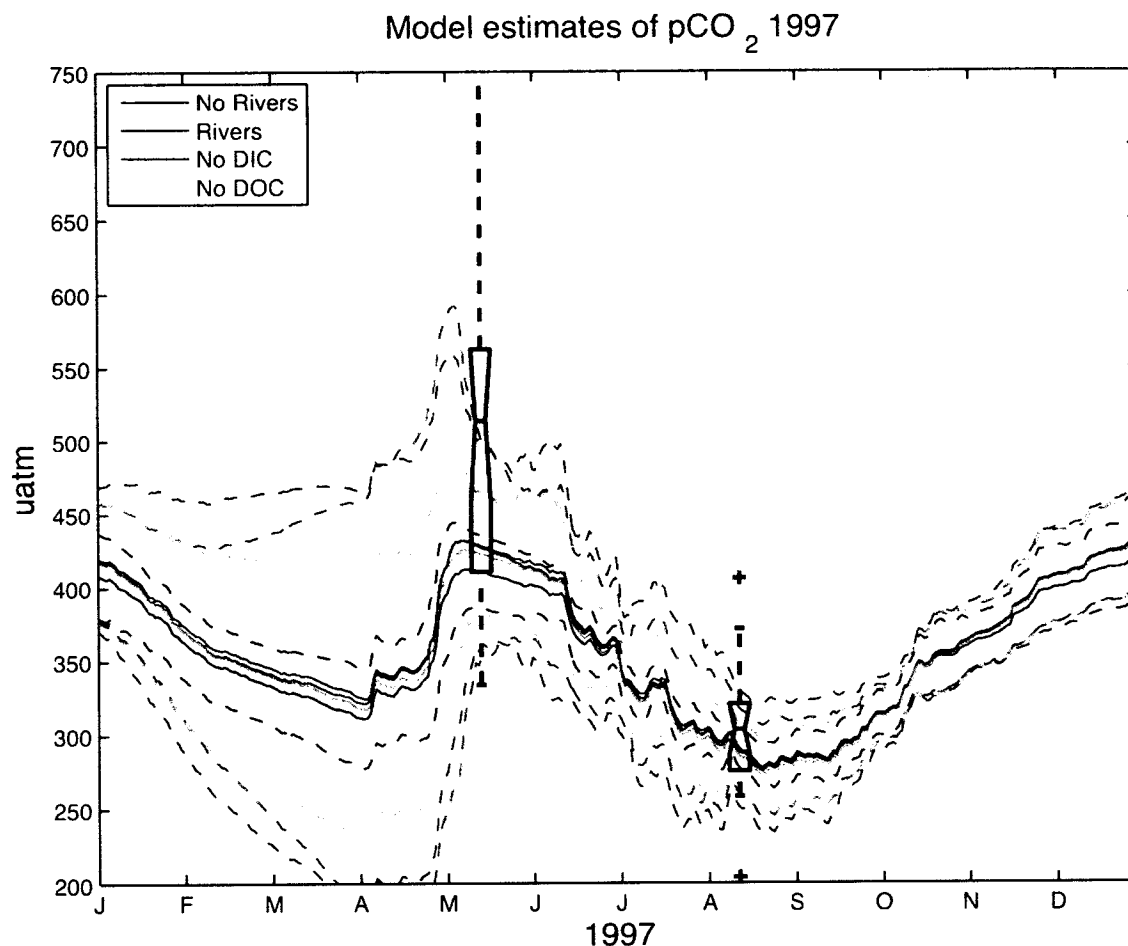


Figure 5-13 Lake-wide mean pCO<sub>2</sub> in NPM river test runs for 1997. Black line is model run including no river effects. The blue line indicates pCO<sub>2</sub> cycle for model run including all river effects. Red and green lines indicate model runs without DIC and DOC, respectively. Dashed lines indicate lake-wide standard deviation of pCO<sub>2</sub> for the corresponding model run.

## Chapter 6

# Respiration Rates in Lake Superior

### 6.1 Introduction

Carbon budgets for Lake Superior put together from observational studies have remained unbalanced, because estimates of lake-wide annual respiration far outweigh production estimates. Estimates of external inputs of organic carbon from rivers, precipitation, groundwater inputs, and sediment re-suspension would have to be off by an order of magnitude to balance the carbon budget. River inputs can be constrained by river concentration and flow observations. Groundwater inputs are believed to be small, and can be constrained by river flow, precipitation, outflow, and lake levels. Many studies of sedimentation rates have been conducted on Lake Superior [eg. *McManus et al., 2003; Chai and Urban, 2004*], and it is unlikely sediment supply of carbon could be orders of magnitude larger than previously suggested. The most likely cause of the imbalance is either an overestimate of respiration or an underestimate of production.

Estimates of primary production and respiration have been limited by spatial and temporal heterogeneity. Historical estimates of net primary production in Lake Superior ranged from 18 - 60 gC/m<sup>2</sup>/yr [Bub, 2001; Fee *et al.*, 1992; Johnson *et al.*, 1982; Maier and Swain, 1978; Vollenweider *et al.*, 1974]. These estimates were made from studies conducted primarily near shore and in the western arm of Lake Superior during stratified conditions. These studies were in part limited by their methods, since very few were *in situ*; none were conducted *in situ* for an entire daylight period; most only measured production in water depths less than 20 m during the stratified season; and many were done without the understanding of trace metal contamination. Sterner [2010] raised these issues in previous NPP estimates and used JGOFS protocol to measure primary productivity during both stratified and un-stratified conditions and throughout the lake. His estimate of annual lake-wide primary production (9.73 TgC/yr) suggests that lake-wide productivity is not an order of magnitude larger than estimated by previous studies and calls into question respiration estimates. No study to date has measured respiration throughout the lake in both stratified and unstratified conditions, as production was measured in his study.

In this chapter, I evaluate the model's ability to capture estimates of respiration off the Keweenaw Peninsula [Urban *et al.*, 2005]. If the model is reasonable, it will be used to estimate annual lake-wide respiration and to close the carbon budget of Lake Superior.

## 6.2 Observations of Respiration

During the Keweenaw Interdisciplinary Transport Experiment in Superior (KITES), Urban *et al.* [2004] measured rates of respiration with bottle incubations at sites off the Keweenaw Peninsula

(Figure 5-1). For a full description of methods used to measure respiration, refer to *Urban et al.*, [2004]. They estimate a lake-wide mean of 9.7  $\mu\text{g C/L/d}$ , or 42.6 TgC/yr during 1999.

### 6.3 Model-Observation Comparisons

Figure 6-1 shows modeled (NPM) and observed rates of respiration along the transect HN, within 5 km from shore, during 1999, when including river inputs from nine major tributaries to Lake Superior (Chapter 5). Modeled rates of respiration include photosynthetic respiration and the decomposition of POC and DOC, although modeled respiration rates are dominated by the decomposition of DOC. Modeled rates of respiration peak when net primary production peaks in the NPM model, during summer, because it is warmest and a substantial amount of autochthonous DOC has been produced by phytoplankton. Modeled rates of respiration at site HN average 6  $\mu\text{g/L/day}$  over the entire year and agree well with *Urban et al.*'s [2005] estimate of 9.7  $\mu\text{g/L/day}$ . Modeled rates of respiration agree well with observations during summer at the surface and to 15 m, but are lower than observed during April-June in the NPM, except for an observation during May, which agrees quite well to model results. This may be due to the lack of other local rivers (eg. Bad River, Keweenaw Waterway) that could increase coastal organic carbon locally, or modeled production may be too low during spring along the peninsula. The large fluctuations in observed rates of respiration suggest that fluctuations in river flows could cause variability in respiration rates as the trapped coastal jet travels along the peninsula (Chapter 3). Both modeled and observed rates of respiration decrease with depth.

Figure 6-2 shows modeled rates of respiration from the NPM near the mouth of the Ontonagon River, within 3 km of shore, compared to observations from *Urban et al.* [2004]. Surface modeled respiration is shown in black and compared to observations in red, including an uncertainty of 12% (10-15% uncertainty, *Urban et al.*, [2005]). Surface respiration values compare very well to measurements in 1999 near the river mouth, suggesting that both primary production and terrestrial inputs of DOC can significantly alter respiration rates. The large fluctuations in respiration rates seen in Figure 2 show river flow influence superimposed on the seasonal cycle of productivity. Subsurface respiration was measured one day during 1999 and is higher than modeled. The model does a reasonable job capturing respiration rates near the river mouth.

Modeled near shore respiration rates compare favorably to discrete measurements taken in 1999 during the KITES project. The model is therefore judged to be suitable to estimate lake wide respiration rates.

## 6.4 Lake-wide Respiration Rates

Figure 6-3 shows the modeled (NPM) annual mean, column-average respiration rates in  $\mu\text{g/L/day}$  for Lake Superior during 1999. Note the logarithmic scale. In the shallow waters near shore, volumetric respiration rates are high within the column. Annual average respiration rates in these shallow waters can be near  $20 \mu\text{g/L/day}$  in close proximity to large river mouths. In the deep, cold waters further from shore, however, column average respiration rates are very low. Annual mean respiration rates in the deepest lake columns are  $<1 \mu\text{g/L/day}$ . Productivity,

temperatures, and river influences are all small in these deep, open waters of Lake Superior (Chapter 5). *Urban et al.*'s [2004] lake-wide volumetric respiration rate of  $9.7 \mu\text{g/L/day}$  is reasonable near shore, as only half of river flow is modeled here, but the model suggests that extrapolation to the whole-lake and entire year is difficult from observations limited to within 21 km of shore.

The middle panel of Figure 6-3 shows column-integrated respiration rates in Lake Superior, averaged over 1999. Although the deep waters have very low rates of respiration, columns that are hundreds of meters thick can respire significant amounts of carbon. Column-integrated respiration is smallest immediately onshore and largest just offshore, where the water is deeper, warm, productive, and effected by rivers. The deepest parts of Lake Superior still have the smallest column-integrated respiration rates. Lake-wide respiration rates average  $71 \text{ gC/m}^2/\text{yr}$ .

Daily average lake-wide respiration rates for 1999 are shown in the bottom panel of Figure 6-3. Respiration has a broad peak during the productive summer months, with lake-wide rates exceeding  $3 \text{ Tg C/yr}$ . During 1999, the modeled lake respired  $5.8 \text{ Tg C}$ , a mere 13% of the rate estimated by *Urban et al.* [2005] ( $46 \text{ Tg C/yr}$ ). This included only half of the river inputs of carbon that would be expected by including 100% of the flow to Lake Superior, but only part of the DOC supplied by rivers is labile and respired within the year. Thus, the lake likely respired additional carbon on the order of  $0.1 \text{ TgC/yr}$  or less.



## 6.5 A New Carbon Budget for Lake Superior

The model captures near shore respiration rates observed during the KITES project just off the Keweenaw Peninsula, yet suggests much lower respiration rates for the entire lake over the year then suggested by *Urban et al.* [2005] or *Cotner et al.*, [2004]. Using modeled and literature values, I suggest that the carbon budget for Lake Superior is not an order of magnitude out of balance (Table 6-1).

### *Inputs*

Modeled net primary production is 3 TgC/yr, but modeled gross primary production is 5.67 TgC/yr. Observational studies have suggested gross primary production as high as 9.73 TgC/yr [*Sterner*, 2010]. Estimated river inputs of dissolved organic carbon in the nine rivers between 1996-2001 used in this study are 0.15-0.32 TgC/yr, constituting ~50% of annual flow. A crude estimate of lake-wide river supply of DOC is thus 0.3-0.64 TgC/yr. Precipitation values are used from previous studies and supply 0.1-0.4 TgC/yr.

### *Outputs*

Losses of DOC from sedimentation and outflow through St. Mary's River are estimated from previous studies as 0.48-0.5 and 0.1 TgC/yr, respectively. Modeled respiration rates are slightly greater than modeled GPP, 5.8 TgC/yr in 1999. Modeled GPP, and thus respiration, is lower than the largest observational study. The modeled net efflux is approximately 50% of the annual river supply of organic carbon, so I put the upper bound of respiration estimates as the sum of the highest production estimate [*Sterner*, 2010] plus 50% of largest river inputs suggested in the literature.

### *Net Efflux*

During 1999, the model effluxes 0.125 TgC/yr from Lake Superior. Assuming the model includes only half of river inputs of organic carbon, it suggests an annual flux of 0.25 TgC/yr during 1999. This flux would vary according to lake respiration, production, and external supplies of carbon.

## **6.6 Discussion and Conclusions**

The model is able to capture the magnitude of near shore respiration rates observed along the Keweenaw Peninsula during 1999, although modeled rates may be low in spring. The model suggests that a significant near to offshore gradient in volumetric respiration rates exists, due to the influence of river DOC near shore. Modeled respiration rates in the open lake are very low. If correct, the carbon budget of Lake Superior is in fact balanced, and air-lake carbon dioxide fluxes are low ( $\sim 0.25$  Tg C / yr).

The model suggests that volumetric near shore respiration far exceeds respiration rates in the offshore waters and that a seasonal cycle in respiration rates exist. Respiration rates have only been measured in the western arm and very near shore. While *Urban et al.*, [2004, 2005] did observe a near to offshore gradient and hypothesized it due to terrestrial carbon sources, more

observational work needs to be done. For whole lake respiration to be evaluated in the model, respiration needs to be routinely measured far from shore, in the open waters of the lake.

Modeled respiration rates are dependent on temperature, which is consistent with the general scientific understanding that community respiration rates increase as temperatures increase. The parameterization of temperature effects on respiration allows for a three-fold increase in respiration rates during summer, consistent with an understanding that bacterial abundance increases at that time [McDonald, 2010]. However, *Urban et al.*, [2004] did not observe a seasonal cycle in respiration rates, although lab measurements indicated a dependence on temperature, and the number of observation dates may have been insufficient to exclude a seasonal cycle in respiration rates. *Urban et al.* [2004] did observe larger respiration rates during the warm El Niño year (1998) compared to the colder 1999, but questions the magnitude of 1998 measurements (personal communication). Measurements were taken in the colder months, as early as April 1, but nearshore regions may already be impacted by river runoff at this time. Flow from the Ontonagon River peaked in early April at 290 m<sup>3</sup>/s, but flow exceeded 210 m<sup>3</sup>/s by March 31 and was high for a week prior. Thus, even cold-water observations nearshore are not necessarily representative of off shore cold-water respiration rates.

Both the model and the observations show high respiration rates close to shore (< 5 km) and lower rates further from shore. The model, however, suggests extremely low respiration rates in the open lake. Surface circulation rates in Lake Superior are generally a few cm/sec or less (Chapter 3), although flow along the Keweenaw can be tens of cm/sec. Sub-surface flows are significantly weaker. Even if all coastal surface flow was 2 cm/sec and directed consistently

away from the river mouth, 50% of the labile terrestrial carbon should be respired before moving 40 km downstream during summer. For scale, *Urban et al.*'s [2004] study was conducted along 70 km of coastline along the Keweenaw Peninsula. Summer surface circulation is counterclockwise along the coasts, so primarily eddy-induced mixing will move terrestrial carbon into the deep, open waters of Lake Superior. Only when the coastal jet is strong and moving in a consistent direction, as it completely reverses direction at times [*Chen et al.*, 2001; Chapter 3], should significant amounts of terrestrial carbon make it to the middle of the lake before being decomposed. Thus, it is reasonable that such a significant near to offshore gradient in respiration rates might exist.

The modeled efflux is limited by the magnitude of carbon deposited by the rivers and is unable to act as a large source of carbon dioxide to the atmosphere on annual time scales. However, near-shore modeled respiration rates are reasonable in 1999. Lake-wide modeled respiration rates are low (5.8 TgC/yr), suggesting that the carbon budget of Lake Superior is indeed more in balance. Sedimentation, re-suspension, and precipitation effects are not considered here; thus, total respiration (5.8 TgC/yr) and efflux (0.12 TgC/yr) are likely greater than modeled, but of the same order of magnitude. Year-round observations of respiration in the open lake are needed to confirm model results. EPA or buoy (Figure 3-1) locations would be appropriate observation locations for such a study.

## Figure Captions

**Figure 6-1** Modeled (line) and observed (circles) respiration rates off the Keweenaw Peninsula at site HN during 1999 (Figure 6-1).. Modeled rates from the NPM with river inputs (Chapter 5).

**Figure 6-2** Modeled (lines) and observed (circles) respiration rates off the Keweenaw Peninsula at site ON during 1999 (Figure 6-1). Modeled respiration rates at the surface are shown in black, and rates from 0-15 m are shown in blue. Modeled rates from the NPM with river inputs (Chapter 5).

**Figure 6-3** The annual mean (1999) column-average respiration rates ( $\mu\text{g/L/day}$ ) in Lake Superior from the NPM are shown in the top panel. Note the logarithmic scale. Annual average column integrated respiration rates for 1999 are shown in the middle panel ( $\text{gC/m}^2/\text{yr}$ ). Daily lake respiration (entire lake volume) respiration is shown for 1999 in the bottom panel.

## Tables

**Table 6-1**

*Inputs of organic carbon to Lake Superior (Tg C / yr)*

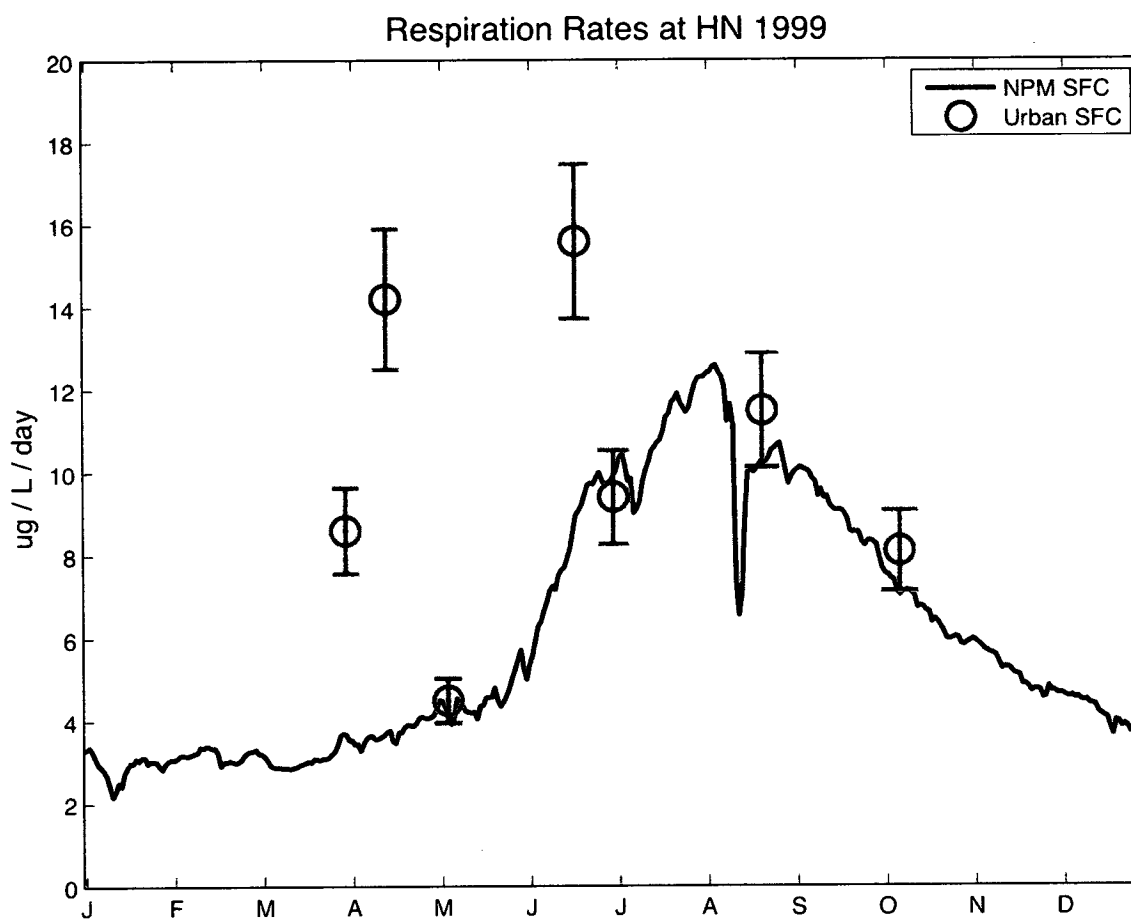
Total Inputs	6.4-10.8	
Rivers Inputs	0.3-0.64, 1	(estimates from this study, <i>Urban et al.</i> , [2005] max is 1 TgC/yr)
Precipitation	0.1-0.4	[ <i>Cotner et al.</i> , 2004; <i>Urban et al.</i> , 2005]
Primary Production	6-9.73	GPP, this study, <i>Sterner</i> , [2010]; [ <i>Cotner et al.</i> , 2004]

*Losses of carbon from Lake Superior (Tg C / yr)*

Total Outputs	6.4-10.8	
Sedimentation	0.48-0.5	[ <i>Cotner et al.</i> 2004; <i>Urban et al.</i> , 2005]
Outflow	0.1	[ <i>Cotner et al.</i> 2004; <i>Urban et al.</i> , 2005]
Respiration	5.8-10.2	(this study ~6 TgC/yr, but GPP estimates are as high as 9.73, include 50% respiration of max river input)

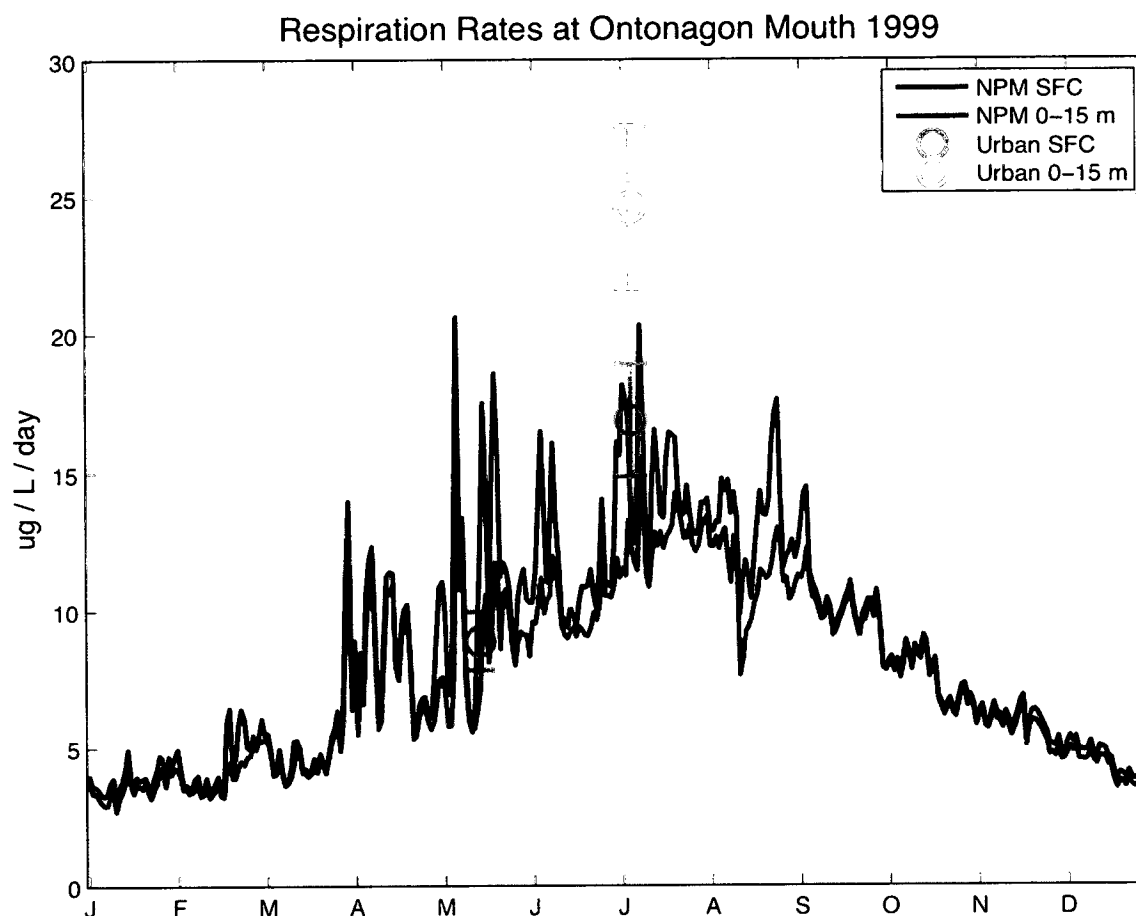
## Figures

**Figure 6-1**



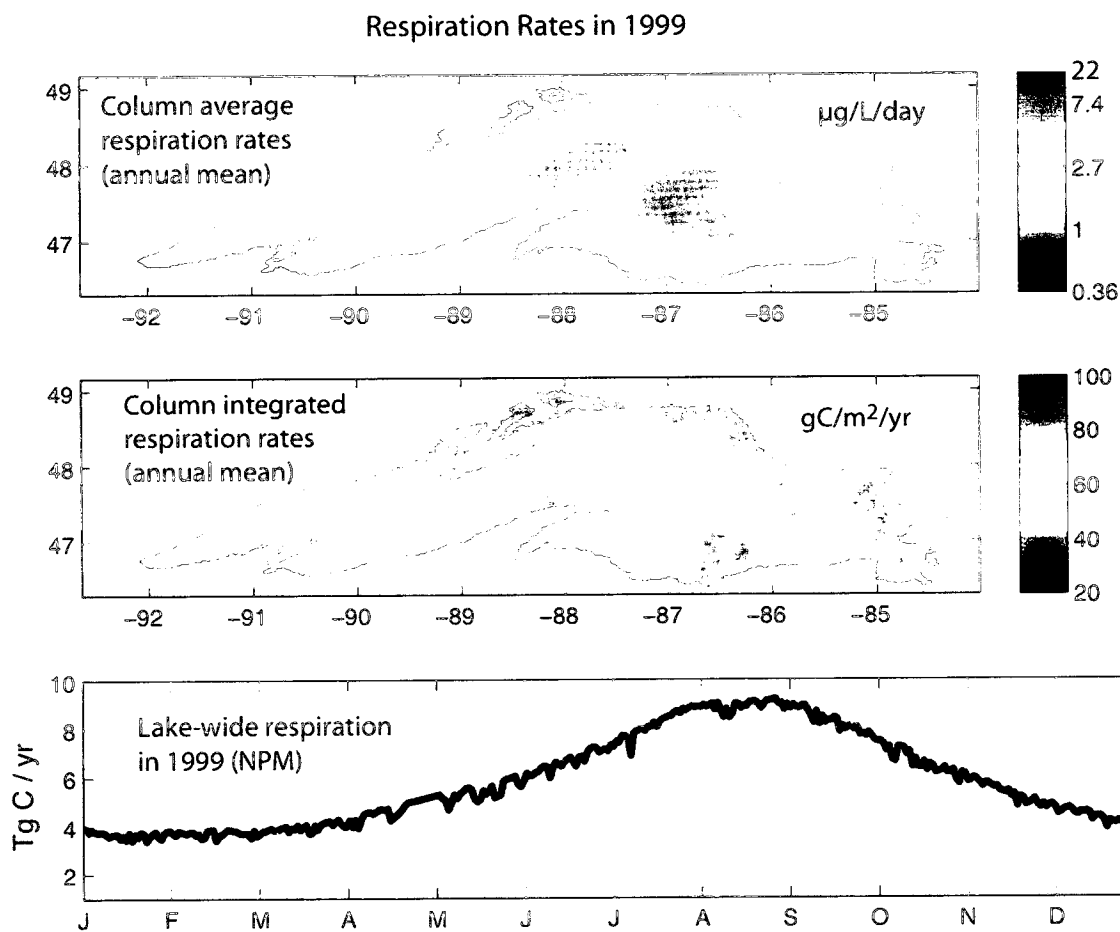
**Figure 6-1** Modeled (line) and observed (circles) respiration rates off the Keweenaw Peninsula at site HN during 1999 (Figure 6-1).. Modeled rates from the NPM with river inputs (Chapter 5).

Figure 6-2



**Figure 6-2** Modeled (lines) and observed (circles) respiration rates off the Keweenaw Peninsula at site ON during 1999 (Figure 6-1). Modeled respiration rates at the surface are shown in black, and rates from 0-15 m are shown in blue. Modeled rates from the NPM with river inputs (Chapter 5).



**Figure 6-3**

**Figure 6-3** The annual mean (1999) column-average respiration rates ( $\mu\text{g/L/day}$ ) in Lake Superior from the NPM are shown in the top panel. Note the logarithmic scale. Annual average column integrated respiration rates for 1999 are shown in the middle panel ( $\text{gC/m}^2/\text{yr}$ ). Daily lake respiration rates (entire lake volume) are shown for 1999 in the bottom panel.

## **Chapter 7**

### **Conclusions and Future Work**

#### **7.1 North Atlantic Flux Variability**

Using a medium-complexity ecosystem model coupled to a regional general circulation model of the North Atlantic Ocean, I investigate whether inter-annual variability in satellite chlorophyll observations is indicative of inter-annual variability in the oceanic sink of atmospheric carbon dioxide. This study shows that although biological production is a strong control on the seasonal cycle of  $p\text{CO}_2$  in the subpolar gyre that production varies in strength by less than 10%, which is insufficient to control annual flux magnitudes. However, year-to-year changes in bloom timing cause significant variability in the local  $p\text{CO}_2$  cycle and should be considered when trying to elucidate trends from observations sparse in time.

##### **7.1.2 Key Issues in North Atlantic Flux Variability**

The model used to study  $\text{CO}_2$  flux variability in the North Atlantic Ocean does well capturing estimates of ocean chlorophyll from satellite measurements. However, chlorophyll is not a direct

measurement of biomass. The model captures the mean seasonal cycle of  $p\text{CO}_2$  suggested by *Takahashi et al.*, [2002], but no individual year of  $p\text{CO}_2$  observations was available to evaluate inter-annual variability in modeled  $p\text{CO}_2$ . No long-term time series of production or  $p\text{CO}_2$  exists in the subpolar gyre but could be used to better constrain modeled  $p\text{CO}_2$  and production. Modeled export also assumes a constant sinking rate that is uniform among all particulate sizes, which is likely a gross simplification of oceanic export out of the mixed layer. The release of Takahashi's  $p\text{CO}_2$  data will likely provide modelers with a better tool to evaluate modeled oceanic  $p\text{CO}_2$  and inter-annual variability in the oceanic carbon sink.

## 7.2 Lake Superior's Carbon Cycle

I investigate whether gross imbalances in previous carbon budgets of Lake Superior are due to spatial and temporal heterogeneity in the lake's carbon cycle. I use a hydrodynamic model configured to Lake Superior bathymetry.

### *Large-Scale Circulation in Lake Superior*

Due to the fact that the large-scale circulation of Lake Superior was poorly documented or unknown, I use the hydrodynamic model to elucidate seasonal patterns of circulation and the mechanisms controlling them. The model adequately captures current directions and magnitudes observed along the Keweenaw Peninsula during the KITES experiment as well as seasonal cycles and synoptic variability in lake surface temperatures measured by the three open lake buoys.

The model shows that circulation patterns are controlled by vorticity in the wind field, and coastal flows are enhanced by near to offshore temperature gradients during summer. These mechanisms create two cyclonic gyres in apparent geostrophic balance in the open lake with a strong coastal jet flowing counterclockwise along the coast. A weak anti-cyclonic gyre exists in the far southwestern arm. Complex lake bathymetry generates a barotropic response and creates small-scale structures in integrated flow throughout the year. Winter circulation is controlled by the wind, as only minimal temperature gradients exist, and are of the opposite sign as summer temperature gradients. Between 1979 and 2006, I find a significant increase in lake surface temperatures ( $0.37^{\circ}\text{C}/\text{decade}$ ) in good agreement with *Austin and Colman* [2007] and an increase in current speed ( $0.37\text{ cm/s}/\text{decade}$ ) driven by increasing wind speeds during the stratified season ( $0.18\text{ m/s}/\text{decade}$ ) [*Desai et al.*, 2009]. Although trends in temperature, wind speeds, and current speed exist, I find that currents vary significantly on synoptic time scales but exhibit similar distributions of speed and direction from one year to the next and exhibit little inter-annual variability.

### *Internal Carbon Cycling in Lake Superior*

I couple two separate ecosystem models to the circulation model to investigate whether the internal carbon cycle of Lake Superior can capture observational estimates of lake  $\text{pCO}_2$  and elucidate the full annual cycle of lake-wide  $\text{pCO}_2$ ,  $\text{CO}_2$  fluxes, and the mechanisms controlling them. The phosphorus model (PM) includes phosphorus dynamics, and thus, more fully couples the lake's physical dynamics to the ecosystem. The PM also has a more rapid rate of

remineralization of autotrophic DOC in order to implicitly include the microbial loop and increase primary production. The no phosphorus model (NPM) ignores phosphorus cycling and determines rates of primary production based solely on light and temperature, as in *Sterner* [2010]. Thus, internal waves and upwelling events may actually decrease net primary production in the NPM via cooling but would increase net primary production in the PM via nutrient supply.

Both models capture discrete observations of chlorophyll at the open lake stations visited by the EPA twice each year, although the NPM does a better job during summer. Annual primary productivity is reasonable in both models, although differing seasonal cycles cause a difference in modeled pCO<sub>2</sub>. The models suggest that Lake Superior is super-saturated with carbon dioxide during spring and early winter, in reasonable agreement with April pCO<sub>2</sub> estimates from EPA observations of temperature, pH, and alkalinity [*Atilla et al.*, 2010], given the large uncertainty. Large rates of lake efflux are possible on a windy winter day (> 10 TgC/yr). During late winter, mid February through mid April, the lake can act as a sink of atmospheric carbon dioxide, when the lake has already out-gassed excess CO<sub>2</sub> and cooled. As the lake warms in spring, it overturns, and effluxes carbon dioxide during. The PM has a strong spring bloom triggered by light and nutrient supply and reduces the magnitude of the spring efflux. During summer, the PM suggests the lake is approximately in equilibrium with the atmosphere, while the NPM suggests that without external inputs to the lake, it should be a sink during summer as primary production peaks. Both models capture observed pCO<sub>2</sub> reasonably, but neither is correct for both seasons, and suggest that the open waters of Lake Superior are not a significant source of carbon dioxide to the atmosphere over the course of a year. Both models suggest that both the seasonal cycle and inter-annual variability in the CO<sub>2</sub> flux are physically driven.

Using EOF analysis, I suggest that spatially coherent variability in the annual CO<sub>2</sub> flux is largest in the deep, open lake, where fewest observations exist. This pattern of contrasting near to offshore variability persists in other variables, indicating a need for offshore monitoring locations. Climatic variability affects the internal carbon cycle of Lake Superior, and years of warmer temperatures have an anomalous efflux, although the model with no external inputs is forced to act as a small (0.015 TgC/yr) sink of the increasing atmospheric carbon dioxide. The Southern Oscillation Index correlates with winter temperatures in Lake Superior and El Niña years are years of lower pCO<sub>2</sub> in the PM and an increase in early winter pCO<sub>2</sub> in the NPM.

#### *Including River Inputs to Lake Superior*

Nearshore estimates of lake surface pCO<sub>2</sub> suggest a significant super-saturation near shore not captured by the models with no external inputs. I add river DOC, DIC, and alkalinity from the nine rivers of greatest annual flow into Lake Superior to see if the models can capture a near to offshore gradient suggested by the observations.

The models capture a large gradient in pCO<sub>2</sub> from near a river mouth to more than 20 km offshore, and nearshore modeled surface pCO<sub>2</sub> is of the same order of magnitude as suggested by the observations. Open lake pCO<sub>2</sub> remains largely unchanged, indicating that the coastal waters of Lake Superior may be sources of atmospheric carbon dioxide as they respire terrestrial organic carbon, but little of this carbon reaches the open lake. Lake-wide annual effluxes are an order of magnitude less than best estimated by *Urban et al.* [2005] (3 TgC/yr). Respiration rates observed near shore in 1999 are well captured by the NPM, although spring respiration may be low near

shore in the model. The model indicates that river DOC causes near shore respiration rates to be up to an order of magnitude larger than open lake respiration rates. River DOC is primarily decomposed near shore as it travels along in the coastal jet during summer, and appears to be more crucial to the whole-lake carbon cycle of Lake Superior than river DIC.

Thus, the model suggests that previous whole-lake respiration estimates are an order of magnitude too large, due to extrapolation from observations in the far western arm and along the Keweenaw Peninsula. Open lake, year-round observations of respiration are necessary to confirm model results, but the model suggests that the carbon budget of Lake Superior may be more or less in balance and that annual net efflux is only  $\sim 0.1$  TgC/yr.

### **7.2.1 Key Issues**

The physical and ecosystem models are imperfect. Mixed layer depths are deeper than observed, and model forcing is too warm, causing a larger lake heat content, premature stratification, and warmer lake surface temperatures during the stratified period. These concerns can affect modeled  $p\text{CO}_2$ , summer surface circulation strength, nutrient supply in the PM, and an early bloom. Both models suggest Lake Superior  $p\text{CO}_2$  is reduced during two periods of the year (summer, late winter) and elevated during two other periods (spring, early winter). However, the capacity to uptake carbon dioxide is impacted by temperature, and, thus, a model that is too warm will have a weaker seasonal cycle of  $p\text{CO}_2$ . The model forcing and resulting error in thermal structure causes large, un-quantified model uncertainty that is increased by ecosystem

error. By including results from two ecosystem models, this study attempts to include as many state spaces as computationally possible. The ecosystem structure alters the magnitude of air-lake CO<sub>2</sub> fluxes throughout the year, indicating that uncertainty in ecosystem parameters and structure significantly affects the modeled carbon cycle. In this study, ecosystem selection causes a maximum difference of nearly 100 μatm in during summer and can double modeled seasonal air-lake CO<sub>2</sub> flux rates. The true uncertainty is unknown.

Once the carbon reaches the lake from the rivers, there is uncertainty in its trajectory due to the selection of model horizontal resolution. In a study of Niagara River discharge into Lake Ontario, *Hayashida et al.* [1999] found that tracer trajectories within a few kilometers of the river mouth were adequately simulated when increasing local model horizontal resolution to 100 m. Offshore trajectories, however, did not require such a high resolution. Thus, the whole-lake paths of DOC modeled here should be accurate, but model trajectory error is a problem when comparing model results to observations taken within a few kilometers of a river mouth. This error is increased when the model is run at 10 km horizontal resolution.

The NPM appears better suited for modeling whole-lake chlorophyll, but may miss the impact of mixing events on primary production. The lack of phosphorus in the NPM would cause a deficiency in modeling inter-annual variability in production, if external phosphorus inputs are considered. The PM likely blooms too soon, but may benefit from river supply of phosphorus during the stratified season. Neither model can be eliminated from the available observations, because lake-wide observations relevant to the carbon cycle are lacking.



The available indirect estimates of  $p\text{CO}_2$  are discrete, do not capture the full seasonal cycle, and their accuracy and precision are currently unknown. They are a poor constraint on the lake's carbon cycle. Chlorophyll observations provide some constraint, but are available only twice during each year at the EPA stations and are an indirect measure of biomass. Productivity has been measured repeatedly in the lake and now lake-wide, suggesting that primary production is well constrained by the observations. Since *Sterner's* [2010] relationship between temperature, light, and primary production is derived from several years of observations, it is likely a mean and will miss variability due to nutrient supply. Respiration observations are clearly lacking in Lake Superior. The model shows that near shore locations can have highly variable respiration rates and that respiration rates far from shore are an order of magnitude less than at a river mouth. There are no observations to confirm modeled respiration results, and model parameters are poorly constrained.

Modeled rates of respiration are dependent on the parameterization of labile fraction of river DOC as well as remineralization rates of organic carbon in the lake. The two ecosystem models have two separate rates of remineralization of autotrophic DOC, and thus, the local impact of river carbon differs between the two models. The labile fraction of river DOC and remineralization rates are unknowns in Lake Superior. Assuming a system in balance, *Cotner et al.* [2004] estimate a residence time of ~30 years for organic carbon in Lake Superior, but *Urban et al.* [2005] suggest a residence time of only 8 years. This may be due to near shore bias in observations, but if the lake is truly out of balance, observations to prove it are lacking.

### 7.3 Future Work

Although the model suggests that lake-wide annual effluxes are small, it does not suggest they are unimportant to our understanding of the regional carbon budget. Statistically different atmospheric  $p\text{CO}_2$  has been observed at Park Falls, WI when air arrives after flowing over the lake than when it arrives after blowing over land [Vasys *et al.*, 2010]. The model also suggests that daily average efflux can exceed a rate of 10 TgC/yr on a windy winter day. This rate is triple the annual estimated rate from Urban *et al.* [2005], indicating that the lake may indeed significantly impact our understanding of the terrestrial carbon cycle within the region. Hourly lake effluxes need to be modeled for 2004 to best gauge the lake's influence on the surrounding land and at Park Falls, WI. Best estimates of lake effluxes will also be provided to the Carbon Tracker program [Peters *et al.*, 2007], so that inverse models may begin to differentiate Lake Superior and its surrounding watershed in its understanding of the continental carbon cycle.

Better constraints for modeled chlorophyll, respiration, and  $p\text{CO}_2$  are needed. Work being done by Colleen Mouw at the University of Wisconsin-Madison to retrieve lake chlorophyll estimates from satellite observations on Lake Superior will provide a greater understanding of the seasonal cycle of lake-wide chlorophyll and its year-to-year variability. Respiration measurements in the open lake and year round are necessary to support or disprove model results. Direct measurements of  $p\text{CO}_2$  in the open lake, perhaps mounted to the three buoys, would better constrain modeled lake-wide  $p\text{CO}_2$ . The buoys are not present in the lake during winter. Thus, permanent subsurface moorings collocated at the buoys could be equipped with  $p\text{CO}_2$  sensors.

By having year-round  $p\text{CO}_2$  cycle in the subsurface and, during the warmer seasons, above, observations would better constrain models used for whole-lake studies. An annual efflux for the open lake could also be established. When estimating  $p\text{CO}_2$  from indirect methods, a strict protocol should be followed and techniques and uncertainties well-documented so that they may be used with confidence. Lability of river DOC and remineralization rates of river DOC, once in the lake, would be of great benefit to this study. Elizabeth Minor at the Large Lakes Observatory and the University of Minnesota-Duluth is investigating these numbers for tributaries in the western arm of Lake Superior. Similar work needs to be done around the rest of the lake.

Model-observation comparisons may be improved by including fine resolution, nested model grids at major river mouths and by including the impacts of river momentum on local flow. This would improve local tracer trajectories and reduce the lake volume subject to instantaneous mixing in the current model setup, thereby allowing for the possibility of larger near to offshore gradients. The model, as it stands, does not include sedimentation, burial, or the effects of precipitation on the lake's carbon cycle. Thus, it would be significantly improved by adding a sediment compartment with a parameterization for re-suspension, which may enhance effluxes during winter and spring mixing. Precipitation effects may be added to the model, although likely less important than sediments.

To truly capture interannual variability in the lake's carbon cycle, it may be necessary to include a river flux of phosphorus and fine tune the PM. The PM model may prove to be more useful when utilizing direct observations of  $p\text{CO}_2$ , as suggested by the SAMI data of 2001. Due to the fact that many model parameters are poorly constrained, fluxes and respiration rates may also be

better constrained by more model sensitivity tests when varying river DOC lability and remineralization rates.

## Appendix A: River Flow and Constituents

The rivers with the nine largest drainage areas within Lake Superior's watershed are included in the model. River flow data was acquired from the United States Geological Survey (USGS) for the St. Louis and Ontonagon Rivers. Water flow gauges maintained by Environment Canada (EC) were used for many rivers in Ontario. The Ontario Power Generation Corporation provided river flow data for several of the rivers in Ontario where hydropower generation alters flow. LoadRunner [Booth *et al.*, 2007] was used as an interface to the USGS program LOADEST [Runkel *et al.*, 2004] to estimate daily average river alkalinity and dissolved inorganic carbon (DIC) concentrations in each of the rivers. River DIC was estimated from same-day measurements of pH, temperature, and alkalinity.

## Appendix A.1. Aguasabon River

The Aguasabon River is located within the Little Pic watershed and has a drainage basin area of 11,500 km<sup>2</sup> [Thompson, 1978] making it the second largest watershed within Lake Superior's drainage basin. The river accounts for 9% of the annual flow into Lake Superior [Thompson, 1978] and outflows into north central Lake Superior just downstream of the Aguasabon Hydroelectric Plant.

Daily average river flow below the Aguasabon Hydroelectric Plant was obtained from the Ontario Power Generation for 1979 through 2009. According to the Lake Superior Management Plan [LaMP, 2000], the average alkalinity in the Aguasabon River is 149.89 mg/L as CaCO<sub>3</sub>. Average pH is 7.54, and average dissolved organic carbon concentration (DOC) is 8.67 mg/L. No in situ measurements of alkalinity, pH, DIC, or DOC were publicly available for the Aguasabon River, so average concentrations are used for the river under all flow conditions. An average concentration of 38.95 mg/L is used for DIC. This was estimated using CO<sub>2</sub>sys [Lewis and Wallace, 1998] assuming a pH of 7.54, temperature of 10°C, and alkalinity of 149.89 mg/L.

## Appendix A.2 Nipigon River

The Nipigon watershed is the largest in Lake Superior's basin and has a drainage area of 25,300 km<sup>2</sup> [Richards, 1990] Twenty six percent of the annual river flow into Lake Superior is from the Nipigon River [Thompson, 1978].

Daily average river flow was obtained from Environment Canada at station 02AD008 (Nipigon River at Pine Portage), located at 49° 18' 28" N and 88° 18' 40" W, near the river mouth. Flow data was available at this station between 1950 and 1994. Nipigon River alkalinity, temperature, and pH were obtained through EPA STORET (<http://>) for site 9000202 at 49.0197°N and 88.2508° W. No statistically significant relationship between flow and alkalinity or time of year and alkalinity existed in this data. Flow along the Nipigon River is regulated due to the Ogoki diversion upstream and the Alexander Hydroelectric Plant downstream near the river mouth. The mean alkalinity of all available data on the Nipigon River was 1458 mmol/m<sup>3</sup>, in agreement with LaMP's estimate of 73.34 mg/L (1466.8 mmol/m<sup>3</sup>). Nipigon River DOC is 7.54 mg/L [LaMP, 2000]. DIC was estimated using CO<sub>2</sub>sys [Lewis and Wallace, 1998] on days when measurements of alkalinity, temperature, and pH were taken. DIC showed no relationship with flow or time of year, and a mean value of DIC (1598 mmol/m<sup>3</sup>) was used for the Nipigon River for all days. For the model runs, daily average flow obtained from Ontario Power Generation below the Alexander Generating Station for 1979-2006 was used, as this flow data is in closest proximity to the river mouth.

### Appendix A.3 Kaministiquia River

The Kaministiquia River accounts for 5% [Thompson, 1978] of the annual flow into Lake Superior and drains 7,820 km<sup>2</sup> [Richards, 1990] into Thunder Bay in western Ontario. Flow in the Kaministiquia River passes through two hydro-power generating stations: Silver Falls and Kakabeka Falls. Flow reaching the mouth of the river is flow through Kakabeka Falls, and flow from the Whitefish and Slate Rivers that join the Kaministiquia River downstream of Kakabeka Falls. Daily average river flow at Kakabeka Falls was obtained from Ontario Power Generation. Whitefish River flow was monitored by Environment Canada at station 02AB017 (48 17'31"N 89 48'35" W) between 1980 and 2008. Flow along the Slate River was monitored by Environment Canada between 2007 and 2008 at station 02AB023 (48 19'32" N 89 24'15" W). During the year in which both Slate River and Whitefish River flows are available, Slate River flow was 25% of daily flow at Whitefish River. For model run years, river flow into Thunder Bay at the Kaministiquia River mouth was assumed to be flow at Kakabeka Falls plus Whitefish River flow plus Slate River flow, which was assumed to be 25% of Whitefish River flow.

In situ measurements of temperature, pH, and alkalinity were taken at station 1010800402 (48.392778N 89.218889 W) at the river mouth. Dissolved inorganic carbon was estimated from temperature, pH, and alkalinity observations using freshwater chemistry [Lewis and Wallace, 1998]. LOADEST [Runkel et al., 2004] was used to separately determine DIC and alkalinity concentrations for the model run period based upon a relationship between concentration and river flow. According to the Lake Superior Management Plan of 2000, the mean concentration of dissolved organic carbon in the Kaministiquia River is 33.08 mg/L [LaMP, 2000], and this value is used for model runs including the effects of DOC.



## Appendix A.4 Michipicoten River

The Michipicoten River drains 5,360 km<sup>2</sup> [Richards, 1990] of the Lake Superior basin and comprises 4.5% [Thompson, 1978] of the annual flow into Lake Superior. River flow data was obtained from Environment Canada's gauge at site 02BD002 (47° 57' 42" N 84° 53' 53" W) between 1920 and 2009. Measurements of river alkalinity between 1969 and 1990 are available for the Michipicoten River on EPA STORET at site 1002900102 (47.9225° N 84.8047° W). This site is located along the Michipicoten River at Highway 17, 5 miles south of Wawa. I assume that the relationship between river flow and alkalinity holds for the remainder of the river downstream of site 1002900102 and for the years after 1990. Using LOADEST [Runkel *et al.*, 2004], I determined the best-fit relationship between river flow at station 02BD002 and alkalinity at site 1002900102, neglecting any trends in the data. I estimated DIC from observations of temperature, pH, and alkalinity when the three measurements were all taken on the same day at site 1002900102 using CO<sub>2</sub>sys [Lewis and Wallace, 1998]. More than 100 estimates of DIC along the Michipicoten River are possible using this method, and I then determined a relationship between river flow and DIC concentration using LOADEST. An average DOC concentration of 6.03 mg/L for the river was used during all flow conditions [LaMP, 2000].

## Appendix A.5 Pic River

Pic River drains into northeastern Lake Superior. It has a drainage basin of 4,270 km<sup>2</sup> [Richards, 1990] and contributes 2% [Thompson, 1978] to the annual river inflow into Lake Superior.

River flow was gauged along the Pic River by Environment Canada from 1970 through 2009 at site 02BB003 (48° 46'26" N, 86° 17'47" W) near Marathon, Ontario. Alkalinity concentrations were measured at site 1006000102 (48.7072° N 86.2836° W) between 1973 and 1993 at Highway 17. These data are available on EPASTORET. The flow and chemical measurements are not co-located, but provide the most information available for this river. LOADEST [Runkel *et al.*, 2004] was used to estimate alkalinity concentrations for all daily river flows between 1973 and the present. DIC was estimated from observations of pH, temperature, and alkalinity [Lewis and Wallace, 1998] measured on the same day at site 1006000102. More than 100 estimates of DIC concentration were possible, and daily average flows for those days were input into LOADEST to estimate river DIC concentrations for all days between 1979 and 2006. According to the Lake Superior Lakewide Management Plan of 2000 [LaMP, 2000], the Pic River has a mean DOC concentration of 14.44 mg/L, and this value was used for all flow conditions for the river.

## Appendix A.6 White River

The White River drains 5,230 km<sup>2</sup> of Lake Superior's watershed [Richards, 1990]. Environment Canada monitored river flow along the White River at station 02BC004 from 1959-2008, just below White Lake (48° 39' 17" N 85° 44' 29" W). By this station, the river has drained 4170 km<sup>2</sup>. I assume that total flow into Lake Superior in the White River is proportional to drainage basin, and I adjust flow along the White River accordingly. Alkalinity, pH, and temperature were measured at station 1005700102 at Highway 17 (48.6606° N, 85.6286° W) and data is available on EPASTORET. There are 203 measurements of river alkalinity on days with river flow data, and LOADEST [Runkel *et al.*, 2004] is used to estimate daily concentrations of alkalinity on White River between 1979 and 2008. On dates that temperature, pH, and alkalinity were measured, I estimate DIC using CO<sub>2</sub>sys [Lewis and Wallace, 1998] and use LOADEST to estimate daily concentrations of DIC between 1979 and 2008. No DOC concentrations were available for the White River. Thus, the mean concentration of DOC for the other rivers modeled, 17 mg/L, was used.

## Appendix A.7      Black Sturgeon River

The Black Sturgeon River drains 2,980 km<sup>2</sup> into northwestern Lake Superior [Richards, 1990]. Environment Canada began monitoring flow along the Black Sturgeon River in 1971 at station 02AC002 by Environment Canada, located at Highway 17 (48° 54' 15" N 88° 22' 36" W).

Alkalinity, temperature, and pH were measured at site 1009200102 at Highway 17 (48.9044° N, 88.3775° W). Daily alkalinity concentrations between 1973 and the present were estimated using LOADEST. DIC was first estimated from river alkalinity, temperature, and pH [Lewis and Wallace, 1998], and then LOADEST [Runkel *et al.*, 2004] was used to obtain daily DIC estimates between 1979 and the present. A mean concentration for DOC of 12.94 mg/L [LaMP, 2000] was used for the Black Sturgeon River under all flow conditions.

## Appendix A.8                      St. Louis River

The St. Louis River is the largest tributary to Lake Superior within the United States. It drains 9,871 km<sup>2</sup> [Richards, 1990] into Lake Superior at Duluth. It contributes an estimated 4% of annual river inflow to Lake Superior [Thompson, 1978]. The United States Geological Survey (USGS) gauges flow in the St. Louis River at station 04024000 (St. Louis River at Scanlon, MN, 46° 42' 12"N, 92° 25' 07"W), and daily river flow is available at [www.usgs.gov](http://www.usgs.gov). Alkalinity measurements taken along the St. Louis River by the EPA and Minnesota Pollution Control Authority are available on EPA STORET. All alkalinity measurements taken below the St. Louis reservoir were used with flow at 04024000 in LOADEST to estimate daily alkalinity in the St. Louis River. I consider all observations to be representative of river conditions on the day measured, and I estimate DIC from temperature, pH, and alkalinity measurements taken downstream of the reservoir using CO<sub>2</sub>sys [Lewis and Wallace, 1998]. 182 days of DIC and flow are input into LOADEST [Runkel et al., 2004] to estimate daily concentrations of DIC in the St. Louis River. The concentration of DOC was assumed to be 22 mg/L [Maier and Swain, 1978].

## Appendix A.9                    Ontonagon River

The Ontonagon River drains 3,470 km<sup>2</sup> [Thompson, 1978; Richards, 1990] into Lake Superior on the western side of the Keweenaw Peninsula. It is the second largest U.S. tributary of Lake Superior and supplies 2.6% of the lake's total annual river inflow [Thompson, 1978]. USGS gauges river flow at site 04040000 near Rockland, Michigan at 46° 43' 15" N, 89° 12' 25" W, where 96% of the river's watershed has already drained into the river. Alkalinity was measured at the river mouth between 1968 and 1973 by the Michigan Department of Environmental Quality and is available on EPA STORET. LOADEST [Runkel *et al.*, 2004] is used to determine the relationship between Ontonagon River flow and alkalinity for 1968 onward. No pH measurements were taken by the Michigan Department of Environmental Quality at the river mouth, so measurements of alkalinity, pH, and temperature taken in the west, east, and middle branches of the Ontonagon River were used to estimate DIC concentrations using CO<sub>2</sub>sys [Lewis and Wallace, 1998] on days when all measurements were available. Measurements were taken by the Michigan Department of Environmental Quality and the USDA Forest Service are available on EPA STORET. Daily estimates of DIC concentration were obtained using LOADEST and flow at USGS 04040000. A mean concentration of 17 mg/L was used for Ontonagon River DOC.

## Appendix A.2 LOADEST Model and Coefficients

Constituent concentrations were estimated for all flow conditions and seasons using the USGS program LOADEST [Runkel *et al.*, 2004] (manual available at: <http://pubs.usgs.gov/tm/2005/tm4A5/pdf/508final.pdf>). I restricted LOADEST to use model 6 for these tributaries of Lake Superior. Model numbers 7 and above include a trend in mean values. While this may be in fact the case during the observational period, LOADEST relationships between flow and constituent concentrations were at times extrapolated to twenty years or more later than the center date of constituent observations. To avoid assuming that a trend over a few years persisted for another twenty years or more, trends in mean values were not included. Fraction of variance ( $r^2$ ) explained by the model did not increase by more than 1% when allowing models 7-11 to be used. Model 6 includes a relationship between flow and constituent concentration as well as seasonality to the constituent:

$$\ln(\text{load}) = a_0 + a_1 \ln Q + a_2 * \ln Q^2 + a_3 \sin(2\pi * \text{dtime}) + a_4 \cos(2\pi * \text{dtime}) \text{ Equation B.21.}$$

where  $\ln Q = \ln(\text{streamflow}) - \text{center of } \ln(\text{streamflow})$

$\text{dtime} = \text{decimal time} - \text{center of decimal time}$

$a_0$ ,  $a_1$ ,  $a_2$ ,  $a_3$ , and  $a_4$  are determined by LOADEST using methods of maximum likelihood. For all rivers, flow is input into LOADEST in units of cubic feet per second (cfs) and constituent concentrations are input as mg/L. The resulting coefficients, centers of decimal time, and centers of  $\ln(\text{streamflow})$  for each river are provided in Tables A-10-1 and A-10-2.

To obtain constituent concentration from river loading, the daily load is divided by the daily flow, accounting for changes in units.

**Table A.10.1** LOADEST MODEL 6 COEFFICIENTS FOR ALKALINITY

River	# Obs	Center Time	Center ln(Q)	r <sup>2</sup>	a0	a1	a2	a3	a4
St. Louis	194	1987.785	7.7536	96.42	12.6271	0.765	-.0095	0.0341	0.0457
Ontonagon	40	1971.194	7.4204	89.71	12.2039	0.816	0.1772	-.0486	0.046
White	203	1983.027	7.6411	94.63	12.6415	0.7473	-0.015	-0.065	-.0363
Black Sturgeon	197	1982.962	6.5434	99.06	11.5148	0.8071	0.0032	-.0103	-.0017
Nipigon	N/A	N/A	N/A	N/A	N/A	N/A	N/A	N/A	N/A
Kaministiquia	145	1986.433	7.3893	97.15	12.0645	0.9307	0.0064	0.002	-.0277
Michipicoten	116	1981.053	7.6196	71.89	11.8438	0.9295	-.2662	-.0365	0.1222
Pic	555	1985.064	7.4543	95.43	12.9157	0.9127	0.0058	-.0845	-.0253
Aguasabon	0	N/A	N/A	N/A	N/A	N/A	N/A	N/A	N/A



**Table A.10.2** LOADEST MODEL 6 COEFFICIENTS FOR DIC

River	# Obs	Center Time	Center ln(flow)	R <sup>2</sup>	a0	a1	a2	a3	a4
St. Louis	179	1987.921	7.7254	81.86	11.3369	0.7479	0.0139	0.115	0.1122
Ontonagon	47	1976.283	6.8778	78.45	10.5361	0.5084	0.0811	- 0.2589	0.163
White	99	1984.389	7.6405	93.8	11.3533	0.8076	0.0069	- 0.0008	- 0.0635
Black Sturgeon	97	1984.816	6.4269	97.33	10.1387	0.8161	0.0006	0.0848	0.0342
Nipigon	N/A	N/A	N/A	N/A	N/A	N/A	N/A	N/A	N/A
Kaministiquia	73	1984.535	7.5918	92.4	11.0419	0.9777	0.0679	0.0351	- 0.0347
Michipicoten	109	1981.161	7.6188	77.59	10.4973	1.0367	0.0245	- 0.0679	0.0962
Pic	108	1983.929	7.1105	95.35	0.0408	0.9769	0.0132	0.0785	- 0.0035
Aguasabon	0	N/A	N/A	N/A	N/A	N/A	N/A	N/A	N/A

## References

- Alin S.R. and T.C. Johnson (2007), Carbon cycling in large lakes of the world: A synthesis of production, burial and lake-atmosphere exchange estimates. *Global Biogeochem. Cycles*, 21,GB3002, doi:10.1029/2006GB002881.
- Assel, R.A. (2003), *An Electronic Atlas of Great Lakes Ice Cover: NOAA Great Lakes Ice Atlas*, Great Lakes Environ. Res. Lab., Ann Arbor, Michigan. (<http://www.glerl.noaa.gov/data/ice/atlas/>)
- Assel, R.A. (2005), Classification of annual Great Lakes ice cycles: Winters of 1973- 2002, *J. Climate*, 18(22), 4895-4905.
- Atila, N., G.A. McKinley, V. Bennington, M. Baehr, N. Urban, M. DeGrandpre, A. Desai, and C. Wu (2010), Observed Variability of Lake Superior  $p\text{CO}_2$ , accepted by *Limnology and Oceanography*.
- Austin, J. A., and S. M. Colman (2007), Lake Superior summer water temperatures are increasing more rapidly than regional air temperatures: A positive ice-albedo feedback, *Geophys. Res. Lett.*, 34, L06604, doi :10.1029/2006GL029021.
- Baehr, M.M. and M.D. DeGrandpre (2002), Under-ice  $\text{CO}_2$  and  $\text{O}_2$  variability in a freshwater lake, *Biogeochemistry*, 61(1), 95-113.
- Baehr, M.M. and M.D. DeGrandpre (2004), In situ  $p\text{CO}_2$  and  $\text{O}_2$  measurements in a lake during turnover and stratification: Observations and modeling, *Limnology and Oceanography*, 49(2), 330-340.
- Baines, S.B., and M.L. Pace (1991), The production of dissolved organic-matter by phytoplankton and its importance to bacteria – patterns across marine and freshwater systems, *Limnology and Oceanography*, 36(6), 1078-1090.
- Barbiero, R.P., and M.L. Tuchman (2004), The deep chlorophyll maximum in Lake Superior, *J. Great Lakes Res.*, 30(Sup 1), 256-268.
- Bender, M., Orchardo, J., Dickson, M.L., et al. (1999), In vitro  $\text{O}_2$  fluxes compared with C-14 production and other rate terms during the JGOFS Equatorial Pacific experiment, *Deep-Sea Res. I: Oceanographic Res.*, 46(4), 637-654.
- Bennett, E.B. (1978), Characteristics of the thermal regime of Lake Superior, *J. Great Lakes Res.*, 4(3-4), 310-319.
- Bennington, V., McKinley, G.A., Kimura, N., and C. Wu (2010), The general circulation of Lake Superior: mean, variability, and trends from 1979-2006, *J. Geophys. Res.- Oceanography* (in press).
- Booth et al., (2007). LoadRunner, Software and website, Yale University, New Haven, CT  
<http://environment.yale.edu/raymond/loadrunner/>
- Bootsma, H.A., Schafer, J.S., and Fillingham, J.H. (2009), Influence of a large rain event on lake- atmosphere carbon dioxide exchange in Lake Michigan, *International Association of Great Lakes Research Conference*, University of Toledo, Toledo, OH.
- Chai, Y, and N. R. Urban (2004),  $^{210}\text{Po}$  and  $^{210}\text{Pb}$  distributions and residence times in the nearshore region of Lake Superior, *J. Geophys. Res.*, 109, C10S07, doi:10.1029/2003JC002081.
- Chen et al. (2002), A model study of the coupled biological and physical dynamics in Lake Michigan, *Ecological Modeling*, 152, 145–168.

- Cole, J. J., N. F. Caraco, G. W. Kling, AND T. K. Kratz (1994), Carbon dioxide super-saturation in the surface waters of lakes, *Science* 265:1568–1570.
- Cole et al., (2007). Plumbing the global carbon cycle: Integrating inland waters into the terrestrial carbon budget. *Ecosystems* 10:171–184.
- Cotner, J.B., B.A. Biddanda, W. Makino, and E. Stets (2004). Organic carbon biogeochemistry of Lake Superior. *Aquatic Ecosystem Health and Management*, 7(4), 451-464.
- DeGrandpre, M.D., Hammar, T.R., Smith, S.P., et al. (1995), In-situ measurements of seawater pCO<sub>2</sub>, *Limnology and Oceanography*, 40(5), 969-975.
- Desai, A.R., Noormets, A.N., Bolstad, P.V., Chen, J., Cook, B.D., Davis, K.J., Euskirchen, E.S., Gough, C.M., Martin, J.G., Ricciuto, D.M., Schmid, H.P., Tang, J.W. and Wang, W. (2008) Influence of vegetation and seasonal forcing on carbon dioxide fluxes across the Upper Midwest, USA: Implications for regional scaling, *Agricultural and Forest Meteorology*, 148(2): 288-308, doi:10.1016/j.agrformet.2007.08.001.
- Dutkiewicz, S., M. Follows, and P. Parekh (2005), Interactions of the iron and phosphorus cycles: a three-dimensional model study. *Global Biogeochemical Cycles*, 19, GB1021, doi:10.1029/2004GB002342.
- Field, C.B., J. Sarmiento, and B. Hales (2007), The carbon cycle of North America in a global context. In: *The First State of the Carbon Cycle Report (SOCCR); The North American Carbon Budget and Implications for the Global Carbon Cycle*. A Report by the U.S. Climate Change Science Program and the Subcommittee on Global Change Research. National Oceanic and Atmospheric Administration, National Climatic Data Center, Asheville, NC, USA, pp. 21-28.
- French, C.R., J.J. Carr, E.M. Daugherty, L.A.K. Eidson, J.C. Reynolds, M.D. DeGrandpre (2002), Spectrophotometric pH measurements of freshwater, *Analytica Chimica Acta* 453,13-20.
- Frouin, R., and R.T. Pinker (1995), Estimating photosynthetically active radiation (PAR) at the Earth's surface from satellite observations, *Remote Sensing of Environment*, 51, 98-107.
- Garcia, H.E. and L.I. Gordon (1992), Oxygen solubility in seawater: better fitting equations. *Limnol. Oceanogr.* 37 (1992), pp. 1307–1312.
- Guildford, S.J., and Hecky, R.E. (2000), Total nitrogen, total phosphorus, and nutrient limitation in lakes and oceans: Is there a common relationship? *Limnol. Oceanogr.* 45:1213–1223.
- Guildford, S.J., et al. (1994), Effects of lake size on phytoplankton nutrient status. *Can. J. Fish. Aquat. Sci.* 51:2769–2783.
- Hanson, P., A. I. Pollard, D. L. Bade, K. Predick, S. R. Carpenter, and J. A. Foley (2004), A model of carbon evasion and sedimentation in temperate lakes. *Glob. Change Biol.* 10: 1285–1298.
- Hecky, R. E., (2000), A biogeochemical comparison of Lakes Superior and Malawi and the limnological consequences of an endless summer. *Aquat. Ecosyst Health Manage.* 3, 23–33.
- Heinen, E.A. and J. McManus (2004), Carbon and nutrient cycling at the sediment-water boundary in western Lake Superior, *J. Great Lakes Res.*, 30(Sup 1), 113-132.
- Kelly, C.A., E. Fee, P.S. Ramlal, J.W. Rudd, R.H. Hesslein, C. Cnema, and E.U. Schindler (2001), Natural variability of carbon dioxide and net epilimnetic production in surface waters of boreal lakes of different sizes, *Limnol. Oceanogr.*, 46(5), 1054-1064.

- Kumar S, Sterner RW, Finlay J. (2008), Nitrogen and carbon uptake dynamics in Lake Superior. *Journal of Geophysical Research – Biogeosciences*. 113:G04003.
- Lake Superior Lakewide Management Plan (LaMP) (2000), United States Environmental Protection Agency.
- Laws, E. A., M.R. Landry, R.T. Barber, M. Bender, L. Campbell, M.-L. Dickson, and J. Marra (2000), Carbon cycling in primary production bottle incubations: Inferences from grazing experiments and photosynthetic studies using  $^{14}\text{C}$  and  $^{18}\text{O}$  in the Arabian Sea, *Deep-Sea Res. II* 47, 1339-1352.
- Lewis, E. and D. W. R. Wallace (1998), Program developed for  $\text{CO}_2$  system calculations, Report 105, Oak Ridge National Laboratory, 33 pp. (available at: <http://cdiac.esd.ornl.gov/oceans/co2rprt.html>).
- Maier, W. J., Swain, W. R. (1978), Lake Superior organic carbon budget. *Water Res.* 12, 403–412.
- Marshall, J., A. Adcroft, C. Hill, L. Perelman, and C. Heisey (1997a), A finite volume, incompressible Navier-Stokes model for studies of the ocean on parallel computers, *J. Geophys. Res.*, 102, 5753-5766.
- Marshall, J., C. Hill, L. Perelman, and A. Adcroft (1997b), Hydrostatic, quasi-hydrostatic, and nonhydrostatic ocean modeling, *J. Geophys. Res.*, 102, 5733-5752.
- McDonald, C. (2010), Improving the reliability of aquatic biogeochemical models: Integrating information and optimizing complexity, PhD Thesis, Michigan Technological University, USA.
- Mesinger, F., et al. (2006). North American Regional Reanalysis. *Bull. Amer. Meteorol. Soc.*, 87, 343-360, doi:10.1175/BAMS-87-3-343.
- Moore et al. (2002), An intermediate complexity marine ecosystem model for the global domain. *Deep-Sea Res. II*, 49, 403-462.
- NOAA Ocean Acidification Steering Committee (2010): NOAA Ocean and Great Lakes Acidification Research Plan, NOAA Special Report, 143 pp.
- Peters et al., (2007) An atmospheric perspective on North American carbon dioxide exchange: CarbonTracker, *PNAS*, 104(48), 18925-18930, doi:10.1073/pnas.0708986104.
- Richards, P.R. (1990), Measures of flow variability and a new flow-based classification of Great Lakes tributaries. *J. Great Lakes Res.*, 16(1), 53-70.
- Runkel, R.L., Crawford, C.G., and Cohn, T.A., 2004, Load Estimator (LOADEST): A FORTRAN Program for Estimating Constituent Loads in Streams and Rivers: U.S. Geological Survey Techniques and Methods Book 4, Chapter A5, 69 p.
- Sarmiento, J. L. and N. Gruber (2006) *Ocean Biogeochemical Dynamics*. Princeton University Press, 503, pp.754.
- Sterner, R.W., et al. (2004) Phosphorus and trace metal limitation of algae and bacteria in Lake Superior. *Limnol. Oceanogr.*, 49(2), 2004, 495–507.
- Sterner, R.W. (2010) In situ-measured primary production in Lake Superior. *J. Great Lakes Res.* 36 139–149.
- Thompson, M.E. (1978), Major ion loadings to Lake Superior. *J. Great Lakes Res.*, 4(3-4), 361-396.
- Tranvik, L. et al. (2009) Lakes and reservoirs as regulators of carbon cycling and climate *Limnol. Oceanogr.*, 54(6, part 2), 2298–2314.
- United States. NOAA. NOAA Ocean Acidification Steering Committee (2010), *NOAA Ocean and Great Lakes*

*Acidification Plan*

- United States. Canada. Lake Superior Binational Program's Superior Work Group (2000), *Lake Superior Lakewide Management Plan (LaMP)*. website: <http://www.epa.gov/glnpo/lakesuperior/lamp2000/index.html>
- Urban, N.R., D.S. Apul, and M.T. Auer (2004), Planktonic respiration rates in Lake Superior. *J. Great Lakes Res.*, 30 suppl. 1, 230-244.
- Urban, N.R., M.T. Auer, S.A. Green, X. Lu, D.S. Apul, K.D. Powell and L. Bub (2005), Carbon Cycling in Lake Superior, *J. Geophys. Res.* 110, C06S90, doi:10.1029/2003JC002230.
- Urban, N.R. (2009), Nutrient cycling in Lake Superior: A retrospective and update. In M. Munawar and I.F. Munawar (Eds.), *State of Lake Superior* (83-115). Ecovision World Monograph Series: Aquatic Ecosystem Health and Management Society.
- Urban, N.R. (2009b), Carbon cycling in Lake Superior: A regional and ecosystem perspective. In M. Munawar and I.F. Munawar (Eds.), *State of Lake Superior* (83-115). Ecovision World Monograph Series: Aquatic Ecosystem Health and Management Society.
- Vasys, V.N., A.R. Desai, G.A. McKinley, V. Bennington, A.M. Michalak, D.N. Huntzinger, and A.E. Andrews (2010). Implications of neglecting large lake carbon cycling for regional tracer transport inversions. *submitted to Geophys. Res. Lett.*
- Vollenwider, R. A., M. Munawar, and P. Stadelmann (1974) A comparative review of phytoplankton and primary production in the Laurentian Great Lakes. *J. Fish. Res. Bd. Can.*, 31, 739-762.
- Wanninkhof, R. (1992), Relationship between wind speed and gas exchange over the ocean, *J. Geophys Res.*, 97, C5, 7373-7382.
- Weiler, R.R. (1978), Chemistry of Lake Superior. *J. Great Lakes Res.* 4, 370-385.